Mechanical Properties and Deformation Behaviour of High-Pressure Die-Cast Magnesium-Aluminium Based Alloys

A thesis submitted in fulfilment of the requirements for the degree of

Doctor of Philosophy

Hua Qian Ang (Vivian)

B.Eng Mechanical Engineering (Hons)

School of Engineering

College of Science Engineering and Health

RMIT University

October 2017

Declaration

I certify that except where due acknowledgement has been made, the work is that of the author alone; the work has not been submitted previously, in whole or in part, to qualify for any other academic award; the content of the thesis is the result of work which has been carried out since the official commencement date of the approved research program; any editorial work, paid or unpaid, carried out by a third party is acknowledged; and, ethics procedures and guidelines have been followed.

Hua Qian Ang (Vivian)

24-October-2017

I would like to dedicate this thesis to the chemical element located in periodic table Group 2 and Period 3 with an atomic number 12- Magnesium

Acknowledgements

I would like to express the deepest appreciation to:

Professor Mark Easton, for his scientific advice, suggestions, supervision and guidance during my PhD studies at RMIT University, and for having unwavering confidence in me even when I had none for myself. He has been both a great supervisor and a good mentor. From him, I was introduced to Magnesium on the 18th of December 2014.

Professor Trevor Abbott, for providing me with the knowledge and skills on modelling and curve fitting, and for the 24-7 assistance via Skype over the past three years. His motivation and enthusiasm for research have truly inspired me and showed me what it truly means to be a Materials Scientist and Engineer. I would not have become a "crystal twister" without him. I also acknowledge Skype for making our discussion fruitful.

Dr. Suming Zhu and *Dr. Chengfan Gu*, for their constant supervision and excellent support in helping me to acquire the experimental skills for carrying out this research. It is always a pleasure to learn from them in formal and informal occassions.

Professor Cuie Wen and *Dr. Dong Qiu*, for being involved in my review committee and providing me with valuable suggestions. *Professor Carlos Cáceres* from University of Queensland, for his very helpful comments on several manuscripts. *Dr. Monir Takla*, for motivating me during my undergraduate studies, to continue with a doctorate work.

Dr. Matthew Field, *Dr. Khurram Munir*, and *Mr. Peter Rummel*, whom provided assistance in various microscopy work, including but not limited to, metallographic sample preparation and microstructural characterisation. I would also like to acknowledge the RMIT Microscopy and Microanalysis Facility for the high-quality electron microscopy equipment.

Mr. Peter Tkatchyk, for enduring my constant need to set up the machine for mechanical testing and for giving me after-hour access to finish my testing. Special thanks to Instron 5569 for breaking down only after my tests were complete.

Big thanks to *RMIT Security* for consistently kicking me out of my lab at late hours, thus forcing me to escape the experimental work and focus on writing thesis and papers. It was during this time that most part of this thesis was produced.

Although we have never met, I would like to thank *Mr. Gary Savage* and his team from CSIRO Manufacturing for the production and supply of the samples.

I also acknowledge the financial support I have received for my research provided by RMIT University [PhD International Scholarship (RPIS)] and Australian Research Council [Grant number LP130100828].

To all PhD students and my friends, if you are still confused about what you are doing, I shall now give you the words of Sir Albert Einstein: “If we knew what it was we were doing, it would not be called research, would it?”

Finally, I wish to express my gratitude to my parents for their unconditional love, support and for cheering me up during the last stage of my PhD. This thesis is only possible because of you. Just a heads up, upon submission of this thesis, I am officially unfunded, and financially dependent on you.

Abstract

Demands for increased fuel efficiency and reduced greenhouse gas emissions led to the need for weight reductions in automotive applications. Because of this, high-pressure die-cast magnesium alloys have attracted a lot of attention for automotive structural applications due to their low density (~ 1.8 g/cm^3) and high specific strength. Replacement of heavy structural components made from aluminum alloys (~ 2.7 g/cm^3), steel and cast iron (~ 7.2 g/cm^3) with die-cast magnesium alloys can offer significant potential for weight reduction.

Structural alloys must have high levels of strength and ductility for energy absorption in vehicle crash situations and for manufacturing processes, such as self-piecing riveting. In order to improve the mechanical properties of existing high-pressure die-cast magnesium alloys for potential structural applications, it is important to first understand how these alloys deform under loading which forms the basis for this research.

The primary aim of this research is to investigate the mechanical properties and deformation behaviour of commercial high-pressure die-cast magnesium-aluminium based alloys Mg-4Al-0.3Mn (AM40), Mg-6Al-0.3Mn (AM60), Mg-9Al-1Zn (AZ91) and Mg-4Al-4RE (AE44) at a broad strain-rate range 10^{-6}-10^{-1} s^{-1}. Both strain rate and aluminium content (main alloying element in these commercial alloys) are important considerations in the design of structural alloys.

Magnesium alloys have a complex progression of deformation mechanisms due to their hexagonal closed-packed crystal structure. This type of crystal structure does not provide sufficient independent basal slip systems to satisfy the von Mises-Taylor criterion and the non-basal slip mechanisms (<a> prismatic and <c+a> pyramidal) only activate at higher stress levels at room temperature. Hence, twinning is activated to accommodate plastic deformation during loading. Twinning in magnesium alloys is unstable in the deformed state and twinning can partially revert during unloading, consequently a large part of the non-linear deformation becomes reversible (anelastic deformation). The deformation behaviour of magnesium alloys can therefore be separated into three stages: elastic, anelastic and plastic. Compared to elasticity and plasticity, relatively less attention has been paid to the anelasticity of magnesium alloys, which manifests as non-linearity or hysteresis loop in the loading-unloading stress-strain curves. The complex deformation behaviour of die-cast magnesium

alloys requires further investigation, especially on the effects of strain rate and aluminium content.

In the first study of this research, the effect of anelasticity on the proof stress measurement of magnesium alloys was investigated. Four standardised proof stress measurement methods were critically reviewed and inconsistencies were found between these methods. It was observed that anelasticity led to ambiguities in proof stress measurement of magnesium alloys. To correct for anelasticity, a more pragmatic approach of using a higher offset strain of 0.45% to achieve 0.2% residual plastic strain in proof stress measurement was proposed for die-cast magnesium alloys. This study is important as it proposes a more consistent proof stress determination method for die-cast magnesium alloys which allows better comparison of alloy's properties for engineering applications. The outcome of this study provides an understanding of the effects of <a> basal slip and reversible twinning on the proof stress of magnesium and alloys.

The second study investigated the effects of strain rate and aluminium content on the deformation behaviour of these commercial alloys at strain rates 10^{-6}-10^{-1} s^{-1}. In this study, alloys with lower aluminium contents in solid solution exhibited higher strain-rate sensitivity, and strain-rate sensitivity was observed to manifest as an increase in work hardening and tensile/yield ratio. This suggests that the performance of magnesium alloys in terms of energy absorption can improve at higher strain rates, and this can benefit crashworthiness, which is beneficial in structural applications. For the first time, the decrease in strain-rate sensitivity in magnesium alloys was observed to be due to the increase in aluminium solute level in the α-magnesium matrix rather than the overall aluminium content and this was related to dynamic strain ageing from the interactions between the aluminium solute and dislocations. Another interesting observation from the second study was the high strain-rate sensitivity of <a> prismatic and <c+a> pyramidal slip.

Therefore, the third study further divided the overall deformation behaviour into three regions: elasticity, anelasticity (reversible twinning) and plasticity (<a> basal slip and <a> prismatic) in order to study their dependences on strain rate and aluminium solute level. Results showed that anelasticity was strain-rate insensitive while plasticity by <a> prismatic slip was strain-rate sensitive. The high strain-rate sensitivity of <a> prismatic slip led to a variation in maximum anelasticity with strain rate. AZ91, which has the most aluminium contents in solution, exhibited the largest maximum anelasticity, as compared to AM40 and AM60. It was proposed that at low aluminium concentrations, solution softening of the <a> prismatic planes reduced the need to twin, whereas at the higher concentrations, solution

hardening of all slip planes (but not twinning) made <a> basal and <a> prismatic slip more difficult, leading to an increased amount of twinning. The effects of strain rate and aluminium solute level on anelasticity and plasticity were systematically studied for the first time. The effect of precipitates on anelasticity was also investigated. Presence of precipitates in aged AE44-T5 was observed to harden not only <a> basal and <a> prismatic slip, but also suppress twinning, decreasing the anelasticity in comparison with as-cast AE44.

In the final study of this research, the knowledge from previous chapters was applied to model the different stages of deformation behaviour of these alloys by constitutive equations. Within the elastic, anelastic and plastic deformation, the stress-strain curve was further separated into four stages, namely elastic (stage I), <a> basal slip and twinning (stage II), <a> prismatic slip (stage III) and <c+a> pyramidal slip (stage IV). Both stages I and III followed a linear relationship and were modelled with a linear equation, while stages II and IV followed a power-law relationship and were modelled with Hollomon's equation. These four stages were first analysed individually and a semi-empirical equation was then established to model the entire stress-strain curve. Overall, the proposed model provided a good fit to the experimental stress-strain curve for most of the alloys, but it slightly overestimated the stress in the stage II-III transition region in the AZ91 alloy. This slight discrepancy was attributed to the delayed onset of stage III, an effect of high aluminium concentration and fully interconnected percolating network, leading to higher strain hardening rate during the stage II-III transition in AZ91.

Overall, this research demonstrates that the deformation behaviour of high-pressure die-cast magnesium-aluminium based alloys can be separated into four stages, elastic, <a> basal slip and twinning, <a> prismatic slip and <c+a> pyramidal slip from the three types of deformations: elastic, anelastic and plastic. Decomposition of stress-strain curve into these different stages has provided insights into the improved measurement of proof strength, the role of aluminium solute in moderating strain-rate sensitivity, the interactions of slip and twinning deformation systems to understand total anelasticity and the contributions of different slip and twinning deformation mechanisms to the overall deformation behaviour of die-cast magnesium alloys. This research is a milestone in developing understanding of the deformation mechanisms in die-cast magnesium alloys and will provide the foundation for future development of improved structural alloys.

Keywords: High-pressure die-casting; magnesium alloys; deformation behaviour; mechanical properties; strain-rate sensitivity; constitutive modelling.

Publications and Presentations

Journal Articles

Ang HQ, Abbott TB, Zhu SM, Gu CF, Easton MA. Proof stress measurement of die-cast magnesium alloys. Mater Des 2016; 112: p. 402-409. (As Chapter 4)
(*SCImago Journal Rank (SJR): 1.751; Impact Factor: 4.364*)

Ang HQ, Zhu SM, Abbott TB, Qiu D, Easton MA. Strain-rate sensitivity of die-cast magnesium-aluminium based alloys. Mater Sci Eng A 2017; 699: p. 239-246. (As Chapter 5)
(*SCImago Journal Rank (SJR): 1.666; Impact Factor: 3.094*)

Ang HQ, Abbott TB, Zhu SM, Easton MA. Anelasticity of die-cast magnesium-aluminium based alloys under different strain rates. Mater Sci Eng A 2017; 707: p. 101-109. (As Chapter 6)
(*SCImago Journal Rank (SJR): 1.666; Impact Factor: 3.094*)

Ang HQ, Abbott TB, Zhu SM, Easton MA. Constitutive modelling of the deformation behaviour of commercial die-cast magnesium-aluminium based alloys. *Submitted to International Journal of Plasticity*. (As Chapter 7)

Conference Papers

Ang HQ, Abbott TB, Zhu SM, Easton MA. Effect of strain rate on mechanical behaviour of commercial die-cast magnesium alloys. Light Metals Technology 2017: Proceedings of the Materials Science & Technology 2017; 2017 Oct 8-12; Pittsburgh, Pennsylvania, USA. p. 164-170.

Easton MA, Zhu SM, Gibson M, Abbott TB, **Ang HQ**, Chen XB, Birbilis N, Savage G. Performance evaluation of high-pressure die-cast magnesium alloys. In: Solanki KN, Orlov D, Singh A, Neelameggham NR, editors. Magnesium Technology 2017: Proceedings of the TMS (The Minerals, Metals & Materials Society); 2017 Feb 26-Mar 2; San Diego, California. Springer International Publishing; 2017. p. 123-129.

Ang HQ, Abbott TB, Zhu SM, Gu CF, Easton MA. Flaws in standardised proof stress determination methods for magnesium alloys. Proceedings of the Third International Academic Conference of Postgraduates, NUAA; 2015 Nov 18-20; Nanjing, China. p. 75-79.

Presentations

Materials Science and Technology 2017: Light Metals Technology
8-12 October, 2017, David L. Lawrence Convention Center,
Pittsburgh, Pennsylvannia, USA

CAMS 2016 Advancing Materials and Manufacturing
6-8 December, 2016, Swinburne University,
Melbourne, Australia

Additive, Innovative Manufacturing, and Light Structures (A.I.L) Symposium
15 July, 2016, RMIT University,
Melbourne, Australia

The Third International Academic Conference for Graduates, NUAA
18-20 November, 2015, Nanjing University of Aeronautics and Astronautics,
Nanjing, China

Trans-Tasman Three Minute Thesis Competition (3MT)
3 November, 2014, University of Western Australia,
Perth, Australia

Table of Contents

List of Figures

Chapter 2 Literature Review

Chapter 4 Proof Stress Measurement of Die-Cast Magnesium Alloys

Chapter 6 Anelasticity of Die-Cast Magnesium-Aluminium Based Alloys under Different Strain Rates

Chapter 8 Conclusions & Recommendations

List of Tables

Chapter 2 Literature Review

Chapter 3 Experimental Techniques & Procedures

Chapter 4 Proof Stress Measurement of Die-Cast Magnesium Alloys

Chapter 5 Strain-rate Sensitivity of Die-Cast Magnesium-Aluminium Based Alloys

Chapter 6 Anelasticity of Die-Cast Magnesium-Aluminium Based Alloys under Different Strain Rates

Chapter 7 Constitutive Modelling of the Deformation Behaviour of Commercial Die-Cast Magnesium-Aluminium Based Alloys

Chapter 1
Introduction

1.1 Background

Magnesium alloys are categorised into cast and wrought alloys. Cast alloys account for over 90% of overall use in automotive and aerospace industries as compared to wrought alloys [1] due to the low cost, high level of automation and short processing time in casting [2]. Furthermore, high-pressure die-cast (HPDC) magnesium alloys also have some advantages over wrought alloys for commercial applications, such as tension-compression isotropy, better mechanical properties at high strain rates and lower corrosion rates [1].

The majority of HPDC magnesium alloy consumption is for automotive applications. The increasing interest in the use of magnesium alloys in vehicle fabrication is mainly due to their low density with one quarter of the density of steel and only two-thirds that of aluminum [3]. Replacement of heavy components made from steel and aluminium alloys with HPDC magnesium alloy components offers an opportunity to increase vehicle efficiency and reduce greenhouse gas emissions.

In the past, there has been considerable focus on high temperature alloy development for powertrain applications [4-6], but in recent years, the focus has shifted to structural applications. With the advent of electric vehicles, this trend is expected to continue due to the greatly simplified nature of electric powertrains compared to those of internal combustion vehicles. This will reduce the demand for powertrain components but the requirements for structural components to form the car body and closures remain.

The requirements for structural alloys differ from those of high-temperature alloys. In particular, there is a need for high room-temperature strength combined with high levels of ductility for energy absorption in vehicle crash situations and during manufacturing processes, such as self-piercing riveting. In both of these situations, strain rate is an important factor, for example in self-piercing riveting, the strain rate produced by the punch speed may vary during rivet insertion due to material resistance to deformation. Understanding the effect of strain rate on the mechanical properties and deformation behaviour of HPDC magnesium alloys is important in the development of improved structural alloys.

The hexagonal close-packed (HCP) crystal structure of magnesium and alloys adds to the complexity of the deformation behaviour. The elastic limit of magnesium alloys is relatively low (< 50 MPa) [7, 8], beyond that plastic deformation occurs. However, the lack of independent basal slip systems and the activation of non-basal slips at higher stress levels in the HCP structure result in profuse twinning to accommodate plastic deformation [9-13]. Twins formed in magnesium alloys are not stable under loading [14]; and twins can revert during unloading [15], consequently a large part of the non-linear deformation in magnesium alloys is reversible. The complex progression of deformation mechanisms in the HCP crystal structure of magnesium alloys requires further investigation and this forms the basis for this research.

To understand the room-temperature tensile deformation behaviour of existing HPDC magnesium alloys, commercially available alloys AM40 (Mg-4Al-0.3Mn), AM60 (Mg-6Al-0.3Mn), AZ91 (Mg-9Al-1Zn) and AE44 (Mg-4Al-4RE) are studied in this research. AZ91 is widely used for some structural components of automobiles (i.e. steering column brackets and brake pedals) because of its good combination of mechanical properties and die-castability; AM40 and AM60 are most commonly used in applications where energy absorption is required, such as seat frames and instrument panels [1, 16, 17]; AE44 has good high-temperature strength and creep resistance and it is ideal for automotive powertrains [18], but it is also seen in structural applications, such as front engine crossmember [19].

In order to properly study the deformation behaviour, the key material properties, such as yield or proof stress, tensile strength and elongation to failure must be clearly defined. Tensile strength and elongation to failure are unambiguous and can be readily determined. Measurement of proof stress in magnesium, however, has been challenging. There are at least four standardised proof stress measurement methods (ISO 6892-1 [20] and ASTM E8M-09 [21]), applicable to magnesium and alloys. This has resulted in a wide range of proof stress values reported in literature for the same alloy, depending on the method used. Establishing a more consistent proof stress measurement method is the first step towards better comparison of alloy's properties.

The non-linear reversible deformation, also known as anelasticity, in magnesium alloys is another interesting aspect of this research. Due to the limited easily activated slip systems available in magnesium alloys, the deformation behaviour can be divided into three stages: elastic, anelastic and plastic [7, 8, 22]. The study of anelasticity is important as it influences several properties, including yield strength [23], fatigue strength [8], apparent stiffness [7, 22] and sound dampening [14].

Although anelasticity plays a major role in the deformation of magnesium alloys, only a few studies, mainly from Cáceres and his co-workers [7, 22, 24] have investigated the solute and grain size dependences of anelasticity on magnesium-zinc and magnesium-aluminium alloys. To the author's knowledge, the effect of strain rate on anelasticity has not been investigated. Understanding the effects of strain rate and aluminium content (aluminium is the main alloying element in the investigated alloys) on the different deformation regions (elastic, anelastic and plastic) can provide insights into the deformation mechanisms of magnesium alloys.

1.2 Research Aims and Objectives

The primary aim of this research is to study the mechanical properties and deformation behaviour of commercial HPDC magnesium alloys AM40, AM60, AZ91 and AE44 across wide strain-rate range 10^{-6}-10^{-1} s^{-1}, and to provide a better understanding of the deformation mechanisms for future development of improved structural alloys. This research is further divided into four objectives:

1) To review the inconsistencies in standardised proof stress determination methods for die-cast magnesium alloys and to propose a better way to measure the proof stress of such alloys by correcting for anelasticity;

2) To investigate the tensile properties and deformation behaviour of commercial die-cast magnesium alloys consisting of different aluminium content at strain rates 10^{-6}-10^{-1} s^{-1};

3) To determine the contributions of elastic, anelastic and plastic deformations and to study their dependences on strain rate and aluminium content;

4) To correlate the deformation mechanisms (different slip and twinning deformation systems) to the different stages of the stress-strain curve and to develop constitutive equations to model these stages.

1.3 Thesis Structure

Chapter 1 provides a brief introduction of this research, including the main aim and research objectives, as well as a summary of the thesis chapters.

Chapter 2 begins by introducing the readers to a basic overview of magnesium and its alloys and their manufacturing processes. It also provides a detailed review that is related to

the deformation behaviour (elastic, anelastic and plastic) of magnesium and alloys. Attention is also brought to the strain-rate sensitivity of magnesium alloys, with particular focus on the effect of aluminium content.

Chapter 3 explains some of the procedural techniques involved in the surface preparation of magnesium alloys for optical and electron microscopy. Special focus is placed on the sample preparation techniques for electron backscattered diffraction (EBSD). The intention of this chapter is to provide a reference for future work on similar alloys, since magnesium is one of the most difficult materials to achieve a satisfactory quality of sample preparation. Mechanical testing procedures are also described.

Chapter 4 is the first published paper related to this research which reviews the inconsistencies in standardised proof stress determination methods for die-cast magnesium alloys. A conversion chart is constructed to enable the determination of the appropriate offset strain in proof stress measurement for a range of magnesium alloys. For die-cast magnesium alloys which have a grain size of less than 10 μm, a higher offset strain of 0.45% shows a closer approximation to the 0.2% permanent plastic strain in proof stress measurement.

Chapter 5 answers the second research objective which is to understand the effects of strain rate (10^{-6}-10^{-1} s^{-1}) and aluminium content on the monotonic tensile behaviour of commercial die-cast magnesium alloys AM40, AM60, AZ91 and AE44. It is observed that strain-rate sensitivity decreases with increasing aluminium solute level and this is proposed to be due to dynamic strain ageing.

Chapter 6 divides the overall deformation behaviour of these alloys into elastic, anelastic (reversible twinning) and plastic (<a> basal slip and <a> prismatic slip) regions and studies their dependences on strain rate and aluminium solute level. This study shows that both anelasticity and plasticity by <a> basal slip are strain-rate insensitive, while plasticity by <a> prismatic slip is strain-rate sensitive. The high strain-rate sensitivity of <a> prismatic slip results in a variation in maximum anelasticity with strain rate. High aluminium concentrations (9 wt.% aluminium) can also make <a> basal slip and <a> prismatic slip more difficult, leading to an increased amount of twinning and anelasticity.

Chapter 7, building on previous chapters, this chapter first separates the stress-strain curve into four stages: elastic (stage I), <a> basal slip and twinning (stage II), <a> prismatic slip (stage III) and <c+a> pyramidal slip (stage IV). A semi-empirical model is then established to predict the entire stress-strain curve. The developed model shows a good agreement with experimental data with one limitation; the model slightly overestimates the experimental data in the stage II-III transition region for the AZ91 alloy.

Chapter 8 summarises the key findings obtained from previous chapters, and discusses some of the research implications and potential future directions that may be derived from the outcomes of this research.

Chapter 1 References

[1] Abbott TB. Magnesium: industrial and research developments over the last 15 years. Corrosion 2015; 71(2): p. 120-7.

[2] Andresen W. Die cast engineering: a hydraulic, thermal, and mechanical process. United States: CRC Press; 2004.

[3] Avedesian M, Baker H. Magnesium and magnesium Alloys—ASM Specialty Handbook, ASM International. Ohio: The Materials Information Society; 1999.

[4] Aghion E, Bronfin B, Von Buch F, Schumann S, Friedrich H. Newly developed magnesium alloys for powertrain applications. Journal of Minerals, Metals and Materials Society 2003; 55(11): p. 30-3.

[5] Luo AA. Recent magnesium alloy development for automotive powertrain applications. Materials Science Forum, Trans Tech Publ 2003; 419-422: p. 57-66.

[6] Bettles CJ, Forwood CT, St. John DH, Frost MT, Jones DS, Qian M et al. AMC-SC1: an elevated temperature magnesium alloy suitable for precision sand casting of powertrain components. In: Kaplan HI, editor. Magnesium Technology. Proceedings of the TMS Annual Meeting; 2003 March 2-6; San Diego, California; p. 223-6.

[7] Cáceres CH, Sumitomo T, Veidt M. Pseudoelastic behaviour of cast magnesium AZ91 alloy under cyclic loading–unloading. Acta Materialia 2003; 51(20): p. 6211-8.

[8] Lu ZJ, Blackmore P. Cyclic stress-strain behaviour of AM60B and AE44 cast magnesium alloys and its impact on LCF characterisation and fatigue analysis. SAE International Journal of Materials and Manufacturing 2014; p. 446-53.

[9] Polmear IJ. Light alloys: metallurgy of the light alloys. London: Metallurgy and Materials Science; 1995.

[10] Pekguleryuz MO, Kainer KU, Kaya AA, editors. Fundamentals of magnesium alloy metallurgy, Cambridge: Woodhead Publishing; 2013.

[11] Yoo MH. Slip, twinning, and fracture in hexagonal close-packed metals. Metallurgical Transactions A 1981; 12(3): p. 409-18.

[12] Koike J, Fujiyama N, Ando D, Sutou Y. Roles of deformation twinning and dislocation slip in the fatigue failure mechanism of AZ31 Mg alloys. Scripta Materialia 2010; 63(7): p. 747-50.

[13] Christian JW, Mahajan S. Deformation twinning. Progress in Materials Science 1995; 39(1): p. 1-157.

[14] Duerig TW, Zadno R. An engineer's perspective of pseudoelasticity. In: Duerig TW, Melton KN, Stöckel D, editors. Engineering aspects of shape memory alloys, 1st ed, UK: Butterworth-Heinemann; 1990, p. 369-93.

[15] Muránsky O, Carr DG, Šittner P, Oliver EC. In situ neutron diffraction investigation of deformation twinning and pseudoelastic-like behaviour of extruded AZ31 magnesium alloy. International Journal of Plasticity 2009; 25(6): p. 1107-27.

[16] Mordike BL, Ebert T. Magnesium: Properties—applications—potential. Materials Science and Engineering A 2001; 302(1): p. 37-45.

[17] Luo AA, Renaud J, Nakatsugawa I, Plourde J. Magnesium castings for automotive applications. Journal of the Minerals, Metals, and Materials Society 1995; 47(7): p. 28-31.

[18] Zhu SM, Easton MA, Abbott TB, Nie JF, Dargusch MS, Hort N et al. Evaluation of magnesium die-casting alloys for elevated temperature applications: microstructure, tensile properties, and creep resistance. Metallurgical and Materials Transactions A 2015; 46(8): p. 3543-54.

[19] Aragones J, Goundan K, Kolp S, Osborne R, Ouimet L, Pinch W. Development of the 2006 Corvette Z06 structural cast magnesium crossmember. SAE Technical Paper 2005-01-0340.

[20] ISO 6892-1 metallic materials tensile testing-part 1: method of test at room temperature. International Standards Organisation; 2009.

[21] ASTM Standard E8M-09 standard test methods for tension testing of metallic materials in annual book of ASTM standards, ASTM. West Conshohocken PA: American Society for Testing and Materials; 2009.

[22] Mann GE, Sumitomo T, Cáceres CH, Griffiths JR. Reversible plastic strain during cyclic loading–unloading of Mg and Mg–Zn alloys. Materials Science and Engineering A 2007; 456(1): p. 138-46.

[23] Carbonneau Y, Sanschagrin A, Renaud J, Tremblay R. On the development of a new approach for the determination of yield strength in Mg-based alloys. Light Metal Age 1998; 56(9-10): p. 50-3.

[24] Nagarajan D, Cáceres CH, Griffiths JR. Anelastic phenomena in Mg-Al alloys. Proceedings of the 12th International Symposium on Physics of Materials; 2011 Sep 4-8; Prague. Czech Republic: Polish Academy of Sciences Institute of Physics; 2012. p. 501-4.

Chapter 2
Literature Review

This chapter surveys the literature most pertinent to the objectives of this thesis. The literature review is divided into five main sections. Section 1 provides a brief overview of magnesium and its alloys, such as their applications, a short explanation on magnesium naming conventions and alloying systems, and deformation modes. Section 2 provides a discussion of the two relevant manufacturing processes: high-pressure die-casting and self-piercing riveting. Section 3 discusses the deformation behaviour (elasticity, anelasticity and plasticity) of magnesium and its alloys and section 4 reviews the strain-rate sensitivity of magnesium alloys. Section 5 concludes with the literature gaps and research hypotheses.

2.1 Magnesium and Magnesium Alloys

Magnesium (Mg) was first discovered in 1808 by Sir Humphrey Davey [1]. Comprising 2.7% of the earth's crust and 0.13% of the earth's ocean water, this makes magnesium a relatively plentiful element [2]. Currently, magnesium has attracted much attention in automotive applications, where weight reduction is important to improve fuel economy and reduce greenhouse gas emissions. This is because magnesium has relatively low density of 1.7 g/cm^3 [3], which is 35% and 61% lower than that of aluminium and titanium, respectively [4]. Although magnesium is commercially available with purities exceeding 99.8%, it is rarely used for engineering applications in its un-alloyed form due to its low strength, low ductility and poor corrosion resistance.

To overcome these limitations, magnesium is alloyed with various alloying elements such as aluminium (Al), zinc (Zn), manganese (Mn), lithium (Li), and rare earth elements (RE). Copper (Cu), nickel (Ni), and iron (Fe) are considered harmful impurities that need to be controlled properly to ensure the quality of magnesium alloys [5].

In terms of the applications of magnesium alloys, both cast and wrought magnesium alloys are available. However, more than 90% of the magnesium parts are manufactured by casting [3]. Currently, some commercially available magnesium alloys are die-cast AM40 (Mg-4Al-0.3Mn), AM60 (Mg-6Al-0.3Mn), AZ91 (Mg-9Al-1Zn) and AE44 (Mg-4Al-4RE).

AZ91 is widely used for some structural components of automobiles (steering column brackets and brake pedals), aircraft, and computers, because of its good combination of mechanical properties and die-castability while AM40 and AM60 are most commonly used in applications where energy absorption is required, such as seat frames and instrument panels [6-8]. AE44 has good combination of strength and ductility and has been applied in automotive front engine crossmember [9].

2.1.1 Alloying Systems

The naming convention of magnesium alloys is based on an alpha-numeric designation system, with the first two letters representing the major alloying elements followed by their respective weight percentage rounded off to whole numbers of these constituents. Sometimes, a serial letter is given at the end (A, B, C, D and E) which designates the stage of development or degree of purity of the alloy. The alloy AZ91D, for example, is an alloy with a nominal content of 9 wt.% aluminium (A) and 1 wt.% zinc (Z). Its development stage is 4 (D). A coding system for the temper designation of magnesium alloys is sometimes used. The designations include as fabricated (F), solution heat-treated (T4) and solution heat-treated and artificially aged (T6). Detailed explanation of this standardised system is reviewed elsewhere [3]. Table 2.1 lists the one letter abbreviations for the most commonly used alloying elements [2, 3, 10].

Table 2.1: ASTM codes for magnesium alloying elements.

Code Letter	Alloying Element	Code Letter	Alloying Element
A	Aluminium	N	Nickel
B	Bismuth	P	Lead
C	Copper	Q	Silver
D	Cadmium	R	Chromium
E	Rare Earths	S	Silicon
F	Iron	T	Titanium
H	Thorium	W	Yttrium
K	Zirconium	Y	Antimony
L	Lithium	Z	Zinc
M	Manganese		

2.1.1.1 Alloying with Aluminium

Aluminium is one of the most important alloying elements in magnesium, and it is also the main alloying element used in this work. Aluminium has high solid solubility in magnesium; the solubility limit of aluminium at eutectic temperature of 437 °C is 11.7 at.% (12.9 wt.%) [11]. Figure 2.1 shows the binary magnesium-aluminium phase diagram [12]. The decreasing solubility from eutectic temperature makes the alloy heat-treatable. The aluminium concentration can vary across a grain or dendrite cell due to microsegregation during solidification. Magnesium near the centre of the grain solidifies first and it has the lowest dissolved aluminium content, while magnesium in the region adjacent to the β-phase will solidify last, and thus, it has higher dissolved aluminium. This results in strong aluminium-rich coring as shown in Figure 2.2 [13]. In die-cast AZ91, the aluminium content in the primary α-Mg has been reported to be approximately 4 wt.% in the centre of the cell and over 11 wt.% in the supersaturated region surrounding the β-phase as measured by SEM and EDX [14].

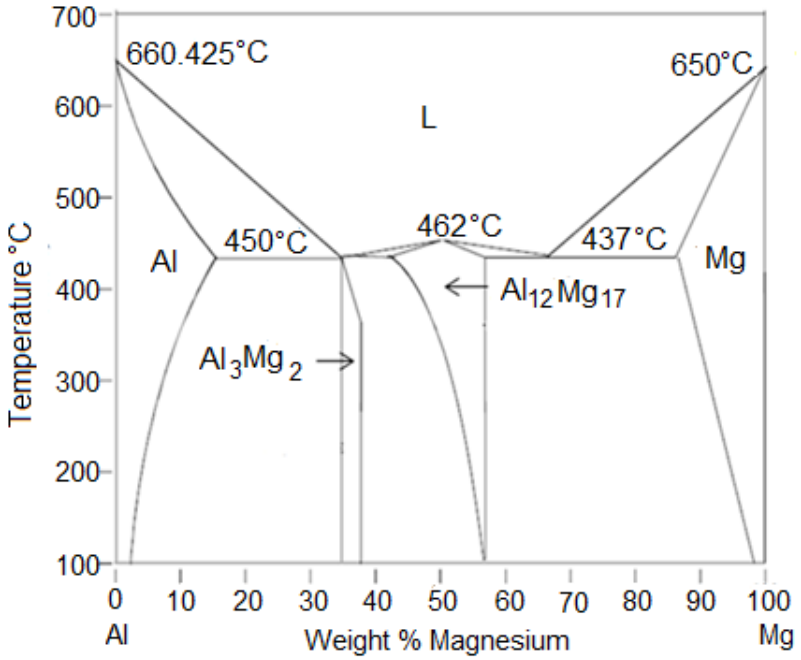

Figure 2.1: Magnesium-aluminium binary phase diagram [12].

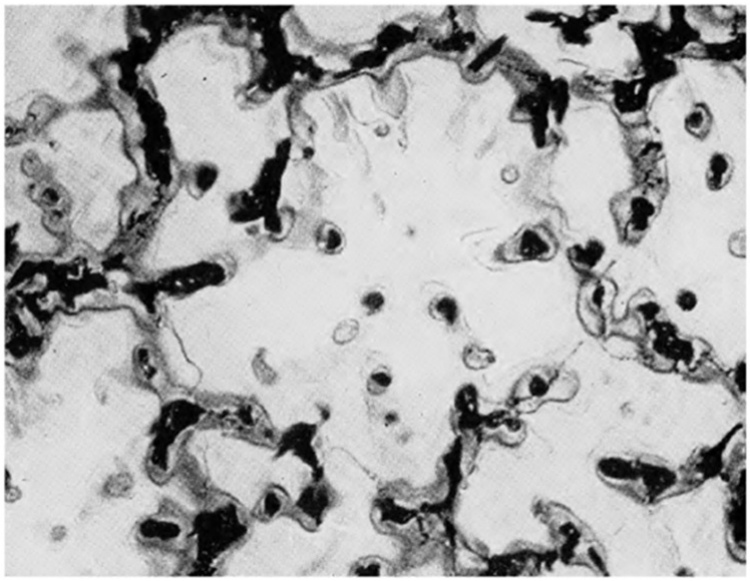

Figure 2.2: Microstructure of chill cast A8 (Mg-8%, Al-0.5%, Zn-0.25% Mn). Note β-$Mg_{17}Al_{12}$ compound (dark) and interdendritic aluminium-rich coring (grey). Electrolytic polish (x250) [13].

Two typical phases are observed in the die-cast microstructure of magnesium-aluminium based alloys, which are the primary α-Mg phase and β-$Mg_{17}Al_{12}$ phase as shown in Figure 2.3. The addition of aluminium in magnesium alloys serves principally as a solid solution strengthening element to further improve the strength [15]. However, the amount of aluminium in magnesium can affect both the die-casting process and mechanical properties. Increasing aluminium content expands the freezing range of the alloy, making the alloy more castable [16], but this can also lead to hot tearing [17] and decreased tendency for die soldering [18]. In terms of mechanical properties, high aluminium content leads to the formation of more brittle intermetallic $Mg_{17}Al_{12}$ phase, increasing the hardness and strength but reducing the ductility [19].

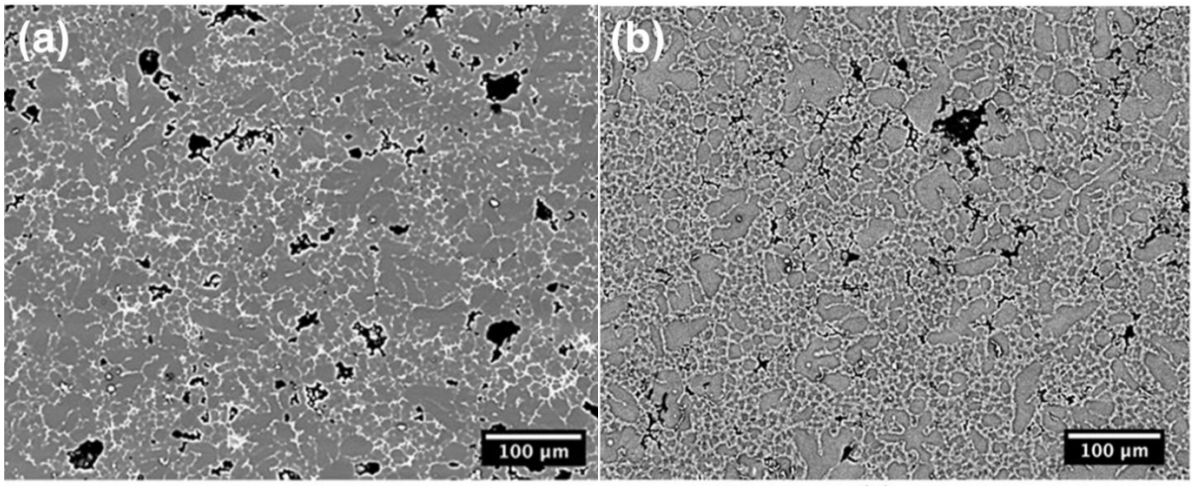

Figure 2.3: Backscattered SEM images of as-cast (a) AZ91 and (b) AM60. Note primary α-Mg phase (dark) and brittle β-$Mg_{17}Al_{12}$ phase (light) [20]. There is a higher volume fraction of bulk $Mg_{17}Al_{12}$ phase in AZ91 due to higher aluminium content.

In die-cast magnesium-aluminium binary alloys with aluminium content varying from 2-18 wt.%, the yield strength of the alloy increased (from 87 to 240 MPa) while elongation to failure decreased (from 19% to 0.7%) with increasing aluminium concentration [21]. A theoretical model accounting for Hall-Petch (strengthening due to grain refinement in die-cast alloys), solid solution and dispersion strengthening mechanisms was established to calculate the yield strength, σ_y of die-cast magnesium-aluminium binary alloys (0.5-12 mass% Al) [22]:

$$\sigma_y=\sigma_{ss}+\sigma_{disp}+\sigma_{hp} \tag{2.1}$$

where solid solution σ_{ss}, dispersion σ_{disp}, and grain boundary σ_{hp} strengthening are defined by Eqs. (2.2) to (2.4):

$$\sigma_{ss} \cong BC^{\frac{2}{3}} \tag{2.2}$$

$$\sigma_{disp} = 135\, f_i \tag{2.3}$$

$$\sigma_{hp} = \sigma_0+kd^{\frac{1}{2}} \tag{2.4}$$

where B = 197.5 MPa, C is either c_{ss} (average solute in solution in the α-Mg grains) or c_E (average solute in solution in the externally solidified grains) for calculation of the solid solution strengthening at the skin and core regions, respectively. c_E is only applicable for

aluminium concentrations above 5.5 mass%, i.e., alloys with distinct skin and core. More information on the cold chamber high-pressure die-cast microstructure can be found in Section 2.2.1.1. f_i is the volume fraction of the dispersed β-$Mg_{17}Al_{12}$ intermetallic particles, σ_0 = 12 MPa [23], k is the strengthening coefficient and d is the average grain diamater.

The theoretical model (Eq. 2.1) [22] showed good prediction for dilute alloys but underestimated the yield strength of most concentrated alloys. This was proposed to be due to the increase in the degree of spatial interconnection of the β-phase intermetallics [24-26] with increasing aluminium concentration. Profuse spatial interconnection can introduce an additional strengthening (4-7 MPa in AZ91 [24]) to the overall strength of the alloy.

2.1.1.2 Alloying with Rare Earth

Rare earths are generally added as mischmetals of various compositions, most commonly rich in cerium (Ce) (52-55 wt.%), followed by lanthanum (La) (23-25wt.%), with smaller amounts of neodymium (Nd) (16-20 wt.%) and sometimes praseodymium (Pr) (5-6 wt.%) [27, 28]. Magnesium-aluminium-rare earth alloys, such as the AE series were first developed by Hydro Magnesium [29] for applications at elevated temperatures [30]. Alloying magnesium-aluminium based alloys with rare earth suppresses the formation of brittle $Mg_{17}Al_{12}$ phase that has poor thermal stability at elevated temperatures as rare earth elements form eutectic systems of limited solubility with magnesium [31]. Therefore, rare earth atoms react with aluminium atoms to form Al-RE intermetallic phases, leaving fewer aluminium atoms to react with magnesium atoms to form the $Mg_{17}Al_{12}$ phase during solidification. The Al-RE intermetallic phases, (i.e. $A1_{11}RE_3$ and $A1_2RE$) are harder and more thermally stable [32].

Apart from improving the strength and creep resistance, alloying magnesium with rare earth elements can improve the ductility of magnesium alloys [33]. For example, alloying additions of rare earth elements to wrought magnesium-zinc sheets assisted the activation of non-basal slip systems; consequently improving room-temperature formability [33]. Bakke et al. [19] observed an increase in elongation to failure of the die-cast AE-series (Mg-Al-RE) alloys relative to the AM (Mg-Al-Mn) alloys, particularly in the 5-9 aluminium at.% range. A plot of elongation to failure against 0.2% proof stress is shown in Figure 2.4. It is apparent that the Mg-Al based alloys forming a reference line with lower elongation to failure at

higher strengths. In contrast, AE-series alloys showed a better combination of elongation to failure and strength.

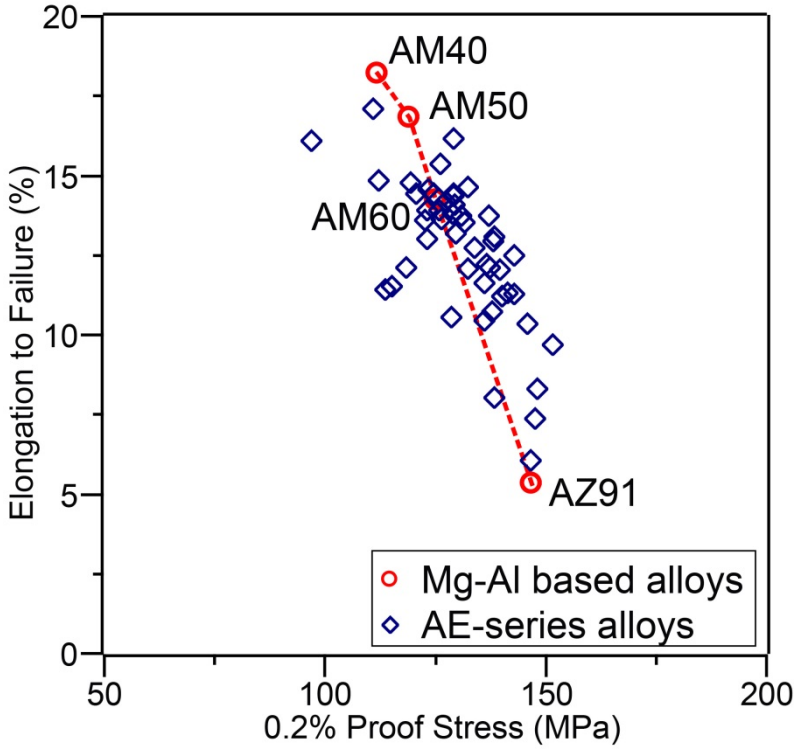

Figure 2.4: Elongation to failure and 0.2% proof stress of magnesium-aluminium based alloys and AE-series alloys [34].

In the past, AE-series alloys were mainly considered for powertrain applications [32], but are now being considered for structural applications, such as automotive front engine crossmember, engine block and auto-body structure [28, 35, 36]. AE-series alloys are composed of primary grains of α-Mg solid solution surrounded by the high volume of intermetallic phases distributed along the grain boundary area [27, 28, 37-44]. The typical microstructure of AE44 consists of a rod-like lamellar phase and polygon/particulate phase as shown in Figure 2.5. EDX analyses from various sources [28, 37, 39, 40, 44-47] have suggested the lamellar phase to be $Al_{11}RE_3$ phase and the particulate phase to be Al_2RE, where RE denotes the type of RE element present.

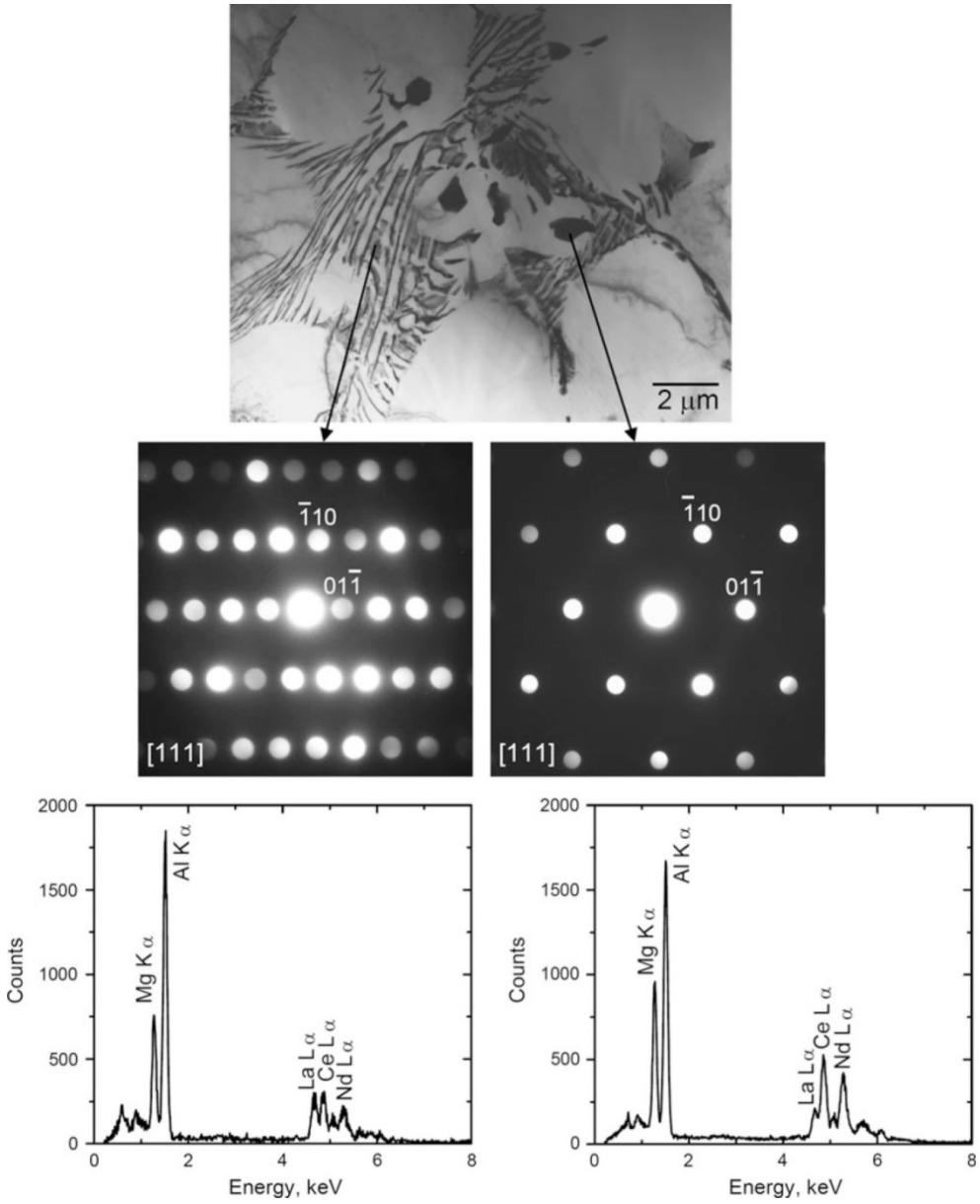

Figure 2.5: TEM bright-field image, microbeam electron diffractions, and EDX spectra showing typical microstructure and identification of intermetallic phases in as-cast AE44. The lamellar-like intermetallic phase was identified to be $Al_{11}RE_3$ (body-centred orthorhombic structure) whereas the particulate-shaped intermetallic phase is Al_2RE (diamond cubic structure) [32].

2.1.2 Deformation Modes in Magnesium

Magnesium solidifies to a hexagonal close-packed (HCP) crystal structure, Figure 2.6, with lattice parameters of a = 0.3209 nm and c = 0.5211 nm (c/a = 1.624, compared to that of an ideal HCP structure 1.633 for perfectly hard spheres), making magnesium nearly perfectly

close-packed [1, 3, 48]. For binary alloys, alloying addition of aluminium decreases the a and c lattice parameters, and increases the c/a ratio [49]. This is expected as the reported atomic bond length of aluminium (≈ 286 pm) is less than that of magnesium (≈ 320 pm) [50]. The magnesium lattice parameters with binary addition of rare earth elements, such as cerium (Ce) and lanthanum (La) have not been reported probably due to their low solid solubility in magnesium matrix (0.23 wt.% for La and 0.74 wt.% for Ce [51]), but the lattice parameters would be expected to increase due to the increase in the atomic bond length (≈394 pm and ≈374 pm for Ce and La, respectively)[50].

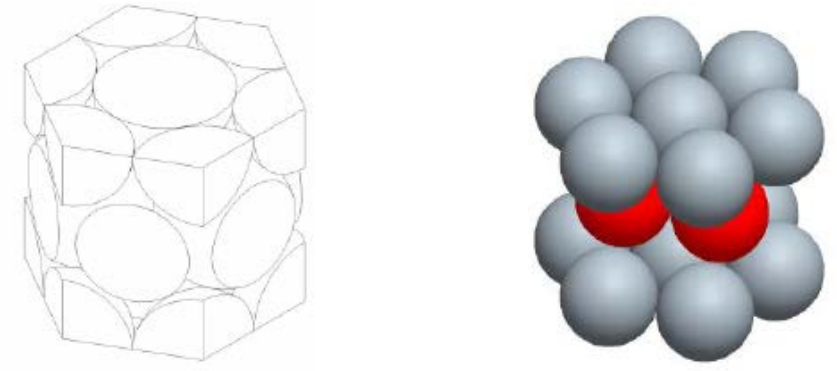

Figure 2.6: Unit cell of hexagonal closed-packed crystal [52].

2.1.2.1 Dislocation Slip

In magnesium, two main types of dislocations are observed, <a> type and <c+a> type. The <a> type dislocations have a Burgers vector of **b** = $\frac{1}{3}$ <11$\bar{2}$0> and can glide on basal, prismatic, or first order pyramidal planes while the <c+a> type dislocations have a Burgers vector of **b** = $\frac{1}{3}$ <11$\bar{2}$3> and glide on second order pyramidal planes [48, 52-58]. The commonly observed slip systems in magnesium and their corresponding slip planes and directions are shown in Figure 2.7.

Requirement of five independent slip systems is necessary to sustain a general homogeneous deformation without generation of cracks or change in volume; this is known as the von Mises-Taylor criterion [59-61]. However, prismatic slip [56, 62], first order pyramidal slip [58] and second order pyramidal slip [63, 64] are not favoured as their critical resolved shear stress (CRSS) at room temperature is several orders of magnitude greater than

that of basal slip [65]. These non-basal dislocations are also easier to activate at higher temperatures. The CRSS for prismatic slip decreases from ~110 MPa at room temperature to ~12 MPa at 270 °C [66], while the CRSS for pyramidal slip also decreases to approximately 3.9 MPa at 330 °C for polycrystalline Mg [67]. It has been reported that the improved ductility and formability at higher temperatures for magnesium is the result of activation of these higher order non-basal slip systems [66, 68].

Hence, it is generally agreed that the main deformation mode at room temperature in magnesium and its alloys is basal slip [69-72] due to its low CRSS. However, basal slip offers only three slip systems, of which two are independent, and this is less than the required five [73]. The limited number of independent basal slip systems in magnesium results in the activation of twinning to accommodate plastic deformation [64, 74, 75].

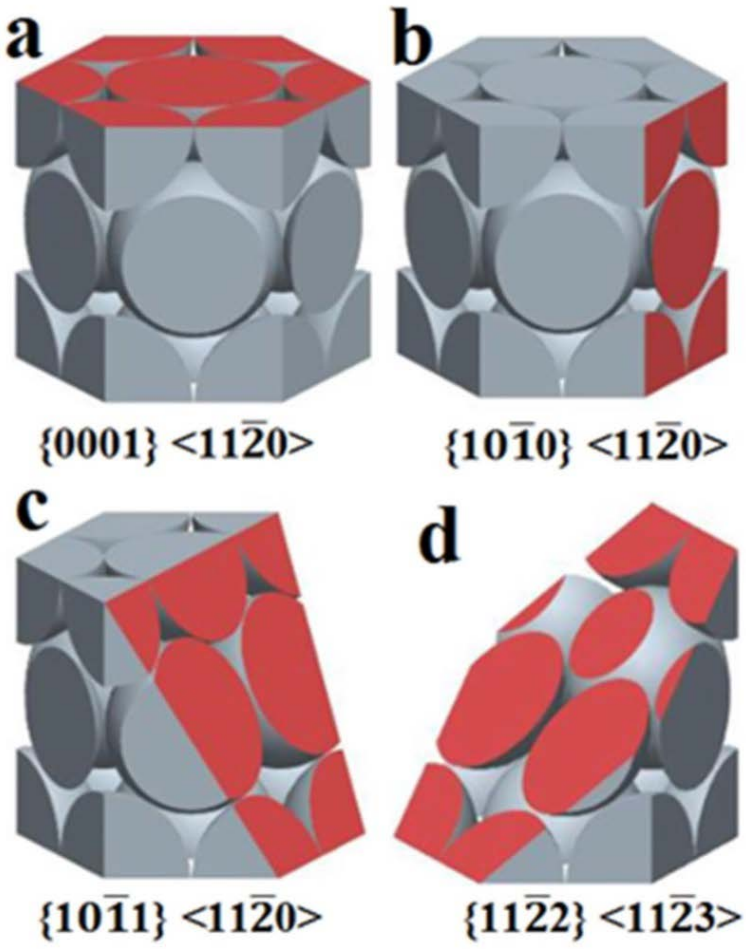

Figure 2.7: Commonly observed slip systems in magnesium: (a) basal slip, (b) prismatic slip, (c) first order pyramidal slip and (d) second order pyramidal slip [52].

The room-temperature CRSSs of the commonly observed slip and twinning mechanisms for single-crystal and polycrystal magnesium and alloys are summarised in Table 2.2. Based on the CRSSs, slip first occurs on the basal plane followed by twinning for polycrystalline magnesium. Note that the CRSSs of basal slip and twinning are less strain-rate dependent [76-80] than that of prismatic and pyramidal slip [76, 78].

Table 2.2: Critical resolved shear stresses (CRSSs) (MPa) of the commonly observed deformation modes of single-crystal and polycrystal magnesium and alloys.

Material/Method	**Basal <a>**	**{10$\bar{1}$2} Extension Twinning**	**Prismatic <a>**	**Pyramidal <a>**	**Pyramidal <c+a>**	**Ref.**
Mg single crystal	0.45-0.81		39-50	0.5		[58, 81, 82] [58] [56, 83]
Mg-0.1% Al single crystal	1		45			[72, 84]
Mg-0.25% Zn single crystal	1.2		45			[62, 72]
Mg polycrystal			110		80	[66] [85]
Mg AZ31* polycrystal EPSC model	20 10	30 30	90 55	65	95 60	[86] [87]
Mg AZ31* polycrystal VPSC model	45		110			[88]

*CRSS values obtained from single-crystal experiments and estimated for polycrystalline AZ31 using elastoplastic self-consistent (EPSC) or viscoplastic self-consistent (VPSC) models.

2.1.2.2 Twinning

Twinning occurs when an applied shear stress results in atomic displacement such that the atoms on one side of a plane (twin boundary) mirror the atoms on the other side [89, 90]. The most common type of twin in magnesium alloys is the {10$\bar{1}$2} extension twin [74], but the activation of {10$\bar{1}$1} and {10$\bar{1}$3} contraction twins and {10$\bar{1}$1}-{10$\bar{1}$2} and {10$\bar{1}$3}-{10$\bar{1}$2} double twins have also been observed [66, 71, 91-94].

{10$\bar{1}$2} extension twins have relatively low CRSS, making them the dominant deformation mode after basal slip (Table 2.2) [64, 95, 96]. They are formed when there is an extension strain component parallel to the c-axis [74], i.e., when tensile stress is applied in

the parallel direction to the c-axis. $\{10\bar{1}1\}$ and $\{10\bar{1}3\}$ contraction twins, on the other hand, can accommodate compression strain along c-axis [97], and they are activated when there is a contraction strain component parallel to this axis or when macroscopic extension is being applied perpendicular to the c-axis. $\{10\bar{1}1\}$-$\{10\bar{1}2\}$ and $\{10\bar{1}3\}$-$\{10\bar{1}2\}$ double twins are also known as secondary twins. They take place within the reoriented primary twins. Contraction twins $\{10\bar{1}1\}$ and $\{10\bar{1}3\}$ form first, after which $\{10\bar{1}2\}$ extension twins are propagated within the original contraction twins [66, 98]. Both types of double twins lead to a contraction along the c-axis.

Considering the above information and the random texture seen in cast magnesium alloys [63, 99, 100], cast samples will consist of several regions with different orientations. Each of these regions may have a favourable orientation for some type of twinning, and therefore, cast magnesium alloys may experience different types of twinning during deformation. Cast AZ31, AZ61 and AZ91 [101] and cast AE42 and AE44 (RE: Yttrium) [102] experienced different types of twinning with $\{10\bar{1}2\}$ extension twinning being the predominant twinning mode after shock loading tests at 800-1400 s^{-1}. Among these alloys, the amount of twinning was observed to decrease with increasing aluminium and yttrium content, respectively.

Electron backscattered diffraction (EBSD) characterisation is useful for determining the exact orientation of each grain in a deformed polycrystal and thus providing quantitative information on the activation of different twin systems. Profuse $\{10\bar{1}1\}$-$\{10\bar{1}2\}$ double twins (purple) were observed from EBSD mapping of polycrystalline AM30 after tensile testing, as shown in Figure 2.8 [96]. Some primary $\{10\bar{1}1\}$ contraction twins (green) were also present, but fewer in number. Only very few $\{10\bar{1}2\}$ extension twins (red) and $\{10\bar{1}3\}$-$\{10\bar{1}2\}$ double twins (blue) were observed.

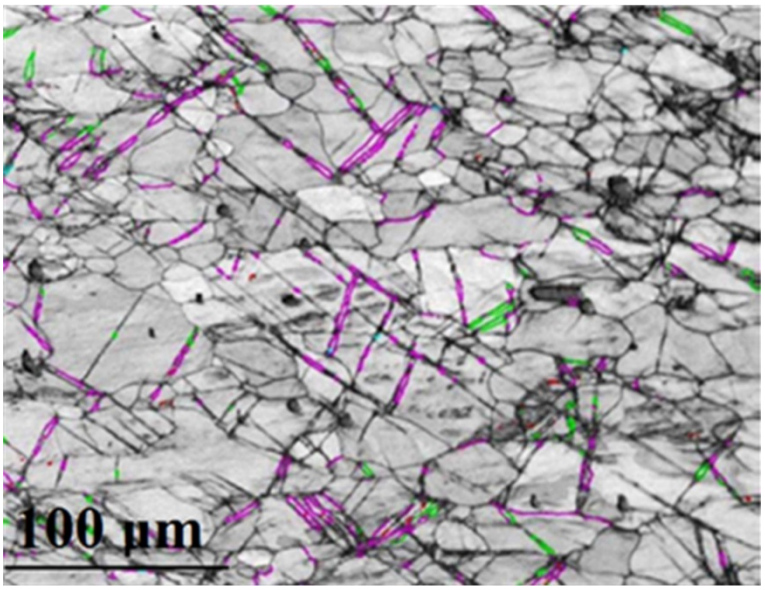

Figure 2.8: EBSD map of AM30 after 8% strain at a temperature of 100 ^{0}C and a strain rate of 0.1 s^{-1}. The tensile axis is horizontal in the map [96].

Apart from EBSD, there are other techniques to measure twins. For example, the sigmoidal shape of a stress–strain curve obtained from mechanical testing [103] and a concave behaviour of work hardening rate are indicative of the occurrence of twinning [101, 103-107]. Deformation twinning results in a sudden reorientation of the volume fraction of the crystal that is being twinned rather than the gradual reorientation that characterises slip. Therefore, due to large disorientation between the twin and the matrix, as twinning proceeds, the required stress for continuing deformation increases. Thus, twinning is associated with a high rate of strain hardening.

2.2 Manufacturing Processes

2.2.1 High-Pressure Die-Casting

High-pressure die-casting (HPDC) is a fully automatic, large volume, high productivity process for the fast production of thin-walled near net shape castings, with part weights ranging from a few grams to more than 15 kg [108, 109]. Other advantages of HPDC include the possibility to obtain fairly complex castings due to the use of movable cores; better surface finish and closer dimensional tolerances, and lower labour cost.

Presently, die-cast alloys are widely used in automotive industry. For instance, automotive components varying from instrument panel beams, steering wheel armatures and seat frames (AM60), to cam covers, clutch housings and steering wheels (AZ91), to high temperature applications such as engine cradles (AE44) have been manufactured with die-cast magnesium alloys [8].

There are two types of HPDC: hot-chamber die-casting and cold-chamber die-casting. Cold-chamber die-casting is used when the casting alloys have a high melting point and cannot be used in hot-chamber machines, for example magnesium-aluminium alloys. Hence, all the alloys involved in this study were cast using a cold-chamber high-pressure die-casting machine as shown in Figure 2.9.

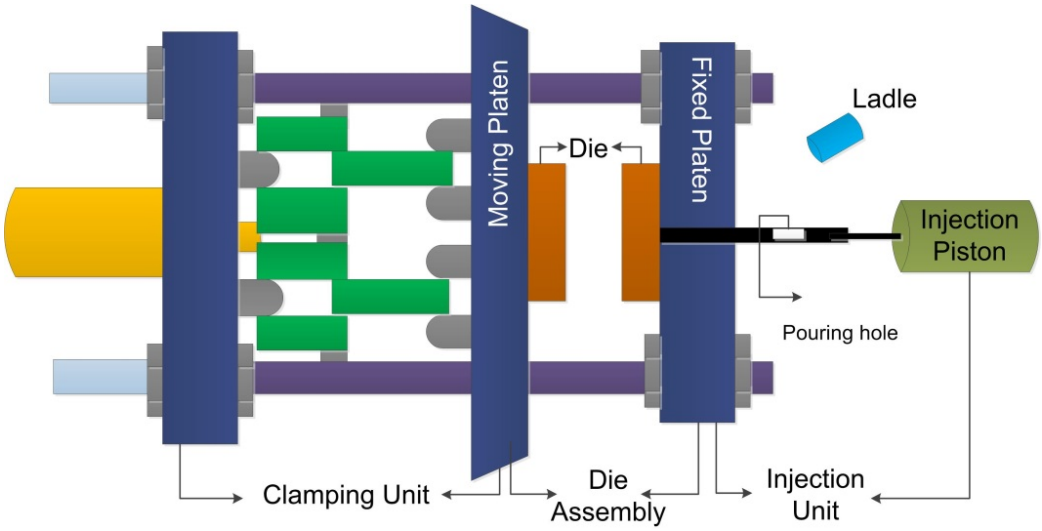

Figure 2.9: Schematic of a cold-chamber HPDC machine which consists of an injection unit, die assembly and clamping unit.

In a cold-chamber machine, molten metal is poured from the ladle into the shot chamber through a pouring hole. An injection piston, powered by hydraulic pressure, forces the molten metal through the shot chamber and into the injection sleeve in the die. The typical injection pressures for a cold-chamber die-casting machine are between 2000 and 20000 psi. After the molten metal has been injected into the die cavity, the injection piston remains forward, holding the pressure while the casting solidifies. After solidification, the hydraulic system retracts the injection piston and the part can be ejected by the clamping unit [110].

2.2.1.1 Microstructure of HPDC Magnesium Alloys

HPDC alloys consist of two well differentiated regions on the casting cross section: a surface region with predominantly fine grains and a higher volume fraction of intermetallic phases, also known as the hard skin, and a centre region (known as the soft core) with relatively larger grains together with large dendritic grains, termed externally solidified grains (ESGs), as shown in Figure 2.10 [22, 111-116].

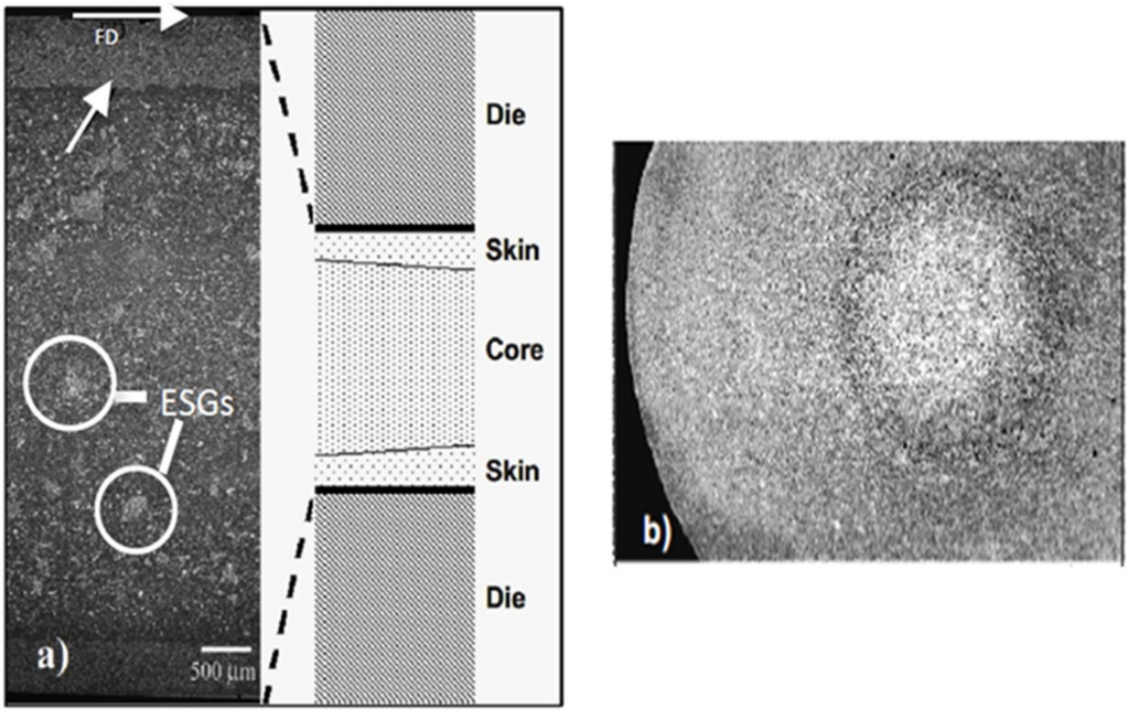

Figure 2.10: Bimodal grain microstructure of a HPDC magnesium alloy. (a) The micrograph and corresponding schematic diagram of the cross-section of a tensile bar normal to the flow direction (FD) showing ‘skin’ and ‘core’ regions and ESGs. (b) ESGs magnified [117].

The ESGs, formed by partial solidification of the melt in the unheated shot sleeve and runner [111, 118, 119], are dispersed in the liquid during the filling of the die [120-122]. The liquid inserted into the die cavity can contain up to 20% solid fraction of ESGs [113, 114]. These ESGs will then migrate to the centre of the die cavity [123] driven by shear flow [114, 121, 124, 125]. The segregation of ESGs towards the centre also ensures that the volume fraction of eutectic is greater near the surface [113].

The difference in grain size between the skin and the core regions leads to non-uniform yielding. Yielding tends to develop first in the softer core while the harder outer skin layer

remains elastic [113]. Non-uniform yielding in the alloy may lead to inconsistency in proof stress measurement. It should be noted, however, that die casting technology is continually improving and these variations are arguably less significant in modern machines.

2.2.1.2 Casting Defects

A few commonly observed casting defects include banded defects, hot tears and porosity. These defects can adversely affect the mechanical properties. Defect bands often appear as narrow regions of positive macro segregation, porosity and/or cracks that follow the contour parallel to the surface of the casting [126-128]. Due to the macroscopic nature of these defects, they cannot be removed during heat treatment and the form they take during solidification remains in the cast product [129]. Examples of defect bands are shown in Figure 2.11. The flow direction is to the right, parallel to the page. Reducing shot sleeve solidification and increasing die and melt temperature can minimize the formation and severity of banded defects [126].

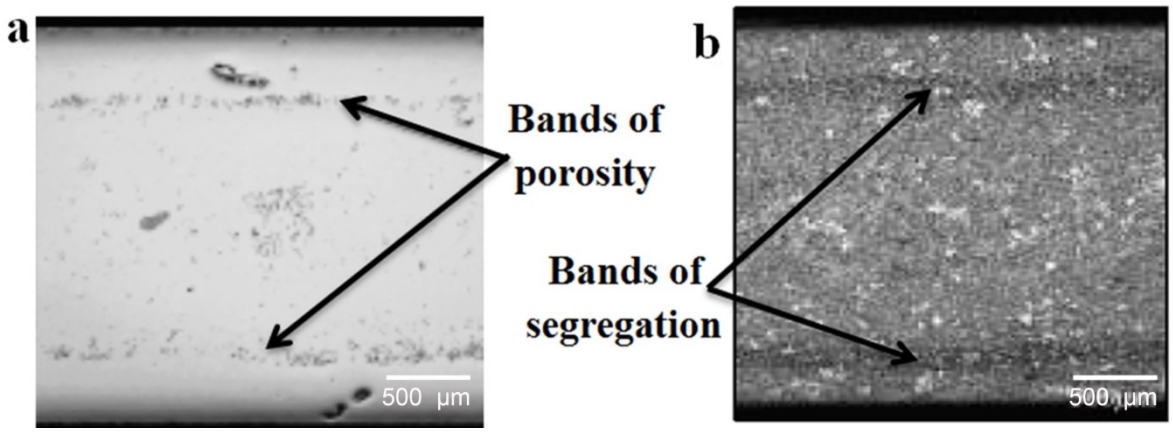

Figure 2.11: (a) Pore bands in magnesium alloy AM60 [121]. (b) Segregation bands in aluminium alloy A356 [130].

Hot tearing or hot cracking is a major defect that can form during casting when the alloy is still in a semi-solid state. Campbell [131] proposed that hot tearing was predominantly controlled by the presence of double oxide films (bifilms) forming during casting. Bifilms are created when a dry film on the surface of the melt is folded and becomes entrained within the melt. Since the folded faces do not bond, and thus form a defect within the casting that can promote crack formation.

Whilst bifilms may act as cracks to tear initiation sites, the alloy content is just as important. It is known that hot tearing susceptibility varies with alloy content through a lambda-curve relationship [132] in most alloy systems, i.e., binary magnesium-aluminium alloys [133, 134]. At low alloy concentrations, the hot-tearing propensity is small; as the alloy content increases, it peaks, and then reduces again at higher concentrations. This behaviour has been attributed to the non-equilibrium solidification range [17], eutectic content [135], solidification paths and phase fractions [136]. For binary magnesium-aluminium alloys (up to 8 wt.% aluminium) by ring casting in a steel mould, hot tearing susceptibility peaks at 0.75 wt.% aluminium [134]. Commercial alloy AZ91 with high aluminium content is known to be relatively resistant to hot tearing [136, 137].

Casting porosity, i.e., gas porosity and shrinkage porosity can be distributed throughout the microstructure of HPDC materials [109]. Porosity leads to significant variability in the fracture sensitive mechanical properties such as ductility [138, 139]. Lee et al. [140] used quantitative fractographic techniques and observed that the amount of porosity present in the fracture surfaces of HPDC AE44 was significantly higher than the average volume fraction of porosity in the bulk three-dimensional microstructure. They believed that the fracture path would preferentially go through the regions of the specimens containing large amounts of localised (clustered) porosity. Hence, ductility could be increased by decreasing the regions of localised clustered pores in the microstructure. This may not necessarily require decreasing the global average volume fraction of the pores in the three-dimensional microstructure as cracks tend to initiate at contraction cavities [141, 142], and propagate by the coalescence of smaller cracks [143].

Porosity can also interfere with subsequent heat treatments performed on the alloy following casting. Due to porosity, HPDC alloys are generally non-heat-treatable because the trapped gas pores can expand during the heat treatment process, causing surface blistering and bulk distortion of cast products [52].

2.2.2 Self-Piercing Riveting

There is an increasing interest in the use of die-cast magnesium alloys in auto-body structure to reduce the weight of vehicle. Vehicle body is usually composed of different lightweight alloys, and hybrid use of these alloys, such as magnesium with aluminium alloys [144] or aluminium with advanced high strength steel [145] can sometimes be difficult or impossible to weld due to differences in thermal, physical and chemical properties.

Self-piercing riveting (SPR) is a cold forming process that is used to fasten together two or more sheets of materials by driving a rivet through the upper sheet and upsetting the rivet in the lower sheet without penetration into the lower sheet. Joining is achieved by rivet locking into the lower sheet. Since the process relies on a mechanical interlock rather than fusion, it can be used with dissimilar materials. Examples are combinations of aluminium alloy A5052 to steel (mild and ultra-high strength steels) [146, 147], to titanium and copper alloy [148], and even to low ductility magnesium alloy AZ31B [144].

SPR was successfully adopted by Audi to join structural panels in the all-aluminium Audi A8 in the 90s [149]. Since then, a significant progression has been the application of SPR technique to both space frame (Audi A2) [150] and monocoque designs (Jaguar) [151, 152].

SPR process can be divided into a few stages as illustrated in Figure 2.12 [153-155]:

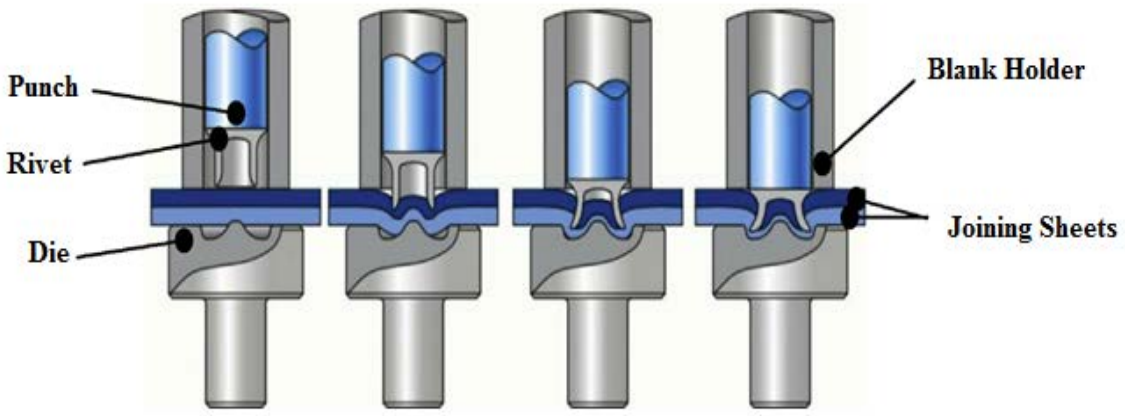

Figure 2.12: Self-piercing riveting process [156].

1) *Clamping and/or Bending:* The sheets to be joined are first clamped together between a blank holder and a die. In some cases, pre-clamping is not involved and sheets bend as rivet being pushed by a punch perpendicularly to the sheet surface. The punch is driven down using either a hydraulic or electrical system. In this phase the rivet clamps the sheets.
2) *Piercing:* The rivet shank acts as a shearing punch that pierces into the entire thickness of the top sheet. The lower sheet is pierced only partially until the rivet reacts against the influence of the die.
3) *Flaring:* The rivet flares into the die and forms a mechanical interlock between the substrates. The lower sheet undergoes plastic deformation and flows into the die cavity

due to the large applied force. The lower sheet conforms to the shape of the cavity, forming a buttonhole at the bottom.

4) *Compressing and Releasing:* The punch continues the stroke, pushing the rivet inside the sheet metals further. The punch stops when it reaches a predetermined force or stroke and then the punch slowly releases.

One of the important factors of SPR is the riveting velocity, which is related to the strain rate of the sheets being joined, has a significant effect on the joint quality. Depending on the SPR equipment, the maximum riveting velocity can range from ≈ 110 mm/s to 400 mm/s [157]. Considering the large variation in rivet length, the strain rate experienced by the sheets can range from 10^{-3}-10^{1} s^{-1} [158], or lower and higher. Riveting velocity may also vary during rivet insertion due to material resistance to deformation. Besides, the punch stops and retracts at the end of riveting is another indication that strain rate during riveting is not constant. Therefore, understanding the strain-rate sensitivity of the parts to be joined can provide insights into the deformation during riveting.

2.2.2.1 Applicability of SPR to Magnesium Alloys

SPR involves large and highly localised plastic deformation [159] that can lead to cracking, especially, in the material used as the lower sheet in the joint. This is particularly the case for magnesium alloys. Cracking of magnesium sheet during SPR is due to the poor room-temperature ductility of magnesium [157], which is mainly attributed to a lack of independent basal slip systems in HCP crystal structure [160]. The ductility of die-cast alloys is also lower than that of wrought alloys at room temperature. Therefore, most studies have focused on SPR of wrought magnesium alloys [144, 158, 161-163]; SPR of die-cast magnesium alloys is sparsely reported [164, 165].

In the riveting of extruded aluminium alloy 6063 (upper) to die-cast magnesium alloy AM50 (lower) as shown in Figure 2.13 (a), cracking of lower magnesium sheet was observed after riveting which may lead to subsequent failure under loading [164]. When similar rivet and die configurations were applied to aluminium alloy 5754 (upper) to join wrought magnesium alloy AZ31B (lower), no crack was found in the joint (Figure 2.13 (b)) [164], probably due to higher ductility of wrought AZ31B compared to die-cast AM50.

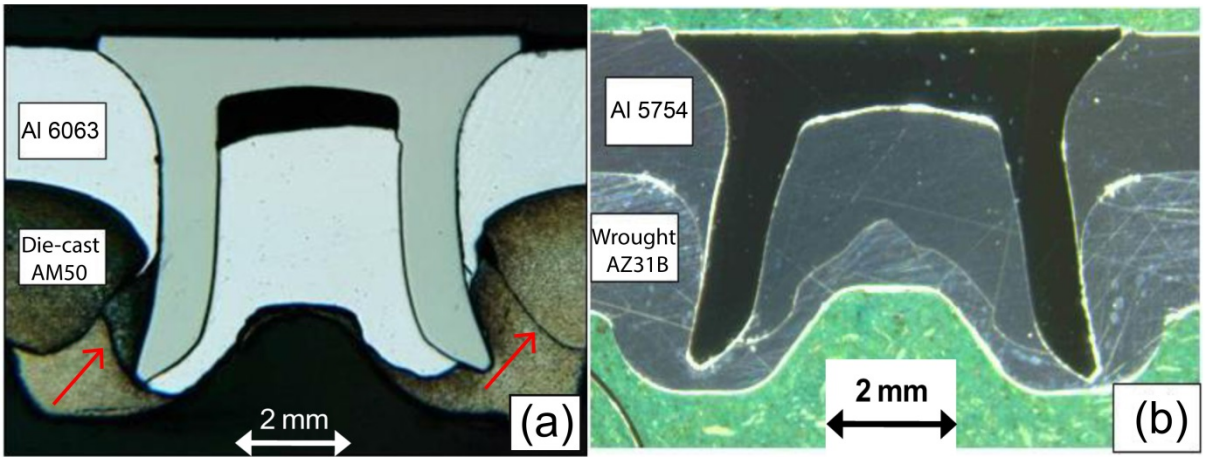

Figure 2.13: Cross-section view of (a) upper extruded aluminium alloy 6063 to lower die-cast magnesium alloy AM50 where cracking is observed on AM50 sheet after riveting and (b) upper wrought aluminium alloy 5754 to lower wrought magnesium alloy AZ31B and no crack is found [164].

To improve the riveting ability of magnesium alloys, preheating them before riveting is an option to increase the plasticity through activation of additional slip systems in the HCP structure [158, 161, 166]. However, machine tools that can quickly deliver the right temperature conditions to achieve heating without increasing the SPR cycle time are rare. Thus, laser beam has been proposed as an add-on machine tool with minimal modification to existing SPR equipment [162]. Lasers have been used to preheat AZ31B-H24 magnesium alloy strips to different temperatures and crack-free joints are achieved when strips are preheated to temperatures above 200 °C before rivet insertion [162]. However, this two-step process increases process complexity and cost, especially when laser heating is used. Therefore, conventional SPR without laser assistance is still preferred in an industrial environment.

Another attempt to improve SPR joining of magnesium alloys was proposed by combining the joining mechanisms of friction stir spot welding and SPR [144, 167, 168], allowing the rivet to rotate at high speed, thus increasing the friction heat to soften the magnesium alloys being joined during the riveting process. This F-SPR process is able to improve the riveting ability of magnesium alloy AZ31B, as compared to the traditional SPR process [144].

2.3 Deformation Behaviour

Materials deformation behaviour, commonly seen in the form of stress-strain curve, is an important graphical measure of a material's mechanical properties. Unlike steel and aluminium which exhibit only elasticity and plasticity, the deformation behaviour of magnesium can be separated into three stages: elastic, anelastic and plastic [169-173] as shown in Figure 2.14.

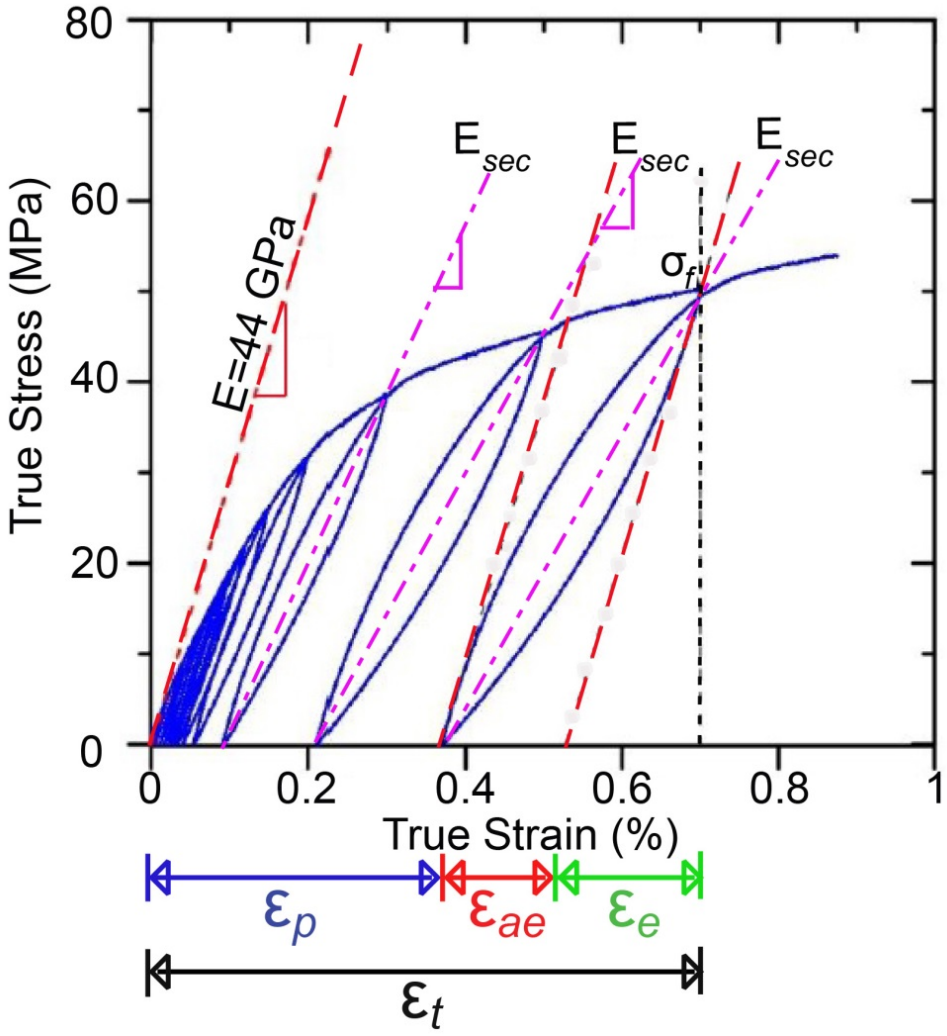

Figure 2.14: An overview of the cyclic tension loading-unloading stress-strain curve of pure magnesium where the total strain (ε_t) can be separated into elastic strain (ε_e), anelastic strain (ε_{ae}) and plastic strain (ε_p). E is the elastic modulus (44 GPa); E_{sec} is the secant elastic modulus, and σ_f is the flow stress at the start of the unloading [172].

2.3.1 Elasticity

The elastic response of magnesium under stress can be described by a linear relationship (Hooke's Law) between the individual stresses and the corresponding strains, where the elastic modulus is measured. The elastic modulus in magnesium and alloys may vary between 44 and 46 GPa [174, 175] depending on grain size and solute content. Hence, the nominal elastic modulus for magnesium and its alloys is commonly taken as 45 GPa [3] as an estimate. During elastic deformation, internal (elastic) strain develops linearly in all grains driven by stretching of atomic bonds, differing only by the elastic anisotropy, which in magnesium is minor [87, 176]. The linear elastic region has been observed to extend up to only ~ 25 MPa for pure magnesium [170, 176] and 40-50 MPa for alloys [171, 177]. The relatively small linear elastic region further complicates the elastic modulus determination, and results in a wide range of measured proof stress values for the same alloy as shown in Table 2.3.

Table 2.3: Comparison of proof stress obtained by conventional 0.2% offset method based on ISO 6892-1 [178] and ASTM E8M-09 [179] for HPDC magnesium alloys reported in literature.

HPDC Magnesium Alloy	0.2% Proof Stress (MPa)	References
AM40	108*-120	[42]
Mg-4Al-1La	110*-133	
Mg-4Al-2La	113*-140	
Mg-4Al-4La	128*-155	
Mg-4Al-1Ce	129*-146	[39]
Mg-4Al-4(Ce/La)	132*-160	[44]
AE44 (RE=Ce-rich mischmetal)	127*-140	[47]
AM60	125-127*	[180]
AZ91D	150-154*	[181]

* Unpublished data taken from Magontec [34].

2.3.2 Anelasticity

Past the linear elastic region, the internal strains begin to diverge from linear elastic loading when grains with a favourable orientation to the stress axis (soft-oriented grains) undergo plastic deformation by basal slip while those with harder orientations undergo

twinning [182]. This often results in non-linearity at low strains even before significant plastic deformation has occurred.

Extensive $\{10\bar{1}2\}$ $<10\bar{1}1>$ twinning in this region leads immediately to anelasticity, also commonly known as pseudo-elasticity. The $\{10\bar{1}2\}$ extension twinning results in an 86.3^0 reorientation of the basal pole [66, 93]. Because of this nearly 90^0 reorientation, de-twining occurs in the twinned areas at subsequent reversed loading [94, 183]. During loading, the positions of twins in the deformed state are not stable [184], and a driving force (provided by the tensile stresses in grains which have just experienced twinning) can cause the twins to return to their original positions during unloading [185]. *In-situ* neutron diffraction studies on pure magnesium and magnesium-7.7 at.% aluminium alloy [186] and magnesium-8.5 wt.% aluminium alloy [187] confirmed that partial reversion of $\{10\bar{1}2\}$ twins is the main cause for anelasticity in magnesium and its alloys. Figure 2.15 illustrates the partial reversal of twins in pure magnesium, when the specimens were under load and subsequently unloaded [170].

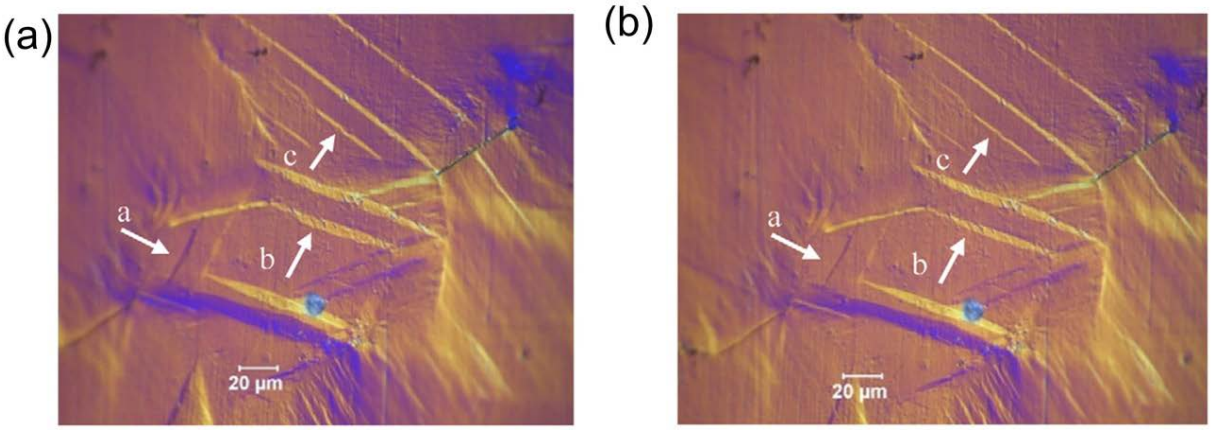

Figure 2.15: Pure magnesium (a) loaded and (b) unloaded. The arrows indicate twins that become thinner upon unloading [170].

This reversible movement of twin boundaries results in large hysteresis loops (Figure 2.14) and the amount of anelasticity is determined from the width of the loop. The closed loop indicates that some energy, in addition to the plastic strain energy, has been introduced into the material (closed loop area) when the external force has been removed [169]. This is believed to be the stacking fault energy due to twinning during deformation.

Similar anelastic behaviour in the form of hysteresis loops has also been observed in sand-cast pure magnesium and magnesium-zinc alloys [170], magnesium-aluminium alloys [188], die-cast AZ91 [171], AM60 and AE44 [169], zirconium [189], and also in other HCP

metals [190] cycled in tension or compression after being plastically deformed. This anelastic behaviour is essentially similar to the superelastic behaviour in shape memory alloys, where it is however, due to stress-induced martensitic transformations [191-193].

Hysteresis loop testing on iron, aluminium, titanium, zinc and magnesium [194] showed that the width of the hysteresis loops (magnitude of anelasticity) differed markedly with the type of metal (Figure 2.16). The loops appeared to be very narrow for iron (body-centred cubic, BCC) and aluminium (face-centred cubic, FCC) that deform mainly by dislocation, whereas they were wider for HCP metals like magnesium that readily undergo mechanical twinning. This further corroborates the idea that twinning and not dislocation is responsible for the hysteresis loops.

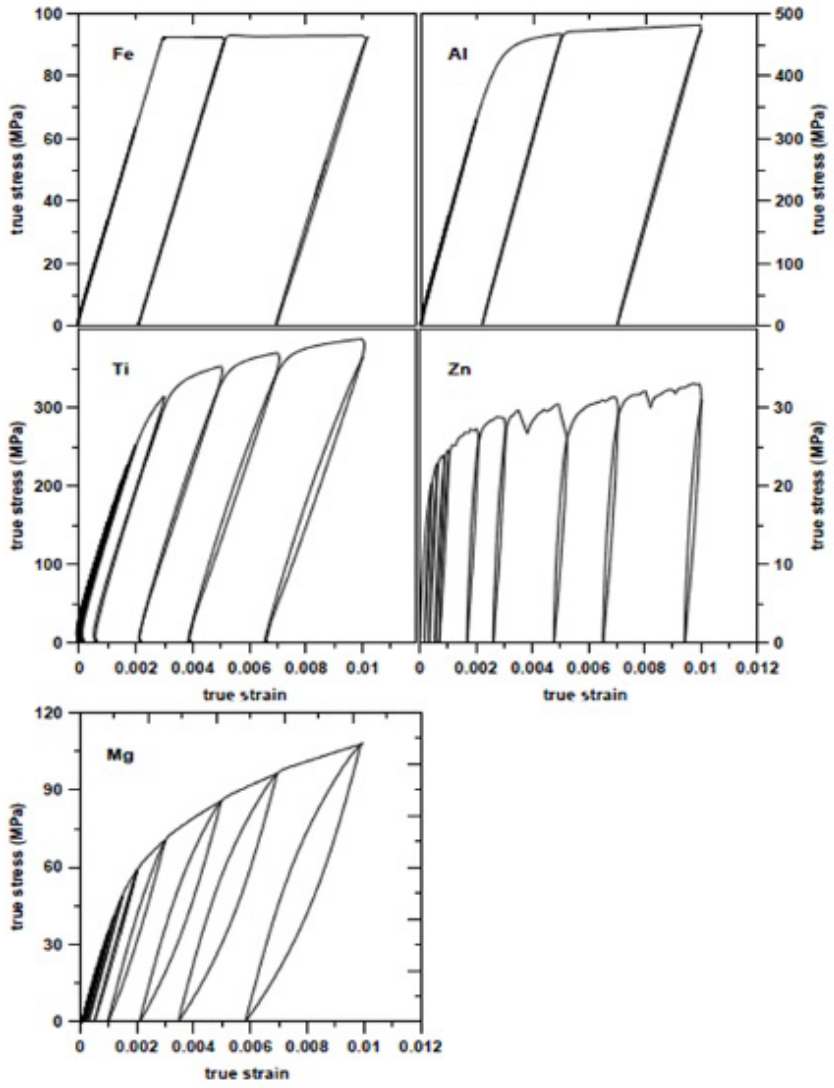

Figure 2.16: Stress-strain hysteresis loops for Fe, Al, Ti, Zn and Mg cycled in tension [194].

As oberved in Figure 2.14, a series of secant moduli, E_{sec}, can be defined. As plastic pre-strain or applied stress amplitude increases, the loop width increases and grows to a maximum after 1–2% plastic strain, becoming slightly narrower afterwards [169-171]. The levelling-off of the hysteresis loop size after a plastic strain of about 1-2% has been ascribed to the combination of two factors [189]: (i) exhaustion of the numbers of twin nuclei; (ii) decreased mobility of the twin boundaries due to increased dislocation activity.

E_{sec} decreases with increasing loop width. E_{sec} decreases to around 60% for die-cast AE44 and AZ91 [169, 171], 53% for sand-cast AZ91 [171], 50% for sand-cast Mg-2Zn and Mg-6Zn [170], of the nominal elastic modulus of magnesium alloys (E=45 GPa) [174]. E_{sec} increases again after 1-2% plastic strain as the loop gets narrower.

The stronger material will show a smaller decrease in E_{sec} [170, 171]. For instance, there was a smaller decrease in E_{sec} in small-grained die-cast AZ91 than large-grained sand-cast AZ91 [171] and a smaller decrease in E_{sec} in alloys compared to pure magnesium [170] when E_{sec} was plotted as a function of applied plastic strain.

The development of anelastic strain when a material is plastically deformed creates a problem to engineers trying to base design on a constant value of elastic modulus. If the anelastic effect is large, conventional formulae relating stress and strain become invalid, as the material may show enhanced damping due to the inherent hysteresis in elastic range. Choosing an appropriate offset strain for proof stress measurement becomes difficult as the transition from elastic to plastic becomes indistinct in the presence of anelasticity. It is, therefore, important to understand the factors that affect the anelastic behaviour of magnesium and its alloys.

2.3.2.1 Effect of Loading Direction

Anelasticity is less affected by loading direction in cast alloys. This is because cast magnesium alloys have random texture and the orientation of grains is relatively random [63, 99, 100, 195]. The amount of anisotropy observed in cast magnesium alloys is very small, and cast alloys are sometimes considered isotropic [196-198]. There was no difference in anelastic strain and E_{sec} in HPDC AE44 cycled in compression and tension [169]. There was only a slight increase in anelastic strain in compression samples as compared to tension samples for sand-cast magnesium-zinc alloys [170] and magnesium-aluminium alloys [188]. The minor difference in anelasticity is because even in a randomly-oriented polycrystalline aggregate, the fraction of grains having their c-axes favourably oriented for $\{10\bar{1}2\}$ twinning

is still smaller than the fraction favourably oriented for $\{10\bar{1}2\}$ twinning in compression [63]. Thus, the anelastic effect that depends on the activation of $\{10\bar{1}2\}$ twinnning is expected to be larger in compression.

In wrought alloys, anelastic-like hysteresis effect has been reported to be more pronounced under compression than tension due mainly to the texture effect [185, 199]. In extruded magnesium-8.5 wt.% aluminium alloy, the anelasticity in compression was almost twice that in tension at 1% plastic strain along the extrusion direction [187]. Observation from in-*situ* neutron diffraction showed that most of the grains were oriented with their c-axes (basal pole) perpendicular to extrusion axis [187]. Hence, $\{10\bar{1}2\}$ extension twinning could be easily activated under compression along the extrusion direction as a result of anisotropy.

2.3.2.2 Effect of Grain Size

Twinning is usually more difficult in the small-grained materials [77, 186]. Since anelasticity is a directly effect of twinning, as twinning becomes more difficult, anelasticity should decrease in small-grained materials. However, contrary to the expectation, smaller-grained materials appear to have larger anelasticity than large-grained [170-173, 175] as shown in Figure 2.17.

The larger anelastic effect in small-grained pure magnesium and alloys has been explained by the effect of grain size on the number and stability of twins [171]. Firstly, for a given strain in a random polycrystalline aggregate of magnesium, the total number of twin nuclei can be expected to be proportional to the number of grains favourably oriented for twinning. Secondly, the grain boundary area, where twins often nucleate, is also larger for small grain size, and this can increase the number of twins. Thirdly, the interfacial energy per unit volume of twinned material is likely to be larger for smaller twins, and small twins will require less accommodation at their ends by dislocation slip, with its concomitant stabilising effect. These effects make smaller twins less stable. Thus, for a given strain, a small grain size can be expected to result in an increased number of small and unstable twins that are more prone to revert upon unloading, magnifying the anelastic strain.

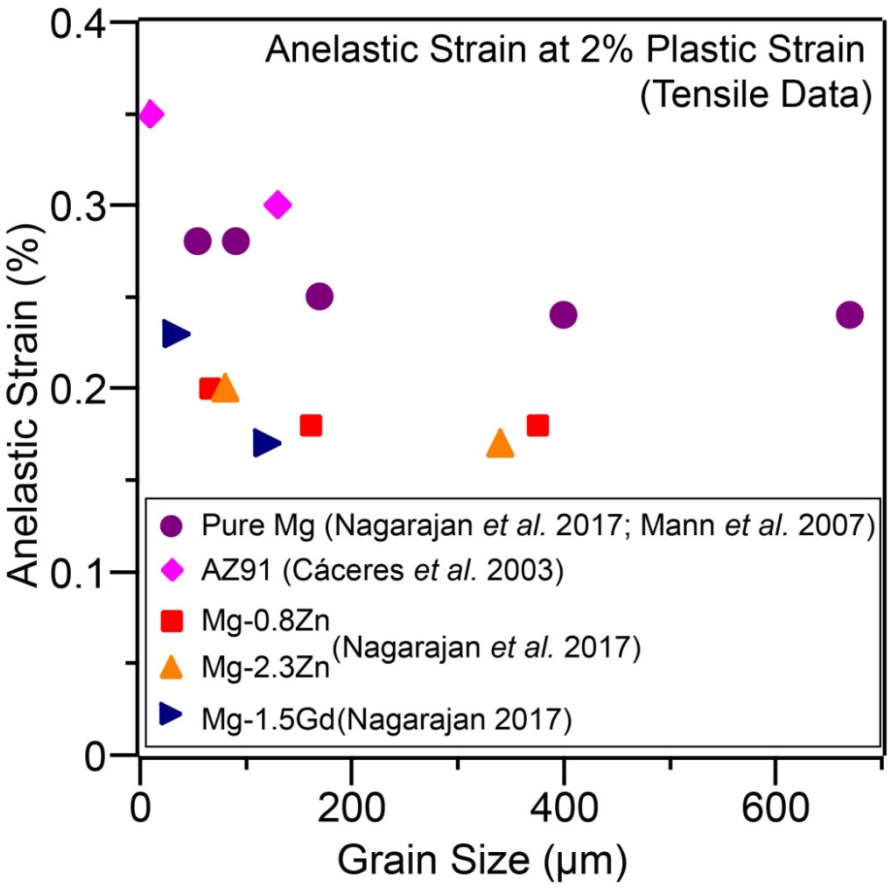

Figure 2.17: Anelastic strain (%) at 2% of plastic strain of pure magnesium [170, 172, 173], AZ91 [171], Mg-0.8Zn and Mg-2.3Zn [173] and Mg-1.5Gd [172] as a function of grain size.

2.3.2.3 Effect of Precipitates

Sand-cast AZ91 alloy that was solution heat-treated at 413 °C for 20 h (denoted as sc T4) and aged for either 16 h or 120 h at 165 °C (labelled sc T6 and sc 120 h, respectively) was compared with die-cast AZ91 alloy in different section thicknesses 1, 2, 6 mm [171]. The anelastic strain of aged sand-cast alloys, regardless of heat-treatment conditions, was significantly lower than that of the die-cast AZ91 in as-cast state as shown in Figure 2.18. But, this reduced anelasticity could also be due to larger grain size in the sand-cast alloy. The effect of precipitates due to heat treatment on anelasticity was not clearly studied.

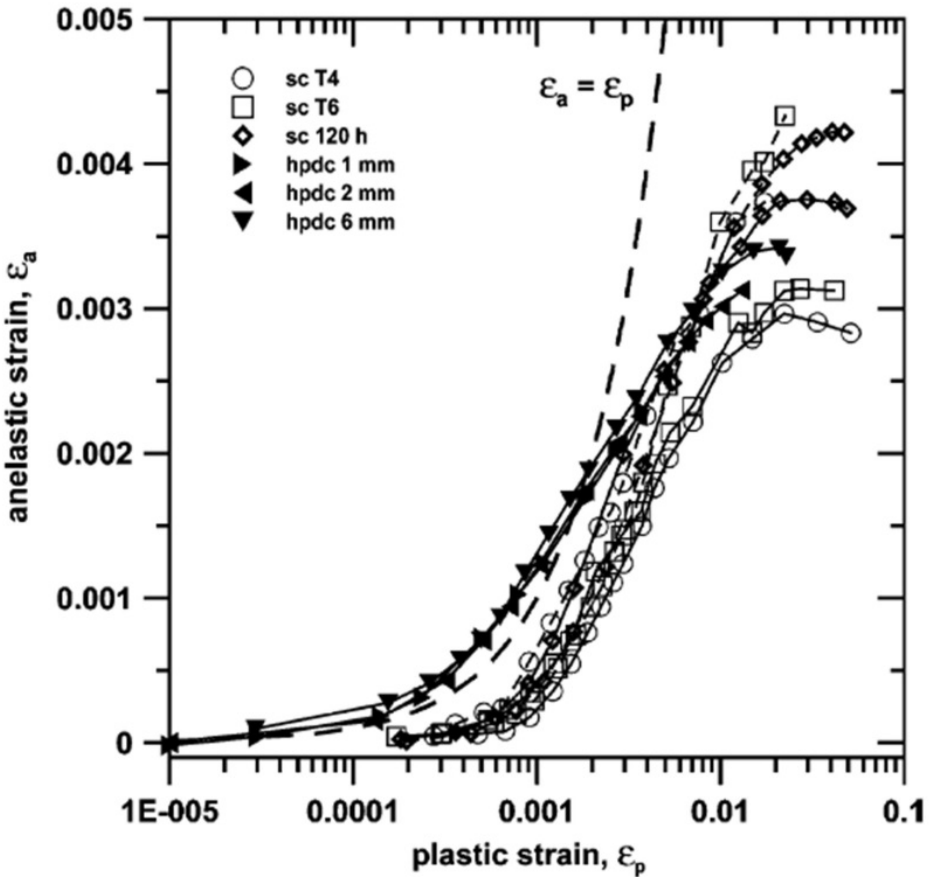

Figure 2.18: The anelastic strain as a function of the applied tensile (solid lines) or compressive (dashed lines) plastic strain, for AZ91 in two different casting conditions: sand-cast (sc) and high-pressure die-cast (hpdc) [171].

The effect of precipitates on anelasticity has not been directly studied, but precipitates have been observed to influence twinning. Precipitates have been reported to induce cross-slip on the prism planes and suppress $\{10\bar{1}2\}$ twins [200], depending also on the shape of precipitate [201].

Robson et al. [202] investigated the effect of precipitates on $\{10\bar{1}2\}$ twinning by deforming a strongly textured magnesium-5 wt.% zinc alloy in an orientation to activate $\{10\bar{1}2\}$ twinning and compared the final microstructures of the age-hardened with unaged specimens. They observed an increase in the number of $\{10\bar{1}2\}$ twins, but decrease in total twinned area fraction in the aged specimens. This suggests that presence of precipitates can suppress $\{10\bar{1}2\}$ twin growth but increase twin nucleation, leading to finer twins in aged specimens.

The $\{10\bar{1}2\}$ twin can grow laterally and consume entire grains in a precipitate-free matrix. In the case of an age-hardened alloy, if the lateral growth of twins is limited by

precipitates then the grain will be subject to higher stress because the imposed strain cannot be accommodated by the twin. This high stress state enables the nucleation of new twins within the grain to accommodate applied strain. This accounts for the formation of more finer twins in the age-hardened condition [203]. Finer twins are more unstable and more likely to revert upon unloading [171].

2.3.2.4 Effect of Solute Content

The addition of solute elements has been observed to decrease the amount of anelasticity, in particular the addition of Zn and Gd. The anelasticity of sand-cast pure magnesium and magnesium-zinc alloys covering a range of zinc contents from dilute (less than 0.4 at.% or 1 wt.% zinc) to concentrated (concentrations up to 2.5 at.% or 6 wt.% zinc) solid solutions has been studied [170]. The largest anelastic effect is observed in pure magnesium and the anelastic effect decreases with increasing zinc solute concentration as shown in Figure 2.19 (a).

Likewise, for magnesium-gadolinium alloys with various gadolinium contents from dilute (gadolinium < 0.4 at.%) to concentrated (up to 4.2 at.%) solid solutions, the addition of gadolinium reduces the magnitude of anelastic strain and shifts the onset of anelastic strain towards larger plastic strains [172, 204] as shown in Figure 2.19 (b).

Although there is a monotonic decrease in anelasticity with increasing zinc and gadolinium contents, the same cannot be said for the effect of aluminium content. Anelasticity is observed to decrease with increasing aluminium content from pure magnesium up to 2 wt.% aluminium; anelasticity then increases significantly in the concentrated magnesium-9 wt.% aluminium alloy [188] as shown in Figure 2.19 (c).

The difference in the effect of solute on the anelastic behaviour of magnesium-zinc, magnesium-gadolinium and magnesium-aluminium alloys can be explained by short range order [188] as decribed below.

Firstly, both zinc and gadolinium have a strong tendency to develop short range order [205] while aluminium forms near random solid solutions [206]. The $\{10\bar{1}2\}$ twins have been described as “shuffling dominated” [207, 208] and they become more difficult when short range order is present [209]. Secondly, presence of small amounts of solutes, like zinc and aluminium causes solid solution softening in magnesium alloys, attributed to the reduction of the CRSS of prismatic slip [62]. Note that softening of prismatic slip has only been confirmed

for zinc and aluminium solute contents up to 0.5 at.% [62], higher solute levels have not been investigated.

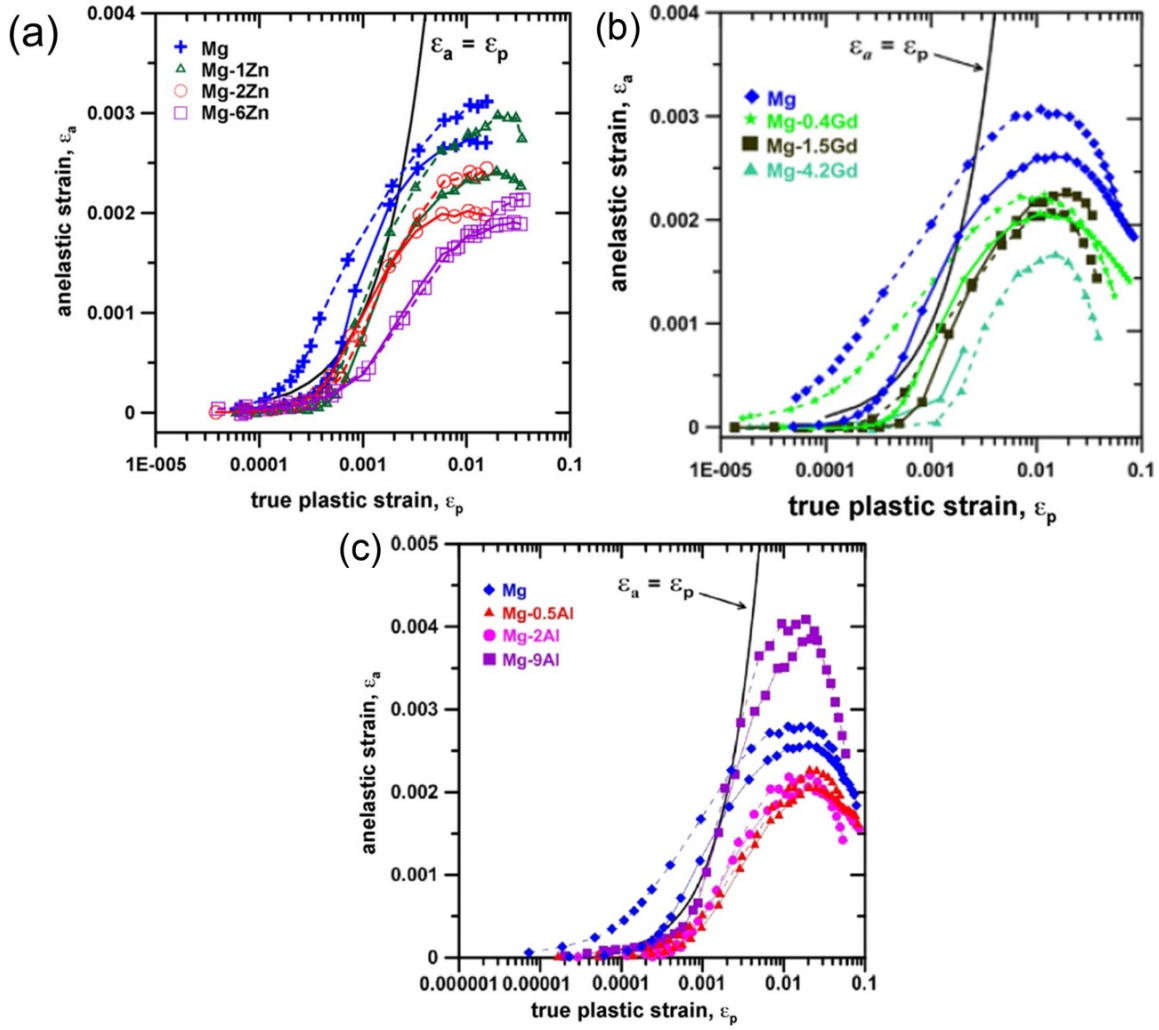

Figure 2.19: Anelastic strain as a function of the tensile (solid lines) and compressive (dashed lines) plastic strain, for pure magnesium and various (a) zinc contents [170], (b) gadolinium contents [172, 204] and (c) aluminium contents [188].

Based on the above information, it is proposed that at low solute concentrations (regardless of the types of solutes), solid solution softening of prismatic slip increases with the solute concentrations, and twinning becomes progressively less necessary as a deformation mechanism, reducing the anelastic effect. At higher concentrations, solid solution hardening of prismatic slip occurs, and twinning gradually becomes a prominent deformation mechanism. But, magnesium-gadolinium and magnesium-zinc alloys also develop short range order, making $\{10\bar{1}2\}$ twinning more difficult. It is likely that the decrease in $\{10\bar{1}2\}$ twinning by short range order is more than the increase in $\{10\bar{1}2\}$

twinning by hardening of slip planes, lowering the anelastic strain in magnesium-gadolinium and magnesium-zinc alloys. In contrast, magnesium-aluminium alloy is strengthened by much weaker random solid solution effects which have little hardening effect on the $\{10\bar{1}2\}$ twinning. At higher concentrations, presumably above 2 wt.% aluminium, prismatic slip becomes more difficult while twinning is not hardened by aluminium; the relative propensity for twinning increases, thereby increasing the anelasticity at high levels of aluminium.

2.3.3 Plasticity

In most HCP metals, including titanium and zirconium, twinning is preceded by gross dislocation plasticity and it is difficult to separate the respective hardening effects [210]. However, twinning in magnesium ($\{10\bar{1}2\}$ twinning) is activated at very low stresses after basal slip [63, 186], with little plastic deformation [170, 174, 211]. The possibility of isolating the hardening effects of twinning from those of dislocation slip was first investigated by Cáceres et al. [212] based on the Kocks-Mecking method of analysis [213, 214] as described below.

When the dominant source of strain hardening is caused by dislocations (this is true for pure FCC and HCP materials where the lattice resistance to dislocation motion is negligibly small), then plastic flow stress, σ_p relates to the dislocation density, ρ as [214-217]:

$$\sigma_p = \sigma - \sigma_y = \alpha\mu b\sqrt{\rho} \tag{2.5}$$

where σ is the flow stress, σ_y is the yield stress, α is a constant assumed independent of the strain, μ is the shear modulus, and b the magnitude of the Burgers vector of the dislocations. σ_p increases with plastic strain, ε_p due to dislocation storage (dislocations stopped by obstacles). The rate of accumulation of dislocations can be written as [214, 216, 218]:

$$\frac{d\rho}{d\varepsilon_p} = \frac{1}{bL} = \frac{\sqrt{\rho}}{\beta b} \tag{2.6}$$

where L is the dislocation mean free path, also defined as the distance traveled by a dislocation segment of length l before it is stopped by obstacles [219], and a constant β. Differentiating Eq. (2.5) and combining with Eq. (2.6) leads to:

$$\sigma_p \frac{d\sigma_p}{d\varepsilon_p} = \frac{(\alpha\mu b)^2}{2} \frac{d\rho}{d\varepsilon_p} \tag{2.7}$$

Eq. (2.7) begins with a linear phase during steady dislocation accumulation, for example when dislocation density increases linearly with deformation. At higher stresses, a mechanism known as dynamic recovery will be activated, allowing some dislocations stopped by obstacles to escape (dislocation annihilation), and Eq. (2.7) starts to drop. This corresponds to the declining slope in stress-strain curves. Note that dynamic recovery is dependent on temperature and strain rate [214].

Eq. (2.7) can be extended to account for the dynamic recovery effect [214, 216]:

$$\sigma_p\Theta = \sigma_p(\Theta_h - \Theta_r)\,(\sigma, \dot{\varepsilon}, T) \tag{2.8}$$

where Θ_h is the athermal contribution to $\Theta = \frac{d\sigma_p}{d\varepsilon_p}$, and Θ_r is the thermal component which describes the dynamic recovery rate, and accounts for any softening effects due to dislocation annihilation as temperature and/or applied stress increase and/or strain rate decreases. Note that Eq. (2.8) embodies two mechanisms, not two stages: both mechanisms may occur simultaneously.

In polycrystals of magnesium and its alloys, the end of anelasticity is marked by the onset of extensive plastic deformation by harder non-basal slip systems. Observations from published work [176, 177, 215, 220] suggest that plastic deformation can be further separated into two stages: deformation first by <a> prismatic slip, followed by <c+a> pyramidal slip systems [182]. Hence, Θ_h in Eq. (2.8) dominates in region with extensive <a> prismatic slip while Θ_r occurs at larger stresses and strains when <c+a> pyramidal slip activates [215].

When most grains become fully plastic by extensive activation of <a> prismatic slip, the strain hardening rate, $\Theta \approx \Theta_h$ becomes linear and drops to a lower value, varying from 1 to 2 GPa (i.e. 1.4 GPa for magnesium-9 mass% aluminium [177] and 1.8 GPa for AZ31 [176]) depending on the alloy compositions, with an average of about 1.4 GPa as observed in pure magnesium polycrystals [177, 215], a value commensurate with athermal accumulation

of forest dislocations [212, 215, 220]. The extent of this linear hardening region is controlled by how easy it is to activate <c+a> pyramidal slip, which might be dependent on factors such as solute content and strain rate. For example, the linear <a> prismatic slip region has been observed to be more extended in pure magnesium than in the Mg-9Al alloy [177]. The reason for this is unknown. It is hypothesised that the increase in solute content in the Mg-9Al delays the onset of <a> prismatic slip, but has little effect on <c+a> pyramidal slip, shortening the transition between <a> prismatic and <c+a> pyramidal slip.

As applied stress and strain increase to a higher level (for instance past 175 MPa at strains above 4~5% for AZ31 as identified by neutron diffraction [176]), <c+a> pyramidal slip activates. The strain hardening rate then decreases slowly in this stage due to dynamic recovery.

Mechanical behavior of magnesium is controlled by the CRSS and hardening responses of a variety of slip and twinning modes. Separating the flow curves into different regions and isolating the hardening effects of each slip and twinning modes can help to better understand the deformation behaviour of magnesium and its alloys.

2.4 Strain-rate Sensitivity of Magnesium Alloys

Pure magnesium and magnesium alloys with low solute concentrations tend to show pronounced strain-rate sensitivity in mechanical testing due to the HCP crystal structure [221]. As shown in Figure 2.20, the flow stress increases with increasing strain rate, $\dot{\varepsilon}$ in a HPDC AS21 magnesium alloy.

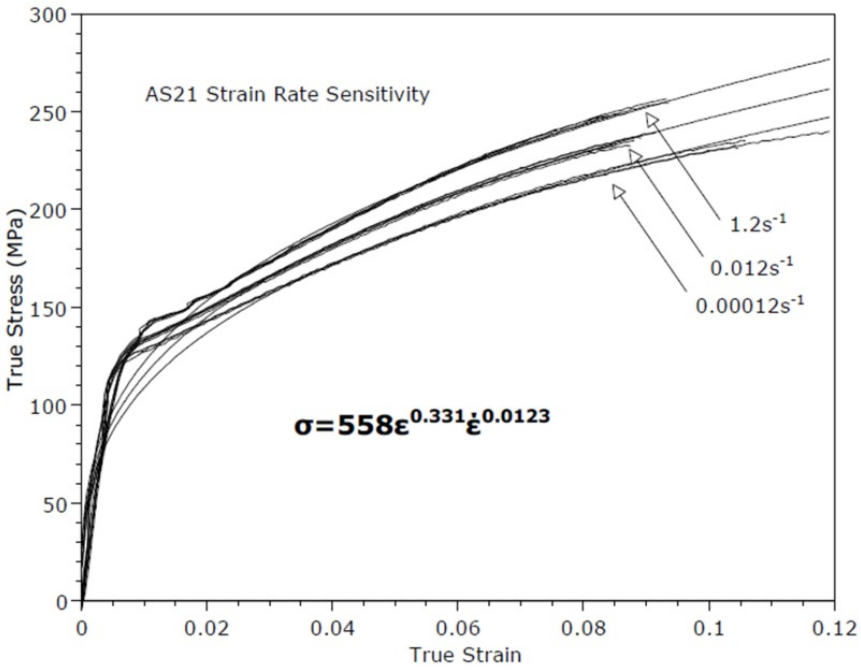

Figure 2.20: Stress-strain curves of HPDC AS21 with a best fit model of stress, σ as a function of strain, ε and strain rate, ε̇ [36].

When there is a change in mechanical response under different strain rates, a material is said to be strain-rate dependent and strain-rate sensitivity becomes an important parameter. The flow stress, σ can be represented by Eq. (2.9) [36] where ε is the strain, *n* is the strain hardening exponent and *m* is the strain-rate sensitivity, also represented by Eq. (2.10) [221-223]:

$$\sigma = \varepsilon^{n}\ \dot{\varepsilon}^{m} \tag{2.9}$$

$$m = \frac{\delta \ln(\sigma)}{\delta \ln(\dot{\varepsilon})} \tag{2.10}$$

The strain-rate sensitivity for magnesium alloys has been observed to increase with increasing temperature [68, 224], and decreasing grain size [106, 225]. In commercial magnesium-aluminium based alloys, the main alloying element, aluminium, is an important factor. In fact, the aluminium content has been observed to influence the strain-rate sensitivity of magnesium alloys [36, 224, 226-228], although the effect reported is still somewhat unclear.

2.4.1 Effect of Aluminium Content

Room temperature tensile and compressive stress-strain data of pure magnesium [106], and various ternary magnesium alloys [36, 228-234] at creep and quasi-static strain-rates, 10^{-6}-10^{0} s^{-1} have been re-analysed from several studies and plotted in Figure 2.21.

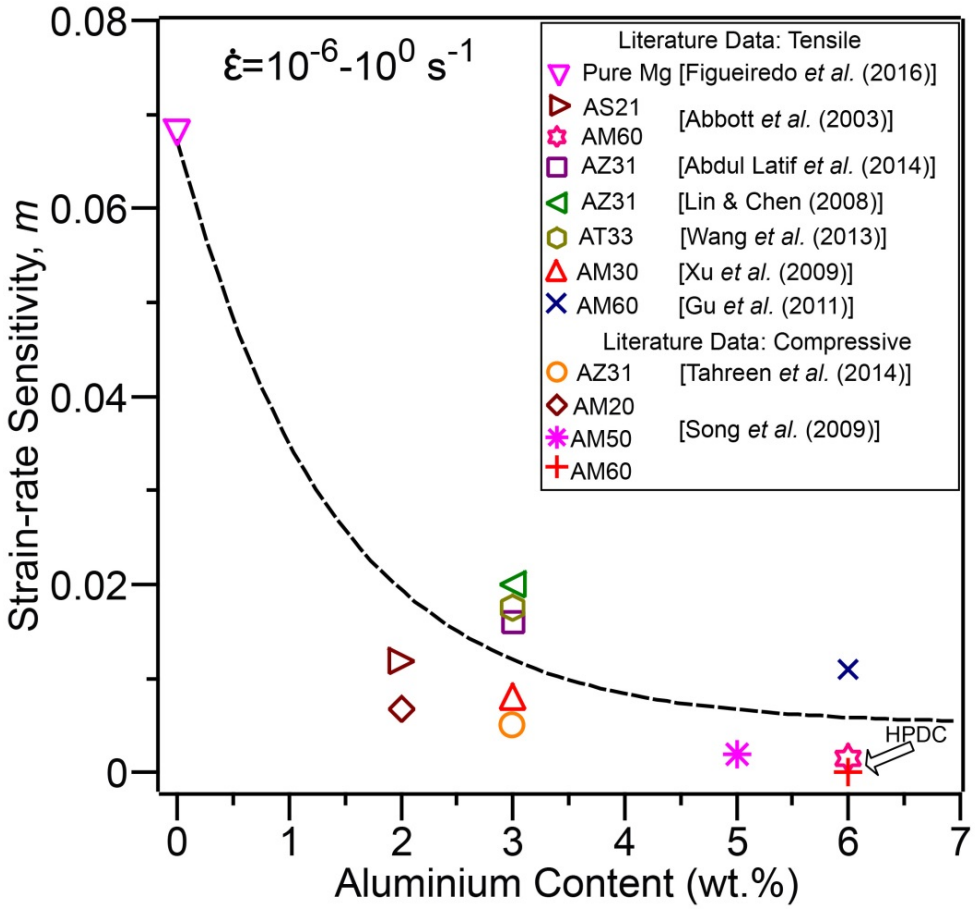

Figure 2.21: Strain-rate sensitivity, *m* versus aluminium content (wt.%) for pure magnesium [106], and various ternary magnesium alloys [36, 228-234]. The arrow indicates the two HPDC AM60 samples which have similar casting procedure [36, 228].

It is observed that pure magnesium has the highest strain-rate sensitivity, and strain-rate sensitivity decreases rapidly with increasing aluminium content with the strain-rate sensitivity becoming negligible when the aluminium content is more than 3 wt.% at these low strain rates. A similar observation was reported [226], but they were not certain if the strain-rate sensitivity was influenced by the aluminium in solid solution or β-$Mg_{17}Al_{12}$ reinforcing phase.

Note that similar HPDC AM60, as annotated in Figure 2.21, showed similar strain-rate sensitivity under both tension [36] and compression [228]. This is expected as HPDC magnesium alloys are isotropic in behaviour [196-198]. The strain-rate sensitivity of an extruded Mg-1Al alloy was observed to be 30% lower than that of pure magnesium at 10^{-4}-10^{-1} s^{-1} [224]. The alloy was solution treated indicating that strain-rate effect is also independent of processing conditions.

The high strain-rate sensitivity in HPDC magnesium alloys with lower aluminium content was observed to manifest as an increase in work hardening rate and tensile to yield ratio at higher strain rates [36]. This may be beneficial during vehicle impact as rapidly deforming regions of magnesium components would exhibit the highest strength, encouraging the spread of deformation to other parts of the components, maximising the energy absorption.

While some observed a correlation between aluminium content and strain-rate sensitivity, others did not. Aune et al. [227] studied the behaviour of die-cast AM50, AM60 and AZ91 alloys at 15-130 s^{-1}, but did not observe a significant variation in strain-rate sensitivity between the alloys despite a difference in aluminium content. This could be due to three factors. Firstly, they only investigated alloys with aluminium contents greater than 5 wt.% when the strain-rate sensitivity is relatively low (Figure 2.21). Secondly, their investigated strain-rate range may be too small (covering less than one order of magnitude) to see the effect of strain rate. Thirdly, their strain rates are significantly higher, falling in between quasi-static (typically $< 10^{0}$ s^{-1}) and dynamic ($\geq 10^{3}$ s^{-1}) domains. The latter two factors may be more plausible since AE44 (reported to have very low aluminium solute in the magnesium matrix $\approx$ 2.3 wt.% [235]) also showed no strain-rate sensitivity in similar strain-rate range (100-300 s^{-1}) [236]. Research on this strain-rate range, 10^{0}-10^{2} s^{-1}, is hard to find due to experimental challenges.

2.4.2 Mechanisms of Strain-rate Sensitivity

The strain rates commonly applied in mechanical testing can be further divided into four categories: creep strain rates ($\leq 10^{-5}$ s^{-1}), quasi-static (10^{-4}-10^{-1} s^{-1}), intermediate (10^{0}-10^{2} s^{-1}) and machining or dynamic strain rates ($\geq 10^{3}$ s^{-1}) as shown in Figure 2.22. Mechanical properties of magnesium alloys are commonly tested at quasi-static and dynamic strain rates due to the availability of testing equipment. Strain-rate sensitivity data are missing in the intermediate (quasi-static to dynamic transition) region, mainly due to experimental

challenges. There is also a severe lack of strain-rate sensitivity data at creep strain rates, because tests in this region are time consuming.

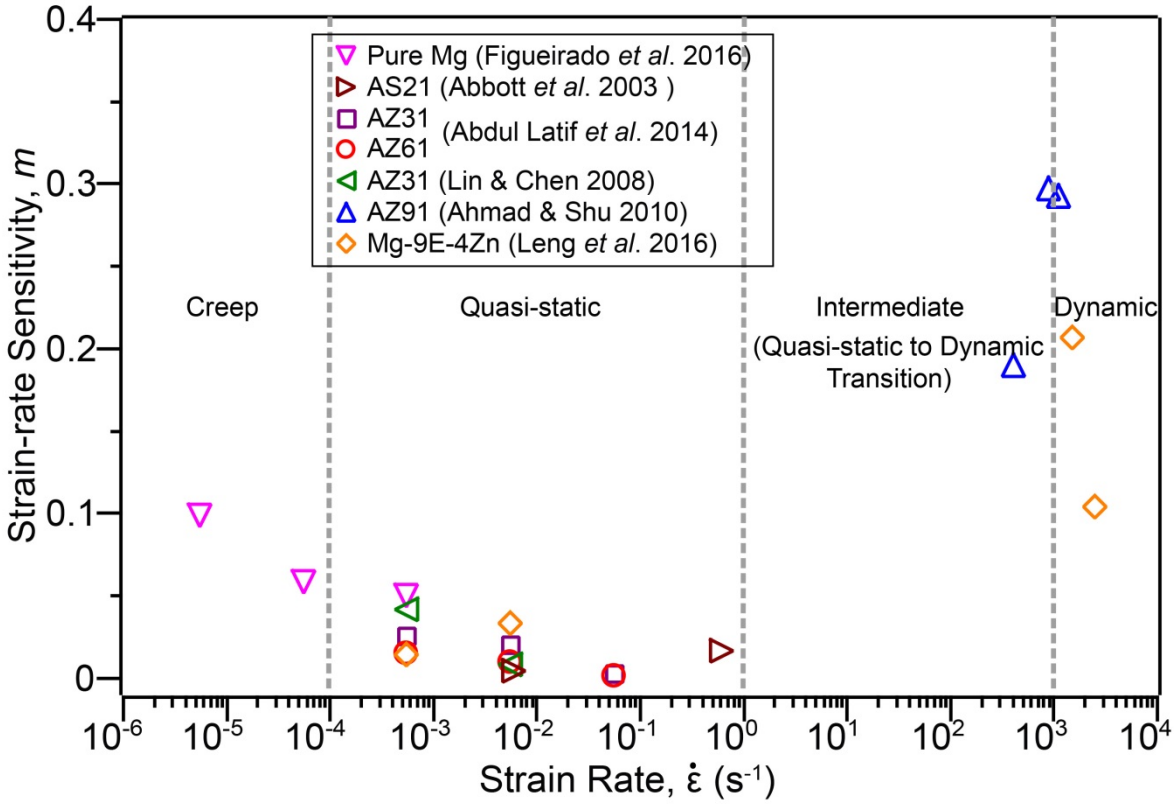

Figure 2.22: Strain-rate sensitivity, *m* as a function of strain rates covering from creep to dynamic strain rates, for pure magnesium [106] and other ternary magnesium alloys [36, 229, 230, 237, 238]. Note the strain rate shown corresponds to the average of the upper and lower values re-analysed from these studies.

As shown in Figure 2.22, strain-rate sensitivity increases with decreasing strain rate at creep strain rates for pure magnesium [106], although further research is required to see if alloys also behave the same way. At dynamic strain rates, in excess of 10^3 s^{-1}, strain-rate sensitivity increases with strain rates in cast Mg-9E-4Zn [238], AZ31 and AZ61 [101] and AZ91 [101, 237] magnesium alloys.

It is also interesting to see that the strain-rate sensitivity at dynamic strain rates is significantly higher than that at quasi-static strain rates. In fact, strain-rate sensitivity has been observed to increase by two orders of magnitude from 10^{-4}-10^{-1} s^{-1} (quasi-static) to 2700 s^{-1} (dynamic) in an extruded Mg-8Li-1Al-1Ce [239]. At dynamic strain rates, the volume

fraction of twinning has been reported to increase significantly and deformation mechanism is a combination of dislocation and twinning [239].

At quasi-static strain rates 10^{-4}-10^{-1} s^{-1}, published results on strain-rate sensitivity are ambiguous. Pure magnesium [106] and extruded AZ31 alloy [229, 240] exhibited high strain-rate sensitivity, and strain rate sensitivity increased with decreasing strain rate. The increase in strain-rate sensitivity with decreasing strain rate was attributed to the suppression of twinning and activation of slip-induced grain boundary sliding [240]. Absence of work hardening in stress-strain curves at low strain rates $\leq 10^{-4}$ s^{-1} [106] further suggests that twinning may be absent and basal slip may be the dominant deformation mechanism.

However, an extruded AZ31 alloy was tensile tested at strain rates between 10^{-5}-10^{-2} s^{-1} and high strain-rate sensitivity observed below 10^{-4} s^{-1}; there was no strain-rate sensitivity in between 10^{-4}-10^{-2} s^{-1} [230]. To give another example, die-cast AM20, AM50, and AM60 showed almost no strain-rate sensitivity between 10^{-3}-10^{0} s^{-1} regardless of the difference in aluminium content [228].

Overall, some observed high strain-rate sensitivity [106, 229, 240], while some observed very low strain-rate sensitivity and strain-rate sensitivity was little affected by strain rates in the quasi-static region [228, 230, 241], regardless of aluminium content. To date, there remains some contradiction in the literature in regard to the strain-rate sensitivity at creep, quasi-static, intermediate and dynamic strain rates.

A change in strain-rate sensitivity often suggests a change in deformation mechanism. This is interpreted from the different fracture surfaces obtained from samples deformed at different strain rates as summarised in Table 2.4.

As shown in Table 2.4, it appears that there is a change in material behaviour from ductile at creep strain rates to brittle at quasi-static strain rates and back to ductile at dynamic strain rates. Brittle fracture has been attributed to deformation by twinning as twin is known to provide a crack path [240], while ductile fracture is frequently associated with an increasing number of slip systems [228].

Table 2.4: Different types of fracture surfaces observed in magnesium alloys deformed at wide strain-rate range.

Strain-rate Region	Applied Strain Rate (s^{-1})	Fracture Surface	References
Creep	10^{-8}	Ductile/Highly-dimpled	Extruded AZ31 [240]
	10^{-5}	Quasi-cleavage fracture with small dimples	Extruded AZ31B [230]
Quasi-static	10^{-4}	Brittle intergranular fracture	Extruded AZ31 [229]
	10^{-3}	Cleavage fracture with surface steps	HPDC AM20 [228]
	10^{-2}		Extruded AZ31B [230]
	10^{-1}	Quasi-cleavage with some shallow dimples	Extruded AZ31 [229]
Dynamic	10^{3}	Ductile fracture with significant amount of micro-dimples	HPDC AM20 [228]

Decreasing strain rate below 10^{-5} hinders twin activation and basal slip becomes the dominant deformation mode in pure magnesium polycrystal [242]. This may be due to less dislocations being piled-up at grain boundaries [243] and better connectivity between grains that are favorably oriented for basal slip [242]. If basal slip can accommodate deformation, twinning becomes less necessary. As strain rate increases, it is generally accepted that at room temperature and quasi-static rates, the deformation mode is a combination of slip and twinning in magnesium and alloys. At dynamic strain rates, deformation heating occurs, and this increases the number of slip systems, leading to a ductile fracture, for example in die-cast AM20 [228].

2.5 Summary: Literature Gaps and Research Hypotheses

From the literature, four gaps are identified and research hypotheses are formulated as shown in Figure 2.23. These gaps will be investigated in the subsequent chapters.

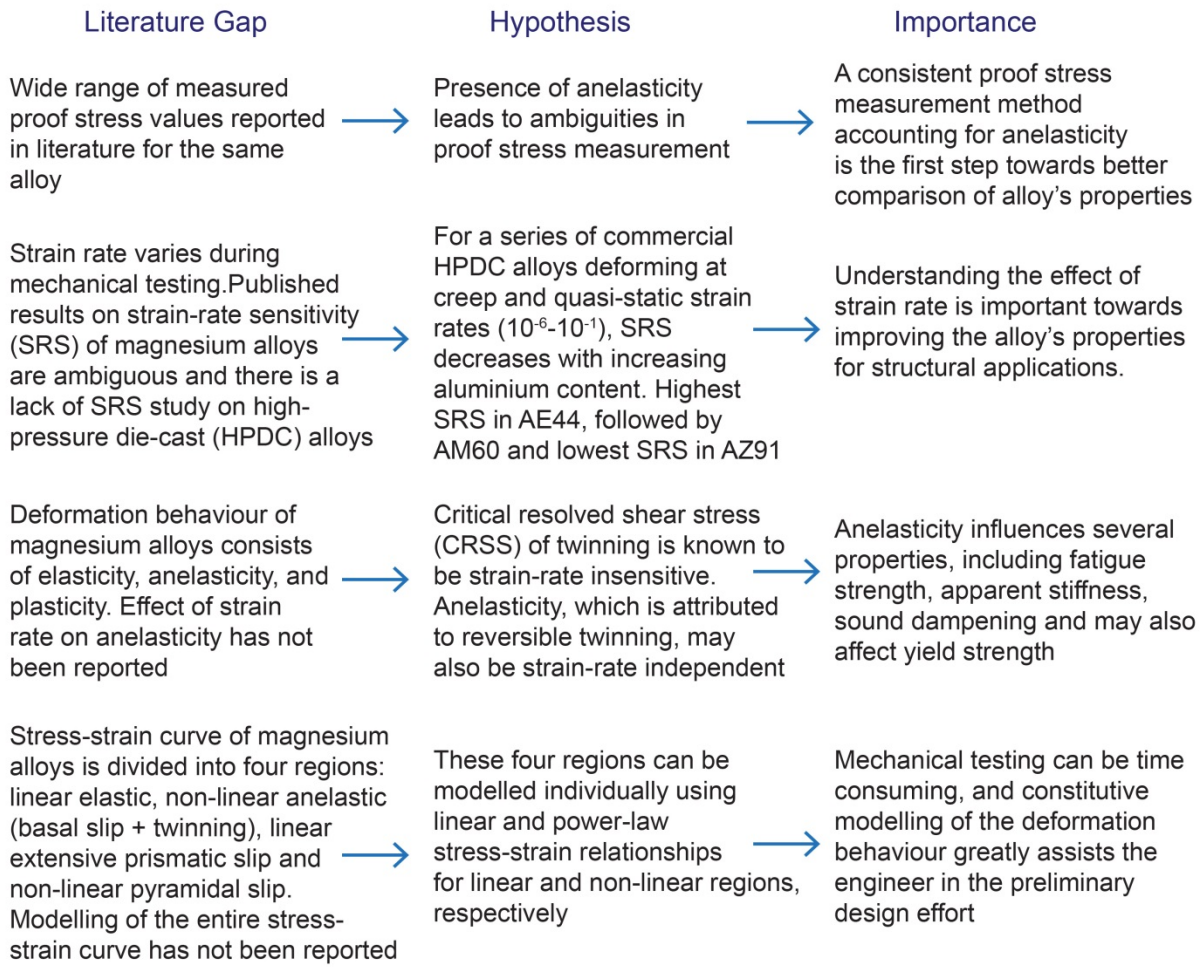

Figure 2.23: Missing gaps in the literature and their respective hypotheses and importance.

The existing issue with the deformation behaviour of magnesium and alloys is the early activation of <a> basal slip at low stress levels. But, the hexagonal closed-packed crystal structure provides only two independent basal slip systems, and this does not satisfy the von Mises-Taylor criterion. To add to the complexity of deformation behaviour, the non-basal slips (<a> prismatic and <c+a> pyramidal slip) only activate at higher stress levels at room temperature. Therefore, twinning is activated to accommodate plastic deformation. Profuse twinning at low stresses and strains further complicates the deformation behaviour of magnesium alloys. This is because twins formed are unstable in the loaded condition, and they can partially revert upon unloading. Presence of non-linear reversible deformation (anelastic deformation) can influence properties, such as fatigue strength, apparent stiffness, sound dampening and yield strength.

Therefore, lowering the critical resolved shear stress (softening) of the non-basal slips or delaying the activation (hardening) of <a> basal slip and twinning can improve the

mechanical properties, such as strength and ductility. Improved strengths and high levels of ductility are required for die-cast magnesium alloys if they were to be considered for structural applications.

The effects of strain rate and aluminium content on the different slip and twinning deformation systems are under reported. Hence, the complex deformation behaviour of die-cast magnesium alloys requires further understanding for future development of improved structural alloys and this forms the basis for this research.

Chapter 2 References

[1] Friedrich HE, Mordike BL. Magnesium technology. Berlin: Springer; 2006.

[2] Polmear IJ. Magnesium alloys and applications. Materials Science and Technology 1994; 10(1): p. 1-16.

[3] Avedesian M, Baker H. Magnesium and magnesium Alloys—ASM Specialty Handbook, ASM International. Ohio: The Materials Information Society; 1999.

[4] Froes FH, Kim YW, Krishnamurthy S. Rapid solidification of lightweight metal alloys. Materials Science and Engineering A 1989; 117: p. 19-32.

[5] Woldman N. Magnesium Casting. Magnesium, ASM International; 1946.

[6] Abbott TB. Magnesium: industrial and research developments over the last 15 years. Corrosion 2015; 71(2): p. 120-7.

[7] Mordike BL, Ebert T. Magnesium: properties—applications—potential. Materials Science and Engineering A 2001; 302(1): p. 37-45.

[8] Luo AA, Renaud J, Nakatsugawa I, Plourde J. Magnesium castings for automotive applications. Journal of the Minerals, Metals, and Materials Society 1995; 47(7): p. 28-31.

[9] Aragones J, Goundan K, Kolp S, Osborne R, Ouimet L, Pinch W. Development of the 2006 Corvette Z06 structural cast magnesium crossmember. SAE Technical Paper 2005-01-0340.

[10] Kainer KU, Kaiser F. Magnesium alloys and technology. New Jersey: John Wiley & Sons; 2003.

[11] Pekguleryuz MO, Friedrich HE, Mordike BL, editors. Magnesium technology: metallurgy, design data, automotive applications. Berlin: Springer; 2006.

[12] Alloy phase diagrams. In: Baker H, Okamoto H, editors. ASM Handbook, Ohio: ASM International; 1992, p. 501.

[13] Emley EF. Principles of magnesium technology. New York: Pergamon; 1966.

[14] Dargusch MS, Dunlop GL, Pettersen K. In: Mordike BL, Kainer KU, editors. Magnesium alloys and their applications, Werkstoff-Informationsgesellschaft, Frankfurt, Germany; 1998, p. 277-82.

[15] Chua BW, Lu L, Lai MO. Deformation behaviour of ultrafine and nanosize-grained Mg alloy synthesized via mechanical alloying. Philosophical Magazine 2006; 86(19): p. 2919-39.

[16] Aghion E, Bronfin B, Von Buch F, Schumann S, Friedrich H. Newly developed magnesium alloys for powertrain applications. Journal of Minerals, Metals and Materials Society 2003; 55(11): p. 30-3.

[17] Easton MA, Gibson MA, Zhu SM, Abbott TB. An a priori hot-tearing indicator to die-cast magnesium-eare earth alloys. Metallurgical and Materials Transactions A 2014; 45(8): p. 3586-95.

[18] Foerster GS. Designing alloys for die casting. Met Eng Q 1973; 13(1): p. 19-22.

[19] Bakke P, Pettersen K, Westengen H. Improving the strength and ductility of magnesium die-casting alloys via rare-earth addition. Journal of Minerals, Metals and Materials Society 2003; 55(11): p. 46-51.

[20] Rettberg LH, Jordon JB, Horstemeyer MF, Jones JW. Low-cycle fatigue behavior of die-cast Mg alloys AZ91 and AM60. Metallurgical and Materials Transactions A 2012; 43(7): p. 2260-74.

[21] Dargusch MS, Pettersen K, Nogita K, Nave MD, Dunlop GL. The effect of aluminium content on the mechanical properties and microstructure of die cast binary magnesium-aluminium alloys. Materials Transactions 2006; 47(4): p. 977-82.

[22] Yang KV, Cáceres CH, Easton MA. Strengthening micromechanisms in cold-chamber high-pressure die-cast Mg-Al alloys. Metallurgical and Materials Transactions A 2014; 45(9): p. 4117-28.

[23] Cáceres CH, Griffiths JR, Reiner P. The influence of microstructure on the Bauschinger effect in an Al-Si-Mg casting alloy. Acta Materialia 1996; 44(1): p. 15-23

[24] Zhang B, Nagasekhar AV, Sivarupan T, Cáceres CH. Deformation behavior of the percolating intermetallic microstructure of high pressure die cast AZ91 alloy. Advanced Engineering Materials 2013; 15(11): p. 1059-67.

[25] Nagasekhar AV, Cáceres CH, Kong C. 3D characterization of intermetallics in a high pressure die cast Mg alloy using focused ion beam tomography. Materials Characterization 2010; 61(11): p. 1035-42.

[26] Zhang B, Yang KV, Nagasekhar AV, Cáceres CH. Deformation behavior of the percolating eutectic intermetallic in HPDC and squeeze-cast Mg alloys. Journal of Minerals, Metals and Materials Society 2014; 66(10): p. 2086-94.

[27] Powell BR, Rezhets V, Balogh MP, Waldo RA. Microstructure and creep behavior in AE42 magnesium die-casting alloy. Journal of Minerals, Metals and Materials Society 2002; 54(8): p. 34-8.

[28] Rzychoń T, Kiełbus A, Dercz G. Structural and quantitative analysis of die cast AE44 magnesium alloy. Journal of Achievements Materials and Manufacturing Engineering 2007; 22(2): p. 43-6.

[29] Bakke P, Westengen H. The role of rare earth elements in structure and property control of magnesium die casting alloys. In: Mathaudhu SN, Luo AA, Neelameggham NR, Nyberg EA, Sillekens WH, editors. Essential Readings in Magnesium Technology, New Jersey: John Wiley & Sons; 2005, p. 313-8.

[30] Bettles CJ, Moss MH, Lapovok R. A Mg–Al–Nd alloy produced via a powder metallurgical route. Materials Science and Engineering A 2009; 515(1): p. 26-31.

[31] Nayeb-Hashemi A. Phase diagrams of binary magnesium alloys. Ohio: ASM International; 1988.

[32] Zhu SM, Nie JF, Gibson MA, Easton MA, Bakke P. Microstructure and creep behavior of high-pressure die-cast magnesium alloy AE44. Metallurgical and Materials Transactions A 2012; 43(11): p. 4137-44.

[33] Bohlen J, Nürnberg MR, Senn JW, Letzig D, Agnew SR. The texture and anisotropy of magnesium–zinc–rare earth alloy sheets. Acta Materialia 2007; 55(6): p. 2101-12.

[34] Magontec. Mechanical properties of die-cast magnesium alloys. Unpublished raw data.

[35] Luo AA. Magnesium casting technology for structural applications. Journal of Magnesium and Alloys 2013; 1(1): p. 2-22.

[36] Abbott TB, Easton MA, Schmidt R. Magnesium for crashworthy components. In: Kaplan HI, editor. Magnesium Technology. Proceedings of the TMS Annual Meeting; 2003 March 2-6; San Diego, California; p. 463-466.

[37] Zhang JH, Liu K, Fang DQ, Qiu X, Tang DX, Meng J. Microstructure, tensile properties, and creep behavior of high-pressure die-cast Mg–4Al–4RE–0.4 Mn (RE= La, Ce) alloys. Journal of Materials Science 2009; 44(8): p. 2046-54.

[38] Zhu SM, Gibson MA, Nie JF, Easton MA, Abbott TB. Microstructural analysis of the creep resistance of die-cast Mg–4Al–2RE alloy. Scripta Materialia 2008; 58(6): p. 477-80.

[39] Zhang JH, Leng Z, Zhang ML, Meng J, Wu RZ. Effect of Ce on microstructure, mechanical properties and corrosion behavior of high-pressure die-cast Mg–4Al-based alloy. Journal of Alloys and Compounds 2011; 509(3): p. 1069-78.

[40] Rzychoń T, Kiełbus A. Effect of rare earth elements on the microstructure of Mg-Al alloys. Journal of Achievements in Materials and Manufacturing Engineering 2006; 18: p. 135-8.

[41] Dargusch MS, Zhu SM, Nie JF, Dunlop GL. Microstructural analysis of the improved creep resistance of a die-cast magnesium–aluminium–rare earth alloy by strontium additions. Scripta Materialia 2009; 60(2): p. 116-9.

[42] Zhang JH, Zhang ML, Meng J, Wu RZ, Tang DX. Microstructures and mechanical properties of heat-resistant high-pressure die-cast Mg–4Al–xLa–0.3 Mn (x= 1, 2, 4, 6) alloys. Materials Science and Engineering A 2010; 527(10): p. 2527-37.

[43] Kiełbus A. Microstructure of AE44 magnesium alloy before and after hot-chamber die casting. Journal of Achievements in Materials and Manufacturing Engineering 2007; 20(1-2): p. 459-62.

[44] Zhang JH, Zhang DP, Tian Z, Wang J, Liu K, Lu HY et al. Microstructures, tensile properties and corrosion behavior of die-cast Mg–4Al-based alloys containing La and/or Ce. Materials Science and Eng A 2008; 489(1): p. 113-9.

[45] Rzychoń T, Kielbus A, Cwajna J, Mizera J. Microstructural stability and creep properties of die casting Mg–4Al–4RE magnesium alloy. Materials Characterization 2009; 60(10): p. 1107-13.

[46] Du WW, Sun YS, Min XG, Xue F, Zhu M, Wu DY. Microstructure and mechanical properties of Mg–Al based alloy with calcium and rare earth additions. Materials Science and Engineering A 2003; 356(1): p. 1-7.

[47] Zhang JH, Yu P, Liu K, Fang DQ, Tang DX, Meng J. Effect of substituting cerium-rich mischmetal with lanthanum on microstructure and mechanical properties of die-cast Mg–Al–RE alloys. Materials and Design 2009; 30(7): p. 2372-78.

[48] Partridge PG. The crystallography and deformation modes of hexagonal close-packed metals. Metallurgical Reviews 1967; 12(1): p. 169-94.

[49] Murray JL, editor. Phase diagrams of binary magnesium alloys. Ohio: ASM International; 1988.

[50] Mitchell AD, Cross LC, editors. Tables of interatomic distances and configuration in molecules and ions. London: Chemical Society; 1958.

[51] Rokhlin LL. Magnesium alloys containing rare earth metals: structure and properties. United States: CRC Press; 2003.

[52] Saddock ND. Microstructure and creep behavior of Mg-Al alloys containing alkaline and rare earth additions [dissertation]. University of Michigan; 2008.

[53] Bacon DJ, Vitek V. Atomic-scale modeling of dislocations and related properties in the hexagonal-close-packed metals. Metallurgical and Materials Transactions A 2002; 33(3): p. 721-33.

[54] Yoo MH, Agnew SR, Morris JR, Ho KM. Non-basal slip systems in HCP metals and alloys: source mechanisms. Materials Science and Engineering A 2001; 319: p. 87-92.

[55] Yoo MH, Morris JR, Ho KM, Agnew SR. Nonbasal deformation modes of HCP metals and alloys: role of dislocation source and mobility. Metallurgical and Materials Transactions A 2002; 33(3): p. 813-22.

[56] Reed-Hill RE, Robertson WD. Deformation of magnesium single crystals by nonbasal slip. Journal of Metals Transactions AIME 1957; 220: p. 496-502.

[57] Groves G, Kelly A. Independent slip systems in crystals. Philosophical Magazine 1963; 8(89): p. 877-87.

[58] Burke EC, Hibbard WR. Plastic deformation of magnesium single crystals. Transactions of the Metallurgical Society of AIME 1952; 194: p. 295-303.

[59] Taylor GI. Plastic strain in metals. Institute of Metals 1938; 62: p. 307-24.

[60] Kocks UF, Westlake DG. The importance of twinning for the ductility of HCP polycrystals. Transactions of the Metallurgical Society of AIME 1967; 239(7): p. 1107-09.

[61] Mises RV. Mechanik der plastischen Formänderung von Kristallen. ZAMM-Journal of Applied Mathematics and Mechanics/Zeitschrift für Angewandte Mathematik und Mechanik 1928; 8(3): p. 161-85.

[62] Akhtar A, Teghtsoonian E. Solid solution strengthening of magnesium single crystals—II the effect of solute on the ease of prismatic slip. Acta Metallurgica 1969; 17(11): p. 1351-6.

[63] Agnew SR, Yoo MH, Tome CN. Application of texture simulation to understanding mechanical behavior of Mg and solid solution alloys containing Li or Y. Acta Materialia 2001; 49(20): p. 4277-89.

[64] Obara T, Yoshinga H, Morozumi S. {11$\bar{2}$2}< 1123> Slip system in magnesium. Acta Metallurgica 1973; 21(7): p. 845-53.

[65] Kleiner S, Uggowitzer PJ. Mechanical anisotropy of extruded Mg–6% Al–1% Zn alloy. Materials Science and Engineering A 2004; 379(1): p. 258-63.

[66] Wonsiewicz BC, Backofen WA. Independent slip systems and ductility of hexagonal polycrystals. Transactions of the Metallurgical Society of AIME 1967; 239: p. 1422-33.

[67] Raynor GV. The physical metallurgy of magnesium and its alloys. 5th ed. Oxford: Pergamon; 1959.

[68] Agnew SR, Duygulu Ö. Plastic anisotropy and the role of non-basal slip in magnesium alloy AZ31B. International Journal of Plasticity 2005; 21(6): p. 1161-93.

[69] Vagarali SS, Langdon TG. Deformation mechanisms in hcp metals at elevated temperatures—II. Creep behavior of a Mg-0.8% Al solid solution alloy. Acta Metallurgica 1982; 30(6): p. 1157-70.

[70] Vagarali SS, Langdon TG. Deformation mechanisms in hcp metals at elevated temperatures—I. Creep behavior of magnesium. Acta Metallurgica 1981; 29(12): p. 1969-82.

[71] Kelley EW, Hosford WF. The deformation characteristics of textured magnesium. Transactions of the Metallurgical Society of AIME 1968; 242(4): p.11.

[72] Akhtar A, Teghtsoonian E. Solid solution strengthening of magnesium single crystals—I alloying behaviour in basal slip. Acta Metallurgica 1969; 17(11): p. 1339-49.

[73] Hull D, Bacon DJ. Introduction to dislocations. 5th ed. Oxford: Elsevier Science and Technology; 2011.

[74] Barnett MR. Twinning and the ductility of magnesium alloys: Part I:"Tension" twins. Materials Science and Engineering A 2007; 464(1): p. 1-7.

[75] Koike J, Kobayashi T, Mukai T, Watanabe H, Suzuki M, Maruyama K et al. The activity of non-basal slip systems and dynamic recovery at room temperature in fine-grained AZ31B magnesium alloys. Acta Materialia 2003; 51(7): p. 2055-65.

[76] Ma Q, Li B, Oppedal AL, Whittington WR, Horstemeyer SJ, Marin EB et al. Strain rate dependence of twinning at 450° C and its effect on microstructure of an extruded magnesium alloy. Materials Science and Engineering A 2013; 559: p. 314-18.

[77] Meyers MA, Vöhringer O, Lubarda VA. The onset of twinning in metals: a constitutive description. Acta Materialia 2001; 49(19): p. 4025-39.

[78] Ulacia I, Dudamell NV, Gálvez F, Yi S, Pérez-Prado MT, Hurtado I. Mechanical behavior and microstructural evolution of a Mg AZ31 sheet at dynamic strain rates. Acta Materialia, 2010. 58(8): p. 2988-98.

[79] Barnett MR. A Taylor model based description of the proof stress of magnesium AZ31 during hot working. Metallurgical and Materials Transactions A 2003; 34(9): p. 1799-1806.

[80] Bettles C, Barnett M. Advances in wrought magnesium alloys: Fundamentals of processing, properties and applications. Cambridge: Woodhead Publishing Limited; 2012.

[81] Schmid E. Articles on the physics and metallography of magnesiums. Z. Elektrochem. 1931; 37: p. 447-59.

[82] Conrad H, Robertson WD. Effect of temperature on the flow stress and strain hardening coefficient of magnesium single crystals. Transactions of the Metallurgical Society of AIME 1957; 209: p. 503.

[83] Flynn PW, Mote J, Dorn JE. On the thermally activated mechanism of prismatic slip in magnesium single crystals. Transactions of the Metallurgical Society of AIME 1961; 221(6): p. 1148-54.

[84] Akhtar A, Teghtsoonian E. Substitutional solution hardening of magnesium single crystals. Philosophical Magazine 1972; 25(4): p. 897-916.

[85] Ando S, Nakamura K, Takashima K, Tonda H. {11$\bar{2}$2}< 1$\bar{1}$23> slip in magnesium single crystal. Keikinzoku/Journal of Japan Institute of Light Metals 1992; 42(12): p. 765-71.

[86] Agnew SR, Brown DW, Tomé CN. Validating a polycrystal model for the elastoplastic response of magnesium alloy AZ31 using in situ neutron diffraction. Acta Materialia 2006; 54(18): p. 4841-52.

[87] Agnew SR, Tomé CN, Brown DW, Holden TM, Vogel SC. Study of slip mechanisms in a magnesium alloy by neutron diffraction and modeling. Scripta Materialia 2003; 48(8): p. 1003-8.

[88] Agnew SR. Plastic anisotropy of magnesium alloy AZ31B sheet. In: Mathaudhu SN, Luo AA, Neelameggham NR, Nyberg EA, Sillekens WH, editors. Essential Readings in Magnesium Technology, New Jersey: John Wiley & Sons; 2016, p. 351-56.

[89] Karabin L. Twinning in magnesium alloys. Magnesium Technology. Metallurgical and Materials Transactions A.

[90] Reed-Hill RE, Abbaschian R. Deformation twinning and martensite reactions. Physical Metallurgy Principles 1998; p. 584-5.

[91] Barnett MR, Keshavarz Z, Beer AG, Ma X. Non-Schmid behaviour during secondary twinning in a polycrystalline magnesium alloy. Acta Materialia 2008; 56(1): p. 5-15.

[92] Yoshinaga H, Obara T, Morozumi S. Twinning deformation in magnesium compressed along the C-axis. Materials Science and Engineering 1973; 12(5): p. 255-64.

[93] Nave MD, Barnett MR. Microstructures and textures of pure magnesium deformed in plane-strain compression. Scripta Materialia 2004; 51(9): p. 881-5.

[94] Roberts CS. The deformation of magnesium. Magnesium and its alloys. New York: John Wiley & Sons; 1960.

[95] Yoo MH. Slip, twinning, and fracture in hexagonal close-packed metals. Metallurgical Transactions A 1981; 12(3): p. 409-18.

[96] Jiang L, Jonas JJ, Luo AA, Sachdev AK, Godet S. Twinning-induced softening in polycrystalline AM30 Mg alloy at moderate temperatures. Scripta Materialia 2006; 54(5): p. 771-5.

[97] Barnett MR. Twinning and the ductility of magnesium alloys: Part II."Contraction" twins. Materials Science and Engineering A 2007; 464(1): p. 8-16.

[98] Jiang L, Jonas JJ, Mishra RK, Luo AA, Sachdev AK, Godet S. Twinning and texture development in two Mg alloys subjected to loading along three different strain paths. Acta Materialia 2007; 55(11): p. 3899-910.

[99] Lu Y, Taheri F, Gharghouri M. Monotonic and cyclic plasticity response of magnesium alloy. Part I. Experimental response of a high-pressure die cast AM60B. Strain 2011; 47: p. 15-24.

[100] Xu S, Tyson WR, Eagleson R, Zavadil R, Liu Z, Mao PL et al. Dependence of flow strength and deformation mechanisms in common wrought and die cast magnesium alloys on orientation, strain rate and temperature. Journal of Magnesium Alloys 2013; 1(4): p. 275-82.

[101] Asgari H, Szpunar JA, Odeshi AG. Texture evolution and dynamic mechanical behavior of cast AZ magnesium alloys under high strain rate compressive loading. Materials and Design 2014; 61: p. 26-34.

[102] Asgari H, Odeshi AG, Szpunar JA, Zeng LJ, Olsson E, Li DY. Effect of yttrium on the twinning and plastic deformation of AE magnesium alloy under ballistic impact. Materials Science and Engineering A 2015; 623: p. 10-21.

[103] Barnett MR, Keshavarz Z, Beer AG, Atwell D. Influence of grain size on the compressive deformation of wrought Mg–3Al–1Zn. Acta Materialia 2004; 52(17): p. 5093-103.

[104] Chun YB, Davies CHJ. Twinning-induced negative strain rate sensitivity in wrought Mg alloy AZ31. Materials Science and Engineering A 2011; 528(18): p. 5713-22.

[105] Figueiredo RB, Száraz Z, Trojanová Z, Lukáč P, Langdon TG. Significance of twinning in the anisotropic behavior of a magnesium alloy processed by equal-channel angular pressing. Scripta Materialia 2010; 63(5): p. 504-7.

[106] Figueiredo RB, Poggiali FSJ, Silva CLP, Cetlin PR, Langdon TG. The influence of grain size and strain rate on the mechanical behavior of pure magnesium. Journal of Materials Science 2016; 51(6): p. 3012-24.

[107] Korla R, Chokshi AH. Strain-rate sensitivity and microstructural evolution in a Mg–Al–Zn alloy. Scripta Materialia 2010; 63(9): p. 913-6.

[108] Thirugnanam M. Modern high pressure die-casting processes for aluminium castings. Transaction of 61st Indian Foundry Congress; 2013 Jan 27-29; Kolkata, India.

[109] Vinarcik EJ. High integrity die casting processes. New Jersey: John Wiley & Sons; 2002.

[110] Guo F. Understanding the microstructure and fatigue behavior of magnesium alloys [dissertation]. University of Leicester; 2009.

[111] Sequeira WP, Dunlop GL, Murray MT. Effect of section thickness and microstructure on the mechanical properties of high pressure die cast magnesium alloy AZ91D. In: Lorimer GW, editor. Proceedings of the Third International Magnesium Conference; 1996 Apr 10-12; Manchester, UK.

[112] Nagasekhar AV, Easton MA, Cáceres CH. Solute content and the grain microstructure of high pressure diecast magnesium–aluminium alloys. Advanced Engineering Materials 2009; 11(11): p. 912-9.

[113] Yang KV, Cáceres CH, Easton MA. A microplasticity-based definition of the skin in HPDC Mg–Al alloys. Materials Science and Engineering A 2013; 580: p. 355-61.

[114] Yang KV, Easton MA, Cáceres CH. The development of the skin in HPDC Mg–Al alloys. Materials Science and Engineering A 2013; 580: p. 191-5.

[115] Pitsaris C, Abbott TB, Davies CHJ, Savage G. Influence of process parameters on the microstructure and mechanical properties of magnesium die castings. In: Kainer KU, editor. Magnesium: Proceedings of the 6th International Conference Magnesium Alloys and Their Applications, Wolfsburg; 2003, p. 695-9.

[116] Chia TL, Easton MA, Zhu SM, Gibson MA, Birbilis N, Nie JF. The effect of alloy composition on the microstructure and tensile properties of binary Mg-rare earth alloys. Intermetallics 2009; 17(7): p. 481-90.

[117] Gjestland H, Westengen H. Advancements in high pressure die casting of magnesium. Advanced Engineering Materials 2007; 9(9): p. 769-76.

[118] Bowles AL, Griffiths JR, Davidson CJ. In: Hryn J, editor. Magnesium Technology 2001, New Orleans: John Wiley & Sons; 2001, p. 161-73.

[119] Shan ZH, Gokhale AM. Utility of micro-indentation technique for characterization of the constitutive behavior of skin and interior microstructures of die-cast magnesium alloys. Materials Science and Engineering A 2003; 361(1): p. 267-74.

[120] Dahle AK, Lee YC, Nave MD, Schaffer PL, StJohn DH. Development of the as-cast microstructure in magnesium–aluminium alloys. Journal of Light Metals 2001; 1(1): p. 61-72.

[121] Laukli HI, Lohne O, Sannes S, Gjestland H, Arnberg L. Grain size distribution in a complex AM60 magnesium alloy die casting. International Journal of Cast Metals Research 2003; 16(6): p. 515-21.

[122] Laukli HI, Gourlay CM, Dahle AK. Migration of crystals during the filling of semi-solid castings. Metallurgical and Materials Transactions A 2005; 36(13): p. 805-18.

[123] Dahle AK, StJohn DH. Rheological behaviour of the mushy zone and its effect on the formation of casting defects during solidification. Acta Materialia 1998; 47(1): p. 31-41.

[124] Mirkovic D, Schmid-Fetzer R. In: Nyberg EA, Agnew SR, Neelameggham NR, Pekguleryuz MO, editors. Magnesium Technology, TMS, New Jersey: John Wiley 7 Sons; 2009, p. 97-100.

[125] Yang KV, Cáceres CH, Easton MA, Gibson MA. The skin effect in a high pressure die cast Mg-RE alloy. Skin 2011; 49(3): p.207-12.

[126] Dahle AK, Sannes S, StJohn DH, Westengen H. Formation of defect bands in high pressure die cast magnesium alloys. Journal of Light Metals 2001; 1(2): p. 99-103.

[127] Gourlay CM, Dahle AK, Laukli HI. Segregation band formation in Al-Si die castings. Metallurgical and Materials Transactions A 2004; 35(9): p. 2881-91.

[128] Otarawanna S, Gourlay CM, Laukli HI, Dahle AK. The thickness of defect bands in high-pressure die castings. Materials Characterization 2009; 60(12): p. 1432-41.

[129] Laukli HI. High pressure die casting of aluminium and magnesium alloys: grain structure and segregation characteristics [dissertation]. Norwegian University of Science and Technology; 2004.

[130] Laukli HI, Graciotti A, Lohne O, Gjestland H, Sannes S. The effect of solidification of metal prior to injection in HPDC on the grain size distribution in a complex die casting. NADCA Trans 2002; 21: p. 1-4.

[131] Campbell J. Complete casting handbook: metal casting processes, techniques and design. 1st ed. UK: Butterworth-Heinemann; 2011.

[132] Campbell J, Clyne TW. Hot tearing in Al-Cu alloys. Cast Metals 1990; 3(4): p. 224-6.

[133] Cao G, Kou S. Hot cracking of binary Mg–Al alloy castings. Materials Science and Engineering A 2006; 417(1): p. 230-8.

[134] Dodd RA, Pollard WA, Meier JW. Hot tearing of magnesium casting alloys. AFS Transactions 1957; 65: p. 110-7.

[135] Cao G, Kou S. Hot tearing of ternary Mg-Al-Ca alloy castings. Metallurgical and Materials Transactions A 2006; 37(12): p. 3647-63.

[136] Cao G, Zhang C, Cao H, Chang YA, Kou S. Hot-tearing susceptibility of ternary Mg-Al-Sr alloy castings. Metallurgical and Materials Transactions A 2010; 41(3): p. 706-16.

[137] Wang Y, Sun B, Wang Q, Zhu Y, Ding W. An understanding of the hot tearing mechanism in AZ91 magnesium alloy. Materials Letters 2002. 53(1): p. 35-9.

[138] Song J, Xiong SM, Li M, Allison J. The correlation between microstructure and mechanical properties of high-pressure die-cast AM50 alloy. Journal of Alloys Compounds 2009; 477(1): p. 863-9.

[139] Song J, Xiong SM, Li M, Allison J. In situ observation of tensile deformation of high-pressure die-cast specimens of AM50 alloy. Materials Science and Engineering A 2009; 520(1): p. 197-201.

[140] Lee SG, Patel GR, Gokhale AM, Sreeranganathan A, Horstemeyer MF. Quantitative fractographic analysis of variability in the tensile ductility of high-pressure die-cast AE44 Mg-alloy. Materials Science and Engineering A 2006; 427(1): p. 255-62.

[141] Eisenmeier G, Holzwarth B, Höppel HW, Mughrabi H. Cyclic deformation and fatigue behaviour of the magnesium alloy AZ91. Materials Science and Engineering A 2001; 319: p. 578-82.

[142] Prakash DGL, Regener D, Vorster WJJ. Microscopic failure modes of hpdc AZ91HP magnesium alloy under monotonic loading. Materials Science and Engineering A 2008; 488(1): p. 303-10.

[143] Horstemeyer MF, Yang N, Gall K, McDowell DL, Fan J, Gullett PM. High cycle fatigue of a die cast AZ91E-T4 magnesium alloy. Acta Materialia 2004; 52(5): p. 1327-36.

[144] Li YB, Wei ZY, Wang ZZ, Li YT. Friction self-piercing riveting of aluminum alloy AA6061-T6 to magnesium alloy AZ31B. Journal of Manufacturing Science and Engineering 2013; 135(6): p. 061007.

[145] Lou M, Li YB, Li YT, Chen GL. Behavior and quality evaluation of electroplastic self-piercing riveting of aluminum alloy and advanced high strength steel. Journal of Manufacturing Science and Engineering 2013; 135(1): p. 011005.

[146] Mori K, Abe Y, Kato T. Self-pierce riveting of multiple steel and aluminium alloy sheets. Journal of Materials Processing Technology 2014; 214(10): p. 2002-8.

[147] Mori K, Kato T, Abe Y, Ravshanbek Y. Plastic joining of ultra high strength steel and aluminium alloy sheets by self piercing rivet. CIRP Annals-Manufacturing Technology 2006; 55(1): p. 283-6.

[148] He XC, Wang YF, Lu Y, Zeng K, Gu FS, Ball A. Self-piercing riveting of similar and dissimilar titanium sheet materials. The International Journal of Advanced Manufacturing Technology 2015; 80: p. 1-11.

[149] Litherland H. Self-piercing riveting for aiuminium applications. In: Ogle MH, Maddox J, Threadgill PL, editors. Joints in Aluminium: INALCO'98, Cambridge: Abington Publishing; 1999, p. 135.

[150] Kochan A. Audi moves forward with all-aluminium cars. Assembly Automation 2000; 20(2): p. 132-5.

[151] Mortimer J. Jaguar uses X350 car to pioneer use of self-piercing rivets. Industrial Robot: An International Journal 2001; 28(3): p. 192-8.

[152] Mortimer J. Jaguar uses castings, extrusions to reduce parts count in new sports car. Assembly Automation 2006; 26(2): p. 115-20.

[153] Atzeni E, Ippolito R, Settineri L. Experimental and numerical appraisal of self-piercing riveting. CIRP Annals-Manufacturing Technology 2009; 58(1): p. 17-20.

[154] Haque R, Williams NS, Blacket SE, Durandet Y. A simple but effective model for characterizing SPR joints in steel sheet. Journal of Materials Processing Technology 2015; 223: p. 225-31.

[155] Haque R, Beynon JH, Durandet Y. Characterisation of force-displacement curve in self-pierce riveting. Science and Technology of Welding and Joining 2012; 17(6): p. 476-88.

[156] Xing B, He X, Wang Y, Yang H, Deng C. Study of mechanical properties for copper alloy H62 sheets joined by self-piercing riveting and clinching. Journal of Materials Processing Technology 2015; 216: p. 28-36.

[157] Chrysanthou A, Sun X, editors. Self-piercing riveting: properties, processes and applications. Cambridge: Woodhead Publishing; 2014.

[158] Wang JW, Liu ZX, Shang Y, Liu LA, Wang MX, Sun RN et al. Self-piercing riveting of wrought magnesium AZ31 sheets. Journal of Manufacturing Science and Engineering 2011; 133(3): p. 031009.

[159] Porcaro R, Hanssen AG, Langseth M, Aalberg A. Self-piercing riveting process: an experimental and numerical investigation. Journal of Materials Processing Technology 2006; 171(1): p. 10-20.

[160] Pekguleryuz MO, Kainer KU, Kaya AA, editors. Fundamentals of magnesium alloy metallurgy, Cambridge: Woodhead Publishing; 2013.

[161] Easton MA, Beer A, Barnett M, Davies C, Dunlop G, Durandet Y et al. Magnesium alloy applications in automotive structures. The Journal of The Minerals, Metals & Materials Society 2008; 60(11): p. 57-62.

[162] Durandet Y, Deam R, Beer A, Song W, Blacket S. Laser assisted self-pierce riveting of AZ31 magnesium alloy strips. Materials & Design 2010; 31: p. S13-S16.

[163] Miyashita Y, Jack Teow YC, Karasawa T, Aoyagi N, Otsuka Y, Mutoh Y. Strength of adhesive aided SPR joint for AM50 magnesium alloy sheets. Procedia Engineering 2011; 10: p. 2532-7.

[164] Luo A, Lee T, Carter J. Self-pierce riveting of magnesium to aluminum alloys. SAE International Journal of Materials and Manufacturing 2011; 4(1): p. 158-65.

[165] Lathabai S, Tyagi V, Ritchie D, Kearney T, Finnin B, Christian S et al. Friction stir blind riveting: a novel joining process for automotive light alloys. SAE International Journal of Materials and Manufacturing 2011; 4(2011-01-0477): p. 589-601.

[166] France LK, Freeman R. Welding and joining of magnesium. In: ATTCE 2001 proceedings, vol. 3. Manufacturing; Spain. Society of Automotive Engineers, Inc. (SAE); 2001. p. 207–11.

[167] Duan HY, Han GK, Wang MX, Zhang XL, Liu ZX, Liu ZY. Rotation friction pressing riveting of AZ31 magnesium alloy sheet. Materials & Design 2014; 54: p. 414-24.

[168] Han GK, Wang MX, Liu ZX, Wang PC. A new joining process for magnesium alloys: Rotation friction drilling riveting. Journal of Manufacturing Science and Engineering 2013; 135(3): p. 031012.

[169] Lu ZJ, Blackmore P. Cyclic stress-strain behaviour of AM60B and AE44 cast magnesium alloys and its impact on LCF characterisation and fatigue analysis. SAE International Journal of Materials and Manufacturing 2014; p. 446-53.

[170] Mann GE, Sumitomo T, Cáceres CH, Griffiths JR. Reversible plastic strain during cyclic loading–unloading of Mg and Mg–Zn alloys. Materials Science and Engineering A 2007; 456(1): p. 138-46.

[171] Cáceres CH, Sumitomo T, Veidt M. Pseudoelastic behaviour of cast magnesium AZ91 alloy under cyclic loading–unloading. Acta Materialia 2003; 51(20): p. 6211-8.

[172] Nagarajan D. Anelasticity in cast Mg-Gd alloys. Materials Science and Engineering A 2017; 695: p. 14-9.

[173] Nagarajan D, Ren X, Cáceres CH. Anelastic behavior of Mg-Al and Mg-Zn solid solutions. Materials Science and Engineering A 2017; 696: p. 387-92.

[174] Sumitomo T, Cáceres CH, Veidt M. The elastic modulus of cast Mg–Al–Zn alloys. Journal of Light Metals 2002; 2(1): p. 49-56.

[175] Sumitomo T. Elastic and pseudoelastic behaviour of Mg-Al-Zn alloys [dissertation]. University of Queensland; 2003.

[176] Yang KV, Cáceres CH, Tomé CN. The elasto-plastic transition in magnesium alloys. In: Mathaudhu SN, Sillekens WH, Neelameggham NR, Hort N, editors. Magnesium Technology 2012: Proceedings of the TMS (The Minerals, Metals & Materials Society); 2012 Mar 11-15; Orlando, Florida; p. 127-131.

[177] Yang KV, Cáceres CH, Nagasekhar AV, Easton MA. Low-strain plasticity in a high pressure die cast Mg–Al alloy. Modelling and Simulation in Materials Science and Engineering 2012; 20(2): p. 024010.

[178] ISO 6892-1 metallic materials tensile testing-part 1: method of test at room temperature. International Standards Organisation; 2009.

[179] ASTM Standard E8M-09 standard test methods for tension testing of metallic materials in annual book of ASTM standards, ASTM. West Conshohocken PA: American Society for Testing and Materials; 2009.

[180] Gu GY, Lin ST, Xia Y, Zhou Q. Experimental study on influence of section thickness on mechanical behavior of die-cast AM60 magnesium alloy. Materials and Design 2012; 38: p. 124-32.

[181] Qi MF, Kang YL, Yang Y, Zhu GM, Liao WN. Comparison of microstructure and mechanical properties of AZ91D alloy formed by rheomolding and high-pressure die casting. Journal of Materials Engineering and Performance 2015; 24(10): p. 3826-34.

[182] Akhtar A, Teghtsoonian E. Solid-solution hardening in magnesium alloys. Materials Transactions (Japan Institute of Metals) 1968; 9: p. 692-7.

[183] Wang H, Wu PD, Tomé CN, Wang J. A constitutive model of twinning and detwinning for hexagonal close packed polycrystals. Materials Science and Engineering A 2012; 555: p. 93-8.

[184] Duerig TW, Zadno R. An engineer's perspective of pseudoelasticity. In: Duerig TW, Melton KN, Stöckel D, editors. Engineering aspects of shape memory alloys, 1st ed, UK: Butterworth-Heinemann; 1990, p. 369-93.

[185] Muránsky O, Carr DG, Šittner P, Oliver EC. In situ neutron diffraction investigation of deformation twinning and pseudoelastic-like behaviour of extruded AZ31 magnesium alloy. International Journal of Plasticity 2009; 25(6): p. 1107-27.

[186] Gharghouri MA, Weatherly GC, Embury JD, Root J. Study of the mechanical properties of Mg-7.7 at.% Al by in-situ neutron diffraction. Philosophical Magazine A 1999; 79(7): p. 1671-95.

[187] Lee SY, Gharghouri MA. Pseudoelastic behavior of magnesium alloy during twinning-dominated cyclic deformation. Materials Science and Engineering A 2013; 572: p. 98-102.

[188] Nagarajan D, Cáceres CH, Griffiths JR. Anelastic phenomena in Mg-Al alloys. Proceedings of the 12th International Symposium on Physics of Materials; 2011 Sep 4-8; Prague. Czech Republic: Polish Academy of Sciences Institute of Physics; 2012. p. 501-4.

[189] Reed-Hill RE, Dahlberg EP, Slippy Jr WA. Some anelastic effects in Zirconium at room temperature resulting from prestrain at 77 deg K. Transactions of the Metallurgical Society of AIME 1965; 233: p. 1766-71.

[190] Jones ERW, Munro W. The “elastic hysteresis” of uranium. Journal of the Mechanics and Physics of Solids 1953; 1(3): p. 182-8.

[191] Rogueda C, Lexcellent C, Bocher L. Experimental study of pseudoelastic behaviour of a CuZnAl polycrystalline shape memory alloy under tension-torsion proportional and non-proportional loading tests. Archives of Mechanics 1996; 48(6): p. 1025-45.

[192] Otsuka K, Wayman CM, Nakai K, Sakamoto H, Shimizu K. Superelasticity effects and stress-induced martensitic transformations in Cu-Al-Ni alloys. Acta Metallurgica 1976; 24(3): p. 207-26.

[193] Perkins J, Sponholz RO. Stress-induced martensitic transformation cycling and two-way shape memory training in Cu-Zn-Al alloys. Metallurgical Transactions A 1984; 15(2): p. 313-21.

[194] Mann GE. Effect of solute concentration on the low strain behaviour and Hall-Petch relationship of cast Mg-Zn alloys [dissertation]. University of Queensland; 2006.

[195] Pérez-Prado MT, Del Valle JA, Contreras JM, Ruano OA. Microstructural evolution during large strain hot rolling of an AM60 Mg alloy. Scripta Materialia 2004; 50(5): p. 661-5.

[196] Easton MA, Song WQ, Abbott TB. A comparison of the deformation of magnesium alloys with aluminium and steel in tension, bending and buckling. Materials and Design 2006; 27(10): p. 935-46.

[197] Altenhof W, Raczy A, Laframboise M, Loscher J, Alpas A. Numerical simulation of AM50A magnesium alloy under large deformation. International Journal of Impact Engineering 2004; 30(2): p. 117-42.

[198] Dørum C, Hopperstad OS, Lademo O-G, Langseth M. Numerical modelling of the structural behaviour of thin-walled cast magnesium components. International Journal of Solids and Structures 2005; 42(7): p. 2129-44.

[199] Gharghouri M. Study of the mechanical properties of Mg-8.5 wt% Al by in-situ neutron diffraction [dissertation]. McMaster University; 1996.

[200] Clark JB. Age hardening in a Mg-9 wt.% Al alloy. Acta Metallurgica 1968; 16(2): p. 141-52.

[201] Robson JD, Stanford N, Barnett MR. Effect of precipitate shape on slip and twinning in magnesium alloys. Acta Materialia 2011; 59(5): p. 1945-56.

[202] Robson JD, Stanford N, Barnett MR. Effect of particles in promoting twin nucleation in a Mg–5wt.% Zn alloy. Scripta Materialia 2010; 63(8): p. 823-6.

[203] Stanford N, Barnett MR. Effect of particles on the formation of deformation twins in a magnesium-based alloy. Materials Science and Engineering A 2009; 516(1): p. 226-34.

[204] Nagarajan D. Grain size hardening effects in Mg and its alloys [dissertation]. University of Queensland; 2014.

[205] Cáceres CH, Blake A. The strength of concentrated Mg–Zn solid solutions. Physica Status Solidi (a) 2002; 194(1): p. 147-58.

[206] Cáceres CH, Rovera DM. Solid solution strengthening in concentrated Mg–Al alloys. Journal of Light Metals 2001; 1(3): p. 151-6.

[207] Li B, Kadiri HEI, Zhang XY, Mathaudhu SN, Ma Q. Structural origin of reversible twinning, non-schmid effect, incoherent twin boundaries and texture of hexagonal close-packed metals. In: Mathaudhu SN, Sillekens WH, Neelameggham NR, Hort N, editors. Magnesium Technology 2012: Proceedings of the TMS (The Minerals, Metals & Materials Society); 2012 Mar 11-15; Orlando, Florida; p. 105-10.

[208] Kelly A, Groves GW, Kidd P. Crystallography and crystal defects. New Jersey: John Wiley & Sons; 2000.

[209] Cahn JW. Thermodynamic and structural changes in deformation twinning of alloys. Acta Metallurgica 1977; 25(9): p. 1021-6.

[210] Kaschner GC, Tomé CN, Beyerlein IJ, Vogel SC, Brown DW, McCabe RJ. Role of twinning in the hardening response of zirconium during temperature reloads. Acta Materialia 2006; 54(11): p. 2887-96.

[211] Klimanek P, Pötzsch A. Microstructure evolution under compressive plastic deformation of magnesium at different temperatures and strain rates. Materials Science and Engineering A 2002; 324(1): p. 145-50.

[212] Cáceres CH, Lukáč P, Blake A. Strain hardening due to {1012} twinning in pure magnesium. Philosophical Magazine 2008; 88(7): p. 991-1003.

[213] Kocks UF. The relation between polycrystal deformation and single-crystal deformation. Metallurgical and Materials Transactions 1970; 1(5): p. 1121-43.

[214] Kocks UF, Mecking F. Physics and phenomenology of strain hardening: the FCC case. Progress in Materials Science 2003; 48(3): p. 171-273.

[215] Cáceres CH, Blake AH. On the strain hardening behaviour of magnesium at room temperature. Materials Science and Engineering A 2007; 462(1): p. 193-6.

[216] Mecking H, Kocks UF. Kinetics of flow and strain-hardening. Acta Metallurgica 1981; 29(11): p. 1865-75.

[217] Lavrentev FF, Pokhil YA. Relation of dislocation density in different slip systems to work hardening parameters for magnesium crystals. Materials Science and Engineering 1975; 18(2): p. 261-70.

[218] Mecking H. Description of hardening curves of fcc single-and polycrystals. Proceedings of the conference on radiation damage in metals; 1975 Nov 9; Cincinnati, Ohio.

[219] Devincre B, Hoc T, Kubin L. Dislocation mean free paths and strain hardening of crystals. Science 2008; 320 (5884): p. 1745-8.

[220] Cáceres CH, Lukáč P. Strain hardening behaviour and the Taylor factor of pure magnesium. Philosophical Magazine 2008; 88(7): p. 977-89.

[221] Meyers MA. Dynamic behavior of materials. New Jersey: John wiley & sons; 1994.

[222] Karimi E, Zarei-Hanzaki A, Pishbin MH, Abedi HR, Changizian P. Instantaneous strain rate sensitivity of wrought AZ31 magnesium alloy. Materials and Design 2013; 49: p. 173-80.

[223] Lee WS, Chen TH. Rate-dependent deformation and dislocation substructure of Al–Sc alloy. Scripta Materialia 2006; 54(8): p. 1463-8.

[224] Stanford N, Sabirov I, Sha G, La Fontaine A, Ringer SP, Barnett MR. Effect of Al and Gd solutes on the strain rate sensitivity of magnesium alloys. Metallurgical and Materials Transactions A 2010; 41(3): p. 734-43.

[225] Del Valle JA, Ruano OA. Influence of the grain size on the strain rate sensitivity in an Mg–Al–Zn alloy at moderate temperatures. Scripta Materialia 2006; 55(9): p. 775-8.

[226] Newland CA, Murray MT. Strain rate dependent behaviour of magnesium-based alloys. Proceedings of the First Australasian Congress on Applied Mechanics; 1996 Feb 21-23; Melbourne, Australia. Australia: Institution of Engineers; 1996.

[227] Aune TK, Albright D, Westengen H, Johnsen TE, Andersson B. Behavior of die cast magnesium alloys subject to rapid deformation. Transactions Journal of Materials and Manufacturing 2000; 109(5): p. 1-7.

[228] Song WQ, Beggs P, Easton MA. Compressive strain-rate sensitivity of magnesium–aluminum die casting alloys. Materials and Design 2009; 30(3): p. 642-8.

[229] Abdul Latif N, Sajuri Z, Junaidi S, Miyashita Y, Mutoh Y. Effect of strain rate on tensile and work hardening properties for Al-Zn magnesium alloys. International Journal of Materials Engineering Innovation 2014; 5(1): p. 28-37.

[230] Lin XZ, Chen DL. Strain hardening and strain-rate sensitivity of an extruded magnesium alloy. Journal of Materials Engineering and Performance 2008; 17(6): p. 894-901.

[231] Wang HY, Xue ES, Nan XL, Yue T, Wang YP, Jiang QC. Influence of grain size on strain rate sensitivity in rolled Mg–3Al–3Sn alloy at room temperature. Scripta Materialia 2013; 68(5): p. 229-32.

[232] Gu GY, Lin ST, Meng Y, Xia Y, Zhou Q. Influence of strain rate and stress state on the mechanical behavior of die-casting AM60 magnesium alloy. Proceedings of the ASME 2011 International Mechanical Engineering Congress and Exposition; 2011 Nov 11-17; Denver, Colorado. New York: ASME; 2012.

[233] Tahreen N, Chen DL, Nouri M, Li DY. Effects of aluminum content and strain rate on strain hardening behavior of cast magnesium alloys during compression. Materials Science and Engineering A 2014; 594: p. 235-45.

[234] Xu S, Tyson WR, Bouchard R, Gertsman VY. Effects of strain rate and temperature on tensile flow behavior and energy absorption of extruded magnesium AM30 alloy. Journal of Materials Engineering and Performance 2009; 18(8): p. 1091-101.

[235] Zhu SM, Easton MA, Abbott TB, Gibson MA, Nie JF. The influence of individual rare earth elements (La, Ce, or Nd) on creep resistance of die-cast magnesium alloy AE44. Advanced Engineering Materials 2016; 18 (6): p. 932-7.

[236] Weiler JP, Wood JT. Strain-rate effects of sand-cast and die-cast magnesium alloys under compressive loading. In: Mathaudhu SN, Sillekens WH, Neelameggham NR, Hort N, editors. Magnesium Technology 2012: Proceedings of the TMS (The Minerals, Metals & Materials Society); 2012 Mar 11-15; Orlando, Florida; p. 365-370.

[237] Ahmad IR, Shu DW. Tensile properties of die-cast magnesium alloy AZ91D at high strain rates in the range between 300 s^{-1} and 1500 s^{-1}. Applied Mechanics and Materials, Trans Tech Publ 2010; 24-25: p. 325-30.

[238] Leng Z, Pan HJ, Niu ZY, Guo CH, Zhang Q, Chang YP et al. Mechanical behavior, deformation and damage mechanisms of Mg–RY–Zn alloy under high strain rate. Materials Science and Engineering A 2016; 651: p. 336-40.

[239] Guo CH, Jiang FC, Wu RZ, Zhang ML. Effect of strain rate on compressive mechanical properties of extruded Mg–8Li–1Al–1Ce alloy. Materials and Design 2013; 49: p. 110-5.

[240] Matsunaga T, Somekawa H, Hongo H,Tabuchi M. Deformation mechanism transition with strain rate in Mg–3Al–1Zn alloy at room temperature. Materials Science and Engineering A 2015; 647: p. 212-5.

[241] Carlson BE. The effect of strain rate and temperature on the deformation of die cast AM60B. Transactions Journal of Materials and Manufacturing 1995; p. 950425.

[242] Cepeda-Jiménez CM, Molina-Aldareguia JM, Pérez-Prado MT. Origin of the twinning to slip transition with grain size refinement, with decreasing strain rate and with increasing temperature in magnesium. Acta Materialia 2015; 88: p. 232-44.

[243] Zhou Q, Li JJ, Wang F, Huang P, Xu KW, Lu TJ. Strain rate sensitivity of Cu/Ta multilayered films: Comparison between grain boundary and heterophase interface. Scripta Materialia 2016; 111: p. 123-6.

Chapter 3

Experimental Techniques & Procedures

This chapter discusses the experimental techniques, procedures and analyses used in this research. This includes the preparation, characterisation, and mechanical testing of commercial high-pressure die-cast magnesium alloys AM40 (Mg-4Al-0.3Mn), AM60 (Mg-6Al-0.3Mn), AZ91 (Mg-9Al-1Zn) and AE44 (Mg-4Al-4RE). Some AE44 specimens were subject to heat treatment to produce a precipitation-hardened structure. Scanning electron microscopy and optical microscopy were used to characterise the microstructure before and after testing. Monotonic and cyclic tension loading-unloading tests were performed to study the deformation behaviour at various strain rates.

3.1 Experimental Materials

Magnesium alloys used in this research were cast at Commonwealth Scientific and Industrial Research Organisation (CSIRO) using a 250 tonne Toshiba cold chamber high-pressure die-cast (HPDC) machine. The nominal compositions of these alloys are given in Table 3.1 and measured compositions of the alloys using inductively coupled plasma atomic emission spectroscopy (ICP-AES) are given in Table 3.2. All compositions are in weight percent (wt.%). The selection of these alloys was influenced by their use as commercial alloys. The casting parameters are given in Table 3.3, although they may vary during each casting operation.

Table 3.1: Nominal compositions (wt.%) of magnesium alloys utilised in this study.

Alloy	Mg	Al	Mn	Zn	RE (Ce + La)
AM40	Bal.	4	0.2	-	-
AM60	Bal.	6	0.3	-	-
AZ91	Bal.	9	-	1	-
AE44	Bal.	4	-	-	4

Table 3.2: Measured compositions (wt.%) by (ICP-AES).

Alloy	Mg	Al	Mn	Zn	RE (Ce + La)
AM40	Bal.	4.44	0.21	0.05	<0.01
AM60	Bal.	6.26	0.29	0.1	<0.01
AZ91	Bal.	8.88	0.19	0.74	<0.01
AE44	Bal.	3.67	0.31	<0.01	2.5 + 1.33

Table 3.3: Casting parameters for HPDC magnesium alloys in this research.

Casting Parameter	Parameter Value
Melt Temperature	740 °C
Oil Heaters in Both Halves of the Die	250 °C
Accumulator Pressure	110 kg/cm^2
Ram Velocities, Slow Speed	Approximately 0.36 ms^{-1}
Ram Velocities, High Speed	Approximately 2.2 ms^{-1}
Average Die Fill Time	600 ms
Die Open Time	4 s

The alloys were cast into a 3-cavity test bar die, consisting of two “dog-bone” shaped tensile bars and one flat test specimen as shown in Figure 3.1. Round “dog-bone” tensile bar has a nominal diameter of 5.6 mm in the gauge length section and flat “dog-bone” shaped tensile bar has a thickness of 3 mm. The dimensions for round and flat specimens are shown in Figure 3.2 (a) and (b) respectively.

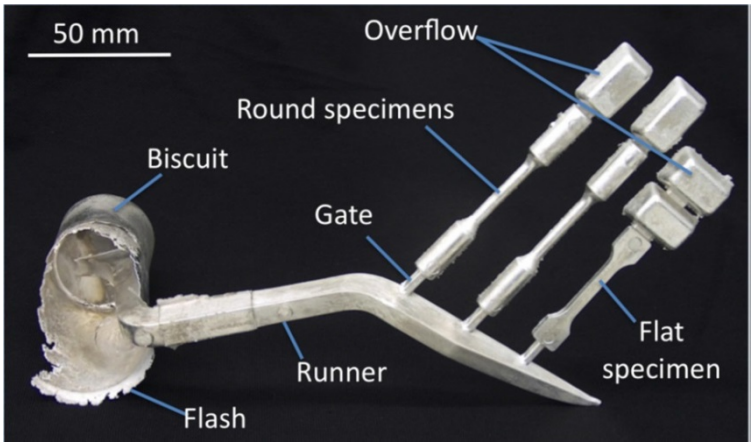

Figure 3.1: A HPDC casting showing two round and one flat tensile samples [1].

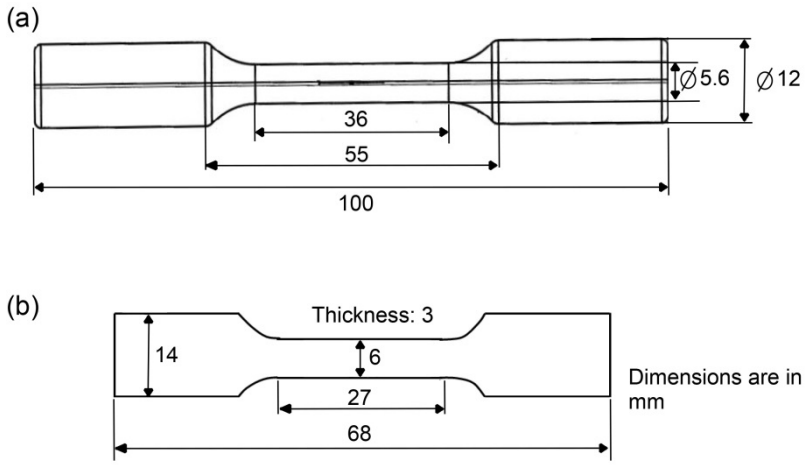

Figure 3.2: Schematic diagrams of (a) round and (b) flat "dog-bone" shaped tensile bars. All dimensions are in mm.

3.1.1 Heat Treatment for AE44

Some AE44 specimens were aged in silicon oil bath at 200 °C for 32 h (labelled T5) without applying a prior solution treatment. This ageing temperature was chosen because it is the typical temperature experienced during coating and painting for magnesium parts in automotive vehicles. HPDC alloys are generally non-heat-treatable because the trapped gas pores can expand during heat treatment process, causing surface blistering and bulk distortion of cast products [2]. Besides, die-cast magnesium-aluminium-rare earth alloys are supposed to be used in the as-cast condition without the application of any heat treatment because it has been taken for granted that heat treatment will not provide benefit to these alloys. However, ageing treatment at 200 °C for 32 h on magnesium-aluminium-rare earth alloy which contains minor manganese addition has been observed to produce significant age hardening as a result of precipitation of nanoscale aluminium-manganese particles without a significant loss in elongation to failure [3]. This interesting finding led to the T5 treatment on AE44 alloy which has 0.3 wt.% manganese in order to investigate the effect of ageing on strain-rate sensitivity in this research. It should be noted that the AE44 specimens did not show any signs of surface blistering or dimensional change after T5 treatment. After T5 treatment, AE44 samples were quenched in a large bucket filled with room-temperature water for convenience. Quenching is not a critical operation in T5.

3.2 Sample Preparation

Electron backscattered diffraction (EBSD) was extensively involved in this research to quantify the types of twins in HPDC magnesium alloys subjected to tensile testing at varying strain rates. A problem arises when the standard polishing procedures for optical microscopy does not necessarily result in a satisfactory surface quality for EBSD. On many occasions, a magnesium alloy specimen was polished to a good surface finish when observed under optical microscopy or scanning electron microscopy (SEM), yet failed to provide a satisfactory EBSD kikuchi pattern. When this occurs, the only solution is to remove the specimen from the SEM vacuum chamber and repolish the surface again. Achieving good surface finishing for EBSD is time-saving in this research. This section summarises the key steps of metallographic preparation procedures, which are cutting, mounting, grinding and polishing, with special attention paid to achieving a satisfactory surface quality for EBSD analysis.

3.2.1 Cutting and Mounting

Samples for SEM/EBSD were cut from the gauge sections of the tensile test specimens and sliced along the planes containing the loading direction using a low speed saw, Figure 3.3. The cutting speeds were always kept to the minimum to avoid introducing any unnecessary twins. The cut specimen was approximately 10 mm long. After cutting, the samples were cold mounted using epoxy resin and hardener with a mixing ratio: 15 parts of resin to 2 parts of hardener. Some cold-mounted samples of magnesium alloys are shown in Figure 3.4. The samples were left to harden in room temperature for one day. Hot mounting was not used in this study in order to prevent any possible microstructural change due to the effect of temperature during sample preparation.

Figure 3.3: Struers Secotom cut-off machine for low speed cutting of magnesium specimens.

Figure 3.4: Cold-mounted magnesium alloys.

3.2.2 Grinding and Polishing

Cold-mounted magnesium samples were manually ground with silicon carbide paper (SiC) with a grit number of 600, with successively finer grit, and finishing at 2400 grit paper at 150 rpm using a Struers RotoForce-21 grinder and polisher machine as shown in Figure 3.5. Each grinding step was first performed by counter rotating grind to remove the prior surface deformation layer generated by the previous grinding step, followed by several turns of static grinding. This static grinding step is to ensure a scratch free, flat surface when the scratches are all marked in same direction. Typically, each grinding step was performed for at least 1 minute or until surface was flat and previous scratches disappeared. An alcohol-based brown lubricant was used to ensure cooling in each grinding step. Automatic grinding was not used because magnesium alloys grind quickly due to their softness, therefore the time and effort-saving aspects of the automated method are not important.

Figure 3.5: Struers RotoForce-21 grinder and polisher machine.

After 2400-grit grinding, samples were polished using the same polisher machine in Figure 3.5. Automatic polishing was carried out first with 3-µm diamond suspension for 7 minutes followed by 1-µm diamond suspension for 3 minutes at 150 rpm on Struers micro polishing cloths, Mol cloth and Nap cloth, respectively. Samples were rotated in the same direction as wheel rotation during polishing. All diamond polishing suspensions used were alcohol-based (DP-Suspension A). An alcohol-based yellow lubricant was also used during these polishing steps to ensure correct cooling of the sample surface. The lubricants and diamond suspensions used are shown in Figure 3.6.

Figure 3.6: Struers lubricants and diamond suspensions used in grinding and polishing steps.

Final polishing is the most critical step in the entire process. For final polishing, 0.05-µm non-drying colloidal silica suspension was used on Struers neoprene polishing cloth

(Chem cloth) and specimen was rotated counter to the wheel direction. To avoid over-etching, ethanol was used as lubricant and the final polishing step should not take longer than 2 minutes. Details of grinding and polishing steps are summarised in Table 3.4. These polishing procedures are purely based on trials for HPDC magnesium alloys, and are not related to the recommendations suggested by the manufacturer.

Table 3.4: Grinding and polishing steps for HPDC magnesium alloys.

Step	Paper or Disc	Lubricant	Speed (rpm)	Rotation Direction (Sample to Disc)	Time (min)	Load (N)
1 (Grinding)	SiC 600	Alcohol-based Brown Lubricant	150	-	1	-
2 (Grinding)	SiC 2400					
3 (3-µm Polishing)	Mol	Alcohol-based Yellow Lubricant		With	7	15
4 (1-µm Polishing)	Nap				3	
5 (0.05-µm Final Polishing)	Chem	Ethanol		Opposite	2	

After each grinding and polishing step, the samples were immediately cleaned with ethanol and dried with compressed air. It should be noted that water is strictly prohibited at any grinding and polishing stages to avoid etching effect. Surfaces of magnesium alloys corrode very quickly when exposed to water. After final polishing, samples were stored in a vacuum desiccator (Figure 3.7) to minimize surface degradation because magnesium, if left unprotected, develops a hydroxide film [4]. Care was taken to prepare samples as close as possible to the time at which EBSD analysis was conducted.

Figure 3.7: Vacuum desiccator connected to vacuum pump.

3.2.2.1 Issues with 0.05-µm Colloidal Silica Final Polishing

There are several factors that could result in poor EBSD results. One of the most common issues is surface damage caused by the 0.05-µm colloidal silica during final polishing. Colloidal silica is reactive to ethanol, and cannot be washed off easily. Having a slight film of silica residue sticking on the sample surface, as shown in Figure 3.8, could result in strong charging of electron beam and poor EBSD contrast.

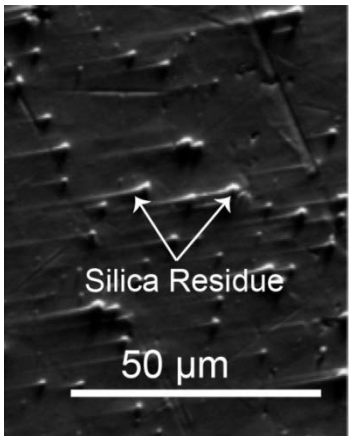

Figure 3.8: Backscattered SEM image showing surface damage caused by colloidal silica residue.

To avoid this issue, immediately after final polishing, the polishing pad (Chem cloth) was scrubbed quickly with ethanol until no silica residue was visible. This was then followed by a short polish with ethanol (less than 10 seconds) to wash off the residue on the specimen surface.

From this stage, the specimen was handled with laboratory gloves to prevent contamination. Care should also be taken when ultrasonic cleaning magnesium specimen in ethanol to remove any excess silica residue that is still embedded on the specimen. Ultrasonic cleaning of 90 seconds is recommended; any longer exposure to ultrasonic cleaning will not be beneficial, since ethanol inevitably contains some water content and therefore causes corrosion. Failure to perform the above workflow properly usually resulted in poor specimen preparation, either by surface oxidation or colloidal silica residue, in both cases causing excessive charging of the specimen surface under SEM, leading to poor EBSD results.

3.3 Microstructural Characterisation

Optical microscopy and SEM equipped with energy dispersive X-ray spectrometer (EDX) and EBSD detectors were used to examine and characterise the microstructure of the alloys in as-cast condition as well as following tensile testing in this research. This includes:

1) Examination and quantification of twinned area fraction in as-cast and deformed samples (optical microscopy and EBSD);
2) Determination of grain orientation and grain size (EBSD);
3) Characterisation of intermetallic phases and morphologies (SEM and EDX);
4) Confirmation of aluminium solute level in magnesium matrix (EDX);
5) Examination of fracture surfaces (SEM).

3.3.1 Optical Microscopy

Optical microscopy was used for general microstructure observations due to its large field of view. This was performed on a Leica optical microscope as shown in Figure 3.9 consisting of a 10× eye piece, five different object lenses with magnifications of 5×, 10×, 20×, 50×, and 100×, a high resolution digital camera, and a high performance computer to carry out detailed analysis. Image analyses were subsequently performed using Image J software, such as to obtain the area fraction of various phases.

Figure 3.9: Leica optical microscope.

3.3.2 Scanning Electron Microscopy (SEM)

Prior to SEM, the samples were thoroughly dried as the scanning electron microscope operates with a vacuum chamber. Both FEI Quanta 200 ESEM and FEI Nova NanoSEM equipped with EDX and EBSD as shown in Figure 3.10 (a) and (b) respectively, were used. Generally, surface finish for optical microscopy is also good for SEM observation. But due to the non-conducting nature of the cold-mounted samples, conductive double-sided adhesive sheets were used to connect the polished sample surface to the epoxy resin. In the SEM, β-secondary phases present as bright and α-magnesium matrix appears dark. For imaging, a typical working distance of 5-10 mm with an accelerating voltage of 15-30 kV, and spot size of 5-6 were utilized for the majority of the microstructural investigations depending on the magnification used. Backscattered electron (BSE) mode was also used to enhance the colour contrast.

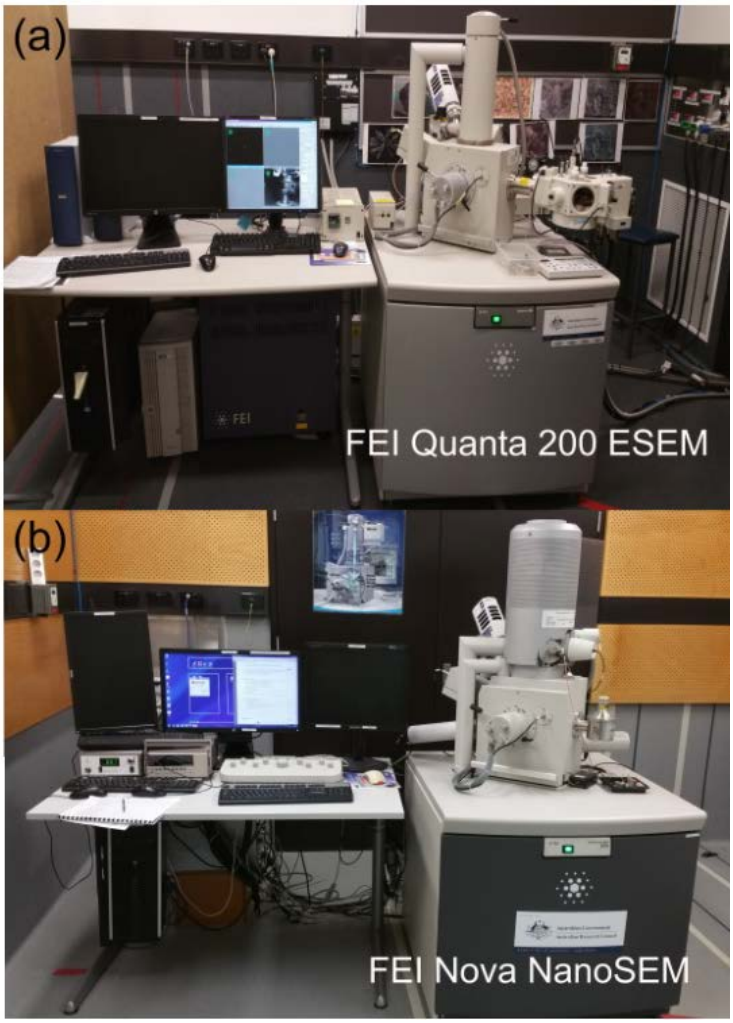

Figure 3.10: Scanning electron microscopes used in the current research. (a) FEI Quanta 200 ESEM and (b) FEI Nova NanoSEM.

3.3.2.1 Energy Dispersive X-ray Spectroscopy (EDX)

EDX was employed to determine the composition of different phases present in eutectic using Aztec software. During EDX measurement, the dead time was usually maintained between 25%-35% and the input count (number of x-rays detected in cps) was maintained about 1000 in order to get good statistical data. This can be controlled by changing the spot size. To measure the aluminium solute level in the α-magnesium matrix, at each sample location, a minimum of 150 points were taken in the magnesium matrix with a spacing of 0.1 µm between each point using EDX line scan. EDX line scan was taken with a holding time of 30 minutes to ensure significant counts above the background. Five locations were analysed for each sample. EDX point scan was sometimes utilized and was taken with a live time of minimum 200 seconds. Figure 3.11 shows the EDX line scan of alloys used in this research.

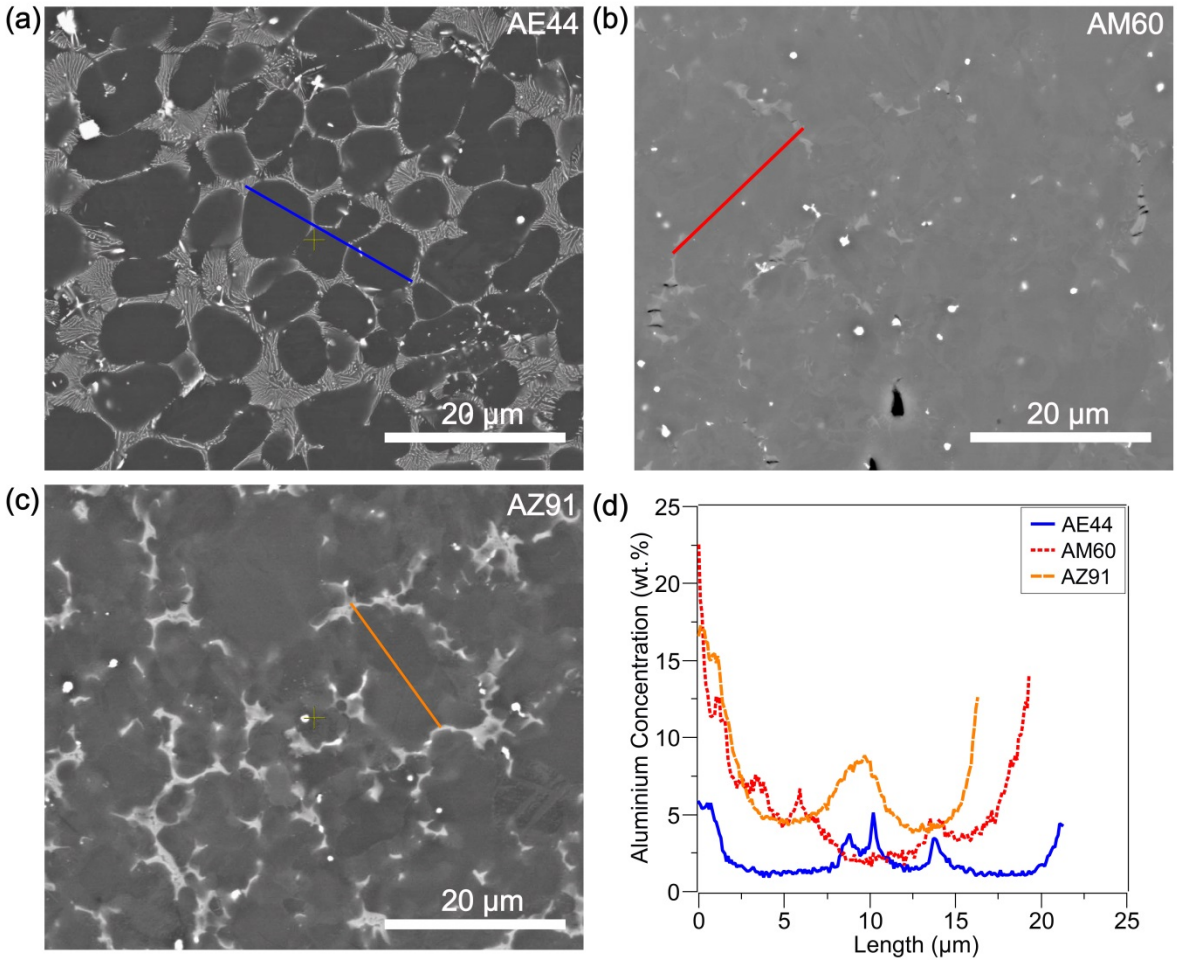

Figure 3.11: Backscattered SEM micrographs and EDX line profiles of the α-magnesium matrix in (a) AE44, (b) AM60 and (c) AZ91. The aluminium concentration (wt.%) across the regions indicated in the SEM micrographs is shown in (d).

3.3.2.2 Electron Backscattered Diffraction (EBSD)

EBSD is a microstructural-crystallographic technique used to examine the crystallographic orientation of the materials. In this study, EBSD measurement was carried out on FEI Nova NanoSEM, Figure 3.10 (b), with an accelerating voltage of 20 kV, together with a working distance of 7-10 mm and a sample tilt angle of 70°. During EBSD mapping, a step size of 0.5 µm was used and a magnification was chosen to allow at least 100 grains to be present in each EBSD scanning window.

EBSD data obtained from Aztec software were then analysed by the acquisition software HKL Channel 5. First, a clean-up procedure was employed in which the orientation of mis-indexed or un-indexed point was replaced with one of its neighbors only if the

orientations of at least six neighbors among eight were alike. With the help of this software, orientation of the crystal can be exactly determined. Apart from the orientation, some other information, for instance, grain/phase boundaries, twin boundaries, and average grain size can also be acquired from the EBSD results. To determine the average grain size, a minimum of 5 EBSD maps were used per alloy and the average grain size was determined from a combination of all maps. Line and circular intercept methods following ASTM standard [5] were also used to confirm the grain size. The die-cast magnesium alloys used in this research have comparable grain sizes of approximately 8 μm, although there is a substantial variation in grain size across the microstructure as shown in Figure 3.12. Twinning types were also identified and quantified based on the misorientation angle and axis relationship between twin and matrix using the acquisition software HKL Channel 5, following EBSD mapping. They are $\{10\bar{1}2\}$ twins (i.e. 86° $<12\bar{1}0>$), $\{10\bar{1}1\}$ twins (i.e. 56° $<12\bar{1}0>$), $\{10\bar{1}3\}$ twins (i.e. 64° $<12\bar{1}0>$), $\{10\bar{1}3\}$-$\{10\bar{1}2\}$ twins (i.e. 22° $<12\bar{1}0>$) and $\{10\bar{1}1\}$-$\{10\bar{1}2\}$ twins (i.e. 38° $<12\bar{1}0>$) [6-8].

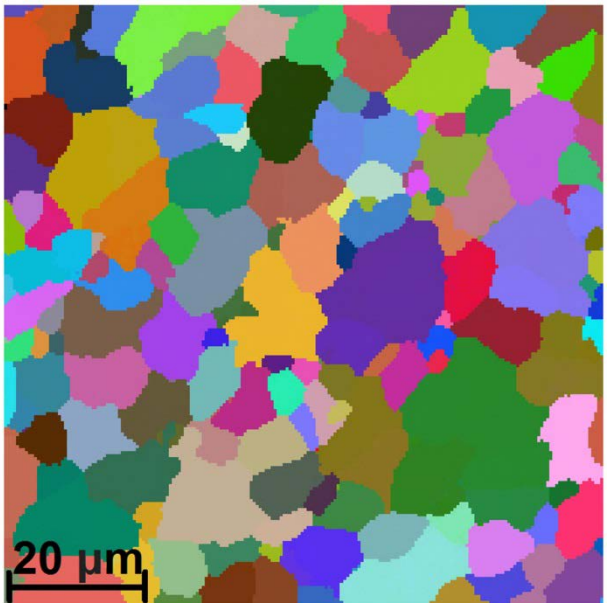

Figure 3.12: EBSD map of as-cast AE44.

3.4 Mechanical Testing

Two types of mechanical tests were conducted: monotonic tension test and cyclic tension loading-unloading test. Both tests were conducted on Instron 5569 with a 50 kN load cell as shown in Figure 3.13. Specimens were mounted using v-grips to align the specimens

with loading axis to minimise the likelihood of any bending during loading. Specimen protect of 2N was enabled to ensure the force on the specimen remains within this pre-set bounds during set-up. The extension of the tensile specimen was measured using an Epsilon 25-mm extensometer with a +50% / -10% measuring range.

Figure 3.13: Instron 5569 Universal Testing Machine.

3.4.1 Monotonic Tension Testing

Monotonic tension testing was performed at wide strain-rate range 10^{-6}-10^{-1} s^{-1} at room temperature. No further higher strain rates can be achieved due to the limitation of the machine. Three samples were tested for each alloy to ensure reproducibility; and the results did not deviate significantly between the three tests. Average of these results was used to compare the key tensile properties such as proof strength, tensile strength and ductility (elongation to failure). Tensile flow curves at strain rate of 10^{-4} s^{-1} for die-cast magnesium alloys used in this research are shown in Figure 3.14. Consistent with literature [9], alloys with higher strength have lower elongation to failure. However, it is interesting to see that the improvement in strength after T5-ageing in AE44 is not accompanied by a loss in elongation in failure. Proof strength was determined by taking both the 0.2% and 0.5% offsets for each stress-strain curve. Necking was not observed in these alloys and tensile strength is also the stress at fracture. The key tensile properties are tabulated in Table 3.5.

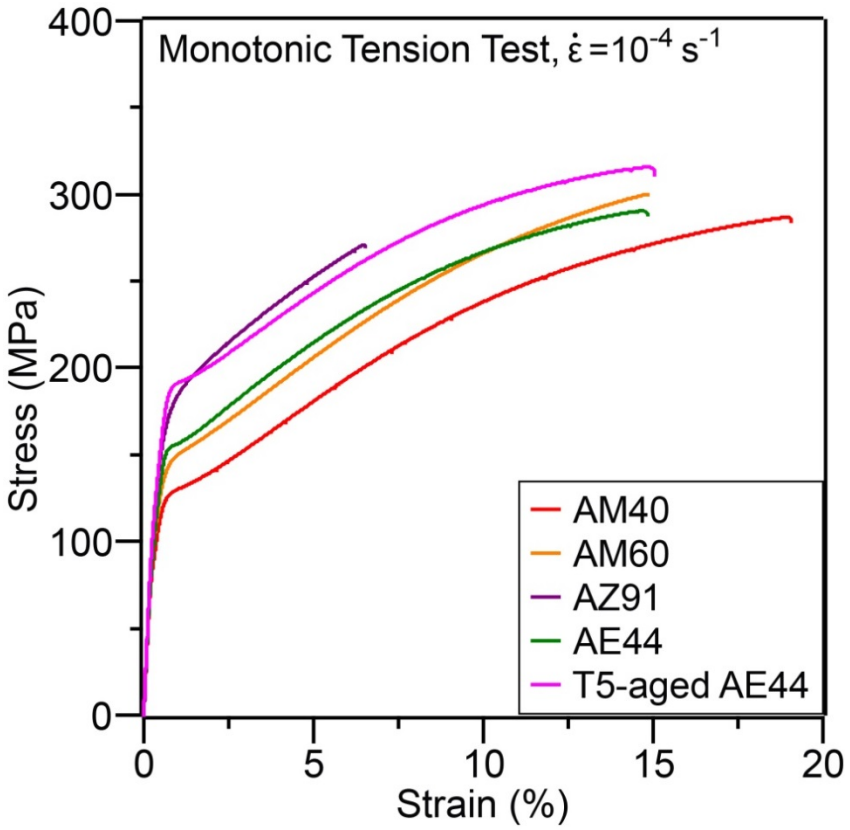

Figure 3.14: Room-temperature monotonic tensile curves of die-cast magnesium alloys AM40, AM60, AZ91, AE44 and T5-aged AE44 at strain rate, $\dot{\varepsilon}$ of 10^{-4} s^{-1}.

Table 3.5: Room-temperature tensile properties of die-cast magnesium alloys at strain rate, $\dot{\varepsilon}$ of 10^{-4} s^{-1}.

Alloy	0.2% Proof Strength (MPa)	0.5% Proof Strength (MPa)	Tensile Strength (MPa)	Elongation to Failure (%)
AM40	110±1.0	128±0.3	290±2.5	19.6±0.6
AM60	126±1.0	147±0.3	302±2.0	15.1±0.3
AZ91	155±0.5	181±0.5	262±9.5	5.90±0.6
AE44	135±0.5	157±1.5	283±8.5	13.0±1.7
T5-aged AE44	168±2.5	191±1.3	308±8.5	13.0±2.2

3.4.2 Cyclic Tension Loading-Unloading Testing

Cyclic tension loading-unloading test was carried out at similar strain-rate range of 10^{-6}-10^{-1} s^{-1} at room temperature. Cycling does not affect the overall plastic behaviour in

comparison with the monotonic tensile curve as shown in Figure 3.15 for AM60 at strain rate 10^{-3} s^{-1}. Monotonic curves are similar to the cyclic stress-strain curves with the absence of hysteresis loops. All cyclic tension loading-unloading tests were strain-controlled, unloading at predetermined strains (i.e. every 0.2% strain increment) to zero stress. Alloys in this research were cyclic tested to 3% strain, except AZ91; AZ91 was tested until failure since it requires a higher strain to see the saturation of anelastic strain. This type of loading-unloading testing was done using the triangle profiler available on Bluehill testing software. Each test was repeated three times. The three types of strains: plastic (ε_p), anelastic (ε_{ae}), and elastic strain (ε_e) indicated in Figure 3.15 were determined and compared between alloys. The effect of strain rate on anelastic strain was also studied.

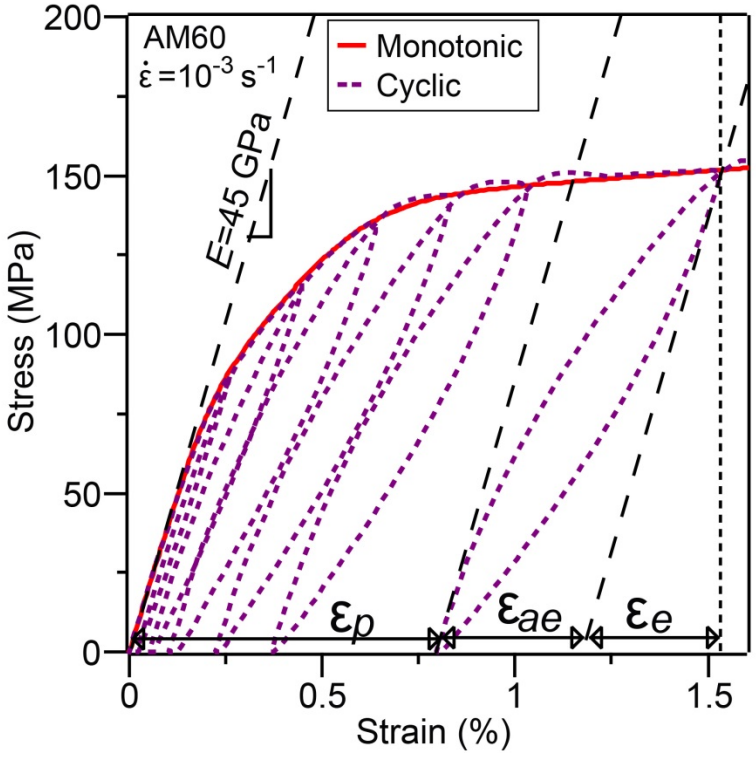

Figure 3.15: A comparison of monotonic and cyclic tensile curves of AM60 at strain rate 10^{-3} s^{-1}.

3.5 Summary

This chapter explains some of the procedural techniques involved in the surface preparation of magnesium alloys for optical and electron microscopy. Special focus is placed on specific techniques for EBSD specimen preparation. The topic of specimen preparation for

microscopy is typically not discussed in detail due to its trivial nature and the presence of already well-established techniques. However, preparation of magnesium alloys for EBSD requires additional efforts due to their soft and highly reactive nature. The specimen preparation techniques developed in this chapter were applied extensively in the subsequent chapters involving the microscopy analysis of magnesium alloys. The intention of this chapter is to provide a reference for future work on similar alloys, since magnesium is one of the most difficult materials to achieve a satisfactory quality of specimen preparation.

Chapter 3 References

[1] Easton MA, Abbott TB, Nie JF, Savage G. In: Pekguleryuz MO, Neelameggham NR, Beals RS, Nyberg EA, editors. Magnesium Technology, New Orleans: TMS Annual Meetings: Magnesium Technology Symposium; 2008, p. 323-28.

[2] Vinarcik EJ. High integrity die casting processes. New Jersey: John Wiley & Sons; 2002.

[3] Zhu SM, Abbott TB, Gibson MA, Nie JF, Easton MA. Age hardening in die-cast Mg–Al–RE alloys due to minor Mn additions. Materials Science and Engineering A 2016; 656: p. 34-8.

[4] Raynor GV. The physical metallurgy of magnesium and its alloys. 5th ed. Oxford: Pergamon; 1959.

[5] ASTM Standard E-112 standard test methods for determining average grain size in annual book of ASTM standards, ASTM. West Conshohocken PA: American Society for Testing and Materials; 2010.

[6] Roberts CS. Magnesium and its Alloys. New York: John Wiley & Sons; 1960.

[7] Wonsiewicz BC, Backofen WA. Independent slip systems and ductility of hexagonal polycrystals. Transactions of the Metallurgical Society of AIME 1967; 239: p. 1422-33.

[8] Nave MD, Barnett MR. Microstructures and textures of pure magnesium deformed in plane-strain compression. Scripta Materialia 2004; 51(9): p. 881-5.

[9] Bakke P, Pettersen K, Westengen H. Improving the strength and ductility of magnesium die-casting alloys via rare-earth addition. Journal of Minerals, Metals and Materials Society 2003; 55 (11): p. 46-51.

Chapter 4

Article 1

Proof stress measurement of die-cast magnesium alloys

Hua Qian Ang[a], Trevor B. Abbott[a,b], Suming Zhu[a], Chengfan Gu[a], Mark A. Easton[a]

[a]*School of Engineering, RMIT University, Bundoora, Victoria 3083, Australia*

[b]*Magontec Limited, Sydney, New South Wales 2000, Australia*

Materials and Design 2016, volume 112, page 402-409

Available online at

https://doi.org/10.1016/j.matdes.2016.09.088

Authorship statement is included in Appendix B.

Materials and Design 112 (2016) 402–409

Contents lists available at ScienceDirect

Materials and Design

journal homepage: www.elsevier.com/locate/matdes

Proof stress measurement of die-cast magnesium alloys

Hua Qian Ang [a], Trevor B. Abbott [a,b], Suming Zhu [a], Chengfan Gu [a], Mark A. Easton [a,*]

[a] School of Engineering, RMIT University, Bundoora, Victoria 3083, Australia
[b] Magontec Limited, Sydney, New South Wales 2000, Australia

HIGHLIGHTS

- The applicability of the standardized proof stress determination methods to die-cast magnesium alloys is evaluated
- The widely used 0.2% offset method is shown to underestimate the proof stress for die-cast magnesium alloys
- The appropriate offset strain corresponding to 0.2% permanent plastic strain is determined for a range of magnesium alloys
- A higher offset strain is shown to have an advantage in reproducibility of proof stress measurement for magnesium alloys

GRAPHICAL ABSTRACT

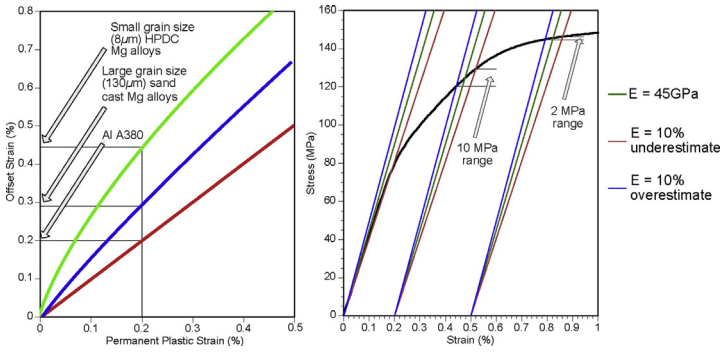

ARTICLE INFO

Article history:
Received 10 August 2016
Received in revised form 12 September 2016
Accepted 26 September 2016
Available online 28 September 2016

Keywords:
Magnesium alloys
High-pressure die-casting
Measurement
Proof stress
Anelasticity

ABSTRACT

Magnesium and its alloys exhibit not only elastic and plastic behaviour but also anelastic behaviour upon loading. The presence of anelastic strain poses a challenge to the measurement of proof stress using conventional methods. As such, the proof stress measurement methods specified by American Society for Testing and Materials (ASTM) and International Standards Organization (ISO) are reviewed and applied to three common die-cast magnesium alloys including AE44, AM60 and AZ91. The methods in the standards give inconsistent results due largely to the inherent anelastic behaviour of these alloys. The widely used 0.2% offset strain method tends to underestimate proof stress while the 0.2% permanent plastic strain method requires repeated loading and unloading. In view of the fact that the non-equivalence between the offset strain and the residual plastic strain for magnesium alloys is a key obstacle to the accurate proof stress measurement, a conversion chart is constructed to enable the determination of the appropriate offset strain for a desired residual plastic strain for a range of magnesium alloys. It is also shown that employing a higher offset strain than 0.2% has an advantage in reproducibility of proof stress measurement.

1. Introduction

Tensile testing is one of the most commonly used methods to assess material properties. The key tensile properties include: yield strength (YS) or proof stress (PS), elastic modulus, tensile strength and elongation to failure. The tensile strength and elongation to failure can be readily determined. Yield strength is used for materials with clear yielding phenomena such as plain carbon steel. For austenitic steels and non-ferrous metals, such as aluminium and magnesium, there is no sharply defined yielding of the material, and hence, proof stress is used as a substitute for yield stress [1]. Studies of high-pressure die-cast magnesium alloys have shown that non-uniform yielding is even more pronounced due to the bimodal grain microstructure [2], where yielding develops first in

* Corresponding author.
E-mail address: mark.easton@rmit.edu.au (M.A. Easton).

http://dx.doi.org/10.1016/j.matdes.2016.09.088
0264-1275/

the softer core [3] consisting of predominantly large externally solidified grains (ESG) while the outer layer of the casting, which consists of mostly fine α-magnesium grains [4], remains elastic (it should be noted, however, that die casting technology is continually improving and these variations are arguably less significant in modern machines).

Proof stress is determined by the stress corresponding to the intersection of the stress-strain curve and a line parallel to the linear elastic part of the curve offset by a definite amount of permanent plastic strain [5]; the permanent strain allowed is an arbitrary choice, ranging from 0.1% for ferrous to 0.5% for some non-ferrous materials [6,7]. For convenience, a permanent plastic strain of 0.2% has been adopted for most metallic materials. The permanent plastic strain can only be determined from a monotonic stress-strain curve if the non-permanent strain can be determined and subtracted. With linear elastic strain this is straightforward, but with non-linear reversible strain (anelastic strain), it is only possible if this anelastic behaviour is fully characterised.

The anelasticity of magnesium alloys manifests itself in a variety of different ways. Under cyclic stress, anelastic behaviour takes the form of a stress-strain hysteresis loop, as identified in magnesium and magnesium-zinc alloys [8], AZ91 (Mg-9Al-0.6Zn) [9], AM60 (Mg-6Al-0.3Mn) and AE44 (Mg-4Al-4RE-rare earth) [10]. The monotonic stress-strain curve of magnesium has a very small linear elastic portion, making elastic modulus determination difficult [11]. The nominal elastic modulus (E) value for magnesium and its alloys is commonly taken as 45 GPa through ultrasonic methods [12], although this value has been shown to vary with solute content, volume fraction of precipitates and porosity [13]. The deviation from elastic behaviour occurs at stresses as low as 20 MPa, due to the activation of basal slip (microyielding) [14]. The variable apparent modulus leads immediately to ambiguities in proof stress determination.

Scientific exchange rests on agreed standards for the measurement of properties. In the case of tensile testing standards (for example ASTM E8M-09 [15] and ISO 6892-1 [16]), four methods are presented for proof stress determination applicable to magnesium as shown in Fig. 1. Detailed descriptions of Methods 1 & 2 can be found in ASTM E8M-09 [15] while Methods 3 & 4 are in ISO 6892-1 [16].

Inconsistencies between and within these methods frustrate attempts to compare alloy properties. AE44, AM60 and AZ91 are commercially available magnesium die-casting alloys for automotive applications, and therefore, they are the focus of this study. In this paper, these alloys are tested according to tensile testing standards and the magnitudes of inconsistencies are determined. More practical proof stress determination methods for magnesium die-casting alloys are discussed.

2. Materials and experimental details

2.1. Materials

Magnesium alloys AE44, AM60 and AZ91, and aluminium alloy A380 were high-pressure die-cast (HPDC) in a 250 ton cold chamber machine. More details about the casting parameters can be found elsewhere [17]. The chemical compositions in wt.% of the three magnesium alloys were analysed using inductively coupled plasma atomic emission spectroscopy (ICP-AES) by Spectrometer Services Pty Ltd. and are listed in Table 1. The study was carried out using cast-to-size cylindrical cross section, dog-bone shaped tensile specimens of gauge diameter 5.6 mm and uniform length of 36 mm.

2.2. Mechanical testing

Both monotonic (Methods 1 and 2) and cyclic tension loading-unloading tests (Methods 3 and 4) were performed on an Instron 5569 Universal Testing Machine (UTS) with a 50 kN load cell at room temperature using a crosshead speed of 5 mm/min. Two to three repeats were performed per alloy composition and test condition. For Method 3, the loading-unloading tests were strain-controlled, unloading at predetermined strains to zero stress. For Method 4, the loading-unloading tests were stress-controlled, unloading at predetermined stress to 10% of the stress obtained. A 25 mm gauge length extensometer was attached to the specimen and digital output files of the flow curves were converted to stress-strain curves.

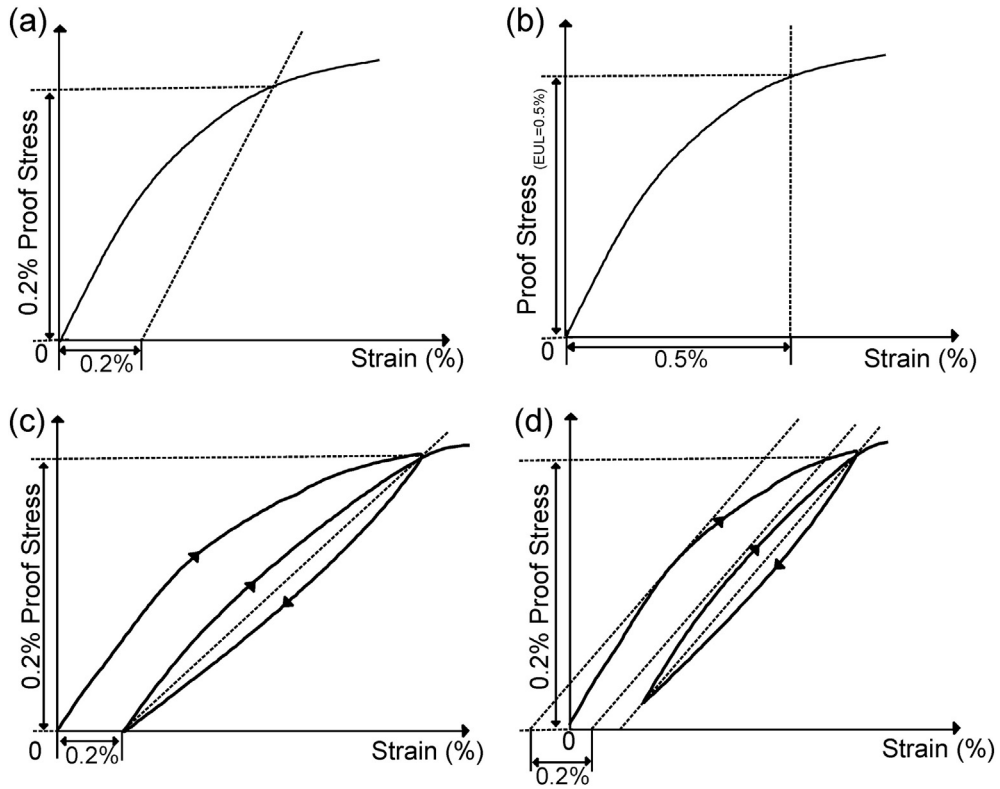

Fig. 1. Proof stress measurement methods: (a) Method 1, (b) Method 2 as specified in ASTM E8M-09 [15] and (c) Method 3 and (d) Method 4 as stated in ISO 6892-1 [16].

Table 1
Chemical compositions (wt.%) determined by ICP-AES for the studied die-cast magnesium alloys.

Alloy	Al	RE (Ce + La)	Zn	Mn	Mg
AE44	3.97	3.76	<0.01	0.18	Bal.
AM60	6.26	<0.01	0.1	0.29	Bal.
AZ91	8.88	<0.01	0.74	0.19	Bal.

3. Results

3.1. Proof stress measurement: Method 1

The engineering stress-strain curves of AE44, AM60, AZ91 and A380 are shown in Fig. 2a. It is seen that the linear elastic behaviour of the three magnesium alloys applies only at low stress levels (<40 MPa), where the elastic modulus of magnesium alloys, $E = 45$ GPa [12] is measured. The aluminium alloy A380, on the other hand, has a more clearly defined linear elastic region (up to >100 MPa) where the elastic modulus value of $E = 70$ GPa can be easily measured.

The relatively small linear elastic region of magnesium alloys makes elastic modulus determination difficult; elastic modulus decreases with increasing stress levels used for modulus determination. As shown in Fig. 2b, the elastic modulus is 45 GPa when it is estimated from the low stress region at 20 MPa; the elastic modulus decreases to 38 GPa when it is estimated from higher stress region at 60 MPa for AE44. Offsetting a lower elastic modulus to 0.2% permanent plastic strain would tilt the offset line forward, leading to higher measured proof stress value (as illustrated in Fig. 2b).

The proof stress values, measured by Method 1 through offsetting a constant elastic modulus of 45 GPa to 0.2% strain are 123 ± 5.5 MPa, 117 ± 3.7 MPa and 154 ± 6.0 MPa, respectively for cast AE44, AM60 and AZ91, whereas the proof stress value for A380 is 185 ± 0.7 MPa through offsetting an elastic modulus of 70 GPa.

3.2. Proof stress measurement: Method 2

Since the linear elastic region of the stress-strain curve in magnesium is not clearly defined, Method 2, extension-under-load (EUL), can be employed. According to the ASTM standard [15], for materials with low yield strengths of <550 MPa, an appropriate value of total extension is 0.005 mm/mm or 0.5% of the gauge length. The proof stress values obtained from Method 2 are 127 ± 2.8 MPa, 122 ± 2.4 MPa, and 148 ± 4.6 MPa respectively, for cast AE44, AM60 and AZ91 and 187 ± 1.4 MPa for A380 as shown in Fig. 3.

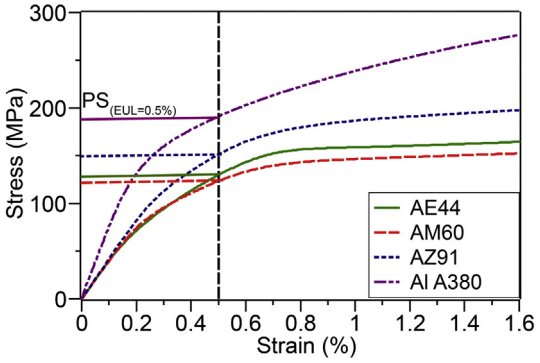

Fig. 3. Tensile curves of die-cast AE44, AM60, AZ91 and A380 showing respectively proof stress values measured by Method 2.

3.3. Proof stress measurement: Method 3

Based on Method 3, a line should be drawn across hysteresis loop unloaded to 0.2% permanent plastic strain. The point at which this line intersects the curve gives the 0.2% proof stress. However, it is often difficult to pre-determine the applied strain and stress that would unload to 0.2% plastic strain due to the uneven hysteresis loops. Hence, each test was unloaded and reloaded six times as indicated by the hysteresis loops formed as shown in Fig. 4 for AE44. Similar hysteresis loops were observed for AM60 and AZ91. A series of secant elastic moduli, E_{sec}, indicated by dashed line, are also defined in Fig. 4.

Here, the hysteresis loops still did not unload to 0.2% plastic strain after several loading-unloading cycles. Hence, 0.2% proof stress is measured by a E_{sec} (as indicated by dotted line in Fig. 4), interpolated from elastic moduli drawn across hysteresis loops unloading to plastic strains before and after 0.2%. The average interpolated E_{sec} at 0.2% strain in Method 3 for AE44, AM60 and AZ91 are 23.9 ± 0.4 GPa, 24.3 ± 0.7 GPa and 26.9 ± 0.6 GPa respectively. The proof stress values measured by Method 3 are summarized in Table 2.

The cyclic stress-strain curve of A380 is also shown in Fig. 5 for comparison. It is worth noting that the loops are small and the elastic modulus remains unchanged ($E = 70$ GPa) with increasing strain. The measured anelastic strains (defined by loop width) are close to zero. The proof stress of A380 measured by Method 3 is 187 ± 0.7 MPa, which is similar to the proof stress values measured by Methods 1 (185 MPa) and 2 (187 MPa).

Generally, E_{sec} decreases with increasing permanent plastic strain when the hysteresis loops become larger until a point where the loops are fully developed. At this point, there will be little change

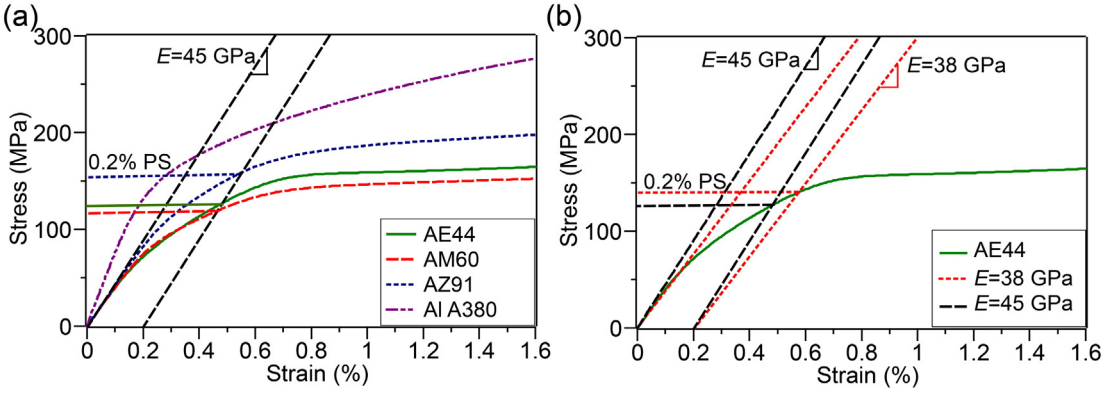

Fig. 2. Proof stress values measurement by Method 1 for die-cast AE44, AM60 and AZ91 alloys, indicated as 0.2% PS in (a) with $E = 45$ GPa determined at low stresses (<40 MPa)·The aluminium alloy A380 is also shown for comparison. It is to be noted that the proof stress measured by Method 1 varies with E, which decreases from 45 GPa to 38 GPa with increasing stress from >40 MPa to ~60 MPa, shown for AE44 in (b).

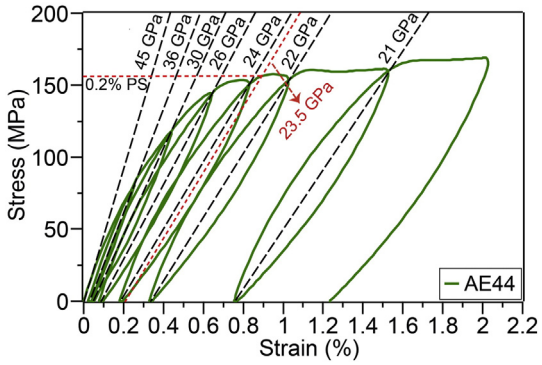

Fig. 4. Cyclic stress-strain curve of AE44 showing proof stress measured by Method 3, by employing a secant elastic modulus, E_{sec} of 23.5 GPa.

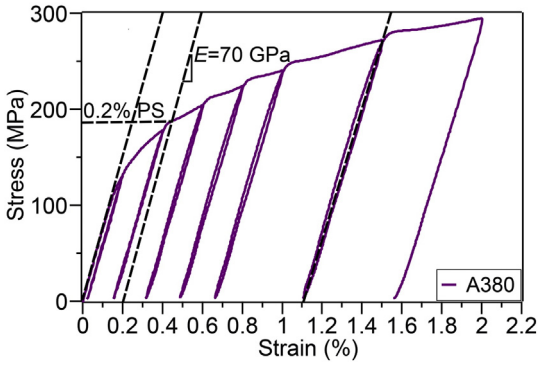

Fig. 5. Cyclic stress-strain curve of A380 showing proof stress measurement by Method 3.

in E_{sec}. This is similar for all the magnesium alloys tested (Fig. 6a). Published work from Mann et al. [8] and Cáceres et al. [9] have been reanalysed and included for comparison. The two HPDC AZ91 2 mm-thick and 6 mm-thick alloys by Cáceres et al. [9] appear to have a higher E_{sec} than the HPDC alloys in this study at 0.2% permanent plastic strain, an indication of smaller hysteresis loops. Stronger materials, i.e. HPDC and aged sand cast, also show a smaller decrease in E_{sec} compared with the lower strength sand cast alloys.

Fig. 6b shows the anelastic strain as a function of permanent plastic strain. It is clear that the anelastic strain is approximately 0.25% at 0.2% permanent plastic strain for all the alloys tested in this study. The two HPDC AZ91 2 mm-thick and 6 mm-thick alloys by Cáceres et al. [9] have a slightly lower anelastic strain (0.2%) than the HPDC alloys tested in this study at 0.2% plastic strain. It is also interesting to note that most sand cast samples, which have larger grain sizes, show lower anelastic strain (0.1–0.15%) at 0.2% plastic strain. Overall, pure magnesium metal shows higher anelastic strain than the alloys for given casting conditions.

3.4. Proof stress measurement: Method 4

Based on Method 4, the stress is reduced to about 10% of the unloading stress when the presumed proof stress is reached to obtain an alternative elastic modulus, E_{alt}, for proof stress determination. But, it is impossible to pre-identify when the proof stress is exceeded unless loading-unloading tests are conducted in advance. Here, based on previously conducted monotonic tests (tensile curves shown in Fig. 2a), AE44, AM60 and AZ91 were unloaded at 123 MPa, 117 MPa and 154 MPa respectively (average proof stress values obtained from Method 1). A380 has constant E_{sec} with increasing strain, and therefore was not subjected to this test. The cyclic stress-strain curve for AE44 and E_{alt} following Method 4 are shown in Fig. 7. According to Method 4, E_{alt} must be tangential to the stress-strain curve and the point where this line crosses the abscissa is taken as the corrected origin. Hence, in this case, E_{alt} is offset from negative strain rather than at the origin (Fig. 7). The average E_{alt} used in Method 4 for AE44, AM60 and AZ91 are 33.3 ± 0.9, 32.1 ± 1.4, and 33.2 ± 1.1 GPa respectively.

One conundrum of Method 4 is to determine where to unload. Unloading at different stress levels yields different alternative elastic moduli, resulting in a variation in proof stress values as illustrated in Fig. 8, ranging from 148 to 158 MPa.

Table 2
Proof stress values measured by Methods 1–4 and the 0.5% offset method.

Alloy	Proof stress (MPa)				
	Method 1	Method 2	Method 3	Method 4	0.5% offset method
AE44	123 ± 5.5	127 ± 2.8	155 ± 0.7	148 ± 1.4	155 ± 1.7
AM60	117 ± 3.7	122 ± 2.4	143 ± 0.5	136 ± 1.0	142 ± 2.1
AZ91	154 ± 6.0	148 ± 4.6	185 ± 2.8	175 ± 0.7	181 ± 4.2
A380	185 ± 0.7	187 ± 1.4	187 ± 0.7	–	–

4. Discussion

4.1. Applicability of the current standardized methods to die-cast magnesium alloys

The proof stress of magnesium alloys reported in literature [18–29] is often defined by Method 1 (0.2% offset) due to its simplicity as compared to Methods 3 and 4. Method 2 is often used to determine the acceptance or rejection of materials whose stress-strain characteristics are well-known from previous tests [30], and hence, is less commonly used in published work. To investigate the inconsistencies in these standardized methods, Figs. 2a and 3 (monotonic stress-strain curves) are overlaid onto Figs. 4 and 7 (cyclic stress-strain curves for Methods 3 and 4 respectively) as shown in Fig. 9 for cast AE44, AM60 and AZ91. The following comments can be made from the comparison of the standardized methods:

(a) The proof stress values measured by Methods 1 and 2 do not leave a 0.2% permanent plastic strain in die-cast magnesium alloys, in fact it is <0.1% plastic strain upon the removal of anelastic deformation, ε_{ae}. Hence, Methods 1 and 2 significantly underestimate the 0.2% proof stress of magnesium alloys.

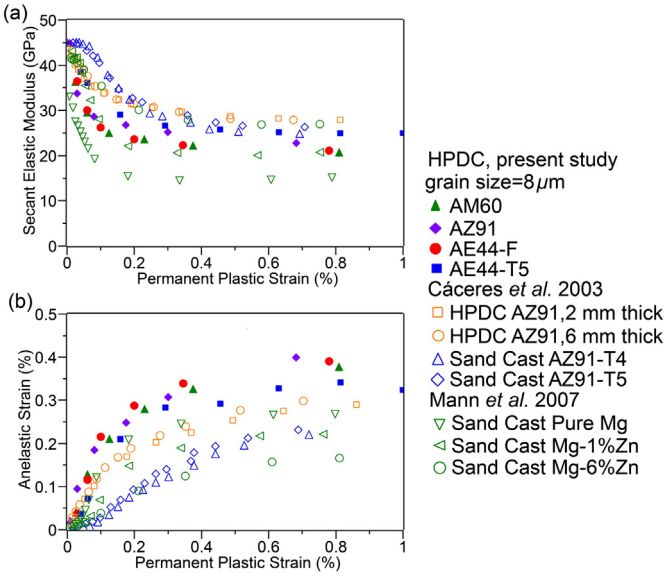

Fig. 6. (a) Secant elastic modulus, E_{sec} (GPa) and (b) anelastic strain (%) as a function of tensile permanent plastic strain (%). Data taken from published work by Mann et al. [8] and Cáceres et al. [9] are included for comparison. For experimental details, refer to original papers.

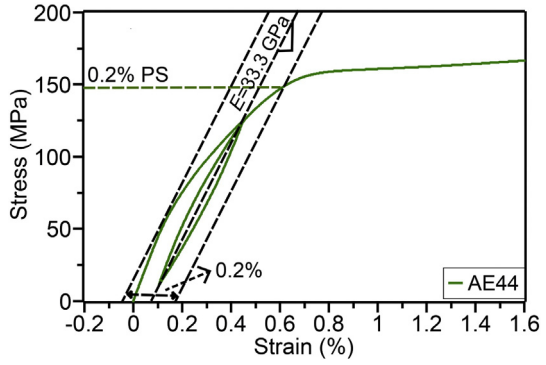

Fig. 7. Proof stress measurement by Method 4 for AE44 where the alternative elastic modulus, E_{alt} is 33.3 GPa.

(b) Method 3 more accurately measures the proof stress of magnesium alloys, but it is almost impossible to pre-determine the stress or strain amplitudes that impart 0.2% permanent plastic deformation upon unloading. Hence, repeated loading-unloading tests have to be conducted, and this becomes time consuming and impractical.

(c) Method 4 itself is inconsistent in that the proof stress value is dependent upon the unloading stress level.

4.2. Appropriate offset strain for magnesium alloys

Methods 1–4 provide different proof stress values for the same magnesium alloy tested. Clearly, proof stress measurement methods specified in ASTM and ISO standard analysis procedures need to be re-evaluated for magnesium and its alloys due to the existence of anelastic strain and for simplicity. Since the monotonic curves are similar to the cyclic stress-strain curves with the absence of hysteresis loops (Fig. 9), for die-cast AE44, AM60 and AZ91, it was found that the 0.2% proof stress values determined by Method 3 could be measured directly from monotonic stress-strain curves with an appropriate offset strain value. This would save considerable amount of time and effort without performing cyclic loading-unloading tests. An appropriate offset strain value should always consider the anelasticity at 0.2% permanent plastic strain.

It is shown in Fig. 10 that the appropriate offset strain for magnesium alloys to achieve a 0.2% permanent strain proof stress can range from 0.3–0.5% depending on the alloy and casting conditions. The HPDC alloys in this study requires a higher offset strain of 0.45% as compared to the HPDC alloys used by Cáceres et al. [9]. This could also be due to grain size effect as those HPDC alloys may have had a greater fraction of large presolidified grains formed in the shot sleeve.

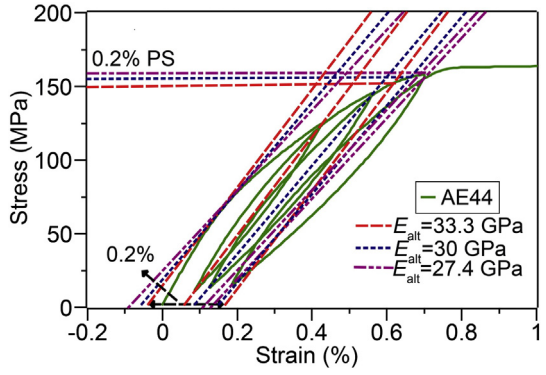

Fig. 8. Inconsistency within Method 4 providing different alternative elastic moduli, E_{alt}, leading to a variation in proof stress values.

Similarly, sand cast samples, with larger grain sizes, show a lower offset strain (≈0.3%) compared to HPDC samples. A small grain size has been reported to result in a greater number of fine {10$\bar{1}$2} twins which are less stable and more prone to revert upon unloading, magnifying the anelastic strain [8,9]. In extension, as anelastic strain increases, so does the offset strain at a given permanent plastic strain.

It is also interesting to note that magnesium-zinc alloys appear to have a lower anelastic strain than pure magnesium for a given casting condition, i.e. the anelastic effect decreases with increasing Zn content (Fig. 6b). This is because the presence of solute (i.e. Zn [8]) is able to enhance the dislocation activity in the prismatic slip system, and hence, twinning becomes progressively less necessary in magnesium alloys [31]. Since anelasticity is known to be caused by the reversible movement of twin boundaries, it is reasonable to believe that decreasing twinning reduces the anelastic strain, and therefore, a slightly lower offset strain is required for the magnesium alloys than pure magnesium. The three die-cast magnesium alloys AE44, AM60 and AZ91 tested in this study also have different Al concentrations, but Al solute appears to have little effect on the anelastic strain compared to Zn. This can be understood by noting that Zn develops short range order [32] while Al forms random solid solutions [33]. Twinning in magnesium is shuffling dominated [34], and therefore, it should be more sensitive to the presence of order [35] than existence of a random solid solution. It is worth noting that the microstructure of AE44 consists of Al-RE intermetallic phases (i.e. $Al_{11}RE_3$ and Al_2RE [36]), while that of AM60 and AZ91 consist of $Mg_{17}Al_{12}$ phase [37]. The difference in intermetallic phases do not seem to affect the anelastic behaviour of the investigated alloys in the present study. These factors are subject to ongoing investigation.

It should also be pointed out that Fig. 10 is only applicable for tensile testing. Depending on the manufacturing process, some magnesium alloys are known to have a larger anelastic strain in compression than tension [8] due to an increased activity of {10$\bar{1}$2} twinning [38], and hence, a larger offset strain might be required fo r compression testing under such condition. However, HPDC samples commonly have isotropic material behaviour [39], therefore, the increase in offset strain should be negligible for HPDC magnesium alloys.

As for twinning-free aluminium alloy A380, due to its negligible anelastic effect, the 0.2% offset strain is able to achieve a 0.2% permanent strain for proof stress measurement.

4.3. Effects of higher offset strain on measurement consistency

The purpose of yield or proof stress is to indicate the stress, above which significant plastic deformation occurs. Fig. 11 shows an example of a stress-strain curve (in this case AM60) with 0.2 and 0.5% offset strains marked. From the inset in Fig. 11, point A (0.5% offset) gives a more diagnostic property value than point B (0.2% offset). The 0.2% offset value lies on the steep part of the curve well before significant plastic deformation has occurred and is of no special significance.

In Section 3.1, it was noted that differences in the stress level chosen for modulus determination could shift the apparent modulus from 45 GPa to 38 GPa. Fig. 11 illustrates that the effect of modulus determination errors is much greater in the 0.2% offset proof stress compared to 0.5% offset proof stress. In the former case the result shifts by 8 MPa while in the later the shift is only 2 MPa. Section 3.1 also illustrated that sample to sample variations at 0.2% offset were also higher, being almost an order of magnitude higher than for aluminium.

The proof stress values measured by the 0.5% offset method for die-cast AE44, AM60 and AZ91 in this study are summarized in Table 2. Regardless of testing methods, AZ91 consistently has the highest proof stress as compared to AE44 and AM60. AZ91 is well-known to be a stronger but less ductile alloy due to the presence of high volume fraction of coarse and brittle β-$Mg_{17}Al_{12}$ phase in the microstructure [40]. It is evident that the values measured by 0.5% offset method correlate well with those measured by Method 3, and they are far larger than

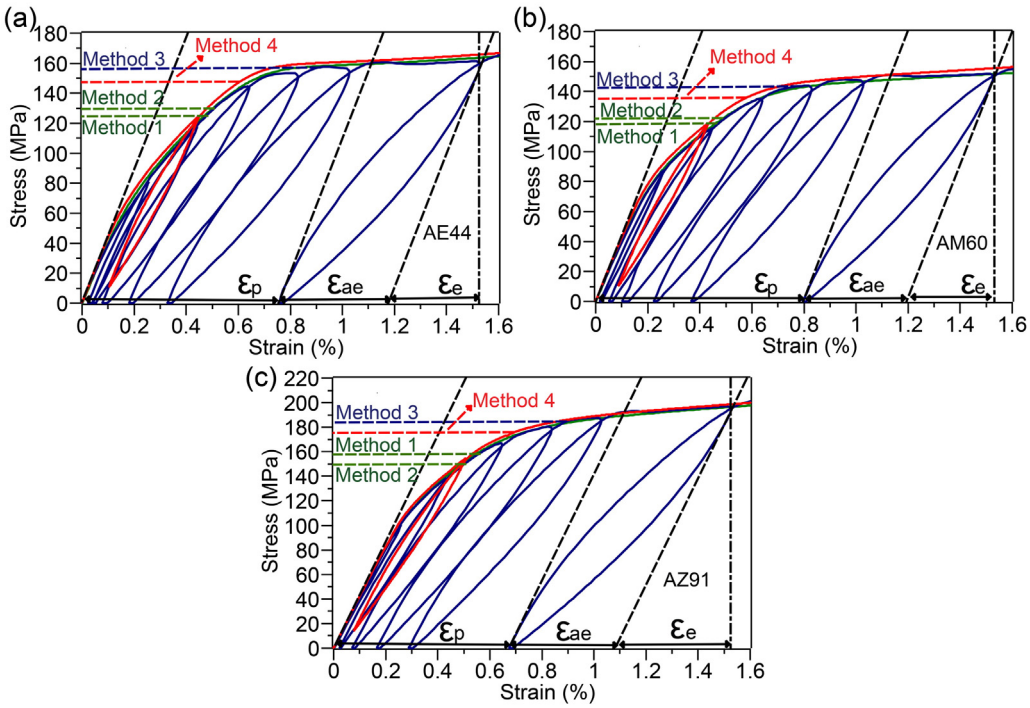

Fig. 9. An overview of monotonic and cyclic stress-strain curves of die-cast (a) AE44, (b) AM60 and (c) AZ91 where the total strain (ε_t) can be separated into plastic strain (ε_p), anelastic strain (ε_{ae}) and elastic strain (ε_e). Proof stress values measured by Methods 1–4 are also shown.

the proof stress values from the 0.2% offset rule (Method 1). Room temperature tensile stress-strain data of high-pressure die-cast magnesium and aluminium alloys from independent studies in the literature have been reanalysed to compare the proof stress obtained by the 0.2% and 0.5% offsets (Table 3). For exact chemical compositions, refer to original studies. By using a higher offset strain, the proof stress of both magnesium and aluminium alloys can increase by up to 20%. Overall, the higher offset method provides a smaller range of proof stress values, and hence, a more consistent measure for magnesium alloys.

However, caution should be taken when considering use of the 0.5% offset method for die-cast magnesium alloys as it has also been shown in Fig. 6 that the anelastic strain is sensitive to factors such as grain size and solute. It should be noted that some of the sand cast magnesium alloys have a lower anelastic strain, and the higher offset strain of 0.5% might overestimate the proof stress.

5. Conclusions

The applicability of the standardized ISO and ASTM proof stress determination methods to magnesium die-casting alloys

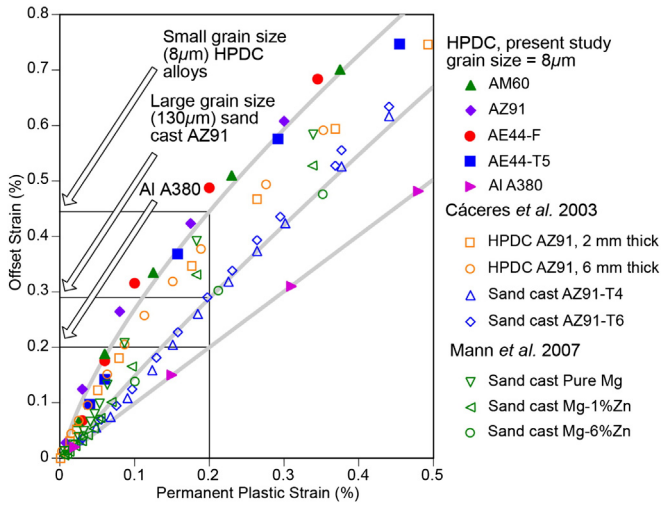

Fig. 10. Permanent plastic strain as a function of offset strain (plastic strain + anelastic strain) for die-cast magnesium alloys. Sand cast magnesium alloys taken from the literature [8,9] are included for comparison.

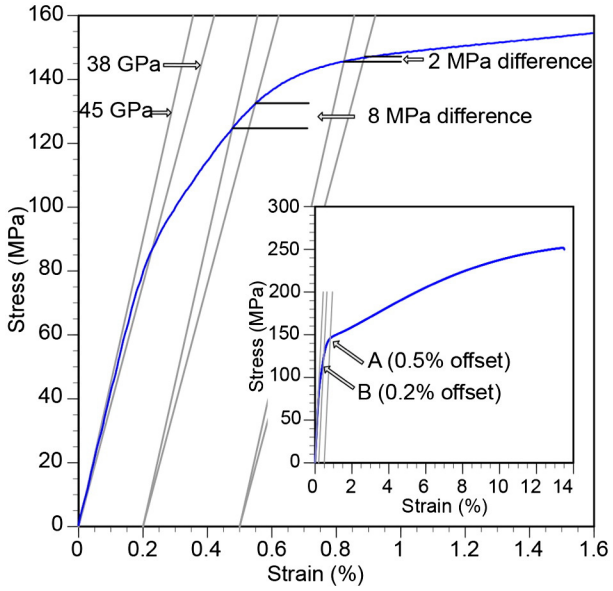

Fig. 11. Stress-strain curve of AM60 showing a comparison of 0.2% and 0.5% offsets and the influence of errors in modulus determination.

Table 3
Comparison of proof stress obtained by 0.2% and 0.5% offsets for HPDC magnesium and aluminium alloys reported in literature.

Alloy	Proof stress (MPa)		Ref.
	0.2% offset	0.5% offset	
Mg alloys			
AM40	108[a]–120	127[a]–133	[41]
Mg-4Al-1La	110[a]–133	129[a]–138	
Mg-4Al-2La	113[a]–140	137[a]–148	
Mg-4Al-4La	128[a]–155	152[a]–162	
Mg-4Al-6La	171	178	
Mg-4Al-3La	123	148	[42]
Mg-4Al-1Ce	129[a]–146	151[a]–152	[43]
Mg-4Al-2Ce	148	153	
Mg-4Al-4Ce	157	162	
Mg-4Al-6Ce	161	168	
Mg-4Al-4(Ce/La)	132[a]–160	161[a]–170	[44]
AE44 (RE = Ce-rich mischmetal)	127[a]–140	149[a]–154[a]	[45]
AM30	116	123	[46]
AM60	125–127[a]	144–148[a]	[47]
AZ91D	150–154[a]	179[a]–185	[48]
AEX422	204	210	[49]
AE42	122	145	[50]
AJ62	126	142	
AS31	127	145	
AXJ530	188	205	
AM-HP2+	175	173	
MRI 153A	164	179	
MRI 153M	162	174	
MRI 230D	179	188	
Mg-3.44La	135	172	[51]
Mg-2.87Ce	135	153	
Mg-3.53Nd	129	135	
Mg-0.47Nd	85	100	
Mg-0.51La	80	98	
Mg-0.53Ce	80	96	
Al alloys			
A380	185	223	This work
A383	150–165	–	[52,53]
A357	143–150	–	[54]
AlMg5.5Si2Mn	183	–	[53]

[a] Unpublished data.

has been investigated. The following conclusions are drawn from this study:

(1) Standardized proof stress determination methods provide inconsistent 0.2% permanent strain proof stress, with a variation of >20%, due largely to the inherent anelastic behaviour of magnesium alloys.

(2) These methods either significantly underestimate the proof stress of magnesium alloys or they are too complex to be considered for routine application.

(3) A conversion chart has been constructed to provide a more accurate determination of 0.2% permanent plastic strain with an appropriate offset strain for a range of magnesium alloys. The appropriate offset strain is shown to vary from 0.3–0.45% depending on the casting conditions.

(4) A more pragmatic approach of using a higher offset strain and its effects are discussed. The high offset strain provides a smaller range of proof stress values as compared to the 0.2% offset strain, and hence, a more consistent measure.

Acknowledgements

This work was supported by the Australian Research Council [Grant number LP130100828]. The authors would like to thank Dr. Carlos Cáceres from the University of Queensland for his very helpful comments on the manuscript and Mr. Gary Savage and his team from CSIRO Manufacturing for the production and supply of the samples.

References

[1] E.C. Rollason, Metallurgy for Engineers, Edward Arnold, London, 1939.
[2] K.V. Yang, C.H. Cáceres, M.A. Easton, A microplasticity-based definition of the skin in HPDC Mg–Al alloys, Mater. Sci. Eng. A 580 (2013) 355–361.
[3] K.V. Yang, C.H. Cáceres, A.V. Nagasekhar, M.A. Easton, The skin effect and the yielding behavior of cold chamber high pressure die cast Mg–Al alloys, Mater. Sci. Eng. A 542 (2012) 49–55.
[4] J.P. Weiler, J.T. Wood, R.J. Klassen, R. Bermortel, G. Wang, The effect of grain size on the flow stress determined from spherical microindentation of die-cast magnesium AM60B alloy, J. Mater. Sci. 40 (22) (2005) 5999–6005.
[5] R.A. Beaumont, Metallurgy for Aircraft Engineers, Inspectors and Engineering Students, Pitman, London, 1946.
[6] F.T. Hill, The Materials of Aircraft Construction, Pitman & Sons, London, 1942.
[7] G.E. Dieter, Mechanical Metallurgy, 3rd ed. McGraw-Hill, New York, 1988.
[8] G.E. Mann, T. Sumitomo, C.H. Cáceres, J.R. Griffiths, Reversible plastic strain during cyclic loading–unloading of Mg and Mg–Zn alloys, Mater. Sci. Eng. A 456 (1) (2007) 138–146.
[9] C.H. Cáceres, T. Sumitomo, M. Veidt, Pseudoelastic behaviour of cast magnesium AZ91 alloy under cyclic loading–unloading, Acta Mater. 51 (20) (2003) 6211–6218.
[10] Z. Lu, P. Blackmore, Cyclic stress-strain behaviour of AM60B and AE44 cast magnesium alloys and its impact on LCF characterisation and fatigue analysis, SAE Int. J. Mater. Manuf. 7 (2014) 446–453.
[11] Y. Carbonneau, A. Sanschagrin, J. Renaud, R. Tremblay, On the development of a new approach for the determination of yield strength in Mg-based alloys, Light Met. Age 56 (9–10) (1998) 50–53.
[12] M. Avedesian, H. Baker (Eds.), ASM Specialty Handbook: Magnesium and Magnesium Alloys, ASM International, Ohio, 1999.
[13] T. Sumitomo, C.H. Cáceres, M. Veidt, The elastic modulus of cast Mg–Al–Zn alloys, J. Light. Met. 2 (1) (2002) 49–56.
[14] A. Zhou, S. Basu, M. Barsoum, Kinking nonlinear elasticity, damping and microyielding of hexagonal close-packed metals, Acta Mater. 56 (1) (2008) 60–67.
[15] ASTM, Standard E8M-09 Standard Test Methods for Tension Testing of Metallic Materials in Annual Book of ASTM Standards, ASTM, West Conshohocken PA, American Society for Testing and Materials, 2009.
[16] ISO 6892-1 Metallic Materials Tensile Testing-part 1: Method of Test at Room TemperatureInternational Standards Organisation 2009.
[17] K.V. Yang, M.A. Easton, C.H. Cáceres, The development of the skin in HPDC Mg–Al alloys, Mater. Sci. Eng. A 580 (2013) 191–195.
[18] Z. Leng, H.J. Pan, Z.Y. Niu, C.H. Guo, Q. Zhang, Y.P. Chang, et al., Mechanical behavior, deformation and damage mechanisms of Mg–RY–Zn alloy under high strain rate, Mater. Sci. Eng. A 651 (2016) 336–340.
[19] J.H. Forsmark, Z. Dowling, K. Gibson, C. Mueller, L. Godlewski, J. Zindel, et al., An investigation of the effects of cast skin on the mechanical properties of an AM60 die-cast magnesium alloy, SAE Int. J. Mater. Manuf. 8 (2015) 714–721.
[20] M. Okayasu, S. Takeuchi, M. Matsushita, N. Tada, M. Yamasaki, Y. Kawamura, Mechanical properties and failure characteristics of cast and extruded $Mg_{97}Y_2Zn_1$ alloys with LPSO phase, Mater. Sci. Eng. A 652 (2016) 14–29.
[21] S. Fintová, L. Kunz, Fatigue properties of magnesium alloy AZ91 processed by severe plastic deformation, J. Mech. Behav. Biomed. Mater. 42 (2015) 219–228.
[22] M.G. Jiang, H. Yan, R. Chen, Microstructure, texture and mechanical properties in an as-cast AZ61 Mg alloy during multi-directional impact forging and subsequent heat treatment, Mater. Des. 87 (2015) 891–900.
[23] Y.Z. Du, X.G. Qian, M.Y. Zheng, D.B. Wang, K. Wu, I.S. Golovin, Effect of microalloying with Ca on the microstructure and mechanical properties of Mg-6 mass% Zn alloys, Mater. Des. 98 (2016) 285–293.
[24] H.Y. Wang, E.B. Zhang, X.L. Nan, L. Zhang, Z.P. Guan, Q.C. Jiang, A comparison of microstructure and mechanical properties of Mg–9Al–1Zn sheets rolled from as-cast, cast-rolling and as-extruded alloys, Mater. Des. 89 (2016) 167–172.
[25] R. Shabadi, R. Ambat, E.S. Dwarakadasa, AZ91C magnesium alloy modified by Cd, Mater. Des. 53 (2014) 445–451.
[26] L. Zhang, J.H. Zhang, Z. Leng, S.J. Liu, Q. Yang, R.Z. Wu, et al., Microstructure and mechanical properties of high-performance Mg–Y–Er–Zn extruded alloy, Mater. Des. 54 (2014) 256–263.
[27] J. She, F.S. Pan, W. Guo, A.T. Tang, Z.Y. Gao, S.Q. Luo, et al., Effect of high Mn content on development of ultra-fine grain extruded magnesium alloy, Mater. Des. 90 (2016) 7–12.
[28] Y. Jiang, Y. Chen, J.J. Gao, Comparative study regarding the effect of Al, Zn, and Gd on the microstructure and mechanical properties of Mg alloy Mg–Sn–Li, Mater. Des. 105 (2016) 34–40.
[29] Q. Yang, F.Q. Bu, F.Z. Meng, X. Qiu, D.P. Zhang, T. Zheng, et al., The improved effects by the combinative addition of lanthanum and samarium on the microstructures and the tensile properties of high-pressure die-cast Mg–4Al-based alloy, Mater. Sci. Eng. A 628 (2015) 319–326.
[30] J.R. Davis (Ed.), Tensile Testing, 2nd ed.ASM international, Ohio, 2004.
[31] A. Akhtar, E. Teghtsoonian, Solid solution strengthening of magnesium single crystals—II the effect of solute on the ease of prismatic slip, Acta Metall. 17 (11) (1969) 1351–1356.
[32] C.H. Cáceres, A.H. Blake, The strength of concentrated Mg–Zn solid solutions, Phys. Status Solidi A 194 (1) (2002) 147–158.
[33] C.H. Cáceres, D.M. Rovera, Solid solution strengthening in concentrated Mg–Al alloys, J. Light. Met. 1 (3) (2001) 151–156.
[34] B. Li, H.E. Kadiri, X.Y. Zhang, S.N. Mathaudhu, Q. Ma, Structural origin of reversible twinning, non-schmid effect, incoherent twin boundaries and texture of hexagonal close-packed metals, in: S.N. Mathaudhu, W.H. Sillekens, N.R. Neelameggham, N.

Hort (Eds.), Magnesium Technology 2012, John Wiley & Sons, London 2012, pp. 105–110.
[35] J.W. Cahn, Thermodynamic and structural changes in deformation twinning of alloys, Acta Metall. 25 (9) (1977) 1021–1026.
[36] S.M. Zhu, M.A. Easton, T.B. Abbott, M.A. Gibson, J.F. Nie, The influence of individual rare earth elements (La, Ce, or Nd) on creep resistance of die-cast magnesium alloy AE44, Adv. Eng. Mater. 18 (6) (2016) 932–937.
[37] L.H. Rettberg, J.B. Jordon, M.F. Horstemeyer, J.W. Jones, Low-cycle fatigue behavior of die-cast Mg alloys AZ91 and AM60, Metall. Mater. Trans. A 43 (7) (2012) 2260–2274.
[38] S.R. Agnew, Ö. Duygulu, Plastic anisotropy and the role of non-basal slip in magnesium alloy AZ31B, Int. J. Plast. 21 (6) (2005) 1161–1193.
[39] M. Easton, W.Q. Song, T. Abbott, A comparison of the deformation of magnesium alloys with aluminium and steel in tension, bending and buckling, Mater. Des. 27 (10) (2006) 935–946.
[40] A. Boby, A. Srinivasan, U.T.S. Pillai, B.C. Pai, Mechanical characterization and corrosion behavior of newly designed Sn and Y added AZ91 alloy, Mater. Des. 88 (2015) 871–879.
[41] J.H. Zhang, M.L. Zhang, J. Meng, R.Z. Wu, D.X. Tang, Microstructures and mechanical properties of heat-resistant high-pressure die-cast Mg–4Al–xLa–0.3 Mn (x = 1, 2, 4, 6) alloys, Mater. Sci. Eng. A 527 (10) (2010) 2527–2537.
[42] S.M. Zhu, T.B. Abbott, M.A. Gibson, J.F. Nie, M.A. Easton, Age hardening in die-cast Mg–Al–RE alloys due to minor Mn additions, Mater. Sci. Eng. A 656 (2016) 34–38.
[43] J.H. Zhang, Z. Leng, M.L. Zhang, J. Meng, R.Z. Wu, Effect of Ce on microstructure, mechanical properties and corrosion behavior of high-pressure die-cast Mg–4Al-based alloy, J. Alloys Compd. 509 (3) (2011) 1069–1078.
[44] J.H. Zhang, D.P. Zhang, Z. Tian, J. Wang, K. Liu, H.Y. Lu, et al., Microstructures, tensile properties and corrosion behavior of die-cast Mg–4Al-based alloys containing La and/or Ce, Mater. Sci. Eng. A 489 (1) (2008) 113–119.
[45] J.H. Zhang, P. Yu, K. Liu, D.Q. Fang, D.X. Tang, J. Meng, Effect of substituting cerium-rich mischmetal with lanthanum on microstructure and mechanical properties of die-cast Mg–Al–RE alloys, Mater. Des. 30 (7) (2009) 2372–2378.
[46] J.H. Zhang, S.J. Liu, Z. Leng, X.H. Liu, Z.Y. Niu, M.L. Zhang, et al., Structure stability and mechanical properties of high-pressure die-cast Mg–Al–La–Y-based alloy, Mater. Sci. Eng. A 531 (2012) 70–75.
[47] G.Y. Gu, S.T. Lin, Y. Xia, Q. Zhou, Experimental study on influence of section thickness on mechanical behavior of die-cast AM60 magnesium alloy, Mater. Des. 38 (2012) 124–132.
[48] M.F. Qi, Y.L. Kang, Y. Yang, G.M. Zhu, W.N. Liao, Comparison of microstructure and mechanical properties of AZ91D alloy formed by rheomolding and high-pressure die casting, J. Mater. Eng. Perform. 24 (10) (2015) 3826–3834.
[49] Q. Yang, K. Guan, F.Q. Bu, Y.Q. Zhang, X. Qiu, T. Zheng, et al., Microstructures and tensile properties of a high-strength die-cast Mg–4Al–2RE–2Ca–0.3 Mn alloy, Mater. Charact. 113 (2016) 180–188.
[50] S.M. Zhu, M.A. Easton, T.B. Abbott, J.F. Nie, M.S. Dargusch, N. Hort, et al., Evaluation of magnesium die-casting alloys for elevated temperature applications: microstructure, tensile properties, and creep resistance, Metall. Mater. Trans. A 46 (8) (2015) 1–12.
[51] T.L. Chia, M.A. Easton, S.M. Zhu, M.A. Gibson, N. Birbilis, J.F. Nie, The effect of alloy composition on the microstructure and tensile properties of binary Mg-rare earth alloys, Intermetallics 17 (7) (2009) 481–490.
[52] G. Hébert, D. Dubé, R. Tremblay, Tensile and fatigue behaviour of thin-walled cast A383.0 components, Mater. Sci. Eng. A 552 (2012) 89–96.
[53] Z.Q. Hu, L. Wan, S.S. Wu, H. Wu, X.Q. Liu, Microstructure and mechanical properties of high strength die-casting Al–Mg–Si–Mn alloy, Mater. Des. 46 (2013) 451–456.
[54] Z. Fan, X. Fang, S. Ji, Microstructure and mechanical properties of rheo-diecast (RDC) aluminium alloys, Mater. Sci. Eng. A 412 (1) (2005) 298–306.

Chapter 5

Article 2

Strain-rate sensitivity of die-cast magnesium-aluminium based alloys

Hua Qian Ang[a], Suming Zhu[a], Trevor B. Abbott[a,b], Dong Qiu[a], Mark A. Easton[a]

[a]*School of Engineering, RMIT University, Bundoora, Victoria 3083, Australia*
[b]*Magontec Limited, Sydney, New South Wales 2000, Australia*

Materials Science and Engineering: A 2017, volume 699, page 239-246

Available online at
https://doi.org/10.1016/j.msea.2017.05.093

Authorship statement is included in Appendix B.

Materials Science & Engineering A 699 (2017) 239–246

Contents lists available at ScienceDirect

Materials Science & Engineering A

journal homepage: www.elsevier.com/locate/msea

Strain-rate sensitivity of die-cast magnesium-aluminium based alloys

Hua Qian Ang[a], Suming Zhu[a], Trevor B. Abbott[a,b], Dong Qiu[a], Mark A. Easton[a,*]

[a] School of Engineering, RMIT University, Bundoora, Victoria 3083, Australia
[b] Magontec Limited, Sydney, New South Wales 2000, Australia

ARTICLE INFO

Keywords:
Magnesium alloys
Strain-rate sensitivity
Dynamic strain ageing
Twinning
Die-casting

ABSTRACT

The strain-rate effect in die-cast magnesium-aluminium based alloys under quasi-static strain rates ranging from 10^{-6} to 10^{-1} s^{-1} was investigated. The strain-rate sensitivity was shown to decrease with increasing aluminium solute level in the matrix. Microstructural examination by electron backscattered diffraction (EBSD) revealed that deformation twinning is more active in the alloys with lower strain-rate sensitivity. It is suggested that the decrease in strain-rate sensitivity with increasing aluminium solute level is likely due to dynamic strain ageing from the interaction between aluminium solute and dislocations. The correlation between strain-rate sensitivity and ductility in AE44 is briefly discussed.

1. Introduction

Magnesium (Mg) tends to show pronounced strain-rate sensitivity in mechanical testing due to the hexagonal close packed crystal structure [1]. Strain-rate sensitivity has been observed to be high in pure Mg [2] and strain-rate sensitivity decreases with increasing aluminium (Al) content in high-pressure die-cast Mg-Al based alloys [2,3]. The high strain-rate sensitivity in high-pressure die-cast Mg alloys with lower Al content led to an increase in work hardening rate and tensile to yield ratio at higher strain rates, with a corresponding increase in energy absorption at higher strain rates [3]. Stanford et al. [4] showed that the strain-rate sensitivity of an extruded Mg-1Al alloy is 30% lower than that of pure Mg at 10^{-4}–10^{-1} s^{-1}. The alloy was solution treated indicating that strain rate effect is also independent of processing conditions.

In contrast, Aune et al. [5] studied the behaviour of die-cast AM50 (Mg-5Al-0.3Mn, wt%), AM60 (Mg-6Al-0.3Mn) and AZ91 (Mg-9Al-1Zn) alloys at 15–130 s^{-1}, but did not observe a significant variation in strain-rate sensitivity between the alloys despite a difference in Al content. This could be due to three factors. Firstly, they only investigated alloys with Al contents greater than 5 wt% when the strain-rate sensitivity is relatively low. Secondly, their investigated strain rate range may be too small to see the effect of strain rate. Thirdly, the strain rates also fall in between quasi-static (typically $< 10^{0}$ s^{-1}) and dynamic ($\geq 10^{3}$ s^{-1}) domains. The latter two factors might be more plausible since Weiler and Wood [6] also reported no strain rate effect for sand-cast AE44 (Mg-4Al-4RE) in similar strain rate range (100–300 s^{-1}). Research in this strain rate range, 10^{0}-10^{2} s^{-1}, is uncommon due to experimental challenges.

At dynamic strain rates ($\geq 10^{3}$ s^{-1}), strain-rate sensitivity has been observed to increase with strain rate in mould cast Mg-9RE-4Zn [7], extruded Mg–8Li–1Al–1Ce [8] and die-cast Mg-Al alloys [9,10]. At quasi-static strain rates ($< 10^{0}$ s^{-1}), published results on the influence of strain rate on strain-rate sensitivity are ambiguous. A greater strain-rate sensitivity was revealed at strain rates below 10^{-4} s^{-1} and 10^{-5} s^{-1} for AZ31 (Mg-3Al-1Zn) [11] and pure Mg [12], respectively. Similarly, strain-rate sensitivity increased from 0.008 to 0.06 with decreasing strain rate from 10^{-3} s^{-1} to 10^{-9} s^{-1} for AZ31 [13]. However, this contrasts with the observations by Carlson [14] and Gu et al. [15], who showed no change in strain-rate sensitivity for die-cast AM60 at strain rates between 10^{0} s^{-1} and 10^{-2} s^{-1}, respectively. Song et al. [16] tested three die-cast Mg alloys AM20 (Mg-2Al-0.3Mn), AM50 and AM60 in compression and observed little change in strain-rate sensitivity between 10^{-3} and 10^{0} s^{-1}.

It is clear that the published research is not completely regarding the effect of Al content on strain-rate sensitivity of Mg-Al based alloys and how the strain-rate sensitivity changes with respect to strain rates, especially at quasi-static strain rates ($< 10^{0}$ s^{-1}). The aim of this work is to measure the strain-rate sensitivity of various die-cast alloys and discern the governing mechanism behind the effect. For this purpose, the tensile behaviour of commercial die-cast Mg alloys with various Al contents, i.e. AM40, AM60, AZ91 and AE44 were investigated over a wide strain rate range 10^{-6}–10^{-1} s^{-1}. AM40 and AM60 are most commonly used in applications where energy absorption is required while AZ91 is widely used for some structural components of automobiles, aircraft, and computers, because of its good combination of

* Corresponding author.
E-mail address: mark.easton@rmit.edu.au (M.A. Easton).

http://dx.doi.org/10.1016/j.msea.2017.05.093
Received 24 April 2017; Received in revised form 23 May 2017; Accepted 24 May 2017
Available online 25 May 2017

Table 1
Chemical compositions (wt%) determined by inductively coupled plasma atomic emission spectroscopy (ICP-AES) for the studied die-cast Mg alloys.

Alloy	Al	Mn	RE (Ce + La)	Zn	Mg
AM40	4.44	0.21	< 0.01	0.05	Bal.
AM60	6.26	0.29	< 0.01	0.1	Bal.
AZ91	8.88	0.19	< 0.01	0.74	Bal.
AE44	3.67	0.31	3.83	< 0.01	Bal.

mechanical properties and die-castability. AE44 was originally developed as a creep resistant alloy, but it has good combination of strength and ductility, especially after ageing [17], this makes it attractive for structural applications [18].

2. Materials and experimental methods

Commercial high-pressure die-cast AM40, AM60, AZ91 and AE44 alloys were used in this study. Details of the casting procedure can be found elsewhere [19]. Some AE44 specimens were given an ageing treatment at 200 °C for 32 h (T5), which produced significant age hardening as a result of precipitation of nanoscale Al-Mn particles [17]. The chemical compositions in wt% of these alloys analysed using inductively coupled plasma atomic emission spectroscopy (ICP-AES) are listed in Table 1.

Dog-bone-shaped cylindrical samples, 100 mm long with a 36 mm parallel section in the gauge length and a diameter of 5.6 mm, were used in this study. Tensile tests were performed on an Instron 5569 Universal Testing Machine at room temperature using a constant rate of crosshead displacement with nominal strain rates in the range 10^{-6}–10^{-1} s^{-1}. Each test was repeated three times.

Electron-backscattered diffraction (EBSD) data was collected in a FEI Nova NanoSEM at 20 kV using a 0.5-μm step size before and after tensile testing. Each sample was scanned three times, covering well over 500 grains. *HKL* Channel 5 Tango subroutine was used to quantify the area fraction of twinning. Five twinning systems were identified based on the misorientation angle/axis between twinned region and matrix. They are {10$\bar{1}$2} twins (i.e. 86° < 12$\bar{1}$0 >), {10$\bar{1}$1} twins (i.e. 56° < 12 $\bar{1}$0 >), {10$\bar{1}$3} twins (i.e. 64° < 12$\bar{1}$0 >), {10$\bar{1}$3}-{10$\bar{1}$2} twins (i.e. 22° < 12$\bar{1}$0 >) and {10$\bar{1}$1}-{10$\bar{1}$2} twins (i.e. 38° < 12$\bar{1}$0 >) [20–22]. The Al solute concentration across grains was measured by energy dispersive X-ray (EDX) spectroscopy. At each sample location, a minimum of 150 points were taken in the α-Mg matrix with a spacing of 0.1 μm between each point using EDX line analysis. Three locations were analysed for each sample. The surfaces of all samples for EBSD and EDX analyses were prepared using standard mechanical polishing procedures and were finished by 0.06 μm OP-S. The fracture surfaces were also investigated by a scanning electron microscopy (SEM) using secondary electron imaging.

3. Results

3.1. Tensile properties

Fig. 1 shows tensile flow curves at various strain rates, $\dot{\varepsilon}$ ranging from 10^{-6} to 10^{-1}, for the as-cast AM40, AM60, AZ91 and AE44, together with the T5-treated AE44. The flow curves of AE44-T5 and as-cast AE44 consistently shift higher with increasing strain rate, and a substantial increase in the proof strength was observed. In contrast, the shift in flow curves of AM40 and AM60 is smaller but still visible, while the changes in flow curves of AZ91 are the barely observable.

The effects of strain rate on strength and ductility are shown in Fig. 2(a) and (b), respectively. In Fig. 2(a), 0.5% proof strength is used because die-cast Mg alloys tend to show pronounced anelasticity and the 0.5% offset is a closer approximation to the 0.2% permanent plastic strain [23]. The 0.5% proof strength shows a more visible increase with strain rate for AE44 and AE44-T5 while the increase is moderate for AM40, AM60 and AZ91. It is noted that tensile strength appears to be

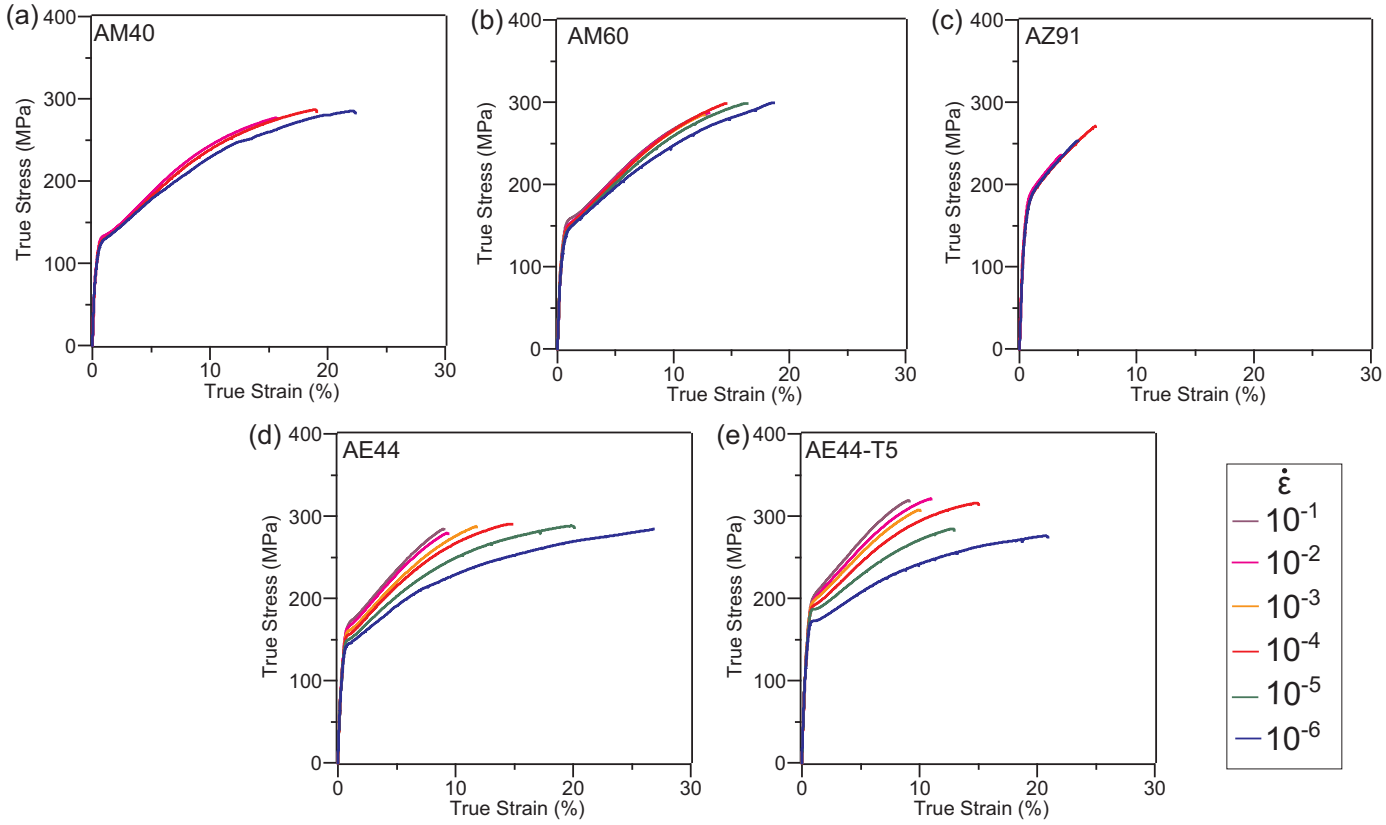

Fig. 1. True stress-strain curves of as-cast (a) AM40, (b) AM60, (c) AZ91, (d) AE44 and T5-aged (e) AE44 at different nominal strain rates, $\dot{\varepsilon}$.

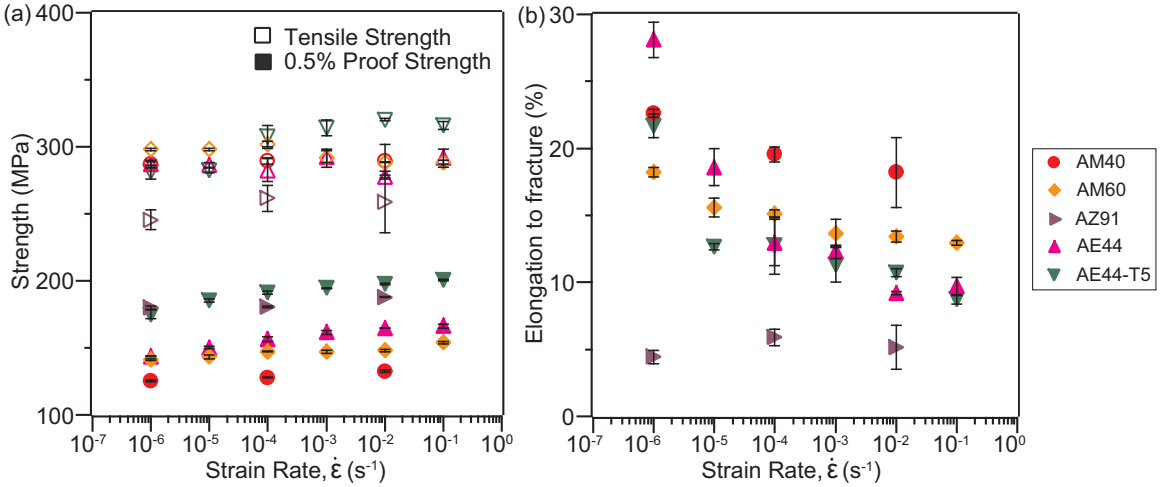

Fig. 2. Effects of strain rate on (a) strength (MPa) and (b) elongation to fracture (%) of as-cast AM40, AM60, AZ91, AE44 and T5-aged AE44. The solid and empty filled symbols in (a) indicate the 0.5% proof strength and tensile strength, respectively.

less sensitive to strain rate and remains almost constant across strain rates for all alloys. This could be due to the fact that the present alloys do not reach necking and the tensile strength is the stress at fracture. Ductility appears to increase with decreasing strain rate in AE44, while the correlation of ductility with strain rate is less visible in AE44-T5, AM40 and AM60. Ductility appears to be independent of strain rate in AZ91.

3.2. Strain rate sensitivity

The differences in the levels of flow stress for different strain rates are indicative of strain-rate sensitivity, represented by $m = \frac{\delta \ln(\sigma)}{\delta \ln(\dot{\varepsilon})}$ [1,24,25]. Fig. 3(a) and (b) show variations of strain-rate sensitivity with true strain and strain rate, respectively. Strain-rate sensitivity increases with strain in both AE44 and AE44-T5, while strain-rate sensitivity first decreases, passes through a minimum then increases again in AM40, AM60 and AZ91 alloys (Fig. 3(a)). In Fig. 3(b), strain-rate sensitivity appears to increase with decreasing strain rate in AE44 and AE44-T5, which is consistent with the observations from studies of pure Mg and other alloys [11–13]. There is no visible change in strain-rate sensitivity observed in AM40 and AZ91. There is, however, no consistent trend in AM60, where the strain-rate sensitivity exhibits a slight decrease, followed by a slight increase with decreasing strain rate. Since, the difference in strain-rate sensitivity is small, it could be assumed that there is no change in strain-rate sensitivity. Overall, AE44-T5 has the highest strain-rate sensitivity, followed by AE44, then AM40, AM60 and AZ91.

3.3. Microstructural characterization

The deformation microstructure in tensile tested AE44, AM60, and AZ91 specimens at different strain rates was examined by EBSD (Fig. 4). The type of twins identified and the fraction of twinned area determined for these alloys are summarized in Table 2. While the starting microstructures (not shown) are twin-free, twins are formed after tensile deformation and the fraction of twinned area shows an increase with increasing strain rate, which is consistent with the previous studies [8,26–28] on Mg alloys. Twinning is most active in AZ91, followed by AM60, and is least active in AE44 for a given strain rate.

Fig. 5 shows the fracture surfaces of AM60, AZ91 and AE44 after tensile testing at the highest and lowest strain rates. Overall, three types of fracture surfaces were observed: quasi-cleavage fracture in all AM60 samples and AE44 deformed at 10^{-5}–10^{-1} s^{-1}, cleavage type of failure in AZ91 samples, and highly-dimpled ductile fracture in AE44 at 10^{-6} s^{-1}. Both AM40 and AE44-T5 (not shown) exhibit similar quasi-cleavage fracture to the AM60 alloy, regardless of the applied strain rates. Cleavage fracture indicates brittle failure, typically controlled by the intermetallic phase [29] while highly-dimpled fracture surface

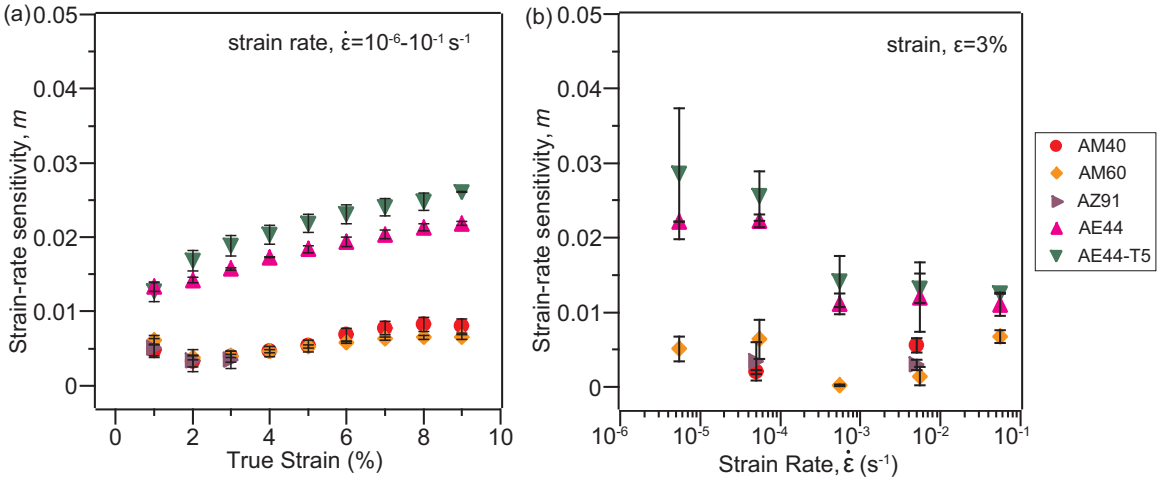

Fig. 3. Variations of strain-rate sensitivity with (a) true strain, covering strain rates, $\dot{\varepsilon}$ from 10^{-6} to 10^{-1} s^{-1} and (b) with strain rate at 3% strain. The strain rate in (b) corresponds to the average of the upper and lower values.

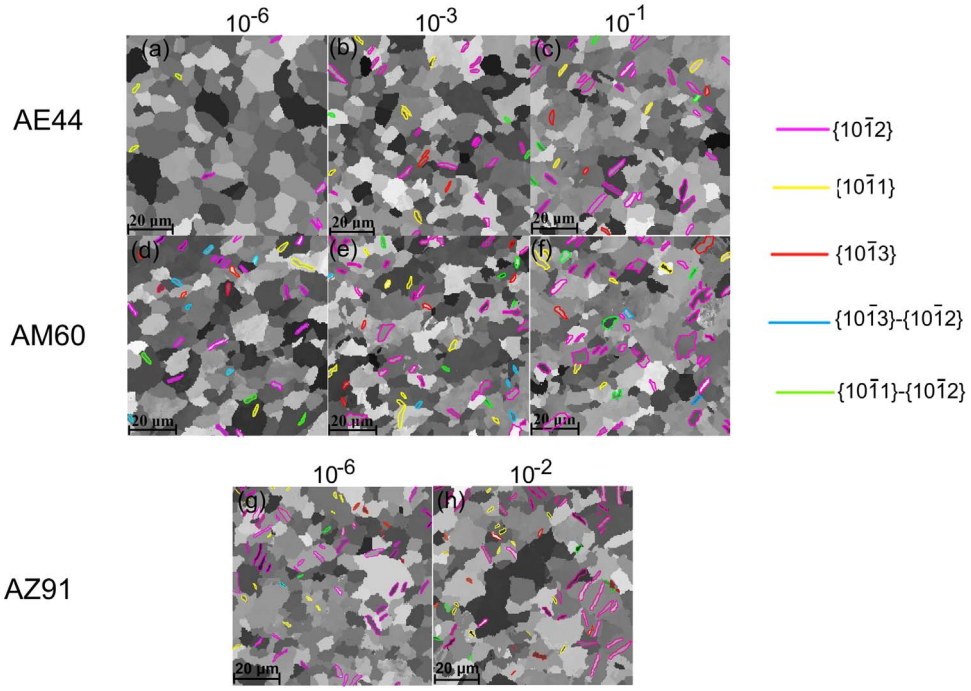

Fig. 4. EBSD maps showing formation of different types of twins in as-cast AE44, AM60, and AZ91 specimens after tensile testing at different strain rates. The loading direction is horizontal. Note that the highest strain rate tested for AZ91 is $10^{-2}\,s^{-1}$.

indicates ductile fracture [30]. Quasi-cleavage fracture surface (Fig. 5(a), (b), (f)) normally contains cleavage planes (P), small and shallow dimples (*S*), along with some secondary cracks (C) on the cleavage plane [31]. Cleavage fracture of AZ91 (Fig. 5(c) and (d)), shows the presence of shrinkage pores (H) (circled) and some facets and steps (F), correlating well with previous work [29]. The fracture surface of AE44 at $10^{-6}\,s^{-1}$ (Fig. 5e) reveals significant amounts of small and large dimples (B), indicating ductile failure. In fact, AE44 at $10^{-6}\,s^{-1}$ shows the capability of accommodating large amounts of plastic strain, with ductility reaching almost 30% strain (Fig. 1(d)).

To provide an indicative distribution of Al solute in the α-Mg grains, line profiles for Al solute concentration in the α-Mg matrix were obtained by EDX as shown in Fig. 6. The Al level at the centre and near grain boundaries are given in Table 3, together with the data predicted by Pandat® [32]. There is an increase in the concentration of Al in the α-Mg towards the grain boundary as would be expected by non-equilibrium solidification with the grain boundary concentrations measured from EDX being between the eutectic concentrations predicted by the Equilibrium and Scheil-Gulliver equation, calculated by Pandat® [32], which is typically used for predicting solute and phase distributions in cast materials. This may indicate some solid state diffusion during the highly non-equilibrium conditions in high-pressure die-casting.

4. Discussion

The strain-rate sensitivity of Mg-Al alloys has been reported to be affected by the alloying content of Al [3,16,33]. However, AM40 and AE44 have similar Al content in composition, but the strain-rate sensitivity of AE44 is significantly higher than AM40. Present results suggest that it is the Al solute level in the α-Mg matrix that influences the strain-rate sensitivity rather than the overall Al content. Fig. 7(a) shows the inverse strain-rate sensitivity as a function of Al solute level in the Mg phase as measured by EDX. Although AE44 has similar overall Al content as AM40, AE44 has significantly lower Al solute in the α-Mg matrix as most of the Al stays is in the form of Al-RE intermetallics [34–36].

The reduced strain-rate sensitivity with increasing Al solute concentration is considered to be related to dynamic strain ageing from the interaction of Al solute and dislocations. The dynamic strain ageing effect does not always manifest itself as serrations on stress-strain curves as reported previously [37,38]. Diffusion of solute elements to dislocations tend to impede their motion [33,37,39,40], leading to a strengthening effect. At higher strain rates the reduced time for diffusion diminishes this strengthening effect [41]. The solute effects, therefore, contribute a negative strain rate sensitivity component, however, in the absence of solute, magnesium has a positive strain

Table 2
The type of twins formed in the tensile tested specimens and the fraction of twinned area determined by EBSD mapping.

Alloy	Strain rate (s^{-1})	Twinned area fraction (%) ± standard deviations					Total twinned area fraction (%)
		{10 $\bar{1}$2}	{10 $\bar{1}$1}	{10 $\bar{1}$3}	{10 $\bar{1}$3}-{10 $\bar{1}$2}	{10 $\bar{1}$1}-{10 $\bar{1}$2}	
AE44	10^{-6}	0.50 ± 0.19	0.19 ± 0.09	[a]			0.69 ± 0.24
	10^{-3}	1.61 ± 0.13	0.39 ± 0.01	0.24 ± 0.16	[a]	0.05 ± 0.07	2.29 ± 0.23
	10^{-1}	2.65 ± 0.42	0.31 ± 0.02	0.26 ± 0.06	0.06 ± 0.10	0.10 ± 0.08	3.38 ± 0.37
AM60	10^{-6}	1.43 ± 0.17	0.20 ± 0.05	0.21 ± 0.05	0.14 ± 0.02	0.11 ± 0.10	2.10 ± 0.34
	10^{-3}	3.68 ± 0.46	0.58 ± 0.02	0.27 ± 0.10	0.15 ± 0.02	0.15 ± 0.06	4.84 ± 0.45
	10^{-1}	4.57 ± 0.50	0.47 ± 0.22	0.16 ± 0.05	0.21 ± 0.14	0.33 ± 0.12	5.80 ± 0.56
AZ91	10^{-6}	5.95 ± 0.32	0.44 ± 0.04	0.31 ± 0.08	0.02 ± 0.001	0.08 ± 0.02	6.81 ± 0.19
	10^{-2}	6.40 ± 0.11	0.39 ± 0.03	0.16 ± 0.03	0.13 ± 0.12	0.21 ± 0.05	7.31 ± 0.17

[a] Insignificant amount.

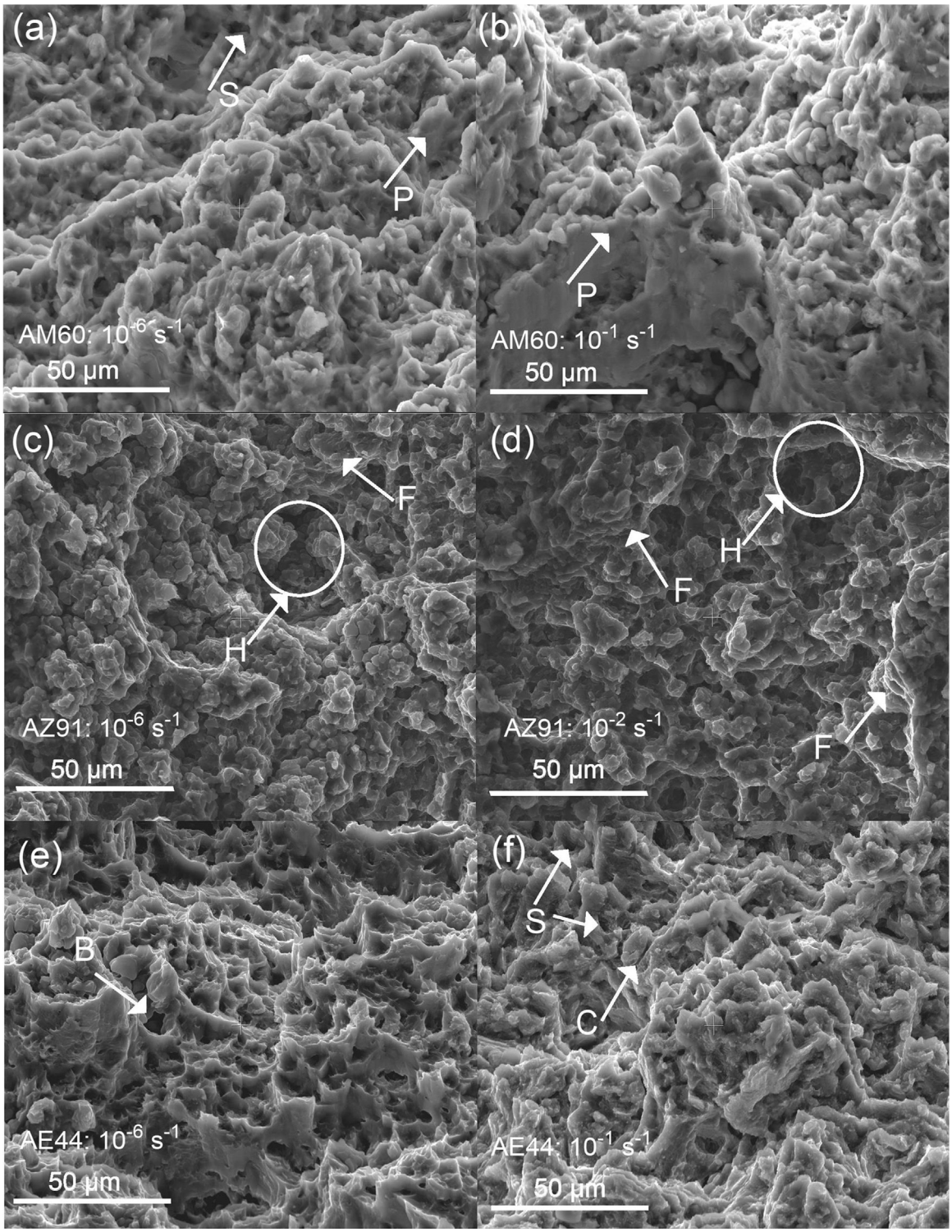

Fig. 5. Secondary electron images of fracture surfaces of (a, b) AM60, (c, d) AZ91 and (e, f) AE44 at different strain rates, showing different features of fracture, such as cleavage plane (P), shrinkage pores (H), facets and steps (F), secondary cracks (C), large dimple (B) and small dimple (S).

rate sensitivity [1]. These two effects are combined in alloys with solute, to result in a lower overall strain rate sensitivity. Increasing Al solute concentration further enhances the dynamic strain ageing effect and reduces the strain-rate sensitivity. Dynamic strain ageing has been previously observed in cast AZ61 and AZ91 alloys due to interactions between Al solute atoms and mobile dislocations by Tahreen et al. [33].

Both AE44 and AE44-T5 have very little Al solute in the α-Mg matrix, and hence they are less likely to be affected by dynamic strain ageing, especially in the T5 condition where even more solute is removed as a result of precipitation [17]. The net result is that the intrinsic strain-rate sensitivity in Mg which is often attributed to the hexagonal closed packed crystal structure [1] is manifested. This is further substantiated by Fig. 3(a). This monotonic increase of strain-rate sensitivity with strain in AE44 and AE44-T5 is the normal behaviour associated with the absence of dynamic strain ageing while the initial decrease of strain-rate sensitivity in AM40, AM60 and AZ91 is a characteristic of dynamic strain ageing [37]. Both AE44 and AE44-T5 show higher strain-rate sensitivity at lower strain rates (Fig. 3(b)).

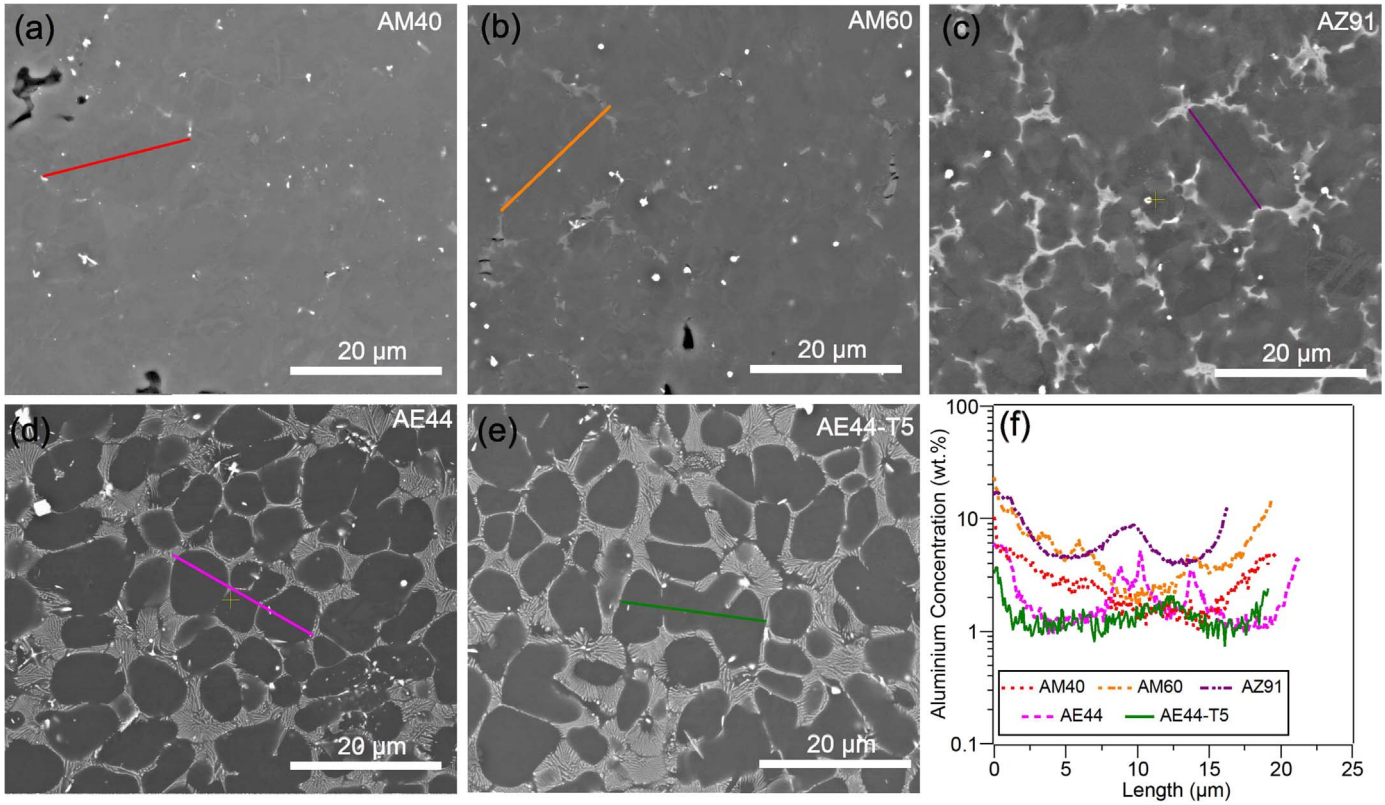

Fig. 6. Backscattered electron images and EDX line profiles of the α-Mg matrix in (a) AM40, (b) AM60, (c) AZ91, (d) AE44, and (e) AE44-T5. The Al concentration (wt%) across the regions indicated in the SEM micrographs is shown in (f). There is an increase in the Al concentration from the centre of the dendrite cells towards the boundaries.

Table 3
Comparison of Al solute concentration (wt%) in the α-Mg matrix obtained by EDX and Pandat®.

Alloy	Al solute concentration (wt%) in α-Mg matrix				
	EDX		Pandat® [32]		
	Centre	Boundaries	Initial Concentration	Solidus (Equilibrium)	Solidus (Scheil)
AM40	2.7	4–5	1.3	3.9	12.5
AM60	3.4	8–10	1.8	5.8	12.5
AZ91	6.5	7–15	2.7	8.7	2.7 (46.5 wt% Zn)
AE44	1.7	2–4	1.2	2.5	12.5
AE44-T5	1.3	2–3	1.2	2.5	12.5

The diminished influence of dynamic strain ageing in AE44 causes the strain-rate sensitivity behaviour to approach that of pure Mg [12].

When dynamic strain ageing takes effect, dislocation movement is restricted by solute and slip becomes more difficult [42]. Consequently other deformation modes such as twinning will be activated to accommodate plastic deformation. The increased twinning activity in the alloys with lower strain-rate sensitivity such as AZ91 is simply a concomitant effect of dynamic strain ageing due to the increased difficulty in slip.

Chun and Davies [27] reported negative strain-rate sensitivity in highly textured wrought AZ31 sheets and suggested that increasing twinning activity would reduce strain-rate sensitivity. As the present alloys have relatively low twinned area fraction and the permanent deformation is more likely to be slip-dominated, the observed differences in strain-rate sensitivity are not considered to be accounted for by twining activity even though the EBSD results seem to be consistent with the dependence of strain-rate sensitivity on twinning activity [27].

The dynamic strain ageing mechanism also provides an alternative explanation for the reported influence of section thickness on strain-rate sensitivity of die-cast AM60 by Gu et al. [15]. They attributed the higher strain-rate sensitivity in the thinner specimen (1.3 mm-thick) to the finer grain size resulting from the faster cooling rate. It might be true that decreasing grain size increases the strain-rate sensitivity, as demonstrated by Figueiredo et al. [12] on pure Mg, however, faster cooling rates also reduce the solute level due to reduced back diffusion during solidification [43]. This is because in non-equilibrium cooling, the microstructure consists of proeutectic α, eutectic α (supersaturated solid solution), and eutectic β. The higher the deviation from equilibrium conditions, the higher the shift of the effective (non-equilibrium) solidus line from the theoretical line. Because of the fast cooling rate in die-casting, the solidus line shifts considerably, leading to a higher amount of eutectic β on the grain boundaries, and a lower amount of aluminium in solid solution [44]. The lowered solute concentration would reduce dynamic strain ageing, leading to higher strain-rate sensitivity for the faster cooled section. Fig. 7(b) shows three similar die-cast AM60 alloy specimens with a variation in strain-rate sensitivity. The increased strain-rate sensitivity in thinner AM60 specimens is more likely due to a lower Al solute concentration. It should be pointed out that present specimens are cylindrical with a 5.6 mm-diameter, and might have a cooling rate in between the 1.3 mm and 6.5 mm-thick flat specimens.

Finally, it is worth briefly discussing the effect of strain-rate sensitivity on tensile ductility (Fig. 2(b)). AE44 with the high strain-rate sensitivity shows larger reduction in ductility and the fracture mode changed from ductile fracture at $10^{-6}\,s^{-1}$ to quasi-cleavage fracture at $10^{-1}\,s^{-1}$. Present results, and results from literature [3,16] have shown that strain-rate sensitivity of die-cast Mg alloys is manifest as an increase in work hardening rate. The higher work hardening rate at $10^{-1}\,s^{-1}$ in AE44 suggests increasing difficulty for dislocations to slip. This could be due to insufficient time for cross-slip or climb of dislocations, leading to more dislocation pile-ups at grain boundaries at

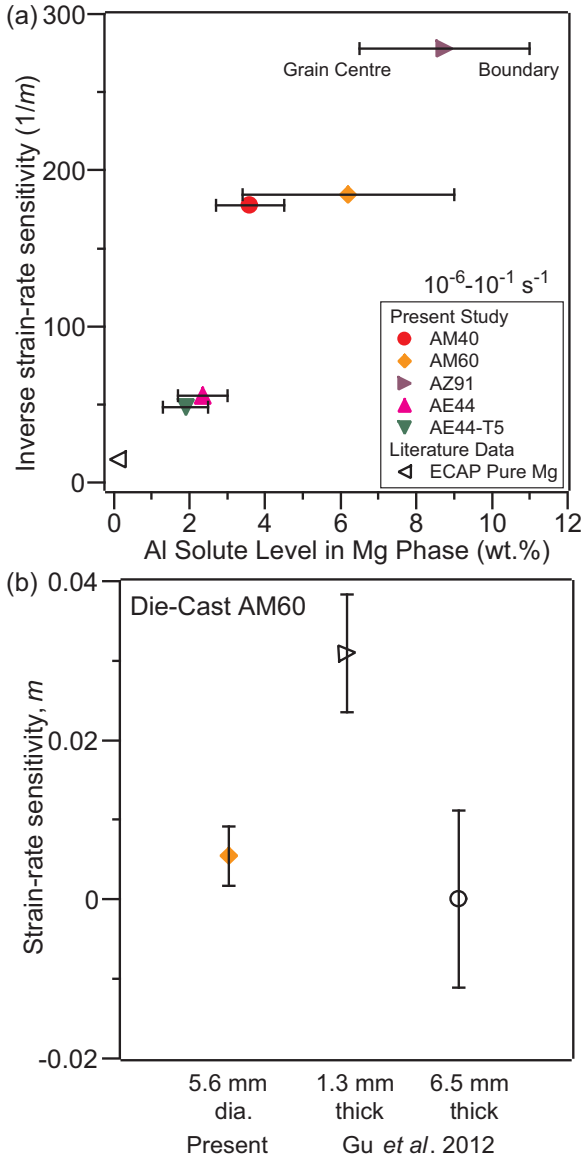

Fig. 7. A correlation of strain-rate sensitivity and Al solute concentration: (a) Inverse strain-rate sensitivity versus Al solute level in Mg phase and (b) strain-rate sensitivity as a function of sample diameter and thicknesses in die-cast AM60. Strain-rate sensitivity of pure Mg [12] and die-cast AM60 [15] taken from literature data are included. Strain-rate sensitivity represents an average for strain rates range 10^{-6}–10^{-1} s^{-1}.

higher strain rates [39], in turn lowering the ductility. While there may be a correlation between strain-rate sensitivity and ductility in AE44, the more brittle fracture of AZ91 is mostly a consequence of the hard and brittle percolating network of $Mg_{17}Al_{12}$ which is abundant and continuous throughout the microstructure, and cracks could easily propagate throughout the material, leading to early fracture [45]. Consequently, ductility is not dependant on strain rate in AZ91.

5. Conclusions

This study has investigated the strain-rate sensitivity in commercial die-cast Mg alloys AM40, AM60, AZ91 and AE44 over a wide strain rate range 10^{-6}–10^{-1} s^{-1}. It is shown that it is the Al solute level in the Mg matrix, rather than the Al content in the alloys in general, that affects the strain-rate sensitivity. The decrease in strain-rate sensitivity with increasing Al solute level is likely related to dynamic strain ageing from the interaction of Al solute with dislocations. The deformation twinning is more active in the alloys with lower strain-rate sensitivity as a result of restricted slip from dynamic strain ageing. The high strain-rate sensitivity in AE44, manifest as an increase in work hardening rate, suggests difficulty in dislocation motion at higher strain rates, reducing the ductility.

Acknowledgements

This work was supported by the Australian Research Council (Grant no. LP130100828). The authors would like to thank Dr. Chengfan Gu, Dr. Matthew Field, Mr. Carmelo Todaro and Mr. Peter Rummel for their technical assistance and acknowledge the use of the RMIT Microscopy and Microanalysis Facility. The authors would also like to thank Dr. Carlos Cáceres from the University of Queensland for his helpful comments on the manuscript.

References

[1] M.A. Meyers, Dynamic Behaviour of Materials, John Wiley & Sons, New York, 1994.
[2] C.A. Newland, M.T. Murray, Strain rate dependent behaviour of magnesium-based alloys, in: Proceedings of the First Australasian Congress on Applied Mechanics, Institution of Engineers, Australia, 1996, pp. 73-76.
[3] T.B. Abbott, M.A. Easton, R. Schmidt, Magnesium for crashworthy components, in: M. Byko (Ed.), Journal of The Minerals, Metals, and Materials Society, TMS Annual Meeting, California, 2003, pp. 227–230.
[4] N. Stanford, M.R. Barnett, Effect of Al and Gd solutes on the strain rate sensitivity of magnesium alloys, Metall. Mater. Trans. A 41 (2010) 734–743.
[5] T.K. Aune, D. Albright, H. Westengen, T.E. Johnsen, B. Anderson, Behavior of die cast magnesium alloys subject to rapid deformation, SAE Technical Paper, 2000. (pp. 2000-01-1116).
[6] J.P. Weiler, J.T. Wood, Strain-rate effects of sand-cast and die-cast magnesium alloys under compressive loading, in: S.N. Mathaudhu, W.H. Sillekens, N.R. Neelameggham, N. Hort (Eds.), Magnesium Technology, 2012 John Wiley & Sons, Florida, 2012, pp. 365–370.
[7] Z. Leng, H.J. Pan, Z.Y. Niu, C.H. Guo, Q. Zhang, Y.P. Chang, et al., Mechanical behavior, deformation and damage mechanisms of Mg–RY–Zn alloy under high strain rate, Mater. Sci. Eng. A 651 (2016) 336–340.
[8] C.H. Guo, F.C. Jiang, R.Z. Wu, M.L. Zhang, Effect of strain rate on compressive mechanical properties of extruded Mg–8Li–1Al–1Ce alloy, Mater. Des. 49 (2013) 110–115.
[9] H. Asgari, J.A. Szpunar, A.G. Odeshi, Texture evolution and dynamic mechanical behavior of cast AZ magnesium alloys under high strain rate compressive loading, Mater. Des. 61 (2014) 26–34.
[10] I.R. Ahmad, D.W. Shu, Tensile properties of die-cast magnesium alloy AZ91D at high strain rates in the range between 300 s^{-1} and 1500 s^{-1}, in: Applied Mechanics and Materials, Trans Tech Publication, Switzerland, 2010, pp. 325–330.
[11] X.Z. Lin, D.L. Chen, Strain hardening and strain-rate sensitivity of an extruded magnesium alloy, J. Mater. Eng. Perform. 17 (2008) 894–901.
[12] R.B. Figueiredo, F. Poggiali, C. Silva, P.R. Cetlin, T.G. Langdon, The influence of grain size and strain rate on the mechanical behavior of pure magnesium, J. Mater. Sci. 51 (2016) 3012–3024.
[13] T. Matsunaga, H. Somekawa, H. Hongo, M. Tabuchi, Deformation mechanism transition with strain rate in Mg–3Al–1Zn alloy at room temperature, Mater. Sci. Eng. A 647 (2015) 212–215.
[14] B.E. Carlson, The effect of strain rate and temperature on the deformation of die cast AM60B, SAE Technical Paper, 1995, p. 950425.
[15] G.Y. Gu, S.T. Lin, Y. Xia, Q. Zhou, Experimental study on influence of section thickness on mechanical behavior of die-cast AM60 magnesium alloy, Mater. Des. 38 (2012) 124–132.
[16] W.Q. Song, P. Beggs, M.A. Easton, Compressive strain-rate sensitivity of magnesium–aluminum die casting alloys, Mater. Des. 30 (2009) 642–648.
[17] S.M. Zhu, T.B. Abbott, M.A. Gibson, J.F. Nie, M.A. Easton, Age hardening in die-cast Mg–Al–RE alloys due to minor Mn additions, Mater. Sci. Eng. A 656 (2016) 34–38.
[18] P. Bakke, K. Pettersen, H. Westengen, Improving the strength and ductility of magnesium die-casting alloys via rare-earth addition, J. Miner. Met. Mater. Soc. 55 (2003) 46–51.
[19] A.V. Nagasekhar, M.A. Easton, C.H. Cáceres, Solute content and the grain microstructure of high pressure die cast magnesium–aluminium alloys, Adv. Eng. Mater. 11 (2009) 912–919.
[20] C.S. Roberts, Magnesium and its Alloys, John Wiley & Sons, New York, 1960.
[21] B.C. Wonsiewicz, W.A. Backofen, Independent slip systems and ductility of hexagonal polycrystals, Trans. Metall. Soc. AIME 239 (1967) 1422–1433.
[22] M.D. Nave, M.R. Barnett, Microstructures and textures of pure magnesium deformed in plane-strain compression, Scr. Mater. 51 (2004) 881–885.
[23] H.Q. Ang, T.B. Abbott, S.M. Zhu, C.F. Gu, M.A. Easton, Proof stress measurement of die-cast magnesium alloys, Mater. Des. 112 (2016) 402–409.
[24] E. Karimi, A. Zarei-Hanzaki, M.H. Pishbin, H.R. Abedi, P. Changizian, Instantaneous strain rate sensitivity of wrought AZ31 magnesium alloy, Mater. Des. 49 (2013) 173–180.
[25] W.S. Lee, T.H. Chen, Rate-dependent deformation and dislocation substructure of Al–Sc alloy, Scr. Mater. 54 (2006) 1463–1468.

[26] C.M. Cepeda-Jiménez, J.M. Molina-Aldareguia, M.T. Pérez-Prado, Origin of the twinning to slip transition with grain size refinement, with decreasing strain rate and with increasing temperature in magnesium, Acta Mater. 88 (2015) 232–244.
[27] Y.B. Chun, C. Davies, Twinning-induced negative strain rate sensitivity in wrought Mg alloy AZ31, Mater. Sci. Eng. A 528 (2011) 5713–5722.
[28] J.W. Liu, D. Chen, Z.H. Chen, H.G. Yan, Deformation behavior of AZ31 magnesium alloy during tension at moderate temperatures, J. Mater. Eng. Perform. 18 (2009) 966–972.
[29] D.G.L. Prakash, D. Regener, W.J.J. Vorster, Microscopic failure modes of hpdc AZ91HP magnesium alloy under monotonic loading, Mater. Sci. Eng. A 488 (2008) 303–310.
[30] J. Song, S.M. Xiong, M. Li, J. Allison, In situ observation of tensile deformation of high-pressure die-cast specimens of AM50 alloy, Mater. Sci. Eng. A 520 (2009) 197–201.
[31] S.G. Lee, G.R. Patel, A.M. Gokhale, A. Sreeranganathan, M.F. Horstemeyer, Quantitative fractographic analysis of variability in the tensile ductility of high-pressure die-cast AE44 Mg-alloy, Mater. Sci. Eng. A 427 (2006) 255–262.
[32] W. Cao, S.L. Chen, F. Zhang, K. Wu, Y. Yang, Y.A. Chang, et al., PANDAT software with PanEngine, PanOptimizer and PanPrecipitation for multi-component phase diagram calculation and materials property simulation, Calphad 33 (2009) 328–342.
[33] N. Tahreen, D.L. Chen, M. Nouri, D.Y. Li, Effects of aluminum content and strain rate on strain hardening behavior of cast magnesium alloys during compression, Mater. Sci. Eng. A 594 (2014) 235–245.
[34] S.M. Zhu, J.F. Nie, M.A. Gibson, M.A. Easton, P. Bakke, Microstructure and creep behavior of high-pressure die-cast magnesium alloy AE44, Metall. Mater. Trans. A 43 (2012) 4137–4144.
[35] S.M. Zhu, M.A. Easton, T.B. Abbott, M.A. Gibson, J.F. Nie, The influence of individual rare earth elements (La, Ce, or Nd) on creep resistance of die-cast magnesium alloy AE44, Adv. Eng. Mater. 18 (2016) 932–937.
[36] M.I. Khan, A.O. Mostafa, M. Aljarrah, E. Essadiqi, M. Medraj, Influence of cooling rate on microsegregation behavior of magnesium alloys, J. Mater. (2014) 1–18.
[37] L.P. Kubin, Y. Estrin, Dynamic strain ageing and the mechanical response of alloys, J. Phys. III 1 (1991) 929–943.
[38] L. Jiang, J.J. Jonas, R. Mishra, Effect of dynamic strain aging on the appearance of the rare earth texture component in magnesium alloys, Mater. Sci. Eng. A 528 (2011) 6596–6605.
[39] A. Van den Beukel, Theory of the effect of dynamic strain aging on mechanical properties, Phys. Status Solidi A 30 (1975) 197–206.
[40] Z. Trojanová, P. Lukác, K.U. Kainer, V. Gärtnerová, Dynamic strain ageing during stress relaxation in selected magnesium alloys containing rare earth elements, Adv. Eng. Mater. 7 (2005) 1027–1032.
[41] G. Rajaram, S. Kumaran, S. Suwas, Effect of strain rate on tensile and compression behaviour of Al–Si/graphite composite, Mater. Sci. Eng. A 528 (2011) 6271–6278.
[42] W.D. Callister, D.G. Rethwisch, Materials Science and Engineering: An Introduction, seventh ed., John Wiley & Sons, New York, 2007.
[43] W. Kurz, D.J. Fisher, Fundamentals of Solidification, fourth ed., Trans Tech Pub, Switzerland, 1998.
[44] S. Spigarelli, M. Regev, E. Evangelista, A. Rosen, Review of creep behaviour of AZ91 magnesium alloy produced by different technologies, Mater. Sci. Tech. 17 (2001) 627–638.
[45] B. Zhang, A.V. Nagasekhar, T. Sivarupan, C.H. Cáceres, Deformation behavior of the percolating intermetallic microstructure of high pressure die cast AZ91 alloy, Adv. Eng. Mater. 15 (2013) 1059–1067.

Chapter 6

Article 3

Anelasticity of die-cast magnesium-aluminium based alloys under different strain rates

Hua Qian Ang[a], Trevor B. Abbott[a,b], Suming Zhu[a], Mark A. Easton[a]

[a]*School of Engineering, RMIT University, Bundoora, Victoria 3083, Australia*
[b]*Magontec Limited, Sydney, New South Wales 2000, Australia*

Materials Science and Engineering: A 2017, volume 707, page 101-109

Available online at
https://doi.org/10.1016/j.msea.2017.09.012

Authorship statement is included in Appendix B.

Materials Science & Engineering A 707 (2017) 101–109

Contents lists available at ScienceDirect

Materials Science & Engineering A

journal homepage: www.elsevier.com/locate/msea

Anelasticity of die-cast magnesium-aluminium based alloys under different strain rates

Hua Qian Ang[a], Trevor B. Abbott[a,b], Suming Zhu[a], Mark A. Easton[a,*]

[a] School of Engineering, RMIT University, Bundoora, Victoria 3083, Australia
[b] Magontec Limited, Sydney, New South Wales 2000, Australia

ARTICLE INFO

Keywords:
Magnesium alloys
Anelasticity
Twinning
Strain-rate sensitivity
High-pressure die-casting

ABSTRACT

Cyclic tension loading-unloading tests were conducted over a wide quasi-static strain rate range $10^{-6}-10^{-1}\ s^{-1}$ on a variety of die-cast Mg-Al based alloys, from which the deformation behaviour, especially the anelasticity, has been systematically studied. At the early stages of deformation, prior to the onset of extensive prismatic slip, the anelastic strain is less dependent on strain rate but varies between the alloys. Upon the activation of extensive prismatic slip, the anelastic strain starts to saturate at a maximum. The maximum increases with increasing strain rate and varies between alloys. The strain-rate dependence of the maximum anelastic strain can be interpreted in terms of solid solution softening/hardening of slip planes and their influence on twinning. Implications of the strain-rate dependence of anelasticity on proof stress measurement of Mg alloys are also discussed.

1. Introduction

The deformation behaviour of magnesium (Mg) alloys is complex due to limited dislocation slip systems [1], leading to difficulties in measuring yield strength [2] and perceived limits to ductility. The limited slip systems results in the activation of twinning to accommodate plastic deformation and the stress-strain curves can be divided into several segments [3–5]. Initial deformation is elastic (stage I) followed by a non-linear region (stage II) in which basal slip and twinning are the dominant deformation mechanisms [6–10]. The twins formed in this region are not stable [11] and can revert during unloading [12], making a large part of stage II deformation reversible. At higher stresses, deformation via prismatic slip takes place leading to extensive plastic deformation (stage III) [3,13]. Eventually the onset of dynamic recovery via the activation of pyramidal slip leads to the final stage of deformation before fracture (stage IV) [13–15].

The focus of this paper is on the reversible component of stage II deformation. The terms anelastic and pseudo-elastic have been used in the past to describe this component [16–20]. The study of anelasticity in stage II is important as it influences several properties including yield strength [2], fatigue strength [21], apparent stiffness [16,17] and sound dampening [11]. The anelastic behaviour of Mg alloys, which manifests as hysteresis loops in loading-unloading stress-strain curves, has been observed in pure Mg and Mg-Zn alloys [17], Mg-Al alloys [22], AZ31 (Mg-3Al-1Zn) [9], AZ91 (Mg-9Al-0.6Zn) [16], AM60B (Mg-6Al-0.3Mn) and AE44 (Mg-4Al-4RE) [21].

This study focuses on high-pressure die-cast alloys. Die-cast alloys account for the large majority of Mg alloy usage and anelasticity contributes significantly to deformation due to the fine grain size. Experiments on pure Mg [23] and die-cast AZ91 [16] have shown that the anelastic effect is more significant in fine-grained alloys. The increase in anelasticity in fine-grained AZ91 was attributed to the formation of fine and unstable twins, which are more prone to revert upon unloading [16]. Anelasticity is also influenced by solute content. The largest anelastic effect has been observed in pure Mg and decreased with increasing Zn [17] and Gd [19] solute concentrations. It was proposed that introduction of solute in solution can lower the critical resolved shear stress (CRSS) for prismatic slip. Consequently, twinning becomes less necessary during deformation, lowering the amount of reversible twinning. Although there was a monotonic decrease in anelasticity with increasing Zn and Gd contents, a similar trend was not observed in Mg-Al alloys; both Mg-0.5Al and Mg-2Al alloys showed similar anelasticity despite the difference in Al content [22]. However, the study was complicated by the fact that the grain size of the Mg-0.5Al alloy was three times larger than that of the Mg-2Al alloy. Anelasticity of Mg alloys has also been observed to be more pronounced in compression than in tension [16,17], due to increased activity of {10 $\bar{1}$ 2} twinning [24].

Recently, the effects of strain rate on the tensile properties and deformation microstructures of a range of Mg die-casting alloys

* Corresponding author.
E-mail address: mark.easton@rmit.edu.au (M.A. Easton).

http://dx.doi.org/10.1016/j.msea.2017.09.012
Received 14 June 2017; Received in revised form 4 September 2017; Accepted 5 September 2017
Available online 08 September 2017

including AM40 (Mg-4Al-0.3Mn), AM60, AZ91, and AE44 (as cast and T5 aged) have been studied by the present authors over a wide strain rate range $10^{-6}-10^{-1}\,s^{-1}$ [25]. It was shown that strain-rate sensitivity decreases with increasing Al solute level in the alloys, due to dynamic strain ageing from the interaction between Al solute and dislocations. It was also shown that deformation twinning is more active in alloys with higher Al solute levels.

The focus of the present work is on the anelastic behaviour of Mg die-casting alloys under a similar strain rate range. The selection of these alloys was influenced in part by their use as commercial alloys, but principally to examine a range of alloy behaviours. AM40, AM60 and AE44-F have moderate strength but good ductility, while AZ91 and AE44-T5 are higher-strength alloys. The strengthening mechanisms within these two alloys are very different with AE44-T5 strengthened by nanoscale precipitates [26] while AZ91 is strengthened, at least in part, by an intermetallic skeleton [27,28]. Comparisons of the amount of anelasticity in these alloys can yield insights into the deformation mechanisms.

2. Materials and experimental details

Mg alloys AM40, AM60, AZ91 and AE44 were high-pressure die-cast in a 250 ton cold chamber machine. More details about the casting process can be found elsewhere [29]. The chemical compositions of these alloys were analysed by inductively coupled plasma atomic emission spectroscopy (ICP-AES) and are listed in Table 1. AE44 specimens were also given an ageing treatment for 32 h at 200 °C (labelled T5).

Cast-to-size cylindrical cross section, dog-bone shaped tensile samples, 100 mm in length with a 36 mm parallel section in the gauge length and a diameter of 5.6 mm were used in this study. Monotonic and cyclic tension loading-unloading tests were performed on an Instron 5569 universal testing machine with a 50 kN load cell at room temperature using a constant rate of crosshead displacement with nominal strain rates in the range from 10^{-6} to $10^{-1}\,s^{-1}$. For the cyclic loading-unloading tests, the samples were loaded to a predetermined strain, unloaded to zero stress and then reloaded again. All alloys were cyclically tested to 3% strain, except AZ91, which was tested to a higher strain (4.5%) in order to determine saturation of anelasticity. Each test was repeated at least twice to ensure reproducibility. Compression tests were not conducted in this study as high-pressure die-cast alloys are relatively isotropic in mechanical properties [30,31].

Deformation microstructures of AE44 after cyclic testing to 3% strain at different strain rates were characterised by electron-backscattered diffraction (EBSD) and transmission electron microscopy (TEM). EBSD data was collected in a FEI Nova NanoSEM at 20 kV using a 0.5-μm step size. HKL Channel 5 Tango subroutine was used to identify the twinning types based on the misorientation angle/axis between the twinned region and matrix. They are {10 $\bar{1}$ 2} twins (i.e. 86° < 12 $\bar{1}$ 0 >), {10 $\bar{1}$ 1} twins (i.e. 56° < 12 $\bar{1}$ 0 >) and {10 $\bar{1}$ 3} twins (i.e. 64° < 12 $\bar{1}$ 0 >) [32–34]. The surfaces of all samples for EBSD analysis were prepared using standard mechanical polishing procedures and were finished by 0.06 μm OP-S. For TEM, the foils were cut from tested specimens and were prepared by ion milling using a Gatan Precision Ion Polishing System (PIPS) at 4 keV with an incident angle of 4°. The thin foils were examined in a JEOL 2100F TEM.

Table 1
Chemical compositions (wt%) determined by ICP-AES for the studied die-cast Mg alloys.

Alloy	Al	Mn	RE (Ce+La)	Zn	Mg
AM40	4.44	0.21	< 0.01	0.05	Bal.
AM60	6.26	0.29	< 0.01	0.1	Bal.
AZ91	8.88	0.19	< 0.01	0.74	Bal.
AE44	3.67	0.31	3.83	< 0.01	Bal.

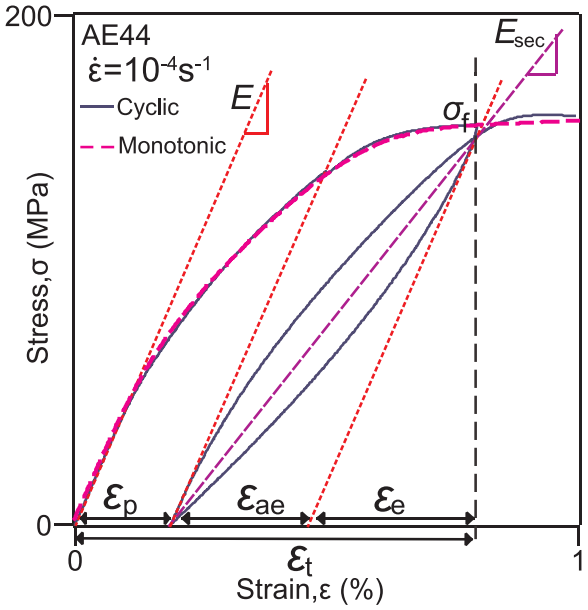

Fig. 1. An overview of cyclic stress-strain curve of die-cast AE44 at $10^{-4}\,s^{-1}$, where the total strain (ε_t) can be separated into linear elastic strain (ε_e), anelastic strain (ε_{ae}) and plastic strain (ε_p). E is the nominal elastic modulus of Mg, taken as 45 MPa [38,39], while E_{sec} is the secant elastic modulus. σ_f is defined as the applied stress where unloading starts. The dashed line is the monotonic tensile flow curve.

3. Results

Fig. 1 shows a typical loading-unloading hysteresis loop for AE44 at $10^{-4}\,s^{-1}$. Several relevant parameters are defined where the total strain (ε_t), is separated into three parts: linear elastic strain (ε_e), anelastic strain (ε_{ae}) and plastic strain (ε_p). Also shown is the corresponding monotonic flow curve. The monotonic flow curve follows closely the cyclic one, indicating that cyclic loading does not have an additional effect on the overall deformation behaviour.

Fig. 2(a) and (b) show the monotonic flow curves of AZ91 and AE44, respectively to illustrate the two extremes of behaviour observed in these experiments. The flow curves of as-cast AE44 consistently shift higher with increasing strain rate while the changes in the flow curves of AZ91 are marginal. The flow curves of aged AE44-T5 show slightly higher strain-rate dependence than that of AE44, while the flow curves of AM40 and AM60 behave more like AZ91, which show a much lower influence of strain rate. Cyclic flow curves (not shown) exhibit the same strain-rate effect as monotonic flow curves.

The monotonic flow curve can also be separated into different stages based on the Kocks-Mecking method of analysis [35,36] extended by Cáceres and his co-workers [3,13,37] for Mg polycrystals. Determination of these stages is illustrated in Fig. 2(c) and (d). Assuming the elastic fraction, f, of the alloy deforms with an elastic modulus, E = 45 GPa [38,39], and the plastically deforming fraction strain hardens at a rate of, Θ_h = 1.4 GPa (pure Mg polycrystals) [3–5], f can be calculated [3]:

$$f = \frac{\frac{d\sigma}{d\varepsilon} - \Theta_h}{E - \Theta_h} \quad (1)$$

Where σ and ε are true stress and strain, respectively. The alloys are fully elastic (stage I) up to ~65 MPa for AZ91 and ~45 MPa for AE44. The departure from pure elasticity indicates the onset of stage II. During stage II, the elastic fraction decreases rapidly due to basal slip and twinning [3–5,37,40,41] and possibly a small amount of prismatic slip. The elastic fraction reaches zero when the alloy becomes fully plastic due to extensive prismatic slip (stage III) [3]. The onsets of these stages are also shown in Fig. 2(a) and (b) and onset values reported in Table 2. Upon extensive activation of prismatic slip, the strain hardening rate

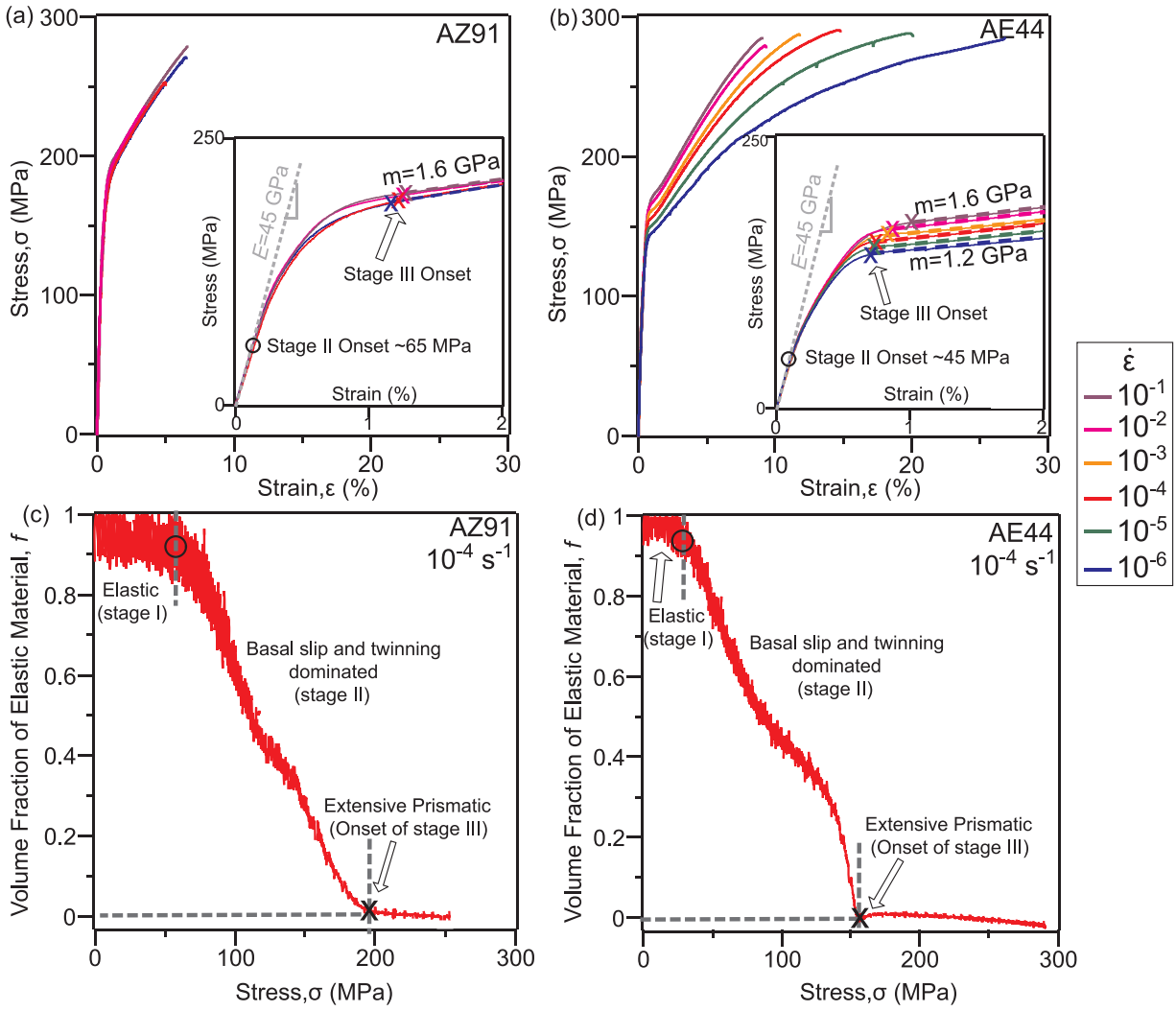

Fig. 2. Monotonic flow curves of (a) AZ91 and (b) AE44 at strain rates $10^{-6}-10^{-1}\,s^{-1}$ which can be separated into different region as illustrated by the volume fraction of (c) AZ91 and (d) AE44 that remained elastic as a function of stress (calculated with Eq. (1)). Onsets of stages II and III are marked by 'O' and 'X', respectively.

Table 2
Stresses and strains at the onsets of stage II and stage III from repeated tests calculated using formalism proposed in literature [3,13,37].

Alloy	Strain rate (s^{-1})	Stage II onset[a]		Stage III onset*	
		Stress (MPa)	Strain (%)	Stress (MPa)	Strain (%)
AM40	10^{-6}	47 ± 2.50	0.12 ± 0.01	126 ± 0.00	0.90 ± 0.02
	10^{-2}	40 ± 0.00	0.11 ± 0.02	132 ± 1.00	0.93 ± 0.02
AM60	10^{-6}	43 ± 0.50	0.10 ± 0.01	147 ± 1.00	1.02 ± 0.08
	10^{-1}	46 ± 4.50	0.11 ± 0.10	155 ± 1.50	1.01 ± 0.03
AZ91	10^{-6}	66 ± 4.00	0.17 ± 0.02	195 ± 3.00	1.25 ± 0.07
	10^{-1}	65 ± 5.00	0.16 ± 0.02	198 ± 0.00	1.29 ± 0.02
AE44	10^{-6}	44 ± 1.00	0.10 ± 0.01	145 ± 3.50	0.79 ± 0.04
	10^{-1}	36 ± 4.00	0.09 ± 0.02	172 ± 0.00	1.14 ± 0.08
AE44-T5	10^{-6}	72 ± 1.00	0.14 ± 0.01	174 ± 2.00	0.82 ± 0.04
	10^{-1}	72 ± 1.00	0.16 ± 0.00	209 ± 2.50	1.28 ± 0.13

[a] The onset values of stage II are taken as the departure from pure elasticity while the onset values of stage III are taken as the start of linear hardening region on the tensile flow curve.

becomes constant (dashed line, prismatic slip-dominated region) at 1.6 GPa in AZ91 and 1.2–1.6 GPa (depending on the strain rate) in AE44, close to the expected value of 1.4 GPa, a value commensurate with athermal accumulation of forest dislocations [5,13]. Comparing AZ91 with AE44, it is interesting to note that in AZ91, the decrease of the elastic fraction towards zero is more asymptotic, indicating a gradual transition from stage II to stage III.

Fig. 3 shows the anelastic strain, ε_{ae} (defined in Fig. 1) as a function of applied strain at strain rates spanning $10^{-6}-10^{-1}\,s^{-1}$. The onset of stage III defined in Fig. 2 is also marked on the anelastic curves. As observed, the anelastic strain saturates at between 0.2% and 0.45%, depending on the alloy and strain rate, after a total strain of 1.5–2%. For a given alloy, the maximum value of anelastic strain increases with strain rate; the changes of this maximum value against strain rate are greatest in aged AE44-T5, followed by AE44, while the changes are lower in AM40, AM60 and AZ91, consistent with the changes in cyclic and monotonic flow curves. While the maximum anelastic strain varies with strain rate, it is interesting to note that anelastic strain is less dependent on strain rate at the early stages of deformation prior to the onset of stage III.

To analyse the difference in deformation microstructures at different strain rates, high strain rate-sensitive alloy, AE44 was examined by EBSD and TEM after cyclic testing to 3% strain as shown in Figs. 4 and 5, respectively. From EBSD analysis, it can be observed that the starting microstructure is twin-free; different types of twins are formed after cyclic tensile deformation with the predominance of {10 $\bar{1}$ 2} extension twins. {10 $\bar{1}$ 2} extension twins also increase with increasing strain rate more than any other twin type (Table 3). {10 $\bar{1}$ 2} extension twinning is more reversible than other twinning types [20,42] because

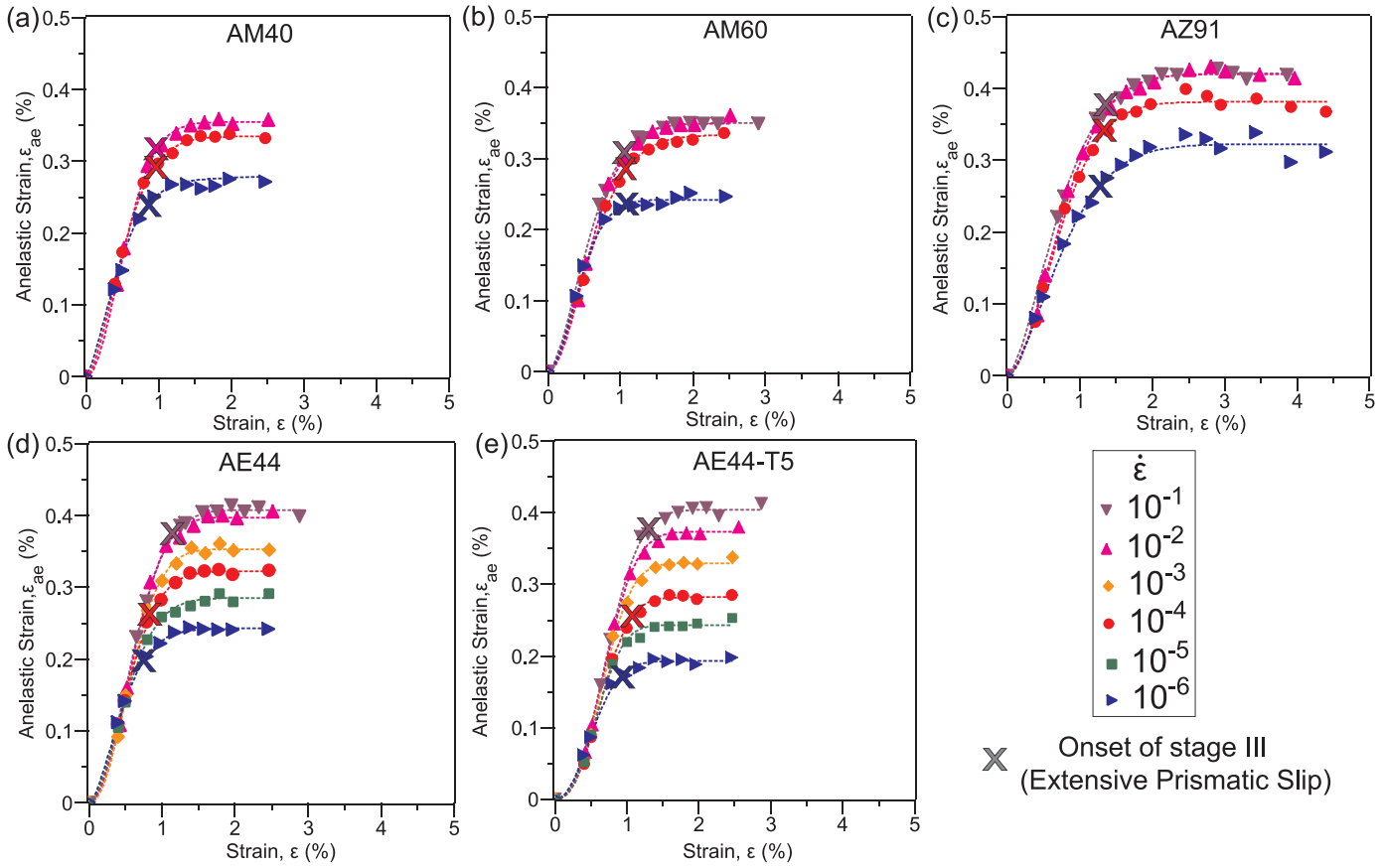

Fig. 3. Anelastic strain (defined in Fig. 1) as a function of strain, for as-cast (a) AM40, (b) AM60, (c) AZ91, (d) AE44 and (e) T5-aged AE44, at strain rate range $10^{-6}-10^{-1}\,s^{-1}$. Onset of stage III, extensive prismatic slip (defined in Fig. 2) is marked by symbol 'X'.

of the near 90° reorientation (86.3°) of the basal pole [33,34]. The increase of {10 $\bar{1}$ 2} twinning with strain rate had also been reported for die-cast AM60 and AZ91 in our previous study [25], although the increase is less in a low strain rate-sensitive alloy AZ91. In TEM images shown in Fig. 5, more dislocations pile-ups are observed when viewed with **g** = [10 $\bar{1}$ 1]. Most dislocation pile-ups become invisible when viewed with **g** = [0002], indicating that they are basal dislocations. Those dislocations that are still visible when viewed with **g** = [0002] are prismatic slip. It is clear that deforming at higher strain rates results in more dislocation pile-ups at twin and grain boundaries.

4. Discussion

The results presented here show that anelasticity is not very strain-rate dependent prior to the onset of stage III (extensive prismatic slip). Upon the onset of stage III, anelasticity starts to saturate, and the maximum anelasticity is strain-rate dependent, suggesting that prismatic slip may influence the anelasticity. In another hexagonal closed-packed metal, Zirconium (Zr) [43], it was observed that a small amount of slip in the Zr matrix may relax the internal stresses which are required to revert the twins during unloading. In this manner, slip dislocations might affect twin reversion. Similarly, later work on pure Mg and Mg-Zn alloys [17] and die-cast AZ91 [16] showed a relationship between reversible twinning and prismatic slip. Easier prismatic slip was thought to reduce the tendency for twinning to occur as a deformation mechanism, with the net result being reduced reversible twinning. The discussion will now consider how strain rate and alloy content affect slip, which in turn results in changes in twinning and consequently anelasticity.

4.1. The effect of strain rate

Prior to the onset of stage III, the changes in anelastic strain with strain rate are smaller (Fig. 3). This is because in stage II, basal slip and twinning are the dominant deformation mechanisms [5,37,40,41]. Since it is well-known that CRSS of basal slip and twinning are strain-rate independent [44–48], it would be expected that the anelastic strain in this region is strain-rate independent. The small variations in anelastic strain in this region could be due to small strain-rate effect of basal slip or presence of small amount of prismatic slip. The latter may be the case for AZ91, which shows a gradual transition from stages II to III (Fig. 2(c)), indicating that prismatic slip may activate early, leading to some strain-rate sensitivity even before the onset of stage III.

Upon onset of stage III, twinning starts to saturate as extensive prismatic slip is activated. Extensive prismatic slip can also reduce the twin boundary mobility [43], and therefore, the anelastic strain starts to saturate (Fig. 3).

The maximum anelasticity then increases with increasing strain rate in the studied alloys. This is due to a delay in the onset of stage III with increasing strain rate, as indicated by the higher onset stress and strain (Fig. 2(a) and (b)). Dislocations are thermally activated [49]. As strain rate increases, there is less time for thermal activation of slip [50], making prismatic slip more difficult to activate at higher strain rates. The CRSS of prismatic slip has also been reported to be dependent on strain rate [44,46]. Firstly, difficulty in activation of prismatic slip at higher strain rate increases the alloys' tendency to twin, in particular {10 $\bar{1}$ 2} twins as shown in Fig. 4 and Table 3. Secondly, the increased dislocation pile-ups at twin and grain boundaries at higher strain rates (Fig. 5) could increase the internal back stresses [51]. Internal back stresses are required to revert the twins [18]. Both phenomena can increase the amount of reversible twinning (larger maximum anelastic

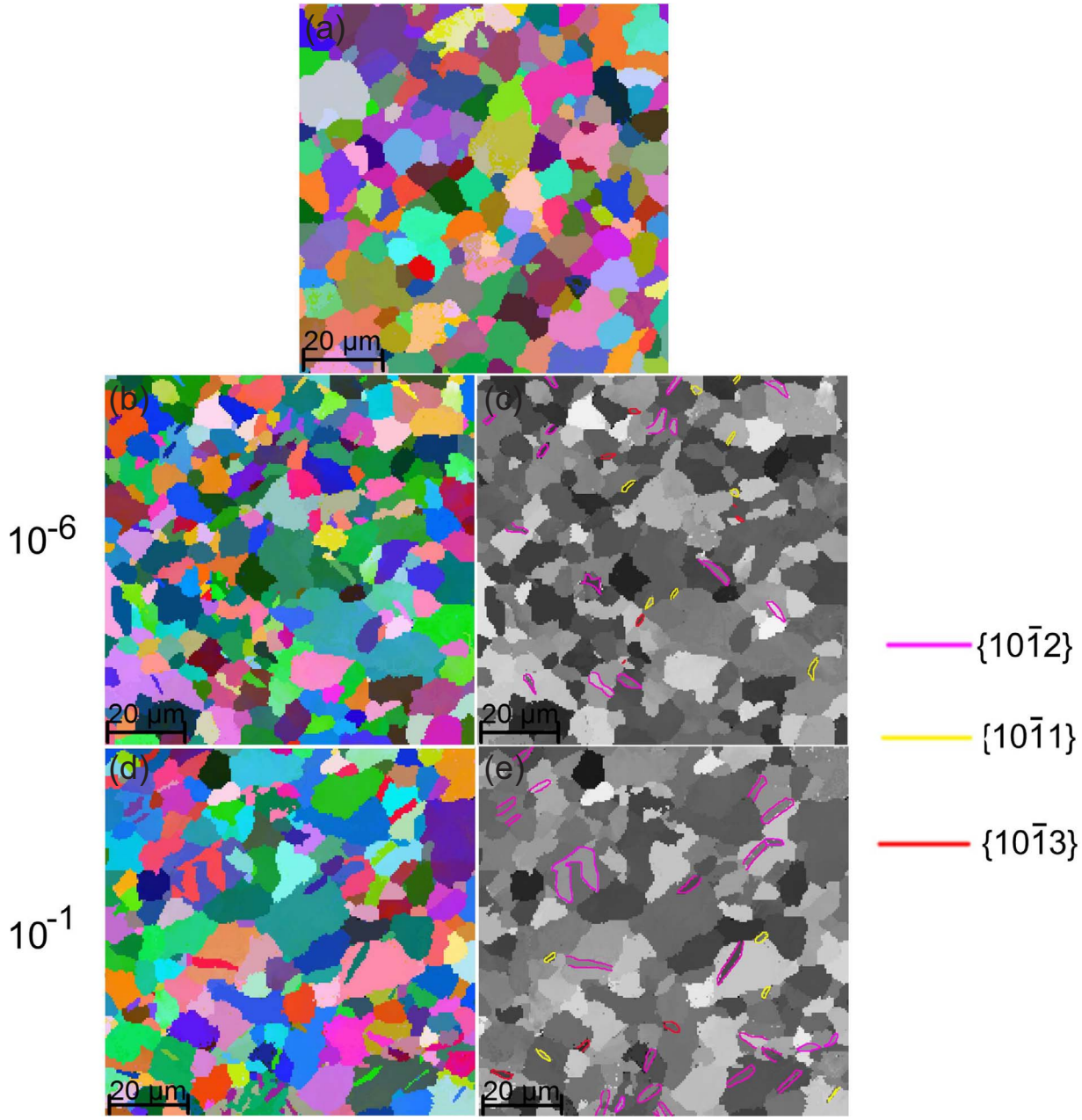

Fig. 4. EBSD maps of AE44 showing (a) twin-free microstructure in as-cast condition and the formation of different types of twins at strain rates of (b, c) $10^{-6}\,s^{-1}$ and (d, e) $10^{-1}\,s^{-1}$ after cyclic testing to 3% strain. The loading direction is horizontal.

strain) at higher strain rates (Fig. 3).

4.2. Inter-alloy comparison

Comparison of Mg-Al alloys AM40, AM60 and AZ91 without RE addition showed that the linear elastic region is extended with increasing Al content due to a delay in the stage II onset (Fig. 6(a)). This suggests that AZ91 has a larger elastic region in comparison with AM40 and AM60. The delay in the stage II onset also reduces the anelasticity in AZ91 at low stresses (Fig. 6(b)). However, AZ91 shows the largest maximum anelastic strain, i.e. the amount at saturation, while AM60 and AM40 show similar maximum anelastic strain (Fig. 7).

The grain sizes of these alloys are similar (~8 μm) so the main difference is the Al content. The major effect of Al at high concentrations such as 9 wt% (AZ91) is solid solution hardening of slip planes [18]. This explains the higher onsets of stage II and III deformation, implying that both basal and prismatic slip are becoming more difficult, respectively. However, Al has little hardening effect on twinning as Al forms near-random solid solutions [52] and does not develop short-range order (SRO) [53]. {10 $\bar{1}$ 2} twinning is shuffling dominated [54,55] and it becomes more difficult when SRO is present. Since both basal and prismatic slip are more difficult in AZ91 while twinning is not hardened by Al; the relative propensity for twinning increases, thereby increasing the maximum anelastic strain.

Another notable observation is the similar maximum anelastic strain in AM40 and AM60 (Fig. 7), despite a notable difference in Al content. This can be rationalised as follows. Additional Al solute up to 2 wt% was found to soften prismatic planes [22], and since Al solute above 9 wt% can harden slip planes [18], the present work suggests that there is a transition from softening to hardening of prismatic planes with increasing Al concentration from 2 to 9 wt%. It is likely that both AM40 and AM60 are near the softening-hardening transition point in which Al content has less of an effect on slip planes, and hence they have similar maximum anelastic strain. This hypothesis is further supported by the

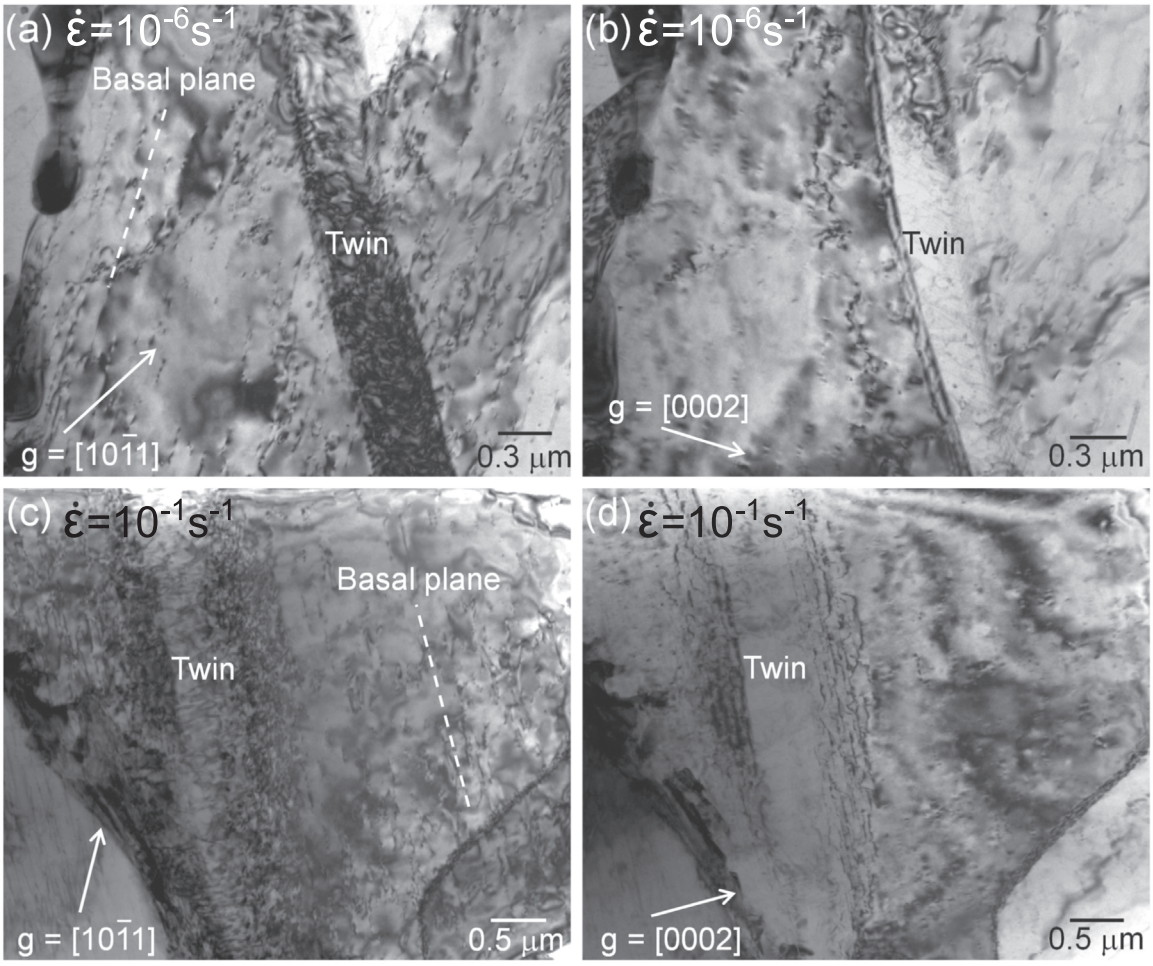

Fig. 5. TEM observations of dislocations pile-ups at twin and grain boundaries in AE44 cyclic tested to 3% strain at (a) $10^{-6}\,s^{-1}$ and (c) $10^{-1}\,s^{-1}$ when viewed with $\mathbf{g} = [10\bar{1}1]$. (b) and (d) are the same area but viewed with $\mathbf{g} = [0002]$.

Table 3
The type of twins formed in high strain rate-sensitive AE44 after cyclic deformation to 3% strain and the twinned area fraction determined by EBSD mapping.

Strain rate (s^{-1})	Twinned area fraction (%)			Total twinned area fraction (%)
	{10 $\bar{1}$ 2}	{10 $\bar{1}$ 1}	{10 $\bar{1}$ 3}	
10^{-6}	1.9 ± 0.10	0.5 ± 0.03	0.2 ± 0.02	2.6 ± 0.11
10^{-1}	3.1 ± 0.10	0.2 ± 0.05	0.1 ± 0.02	3.4 ± 0.07

fact that there is barely any difference between the onsets of stages II and III in AM40 and AM60 (Fig. 6(a)).

Another conundrum arising from the present results is that both AE44 and AE44-T5 have smaller maximum anelastic strain below $10^{-3}\,s^{-1}$; whilst above $10^{-3}\,s^{-1}$, the maximum anelastic strain is observed to increase to be greater than that found in AM40 and AM60 (Fig. 7). AE44, which has a lower amount of Al in solid solution [25], consists of Al-RE intermetallics which are not found in the AM40, AM60 and AZ91 alloys [56,57]. Recent studies on other die-cast Mg alloys showed a measurable strengthening effect of the percolating intermetallic [27,28,58,59], but it is not known if it has an effect on the anelastic deformation. Comparison between Mg-Al-RE and Mg-Al alloys is more complex due to the microstructural differences, and requires further investigation.

Interestingly, in Fig. 7, the increase in the maximum anelastic strain with strain rate is smaller when the prismatic slip (stage III) onset is less strain-rate sensitive, e.g. in AM40, AM60, and AZ91. This further proves that prismatic slip has an indirect effect on the overall anelastic behaviour. The question of interest here is why prismatic slip is more strain-rate sensitive in AE44 and T5-aged AE44. The effect of strain rate on the tensile behaviour of similar die-cast alloys has been investigated in previous work [25], which showed that increasing Al in solution decreases the strain-rate sensitivity in stage III. The reduction in strain-rate sensitivity was explained by dynamic strain ageing due to the interaction of Al solute with dislocations [25]. Both AE44 and AE44-T5 have very little Al solute in the α-Mg matrix, especially in the T5 condition where even more solute is removed as a result of precipitation [26]. Consequently, as previously reported [25] these alloys are less likely to be affected by dynamic strain ageing and the intrinsic strain-rate sensitivity in Mg which is often attributed to the hexagonal closed-packed crystal structure [60] is manifested, especially in the stage III region. Overall, it is the strain-rate dependence of prismatic slip that leads to a variation in maximum anelasticity with strain rate, even though twinning is strain-rate insensitive.

4.3. Effect of precipitation

It has recently been observed that a T5 heat treatment leads to a significant increase in the strength of AE44 with the main change in microstructure being the precipitation of Al-Mn phases and a consequent reduction in solute in the matrix [26]. In Fig. 6(a), the onset of stage II deformation in AE44 and AE44-T5 occurs at stresses ~45 MPa and ~70 MPa, respectively. The extended linear elastic region in AE44-T5 suggests that basal slip is delayed, presumably due to precipitation hardening. Besides the hardening of basal slip, there is also evidence of

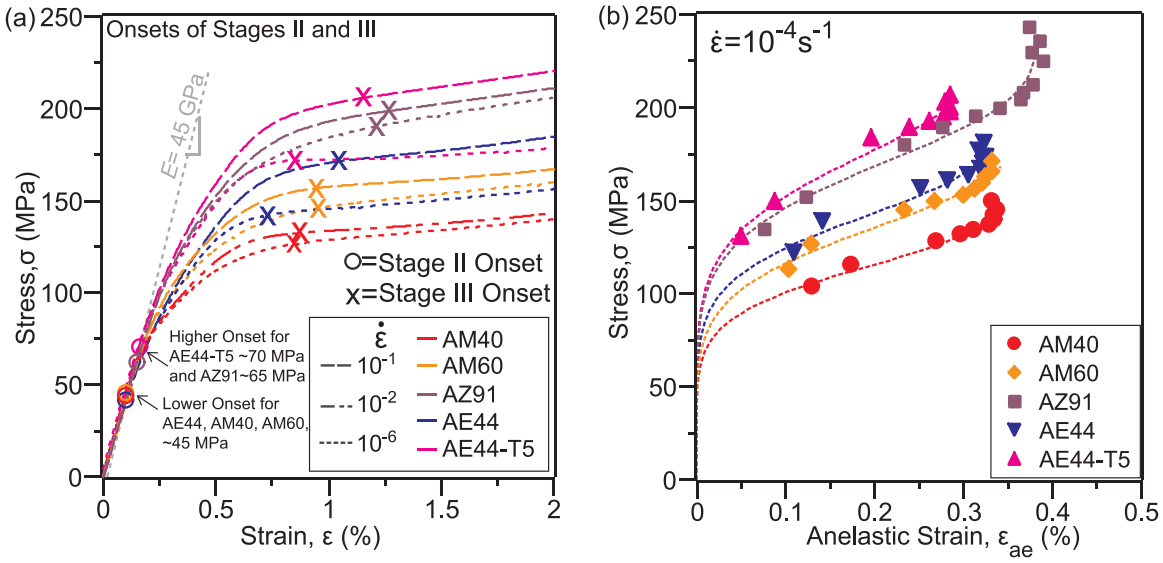

Fig. 6. A correlation between onsets of stages II and III with anelastic strain. (a) Monotonic tensile flow curve with the onsets of stage II marked by 'O' and stage III marked by 'X' and (b) stress as a function of anelastic strain at strain rate $10^{-4}\,s^{-1}$. For onset values, refer to Table 2.

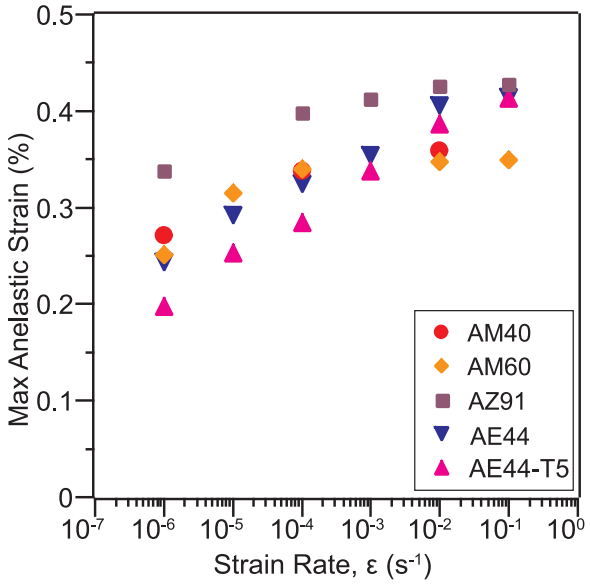

Fig. 7. Maximum anelastic strain as a function of strain rate, for all alloys tested.

hardening of prismatic slip (higher onset of stage III) in AE44-T5. Since both basal and prismatic slip are more difficult in AE44-T5, the total amount of anelastic strain in AE44-T5 should be more than that in AE44 given the argument provided for AZ91, but the present results (Fig. 7) suggest otherwise.

The lower maximum anelastic strain in AE44-T5 compared to AE44 suggests a reduced tendency to de-twin in AE44-T5. In the presence of precipitates, twinning will encounter these precipitates as it propagates along the twin boundaries [61]. An additional stress is required to bow twinning around the particles. If twinning is more difficult due to the presence of precipitates, the amount of de-twinning and consequently anelasticity will also reduce.

In fact, studies have shown that precipitates can suppress different deformation mechanisms, depending on the precipitate morphology [62,63]. For example, rod-like precipitates are more effective in strengthening basal slip than prismatic slip [64], while plate-like precipitates are more effective in inhibiting twinning compared to sphere-like precipitates [61]. The AE44-T5 alloy used in the present study has been characterised by TEM and results showed that the Al-Mn precipitates formed in this alloy are nano-scale particles [26]. Hence, they are likely to have the same strengthening effect on any deformation modes. The presence of precipitates may suppress all deformation mechanisms, leading to a smaller total strain at a given stress (comparing AE44 and AE44-T5 in Fig. 6(a)).

4.4. The effect of anelastic strain on the offset strain for proof stress measurement

The presence of anelasticity in Mg and its alloys has been observed to delay the onset of yielding and make proof stress measurement difficult [2]. A more accurate and consistent proof stress measurement method was previously proposed and it was shown that an appropriate offset strain for 0.2% proof stress should always consider the anelasticity at 0.2% plastic strain [2]. Since the present results show a change in anelastic strain with strain rate, the appropriate offset strain to achieve a 0.2% permanent strain proof stress for AZ91 and AE44 can range from 0.39% to 0.48% and 0.37 to 0.51% respectively, depending on the applied strain rate as shown in Fig. 8. A wider range of offset strain in AE44 compared to AZ91 is a consequence of a larger variation in anelastic strain due to the high strain-rate dependence of prismatic slip in AE44.

5. Conclusions

The anelasticity of commercial die-cast Mg-Al based alloys has been studied across quasi-static strain rates $10^{-6}-10^{-1}\,s^{-1}$. The following conclusions are drawn from this study:

1. Anelastic strain increases with stress and strain at early stages of deformation when basal slip and twinning dominate. The strain-rate insensitivity of these two deformation modes results in little variation of anelastic strain with strain rate in this region. As deformation continues, the anelasticity begins to saturate to a maximum upon activation of extensive prismatic slip. The strain-rate sensitivity of prismatic slip leads immediately to the high strain-rate dependence of maximum anelastic strain.
2. AZ91 has smaller anelastic strain at low stress levels, but it exhibits the largest maximum anelastic strain, when compared to AM40 and AM60. It is proposed that at low Al contents, solution softening of the prismatic planes reduces the need to twin, whereas at the higher concentrations, solid solution hardening in all slip systems (but not

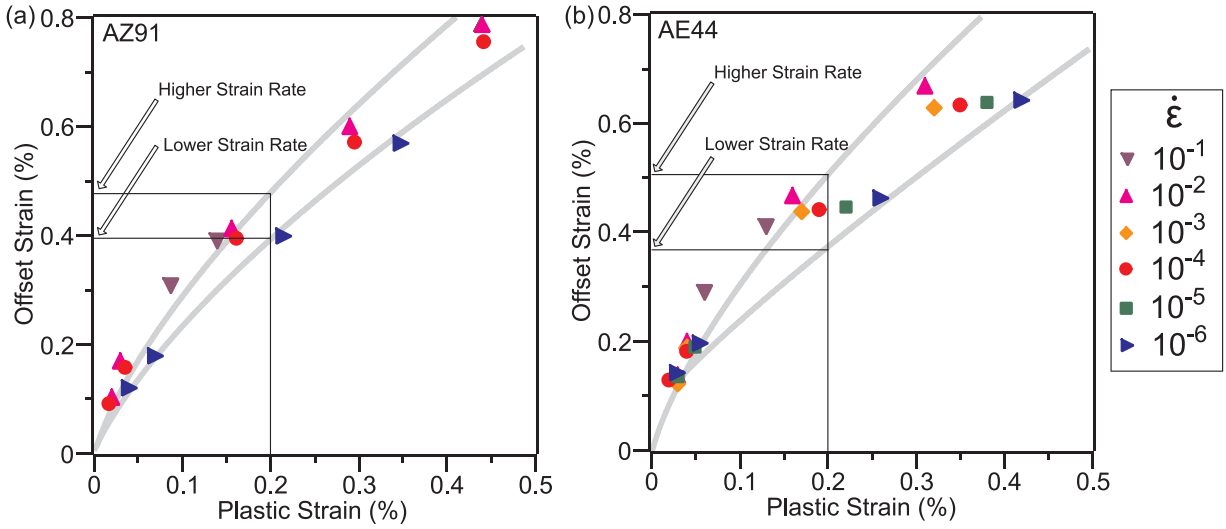

Fig. 8. Offset strain (plastic strain + anelastic strain) as a function of permanent plastic strain for (a) AZ91 and (b) AE44 at strain rate range $10^{-6}-10^{-1}\,s^{-1}$.

twinning) makes dislocation slip more difficult, leading to an increased amount of twinning. The small anelastic strain of AZ91 at low stresses is due to its extended linear elastic region, resulting in a delay in the onset of anelasticity.

3. The presence of precipitates in aged AE44-T5 is observed to harden not only basal and prismatic slip, but also suppress twinning, lowering the anelastic strain in comparison with as-cast AE44.
4. The variation in anelastic strain with strain rate leads to a wide range of offset strains required to achieve a 0.2% permanent strain proof stress even for the same alloy.

Acknowledgements

This work was supported by the Australian Research Council [Grant number LP130100828]. The samples were produced by the CSIRO Manufacturing Flagship with acknowledgement of Mr. Gary Savage and Mr. Andrew Yob. The authors would like to thank Dr. Carlos Cáceres from the University of Queensland for his very helpful comments on the manuscript and acknowledge the use of the RMIT Microscopy and Microanalysis Facility.

References

[1] P.G. Partridge, The crystallography and deformation modes of hexagonal close-packed metals, Metall. Rev. 12 (1967) 169–194.
[2] H.Q. Ang, T.B. Abbott, S.M. Zhu, C.F. Gu, M.A. Easton, Proof stress measurement of die-cast magnesium alloys, Mater. Des. 112 (2016) 402–409.
[3] K.V. Yang, C.H. Cáceres, A.V. Nagasekhar, M.A. Easton, Low-strain plasticity in a high pressure die cast Mg–Al alloy, Model. Simul. Mater. Sci. Eng. 20 (2012) 024010.
[4] K.V. Yang, C.H. Cáceres, C.N. Tomé, The elasto-plastic transition in magnesium alloys (2012 Mar 11–15), in: S.N. Mathaudhu, W.H. Sillekens, N.R. Neelameggham, N. Hort (Eds.), Magnesium Technology 2012: Proceedings of the TMS (The Minerals, Metals & Materials Society), John Wiley and Sons, Orlando, Florida, New York, 2012, pp. 127–131.
[5] C.H. Cáceres, P. Lukáč, Strain hardening behaviour and the Taylor factor of pure magnesium, Philos. Mag. 88 (2008) 977–989.
[6] I.J. Polmear, Light alloys: metallurgy of the light alloys, Metall. Mater. Sci. (1995) 168–195.
[7] M. Pekguleryuz, K. Kainer, A. Kaya, Fundamentals of Magnesium Alloy Metallurgy, first ed., Woodhead Publishing, Cambridge, 2013.
[8] M.H. Yoo, Slip, twinning, and fracture in hexagonal close-packed metals, Metall. Trans. A 12 (1981) 409–418.
[9] J. Koike, N. Fujiyama, D. Ando, Y. Sutou, Roles of deformation twinning and dislocation slip in the fatigue failure mechanism of AZ31 Mg alloys, Scr. Mater. 63 (2010) 747–750.
[10] J.W. Christian, S. Mahajan, Deformation twinning, Prog. Mater. Sci. 39 (1995) 1–157.
[11] T.W. Duerig, R. Zadno, An engineer's perspective of pseudoelasticity, in: T.W. Duerig, K.N. Melton, D. Sto¨ckel, C.M. Wayman (Eds.), Engineering Aspects of Shape Memory Alloys, Butterworth-Heinemann Publisher, Oxford, 1990, pp. 369–393.
[12] O. Muránsky, D.G. Carr, P. Šittner, E.C. Oliver, In situ neutron diffraction investigation of deformation twinning and pseudoelastic-like behaviour of extruded AZ31 magnesium alloy, Int. J. Plast. 25 (2009) 1107–1127.
[13] C.H. Cáceres, A.H. Blake, On the strain hardening behaviour of magnesium at room temperature, Mater. Sci. Eng. A 462 (2007) 193–196.
[14] B.C. Wonsiewicz, Plasticity of Magnesium Crystals [Dissertation], Massachusetts Institute of Technology, Cambridge, 1966.
[15] G. Dieter, Mechanical Metallurgy, SI Metric ed., McGraw-Hill, London, 1988.
[16] C.H. Cáceres, T. Sumitomo, M. Veidt, Pseudoelastic behaviour of cast magnesium AZ91 alloy under cyclic loading–unloading, Acta Mater. 51 (2003) 6211–6218.
[17] G.E. Mann, T. Sumitomo, C.H. Cáceres, J.R. Griffiths, Reversible plastic strain during cyclic loading–unloading of Mg and Mg–Zn alloys, Mater. Sci. Eng. A 456 (2007) 138–146.
[18] D. Nagarajan, X. Ren, C.H. Cáceres, Anelastic behavior of Mg-Al and Mg-Zn solid solutions, Mater. Sci. Eng. A 696 (2017) 387–392.
[19] D. Nagarajan, Anelasticity in cast Mg-Gd alloys, Mater. Sci. Eng. A 695 (2017) 14–19.
[20] S.Y. Lee, M.A. Gharghouri, Pseudoelastic behavior of magnesium alloy during twinning-dominated cyclic deformation, Mater. Sci. Eng. A 572 (2013) 98–102.
[21] Z. Lu, P. Blackmore, Cyclic stress-strain behaviour of AM60B and AE44 cast magnesium alloys and its impact on LCF characterisation and fatigue analysis, SAE Int. J. Mater. Manuf. 7 (2014) 446–453.
[22] D. Nagarajan, C.H. Cáceres, J.R. Griffiths, Anelastic phenomena in Mg Al alloys, in: F. Chmelík, R. Král, J.L. Martin (Eds.), Proceedings of the 12th International Symposium on Physics of Materials, Acta Phys. Polonica A, 122 2012 (No. 3).
[23] C.H. Cáceres, G.E. Mann, J. Griffiths, Grain size hardening in Mg and Mg-Zn solid solutions, Metall. Mater. Trans. A 42 (2011) 1950–1959.
[24] S.R. Agnew, Ö. Duygulu, Plastic anisotropy and the role of non-basal slip in magnesium alloy AZ31B, Int. J. Plast. 21 (2005) 1161–1193.
[25] H.Q. Ang, S.M. Zhu, T.B. Abbott, D. Qiu, M.A. Easton, Strain-rate sensitivity of die-cast magnesium-aluminium based alloys, Mater. Sci. Eng. A 699 (2017) 239–246.
[26] S.M. Zhu, T.B. Abbott, M.A. Gibson, J.F. Nie, M.A. Easton, Age hardening in die-cast Mg–Al–RE alloys due to minor Mn additions, Mater. Sci. Eng. A 656 (2016) 34–38.
[27] B. Zhang, A.V. Nagasekhar, T. Sivarupan, C.H. Cáceres, Deformation behavior of the percolating intermetallic microstructure of high pressure die cast AZ91 alloy, Adv. Eng. Mater. 15 (2013) 1059–1067.
[28] B. Zhang, K.V. Yang, A.V. Nagasekhar, C.H. Cáceres, M.A. Easton, Deformation behavior of the percolating eutectic intermetallic in HPDC and squeeze-cast Mg alloys, JOM 66 (2014) 2086–2094.
[29] A.V. Nagasekhar, M.A. Easton, C.H. Cáceres, Solute content and the grain microstructure of high pressure die cast magnesium–aluminium alloys, Adv. Eng. Mater. 11 (2009) 912–919.
[30] C. Dørum, O.S. Hopperstad, O.G. Lademo, M. Langseth, Numerical modelling of the structural behaviour of thin-walled cast magnesium components, Int. J. Sol. Struct. 42 (2005) 2129–2144.
[31] M.A. Easton, W.Q. Song, T.B. Abbott, A comparison of the deformation of magnesium alloys with aluminium and steel in tension, bending and buckling, Mater. Des. 27 (2006) 935–946.
[32] C.S. Roberts, Magnesium and its Alloys, John Wiley & Sons, New York, 1960.
[33] B.C. Wonsiewicz, W.A. Backofen, Independent slip systems and ductility of hexagonal polycrystals, Trans. Metall. Soc. AIME 239 (1967) 1422–1433.
[34] M.D. Nave, M.R. Barnett, Microstructures and textures of pure magnesium deformed in plane-strain compression, Scr. Mater. 51 (2004) 881–885.
[35] U.F. Kocks, The relation between polycrystal deformation and single-crystal deformation, Metall. Mater. Trans. 1 (1970) 1121–1143.
[36] U.F. Kocks, H. Mecking, Physics and phenomenology of strain hardening: the FCC case, Prog. Mater. Sci. 48 (2003) 171–273.

[37] C.H. Cáceres, P. Lukáč, A.H. Blake, Strain hardening due to {10 1 2} twinning in pure magnesium, Philos. Mag. 88 (2008) 991–1003.
[38] M. Avedesian, H. Baker, Magnesium and Magnesium Alloys—ASM Specialty Handbook Vol. 52 ASM International, The Materials Information Society, Ohio, 1999.
[39] T. Sumitomo, C.H. Cáceres, M. Veidt, The elastic modulus of cast Mg–Al–Zn alloys, J. Light Met. 2 (2002) 49–56.
[40] S.R. Agnew, C.N. Tomé, D.W. Brown, T.M. Holden, S.C. Vogel, Study of slip mechanisms in a magnesium alloy by neutron diffraction and modeling, Scr. Mater. 48 (2003) 1003–1008.
[41] Y. Chino, K. Kimura, M. Mabuchi, Twinning behavior and deformation mechanisms of extruded AZ31 Mg alloy, Mater. Sci. Eng. A 486 (2008) 481–488.
[42] M.A. Gharghouri, G.C. Weatherly, J.D. Embury, J. Root, Study of the mechanical properties of Mg-7.7 at% Al by in-situ neutron diffraction, Philos. Mag. A 79 (1999) 1671–1695.
[43] R.E. Reed-Hill, E.P. Dahlberg, W.A. Slippy Jr, Some anelastic effects in zirconium at room temperature resulting from prestrain at 77 deg K, Trans. Met. Soc. AIME 233 (1965) 1766–1770.
[44] Q. Ma, B. Li, A.L. Oppedal, W.R. Whittington, S.J. Horstemeyer, E.B. Marin, et al., Strain rate dependence of twinning at 450° C and its effect on microstructure of an extruded magnesium alloy, Mater. Sci. Eng. A 559 (2013) 314–318.
[45] M.A. Meyers, O. Vöhringer, V.A. Lubarda, The onset of twinning in metals: a constitutive description, Acta Mater. 49 (2001) 4025–4039.
[46] I. Ulacia, N.V. Dudamell, F. Gálvez, F., S. Yi, M.T. Pérez-Prado, I. Hurtado, Mechanical behavior and microstructural evolution of a Mg AZ31 sheet at dynamic strain rates, Acta Mater. 58 (2010) 2988–2998.
[47] M.R. Barnett, A. Taylor, model based description of the proof stress of magnesium AZ31 during hot working, Metall. Mater. Trans. A 34 (2003) 1799–1806.
[48] C. Bettles, M. Barnett (Eds.), Advances in Wrought Magnesium Alloys: Fundamentals of Processing, Properties and Applications, Woodhead Publishing, Cambridge, 2012.
[49] U.F. Kocks, A.S. Argon, M.F. Ashby, Thermodynamics and kinetics of slip, in: B. Chalmers, J.W. Christian, T.B. Massalski (Eds.), Progress in Materials Science, Pergamon Press, Oxford, 1975, pp. 110–170.
[50] J.W. Morris Jr, Overview of dislocation plasticity, in: K.H.J. Buschow, R. Cahn, M. Flemings, B. Ilschner, E. Kramer, S. Mahajan, P. Veyssiere (Eds.), Encyclopedia of Materials: Science and Technology, Pergamon Press, Oxford, 2001, pp. 4986–4994.
[51] Q. Zhou, J.J. Li, F. Wang, P. Huang, K.W. Xu, T.J. Lu, Strain rate sensitivity of Cu/Ta multilayered films: comparison between grain boundary and heterophase interface, Scr. Mater. 111 (2016) 23–126.
[52] C.H. Cáceres, D.M. Rovera, Solid solution strengthening in concentrated Mg–Al alloys, J. Light Met. 1 (2001) 151–156.
[53] D. Nagarajan, C.H. Cáceres, J.R. Griffiths, Grain Size Hardening Effects in Mg and Its Alloys (Dissertation), University of Queensland, Brisbane, 2014.
[54] B. Li, H.E.I. Kadiri, X.Y. Zhang, S.N. Mathaudhu, Q. Ma, Structural origin of reversible twinning, non-schmid effect, incoherent twin boundaries and texture of hexagonal close-packed metals (11–15 Mar 2012), in: S.N. Mathaudhu, W.H. Sillekens, N.R. Neelameggham, N. Hort (Eds.), Magnesium Technology 2012: Proceedings of the TMS, The Minerals, Metals & Materials Society, Orlando, Florida, 2012, pp. 105–110.
[55] A. Kelly, G.W. Groves, P. Kidd, Crystallography and Crystal Defects, John Wiley & Sons, New Jerseys, 2000.
[56] S.M. Zhu, M.A. Easton, T.B. Abbott, M.A. Gibson, J.F. Nie, The influence of individual rare earth elements (La, Ce, or Nd) on creep resistance of die-cast magnesium alloy AE44, Adv. Eng. Mater. 18 (2016) 932–937.
[57] S.M. Zhu, M.A. Easton, T.B. Abbott, J.F. Nie, M.S. Dargusch, N. Hort, et al., Evaluation of magnesium die-casting alloys for elevated temperature applications: microstructure, tensile properties, and creep resistance, Metall. Mater. Trans. A 46A (2015) 3543–3554.
[58] B. Zhang, S. Gavras, A.V. Nagasekhar, C.H. Cáceres, M.A. Easton, The strength of the spatially interconnected eutectic network in HPDC Mg-La, Mg-Nd, and Mg-La-Nd alloys, Metall. Mater. Trans. A 45 (2014) 4386–4397.
[59] B. Zhang, A.V. Nagasekhar, X.M. Tao, Y.F. Ouyang, C.H. Cáceres, M.A. Easton, Strengthening by the percolating intergranular eutectic in an hpdc Mg–Ce alloy, Mater. Sci. Eng. A 599 (2014) 204–211.
[60] M.A. Meyers, Dynamic Behaviour of Materials, John Wiley & Sons, New York, 1994.
[61] J.D. Robson, N. Stanford, M.R. Barnett, Effect of precipitate shape on slip and twinning in magnesium alloys, Acta Mater. 59 (2011) 1945–1956.
[62] J.F. Nie, Effects of precipitate shape and orientation on dispersion strengthening in magnesium alloys, Scr. Mater. 48 (2003) 1009–1015.
[63] N. Stanford, M.R. Barnett, Effect of particles on the formation of deformation twins in a magnesium-based alloy, Mater. Sci. Eng. A 516 (2009) 226–234.
[64] J.D. Robson, N. Stanford, M.R. Barnett, Effect of particles in promoting twin nucleation in a Mg–5wt% Zn alloy, Scr. Mater. 63 (2010) 823–826.

Chapter 7
Article 4

Constitutive modelling of the deformation behaviour of commercial die-cast magnesium-aluminium based alloys

Hua Qian Ang[a], Trevor B. Abbott[a,b], Suming Zhu[a], Mark A. Easton[a]

[a]*School of Engineering, RMIT University, Bundoora, Victoria 3083, Australia*
[b]*Magontec Limited, Sydney, New South Wales 2000, Australia*

(Manuscript submitted to International Journal of Plasticity)

Authorship statement is included in Appendix B.

Constitutive modelling of the deformation behaviour of commercial die-cast magnesium-aluminium based alloys

Hua Qian Ang[a], Trevor B. Abbott[a,b], Suming Zhu[a], Mark A. Easton[a, *]

[a]*School of Engineering, RMIT University, Bundoora, Victoria 3083, Australia*
[b]*Magontec Limited, Sydney, New South Wales 2000, Australia*

Abstract

Magnesium and its alloys have a complex progression of deformation mechanisms due to the hexagonal closed-packed crystal structure. The deformation behaviour is marked by the commencement of elastic (Stage I), followed by <a> basal slip and twinning (Stage II), <a> prismatic slip (Stage III) and finally <c+a> pyramidal slip (Stage IV). These deformation mechanisms result in four distinct stages of strain hardening in the stress-strain curve. In this study, the four stages of deformation behaviour of a range of commercial die-cast magnesium-aluminium based alloys are modelled. A semi-empirical equation is then proposed to model the entire stress-strain curve. It is shown that both Stages I and III can be described by a linear equation while Stages II and IV follow a power-law relationship and are modelled with the Hollomon's equation. The proposed model provides a good fit to the experimental stress-strain data for AM40, AM60 and AE44. However, there is a slight discrepancy with the experimental data for AZ91 in the Stage II-III transition region. The possible cause for the observed discrepancy in AZ91 is discussed.

Keywords: B. Constitutive behaviour; B. Plasticity; A. Dislocations; A. Twinning; Magnesium alloys; Strain-rate sensitivity

[*] *Corresponding author. Tel: +61 3 9925 6278*
E-mail address: mark.easton@rmit.edu.au

1. Introduction

Die-cast magnesium (Mg) alloys have low density and high specific strength and have found many applications in automotive structural parts, for example, AZ91 (Mg-9Al-1Zn) in steering column brackets and brake pedals, AM40 (Mg-4Al-0.3Mn) and AM60 (Mg-6Al-0.3Mn) in seat frames and instrument panels, and AE44 (Mg-4Al-4RE) in an automotive front engine cradle (Avedesian and Baker, 1999; Bakke et al., 2003; Mordike and Ebert, 2001). A good knowledge of deformation behaviour, especially strain-rate sensitivity is important for understanding the crashworthiness of these alloys.

Recently, the effect of strain rate on the tensile properties (Ang et al., 2017b) and deformation behaviour (Ang et al., 2017a) of similar Mg alloys has been studied by the present authors at strain-rate range 10^{-6}-10^{-1} s^{-1}. It is observed that the deformation behaviour of Mg and alloys can be separated into three regions: elastic, anelastic and plastic (Ang et al., 2016; Cáceres et al., 2003; Mann et al., 2007; Nagarajan, 2017; Nagarajan et al., 2017). Within these regions, the stress-strain curve can be further divided into four stages (Cáceres and Lukáč, 2008; Yang et al., 2012a; Yang et al., 2012b).

Stage I - Elastic deformation is a reversible process which involves stretching of the atomic bonds. The elastic limit of Mg and alloys are relatively low (< 40 MPa), with a consequently short linear region (Ang et al., 2016; Lu and Blackmore, 2014).

Stage II - Beyond the elastic deformation is the onset of anelasticity and plasticity. During this stage, grains with a favorable orientation to the stress axis (soft-oriented grains) deform first via <a> basal slip until they are stopped by obstacles, i.e. grain boundaries, while grains with harder orientations either remain elastic or twin (Akhtar and Teghtsoonian, 1968). As soft-oriented grains diminish their share of elastic strain, hard-oriented grains compensate by becoming more highly stressed. The overall hardening rate in this stage is determined by load sharing between soft and hard-oriented grains (Agnew et al., 2003). <a> Basal slip induces plasticity while reversible twinning contributes to anelasticity (Wang et al., 2013). Due to the limited independent <a> basal slip systems in Mg (Partridge, 1967), twinning is essential to deformation in this region. The anelastic deformation in this stage is reported to be greater than plastic deformation, for example in die-cast AZ91 (Mg-9Al-1Zn) (Cáceres et al., 2003).

Stage III - As deformation continues at a higher stress level, the first available non-basal slip system, i.e. <a> prismatic slip (Akhtar and Teghtsoonian, 1968; Qiao et al., 2015; Stanford and Barnett, 2013) will be activated. In this stage, a combination of <a> prismatic slip and <a> basal slip offers only four independent slip systems (Partridge, 1967) and this still does not satisfy the Von Mises-Taylor criterion (Mises, 1928; Taylor, 1938), therefore, twinning must still be present in this stage. Activation of <a> prismatic slip allows the <a> basal dislocations which were retarded by obstacles in the previous stage to cross slip (change of slip plane from basal to prismatic) to bypass obstacles, creating a forest of dislocations. The strain hardening rate in this stage drops to about 1.4 GPa for pure Mg, a value consistent with athermal accumulation of forest dislocations (Cáceres and Blake, 2007; Cáceres et al., 2008; Kocks and Mecking, 2003).

Stage IV - The end of Stage III is marked by onset of a second non-basal slip system, which experiments show is <c+a> pyramidal slip (Wonsiewicz, 1966). Activation of <c+a>

pyramidal slip reduces the pile-up stresses (back stresses) at obstacles as dislocations piled up at obstacles in previous deformation stages are allowed to escape. This is also known as dynamic recovery (Cáceres and Blake, 2007; Dieter, 1988) which further reduces the strain hardening rate until fracture occurs.

Note that the different stages of deformation behaviour are referring to the different dominating mechanisms themselves (e.g. bond stretching, <a> basal slip, twinning, <a> prismatic and <c+a> pyramidal slip), and the deformation mechanisms in previous stages do not necessarily stop as the next stage commences. Since the stress-strain curve is largely dependent on the strain hardening behaviour of these mechanisms, modelling these different stages individually provides insights into the contribution of each deformation mechanism and this will provide the foundation for future development of improved structural alloys.

To date, modelling of the complete stress-strain curve of Mg and alloys has not been reported, and published work only focused on certain stages of deformation. In the modelling of Mg alloy AZ31 sheet (Takuda et al., 2005), a power law was proposed to express tensile stress as a function of strain, strain rate and temperature. However, their proposed equation is only valid in between 5-7% strain for strain rates of 10^{-2}-10^{0} s^{-1} and temperatures of 423-573 K. Their model does not provide a good fit at the early stages of deformation. The model developed for $\{10\bar{1}2\}$ twinning (Barnett et al., 2015) in an extruded AZ31 can predict the stress-strain curve at low strains, up to 1.5%. However, the model is not able to extend to higher strains due to complex phenomena involved such as interactions between slip and twinning and saturation of twin nucleation at higher strains. Applying the Kocks-Mecking method of analysis (Kocks, 1970; Kocks and Mecking, 2003), Cáceres and his co-workers have analysed the Stage III deformation of permanent mould-cast pure magnesium (Cáceres and Blake, 2007) and die-cast Mg-9Al alloy (Yang et al., 2012a) with a simple linear equation, but other stages of deformation were not investigated. In this work, based on the analysis of deformation mechanisms at different stages, the entire stress-strain curves of a range of die-cast Mg-Al based alloys with various Al contents, i.e. AM40, AM60, AZ91 and AE44 in a wide strain-rate range 10^{-6}-10^{-1} are modelled by a semi-empirical constitutive equation.

2. Deformation Behaviour at Different Strain Rates

Commercial high-pressure die-cast AM40, AM60, AZ91 and AE44 alloys of similar grain sizes (~ 8 μm) were used in this study. Some AE44 specimens were also given an ageing treatment for 32 h at 200 °C (labelled T5). Apart from their commercial importance, these alloys were selected to understand the deformation behaviour of high-strength alloys (AZ91 and AE44-T5) and low-strength alloys (AM40, AM60 and AE44). Both monotonic and cyclic tension loading-unloading tests were carried out at a wide strain-rate range 10^{-6}-10^{-1} s^{-1}. Details of the materials compositions and mechanical testing can be found in recent publications by the authors (Ang et al., 2017a; Ang et al., 2017b).

Fig. 1 shows the monotonic (taken from (Ang et al., 2017b)) and cyclic stress-strain curves at different strain rates for AZ91 and AE44 (alloys with the most different behaviour observed in these experiments). The flow curves of as-cast AE44 consistently shift higher

with increasing strain rate while the changes in the flow curves of AZ91 are smaller. It should be noted that the flow curves of aged AE44-T5 show slightly higher strain-rate dependence than that of AE44, while the flow curves of AM40 and AM60 behave more like AZ91, which show a much reduced effect of strain rate under both monotonic and cyclic testing. The original paper (Ang et al., 2017b) showed that the reduction in strain-rate sensitivity with increasing Al contents in solution was due to dynamic strain ageing from the interaction between Al solute and dislocations. As also reported (Ang et al., 2017b), both AE44 and AE44-T5 have very little Al solute in the α-Mg matrix, especially in the T5 condition where even more solute is removed as a result of precipitation (Zhu et al., 2016), and therefore they are less likely to be affected by dynamic strain ageing and the intrinsic strain-rate sensitivity in Mg attributed to its hexagonal closed-packed crystal structure (Meyers, 1994) is observed. Cycling does not affect the strain hardening behaviour as monotonic flow curve (dashed line) follows closely with the cyclic one.

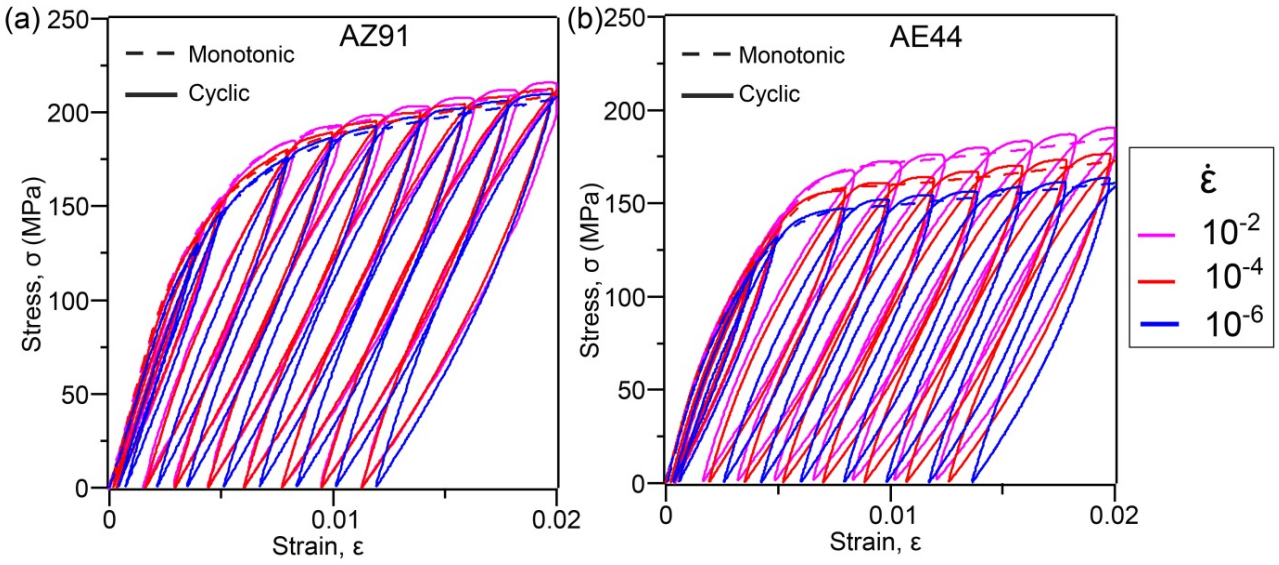

Fig. 1. Monotonic (dashed) and cyclic (solid) stress-strain behaviour of (a) AZ91 and (b) AE44 at different strain rates, $\dot{\varepsilon}=10^{-6}$-$10^{-2}$ s^{-1}.

3. Constitutive Modelling of Deformation Behaviour

3.1 Stage I: Elasticity

Elastic deformation is well understood as a change in shape of a material at low stress that is recoverable after the applied stress is removed. In this stage, the applied stress, σ is proportional to elastic strain, ε_I and the deformation behaviour is governed by Hooke's law:

$$\sigma = E\,\varepsilon_I \tag{1}$$

For Mg and alloys, the stress-strain curve has very small linear elastic region which applies only at low stress levels (< 40MPa) (Ang et al., 2016; Lu and Blackmore, 2014;

Nagarajan, 2017; Nagarajan et al., 2017), where the elastic modulus of Mg, E=45 GPa (Avedesian and Baker, 1999; Sumitomo et al., 2002) is measured.

3.2 Stage II: <a> Basal Slip and Twinning

The departure of linear elasticity is marked by the onset of anelastic and plastic deformations. During this stage, soft-oriented grains will undergo plastic deformation first by <a> basal slip. However, due to the hexagonal closed-packed crystal structure of Mg and alloys, <a> basal slip provides only two independent slip systems (Partridge, 1967) and this does not satisfy the von Mises-Taylor criterion (Mises, 1928; Taylor, 1938) for homogeneous deformation. Therefore, most grains in this region will undergo twinning (Christian and Mahajan, 1995; Pekguleryuz et al., 2013; Yoo, 1981). However, twins formed during loading are not stable (Duerig and Zadno, 1990); and they can revert during unloading (Muránsky et al., 2009), giving rise to large hysteresis loops as observed in cyclic stress-strain curves (Fig. 1). The anelastic strain is measured from the width of these hysteresis loops (Cáceres et al., 2003; Lu and Blackmore, 2014; Nagarajan et al., 2017). Therefore, this stage is a mix of anelasticity and plasticity. For the sake of the following discussion, the term anelastic strain, ε_{ae} is associated only with reversible twinning; while Stage II strain, ε_{II} is made up of anelasticity and plasticity, and is composed of all three mechanisms, <a> basal slip, irreversible twinning and reversible twinning.

To examine the relationship between ε_{II} and ε_{ae}, ε_{II} taken from monotonic flow curve and ε_{ae} taken from hysteresis loops in cyclic flow curve are plotted in Fig. 2. It is clear that ε_{ae} (dotted) is proportional to ε_{II} (dashed) and ε_{II} is composed of 60-75% of ε_{ae} depending on the alloy. In short, twinning dominates in Stage II and most twins that form revert upon unloading, correlating well with the literature for fine-grained high-pressure die-cast Mg alloys (Cáceres et al., 2003; Mann et al., 2007).

It is observed that ε_{ae} is insensitive to strain rate prior to reaching the maximum value. This is because at early stages of deformation when <a> prismatic slip is absent, deformation is controlled by <a> basal slip and twinning which are less strain-rate sensitive (Barnett, 2003; Bettles and Barnett, 2012; Ma et al., 2013; Meyers et al., 2001; Ulacia et al., 2010). As deformation continues, anelasticity begins to saturate to a maximum upon extensive activation of <a> prismatic slip. The strain-rate sensitivity of <a> prismatic slip (Ma et al., 2013; Ulacia et al., 2010) leads immediately to the high strain-rate dependence of maximum anelastic strain (Ang et al., 2017a).

Since ε_{II} is made up of 60-75% of ε_{ae} (Fig. 2), and the irreversible twinning fraction was observed to be less than 10% in these die-cast alloys (Ang et al., 2017b), a simple assumption is made that ε_{II} can be modelled like ε_{ae}, being strain-rate insensitive at early stages of deformation prior to reaching a maximum.

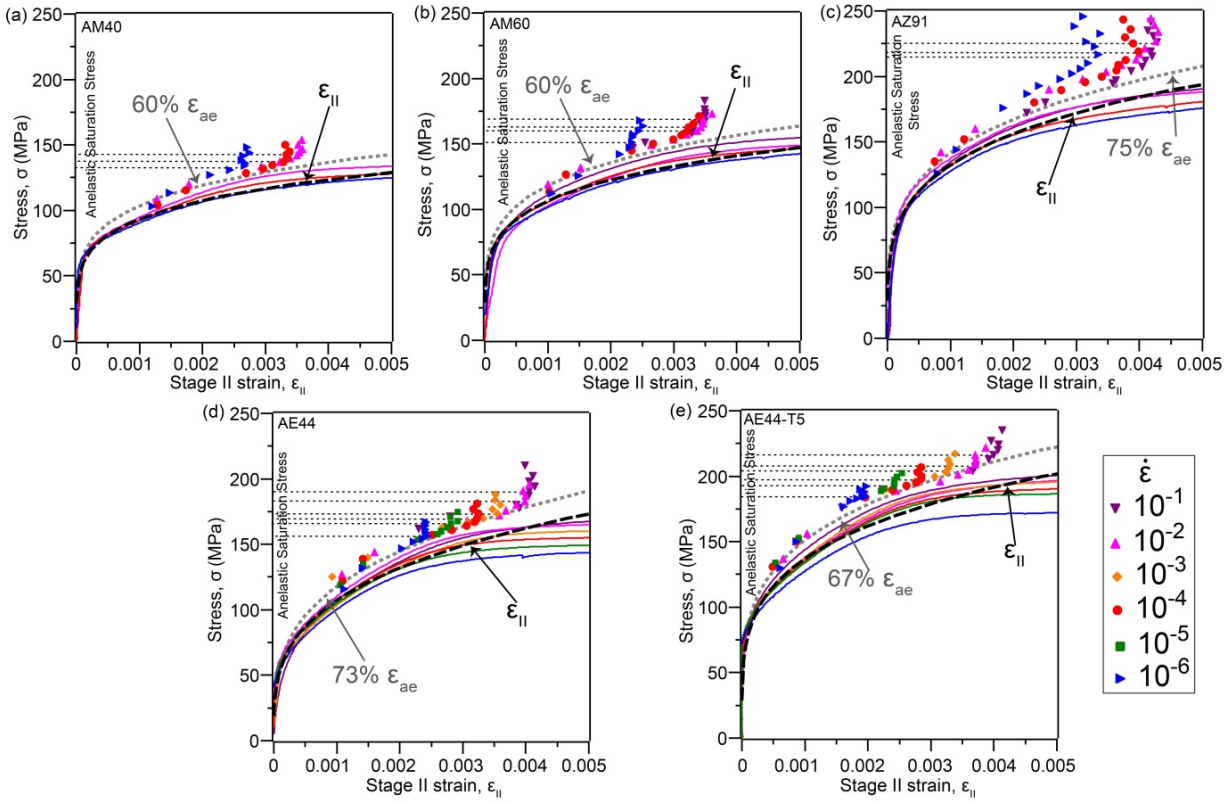

Fig. 2. Applied stress as a function of Stage II strain, for as-cast (a) AM40, (b) AM60, (c) AZ91, (d) AE44 and (e) AE44-T5, at strain-rate range 10^{-6}-10^{-1} s^{-1}. Dotted line is the anelastic strain and dashed line represents the stage II strain which is composed of 60-75% of anelastic strain.

Modelling of Stage II deformation has not yet been reported but anelasticity which follows the same trend as Stage II has been modelled with a Weibull function for its sigmoidal relationship with applied stress (Mann et al., 2007):

$$\varepsilon_{ae} = \varepsilon_{ae,\,max}\,[\,1 - \exp\{-(\frac{\sigma}{\sigma_1})^{m_e}\}\,] \qquad (2)$$

where $\varepsilon_{ae,max}$ is the maximum anelastic strain, σ_1 is the stress where anelasticity increases the fastest and m_e is the Weibull modulus. However, anelasticity can be further divided into strain-rate insensitive and sensitive components as observed in Fig. 2. The Weibull function cannot clearly reflect these two distinct regions of anelasticity because any changes to the Weibull function parameters change the entire function curve and not just the maximum. This is illustrated in Fig. 3(a) using the ε_{ae} measured from AE44 at 10^{-4} s^{-1} as an example. In contrast, Fig. 3(b) shows that a much simpler power-law relationship is able to model the strain-rate insensitive component of the anelasticity while the strain-rate sensitive component (maximum anelastic strain) can be included in the modelling of Stage III deformation as discussed in Section 3.3.

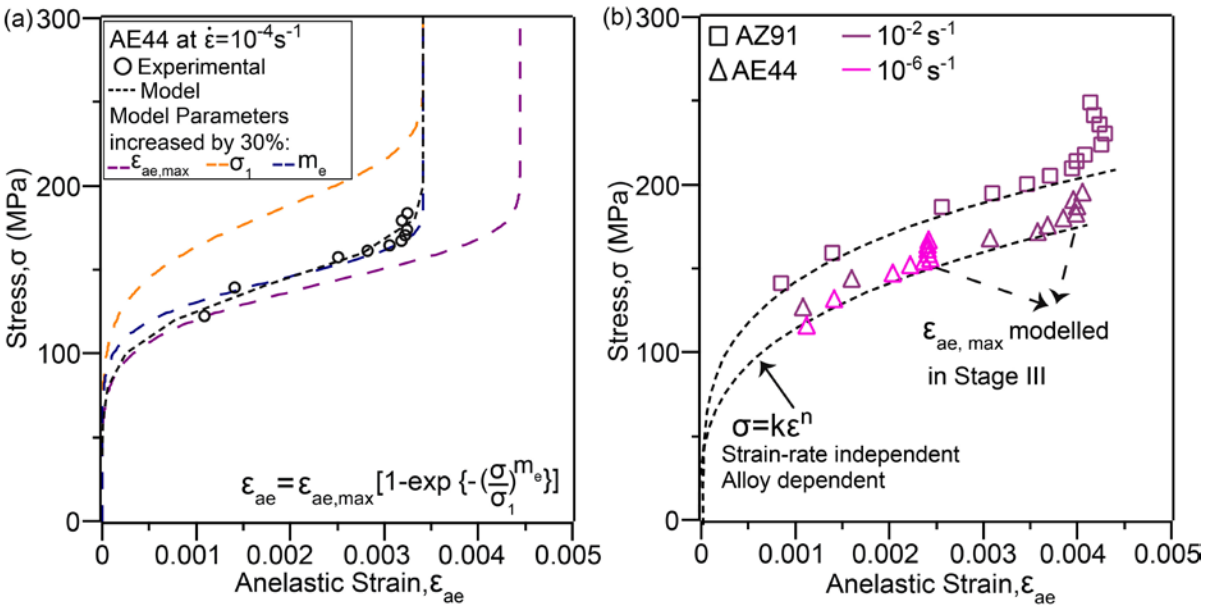

Fig. 3. Comparison of Weibull function and power law. (a) A Weibull function diagram illustrating any changes in Weibull function parameters can change the entire function curve and cannot reflect the strain-rate insensitive and sensitive components of anelasticity, and (b) a power law modelling the strain-rate insensitive region of anelasticity.

Due to this dilemma, we suggest modelling the strain-rate insensitive component of Stage II with:

$$\sigma = K_{II}\,\varepsilon_{II}^{n_{II}} \tag{3}$$

where K_{II} is the strength coefficient and n_{II} is the strain hardening exponent in Stage II. The next step is to determine the upper limit of Eq. (3) to describe the strain-rate sensitivity of the maximum anelasticity.

To find this upper limit, the strain-rate sensitive maximum anelasticity needs to be reviewed. There seems to be a correlation between maximum anelastic stress, $\sigma_{ae,max}$ and the stress when Stage III strain reaches 0.01 (for AM40, AM60, AE44) and 0.015 (for AZ91) as shown in Fig. 4. $\sigma_{0.01,III}$ and $\sigma_{0.015,III}$ denote the stresses when Stage III strain (also known as <a> prismatic strain), ε_{III}, reaches 0.01 and 0.015, respectively. Unlike the rest of the alloys, $\sigma_{0.01,III}$ in AZ91 does not match its $\sigma_{ae,max}$ (symbol deviates from dashed line), indicating that the maximum anelasticity in AZ91 saturates at a higher ε_{III} of 0.015. Determination of ε_{III} is covered in Section 3.3.

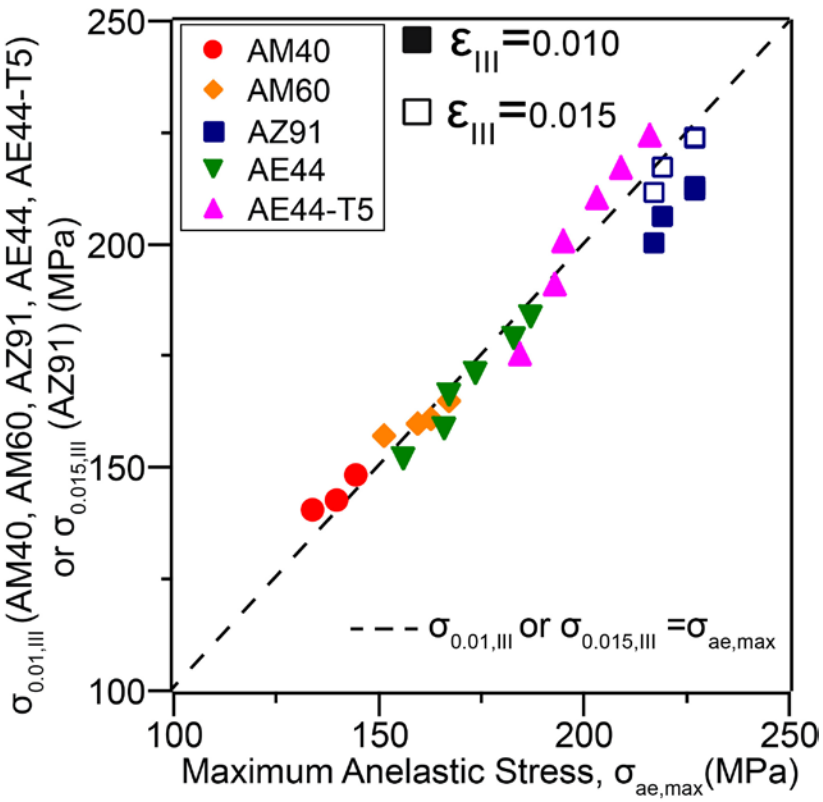

Fig. 4. Stress when ε_{III} reaches 0.01 for as-cast AM40, AM60, AZ91, AE44 and AE44-T5 and 0.015 for AZ91 as a function of maximum anelastic stress.

The possibility of anelasticity reaching a maximum at ε_{III} of ~ 0.01-0.015 is consistent with other work. Previous experiments showed that maximum anelasticity occurred at a plastic strain of ~ 0.01 for mold-cast Mg-Gd alloys (Nagarajan, 2017), ~ 0.015 for sand-cast pure Mg and Mg-Zn alloys (Mann et al., 2007) and die-cast AZ91 (Cáceres et al., 2003), ~ 0.02 for sand-cast Mg-Al alloys (Nagarajan et al., 2012). When deformation is small, less than a strain of 0.01, twins can multiply undisturbed, and anelasticity increases with stress and strain. When deformation is large, exceeding a strain of 0.01, activation of other slip systems, such as <a> prismatic slip, in the matrix surrounding the twins will decrease the twin boundary mobility. Consequently, reversible twinning is restricted (Cui et al., 2017; Reed-Hill et al., 1965). Considering this information, an assumption is made that Stage II saturates (due to saturation of reversible twinning) when anelasticity reaches a maximum upon extensive activation of <a> prismatic slip at ε_{III} of 0.01 for AM40, AM60 and AE44 and 0.015 for AZ91.

With this assumption in mind, Fig. 5 compares the experimental Stage II curves with those computed by Eq. (3) at low ε_{II} of no more than 0.0015 for AZ91 and AE44. This low ε_{II} value was chosen to ensure no involvement of <a> prismatic and <c+a> pyramidal slip in the modelling of Stage II. It is observed that Stage II starts at about 25 MPa for AE44 and about 40 MPa for AZ91 when ε_{II} becomes significant, indicating that AZ91 has a larger elastic region. The experimental flow curves (solid) in this stage show no strain-rate dependency. The slight difference between the flow curves is due to experimental variation,

and an average flow curve (dashed) is fitted. The K_{II} and n_{II} values for each strain rate and alloy from repeated tests are summarised in Table 1.

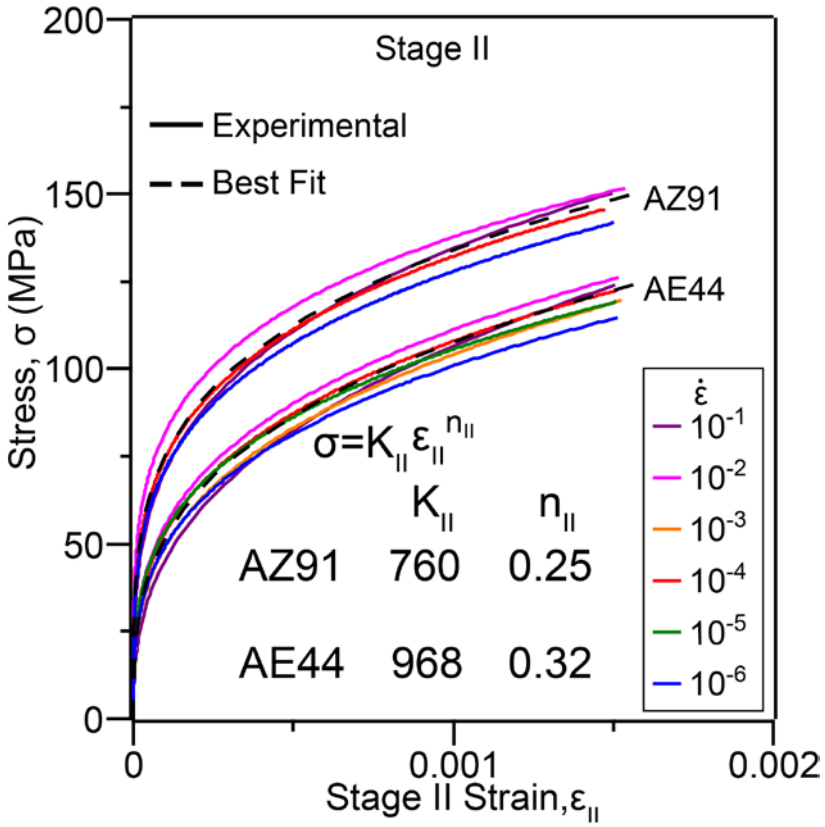

Fig. 5. Average deformation behaviour of Stage II for AZ91 and AE44, best fit using Eq. (3) (dashed) are compared with experiments (solid).

Table 1. Parameters in Stage II: K_{II} (MPa) and n_{II} of best fit of Eq. (3).

$\dot{\varepsilon}$	AM40		AM60		AZ91		AE44		AE44-T5	
	K_{II}	n_{II}	K_{II}	n_{II}	K_{II}	n_{II}	K_{II}	n_{II}	K_{II}	n_{II}
10^{-6}	337±0.84	0.19±0.00	507±59.2	0.23±0.02	1049±316	0.30±0.05	794±61.7	0.30±0.01	565±42.9	0.21±0.02
10^{-5}	-	-	-	-	-	-	864±67.7	0.30±0.01	679±0.42	0.23±0.00
10^{-4}	411±31.6	0.22±0.01	455±1.50	0.21±0.00	591±148	0.21±0.04	955±59.7	0.32±0.01	714±25.4	0.24±0.01
10^{-3}	-	-	-	-	-	-	987±2.17	0.33±0.00	757±4.10	0.25±0.00
10^{-2}	412±1.44	0.21±0.00	610±77.7	0.26±0.02	654±0.26	0.23±0.00	898±5.37	0.31±0.00	766±0.11	0.25±0.00
10^{-1}	-	-	638±2.32	0.26±0.00	916±0.07	0.28±0.00	1369±1.25	0.37±0.00	791±1.47	0.25±0.00
Average	387±39.5	0.21±0.01	552±89	0.24±0.02	803±256	0.25±0.05	978±190	0.32±0.02	712±77.9	0.24±0.01

3.3 Stage III: <a> Prismatic

The end of Stage II is determined by the onset of <a> prismatic slip. In this stage, any <a> basal plane dislocations inhibited by obstacles (i.e. grain boundaries) are allowed to cross slip, relaxing the dislocation pile-up stresses at grain boundaries. Activation of <a> prismatic slip allows cross slip to occur and creates a forest of dislocations in the process. The strain

hardening rate in this stage is linear and follows an equation of the form (Cáceres and Blake, 2007; Dieter, 1988; Kocks and Mecking, 2003):

$$\sigma = \Theta\, \varepsilon_{III} + \sigma_y \tag{4}$$

where ε_{III} is the <a> prismatic strain, σ_y is the <a> prismatic yield stress, and Θ is the strain hardening rate in Stage III (slope), with the definition (Kocks and Mecking, 2003; Mecking and Kocks, 1981):

$$\Theta = \Theta_h - \Theta_r(\dot{\varepsilon}, T) \tag{5}$$

The first term Θ_h is the athermal component of strain hardening rate which is between 1-2 GPa (Cáceres and Blake, 2007). Θ_h is ≈ E/32 ≈ 1.4 GPa for pure Mg (Cáceres and Blake, 2007) and Mg-9Al (Yang et al., 2012a), and ≈ E/25 ≈ 1.8 GPa for AZ31 (Yang et al., 2012b), where E is the elastic modulus of Mg (45 GPa (Avedesian and Baker, 1999)). Θ_h is insensitive to many variables and it varies only slightly from one metal to another (within a factor of 2) (Hirsch and Mitchell, 1967; Kocks, 1966). For face-centred cubic polycrystals (Kocks and Mecking, 2003), $\Theta_h \approx E/50$.

The second term Θ_r is the thermal component which describes the dynamic recovery rate. Θ_r is both strain-rate and temperature dependent and it accounts for any softening effects due to dislocation annihilation as temperature (T) increases and/or strain rate ($\dot{\varepsilon}$) decreases. At the limit of the highest strain rate or lowest temperature, Θ_r approaches zero, and $\Theta = \Theta_h$.

The modelling of Θ is not very well defined. Kocks and Mecking (2003) defined Θ as

$$\Theta = \Theta_h\left(1 - \frac{\sigma_y/\mu}{r(\dot{\varepsilon},T)\,\sigma_{y_0}/\mu_0}\right) \tag{6}$$

and r:

$$r = \left\{1 - \sqrt{\left(\frac{1}{g_0}\,\frac{kT}{\mu b^3}\,\ln\frac{\dot{\varepsilon}_0}{\dot{\varepsilon}}\right)}\right\}^2 \tag{7}$$

where σ_{y_0} is a mechanical threshold (<a> prismatic yield stress at 0 K); μ is the shear modulus, μ_0 is the shear modulus at 0 K; g_0 is an extrapolated value from Fig. 26 in (Kocks and Mecking, 2003) and has no identified physical meaning; k is the Boltzmann constant; b the magnitude of the Burgers vector of the dislocations and $\dot{\varepsilon}_0$ is a constant (Kocks and Mecking, 2003).

Here, by combining Eqs. (6) and (7), Θ is calculated using

$$\Theta = \Theta_h - \Theta_h \frac{A}{\left\{1 - \sqrt{B\,T\ln\left(\frac{C}{\dot{\varepsilon}}\right)}\right\}^2} \tag{8}$$

where A, B, C are grouped constants made up of individual functional dependence:

$$A = \frac{\sigma_y/\mu}{\sigma_{y_0}/\mu_0} \quad (9)$$

$$B = \frac{1}{g_0}\frac{k}{\mu b^3} \quad (10)$$

$$C = \dot{\varepsilon}_0 \quad (11)$$

and <a> prismatic yield stress, σ_y can be modelled as Eq. (12) as reported (Mecking and Kocks, 1981):

$$\sigma_y = \sigma_{y_0}\left(\frac{\dot{\varepsilon}}{\dot{\varepsilon}_0}\right)^n \quad (12)$$

where n is the temperature dependent exponent, $n = \frac{kT}{\mu b^3}$.

The straight lines (dashed) in Fig. 6 are the linear approximations of the experimental flow curves (solid) in stage III, which follow Eq. (4). The measured values of Θ and σ_y from two sets of data are summarised in Table 2.

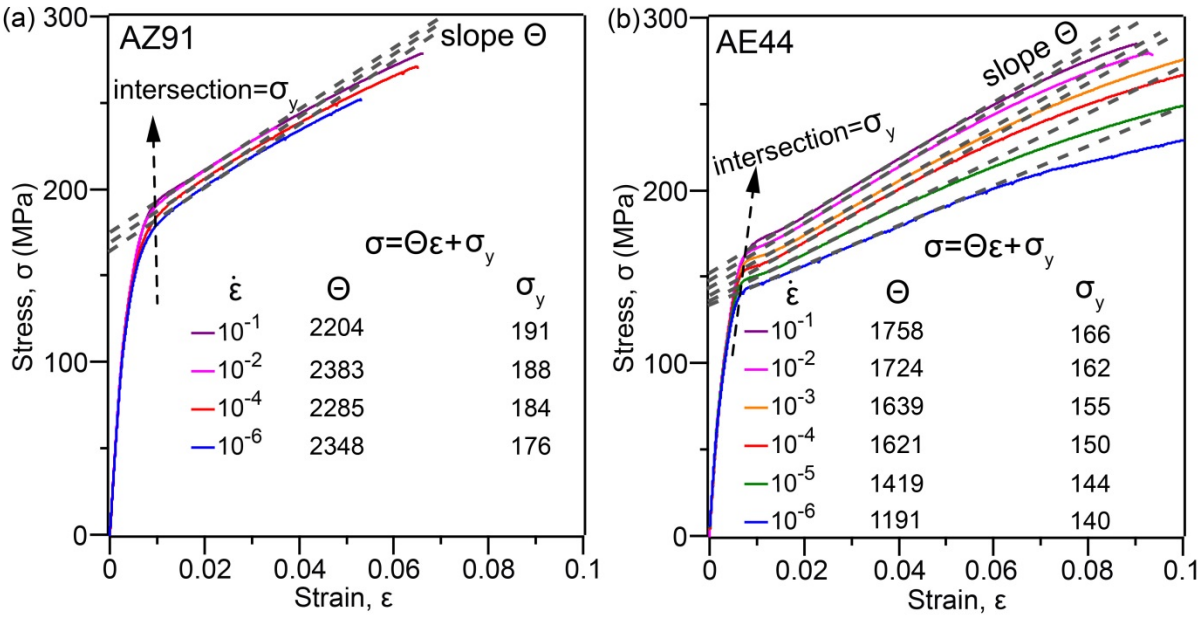

Fig. 6. Experimental flow curves (solid) of (a) AZ91 and (b) AE44 at strain rates 10^{-6}-10^{-1} s^{-1} are compared with best fit linear lines (dashed) according to Eq. (4).

Table 2. Parameters in Stage III: Θ (MPa) and σ_y (MPa) of best fit of Eq. (4) measured from experimental flow curves.

$\dot{\varepsilon}$	AM40		AM60		AZ91		AE44		AE44-T5	
	Θ	σ_y	Θ	σ_y	Θ	σ_y	Θ	σ_y	Θ	σ_y
10^{-6}	1299±27	127±0.4	1334±33	145±1.1	2264±84	180±3.4	1187±4.7	142±1.4	977±11	169±4.0
10^{-5}	-	-	-	-	-	-	1400±19	145±1.0	1203±2.3	178±0.6
10^{-4}	1437±16	126±0.6	1479±9.6	148±1.9	2271±13	185±1.9	1606±16	151±1.3	1435±8.1	188±1.3
10^{-3}	-	-	-	-	-	-	1645±5.7	156±1.3	1555±2.6	194±0.9
10^{-2}	1512±18	131±2.2	1509±0.1	147±0.6	2381±1.9	188±0.2	1693±31	162±0.5	1601±17	201±0.2
10^{-1}	-	-	1512±32	150±1.2	2252±48	190±0.8	1776±18	165±1.4	1728±9.1	206±1.9

Fig. 7 compares the measured Θ from Eq. (4) with the modelled Θ predicted from Eq. (8). The values of Θ_h which provide the lowest scatter for AM40, AM60, AZ91, AE44 and AE44-T5 are also shown and it is clear that they fall within the expected range of 1000-2000 MPa (Cáceres and Blake, 2007) for AM40, AM60, AE44 and AE44-T5. AZ91, however, has a higher Θ_h of 2300 MPa. Overall, Eq. (8) describes the behaviour of Θ well.

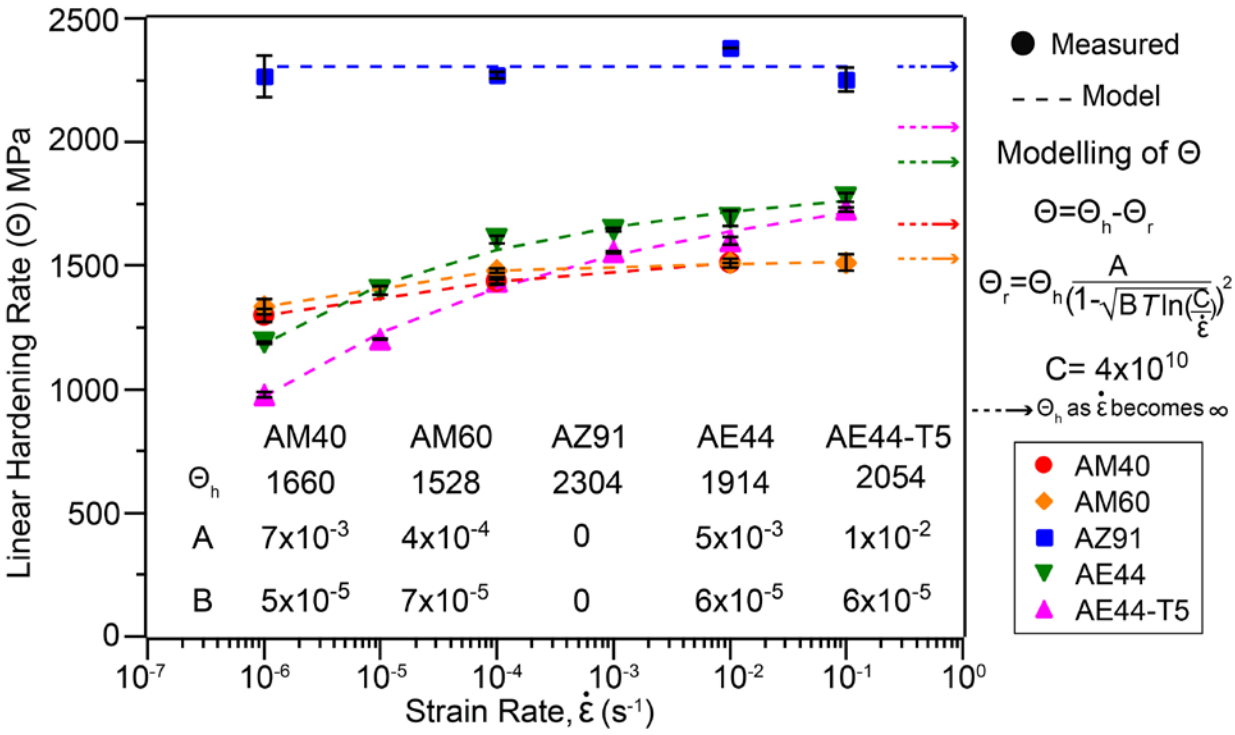

Fig. 7. The strain hardening rate, Θ in Stage III for present alloys at different strain rates. The solid filled symbol and dashed line indicate the measured Θ using Eq. (4) and the modelled Θ with Eq. (8), respectively. The values of Θ_h and constants A, B, and C for each alloy are shown.

It is interesting to see that the optimum value of constant C which provides the lowest scatter is ~10^{10} s^{-1} for present die-cast alloys. For FCC metal, this value is ~10^7 s^{-1} determined by trial and error in (Kocks and Mecking, 2003).

To model σ_y, the temperature dependent exponent, n in Eq. (12) is first calculated. By using a Boltzmann constant, k of 1.38 x 10^{-23} m^2 kg s^{-2} K^{-1}, shear modulus, μ of Mg (17 GPa), the magnitude of the Burgers vector, b of magnesium (0.32 nm) (Callister and Rethwisch, 2007) at room temperature T = 295.15 K, the temperature dependent exponent, n in Eq. (12) is calculated to be 0.0073. The n value correlates well with the literature data where n is reported to be 0-0.03 (Kocks and Mecking, 2003) within a strain-rate range of 10^{-4}-10^{0} s^{-1}, at room temperature.

Applying n of 0.0073 and $\dot{\varepsilon}_0$ of 4x10^{10} s^{-1} (constant C in Fig. 7), σ_y is modelled and compared with measured σ_y from experimental flow curves as shown in Fig. 8. There is a good agreement between the measured σ_y and modelled σ_y, confirming the values of $\dot{\varepsilon}_0$ and n determined.

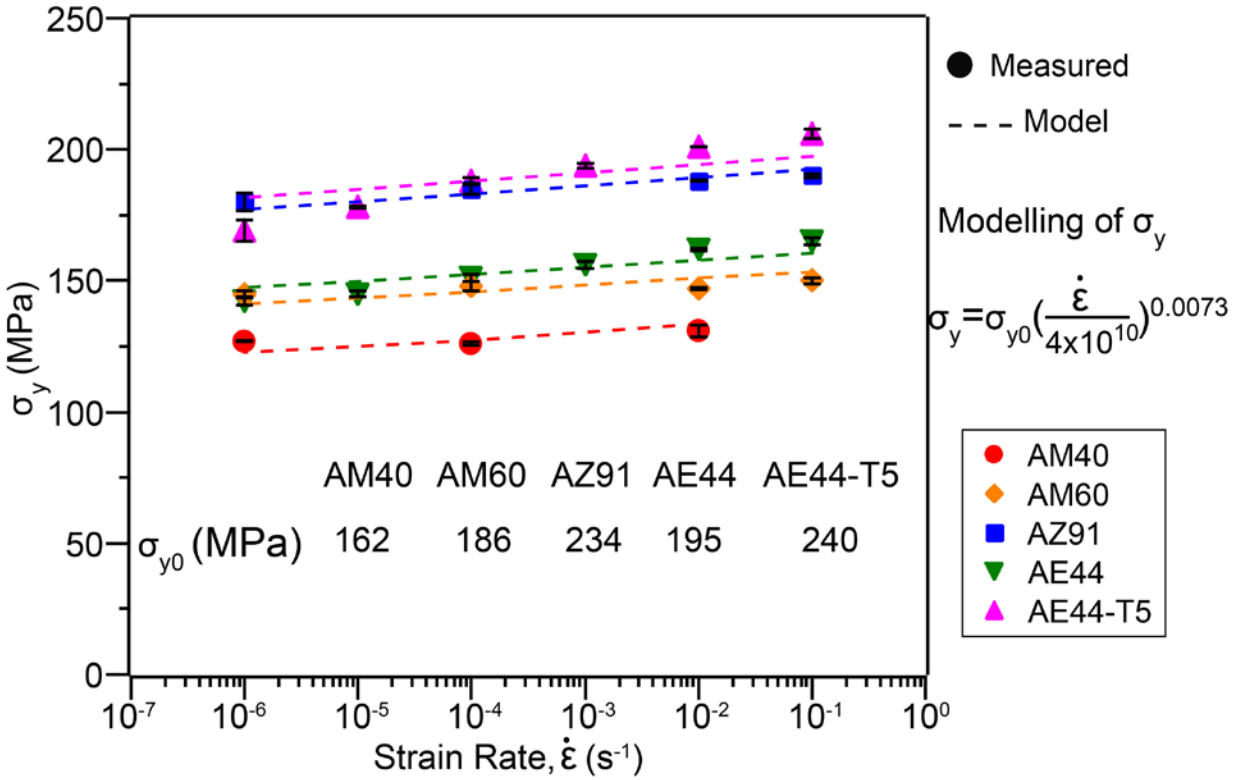

Fig. 8. The <a> prismatic yield stress, σ_y of present alloys at different strain rates. The solid filled symbol and dashed line indicate σ_y measured from experimental flow curves using Eq. (4) and the modelled σ_y with Eq. (12), respectively. The value of σ_{y_0} (MPa) for each alloy is shown.

3.4 Stage IV: <c+a> Pyramidal

As deformation continues, the internal stresses are high enough to activate additional non-basal slip systems, which in Mg and alloys is <c+a> pyramidal slip (Agnew et al., 2001). Activation of an additional slip system allows dislocations piled-up at obstacles due to cross slip in the previous stage to escape, reducing the internal-strain field. This process is called dynamic recovery, and strain hardening decreases until fracture occurs (Yang et al., 2012b). This stage is also more sensitive to strain rate and temperature than Stage III (<a> prismatic

slip-dominated stage), and may limit the extent of Stage III deformation, especially at low strain rates or high temperatures when <c+a> pyramidal slip activates early (Dieter, 1988). The stress-strain curve in this stage has been reported to follow Hollomon's equation: a power-law relationship between stress and amount of <c+a> pyramidal strain (Agnew and Duygulu, 2005; Hollomon, 1945; Kleemola and Nieminen, 1974):

$$\sigma = K_{IV}\, \varepsilon_{IV}^{n_{IV}} \tag{13}$$

where ε_{IV} is the Stage IV strain or <c+a> pyramidal strain, K_{IV} is the strength coefficient and n_{IV} is the strain hardening exponent in Stage IV.

Fig. 9 compares the experimental (solid) and best fit (dashed) stress-strain curve of Stage IV; the parameters K_{IV} and n_{IV} from two sets of data are summarised in Table 3. It is clear that Eq. (13) can describe this part of the flow curve reasonably well. It is also interesting to see that <c+a> pyramidal slip starts to dominate above an applied stress of ~ 200 MPa for both AZ91 and AE44; slightly higher with increasing strain rates. Below 200 MPa, <c+a> pyramidal strain, ε_{IV} is insignificant. It is also observed that AZ91 has considerably less total <c+a> pyramidal strain as compared to AE44 (the scale on the x-axis of AZ91 is smaller). This is because AZ91 fractures early before <c+a> pyramidal strain becomes too extensive.

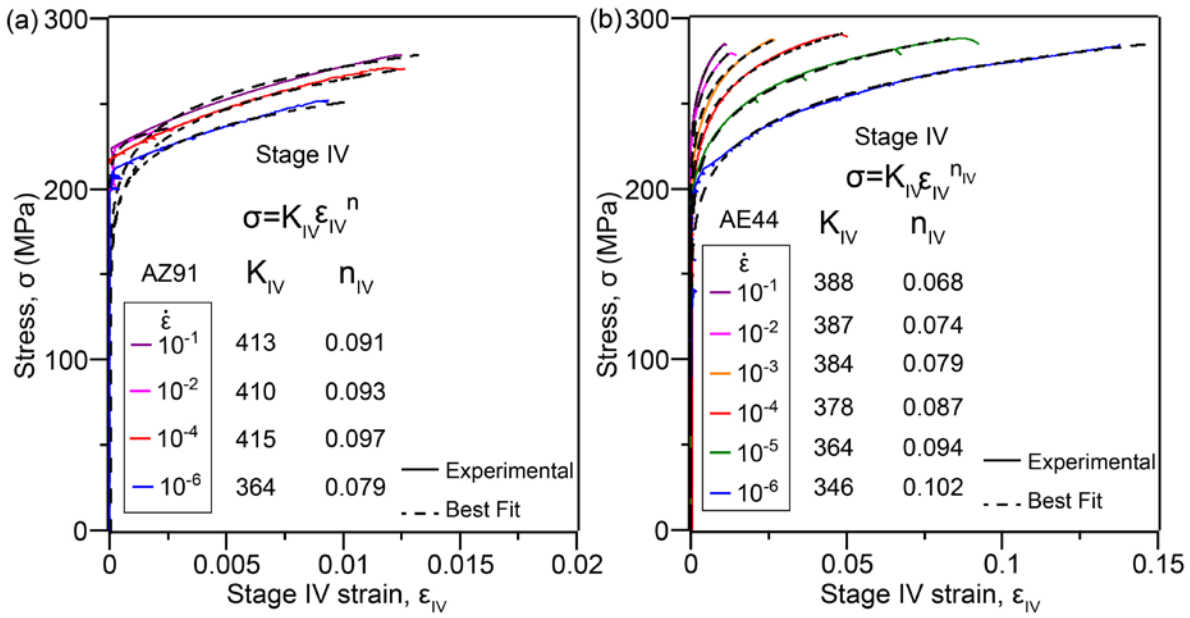

Fig. 9. Experimental (solid) and best fit (dashed) stress-strain curve of Stage IV for (a) AZ91 and (b) AE44. Note the different scales on the x-axis between the two alloys.

Table 3. Parameters in Stage IV: K_{IV} (MPa) and n_{IV} of best fit of Eq. (13).

$\dot{\varepsilon}$	AM40		AM60		AZ91		AE44		AE44-T5	
	K_{IV}	n_{IV} (10^{-3})	K_{IV}	n_{IV} (10^{-3})	K_{IV}	n_{IV} (10^{-3})	K_{IV}	n_{IV} (10^{-3})	K_{IV}	n_{IV} (10^{-3})
10^{-6}	373±1.6	106±0.8	396±1.4	97±2.7	363±0.6	76±3.3	347±1.3	101±0.8	334±4.0	73±0.4
10^{-5}	-	-	-	-	-	-	366±2.4	92±1.6	361±0.5	68±0.2
10^{-4}	376±3.6	96±2.3	399±3.2	85±0.5	415±0.0	97±0.0	377±1.0	85±1.1	385±1.2	63±0.2
10^{-3}	-	-	-	-	-	-	389±5.1	81±1.2	394±0.7	59±0.0
10^{-2}	379±5.6	95±0.8	382±0.9	79±0.9	410±0.0	93±0.0	384±2.3	72±1.6	399±2.6	55±0.5
10^{-1}	-	-	378±1.1	74±0.4	422±8.3	94±3.2	389±1.7	68±0.0	402±0.0	51±0.6

The parameters K_{IV} and n_{IV} from Eq. (13) can be further defined in the form of Ludwik's empirical equation (Ludwik, 1909) as shown in Eq. (14) or Hollomon's equation (Hollomon, 1945) in Eq. (15):

$$K_{IV} \text{ or } n_{IV} = a\,[1\text{-}b\,\dot{\varepsilon}^{c}\,] \tag{14}$$

$$K_{IV} \text{ or } n_{IV} = d\,\dot{\varepsilon}^{f} \tag{15}$$

where a, b, c, d and f are constants. To find out which model is valid for present die-cast alloys, both Ludwik's and Hollomon's constitutive models are compared with the measured K_{IV} and n_{IV} obtained from best fit of Eq. (13) (Table 3), as shown in Fig. 10 for AE44.

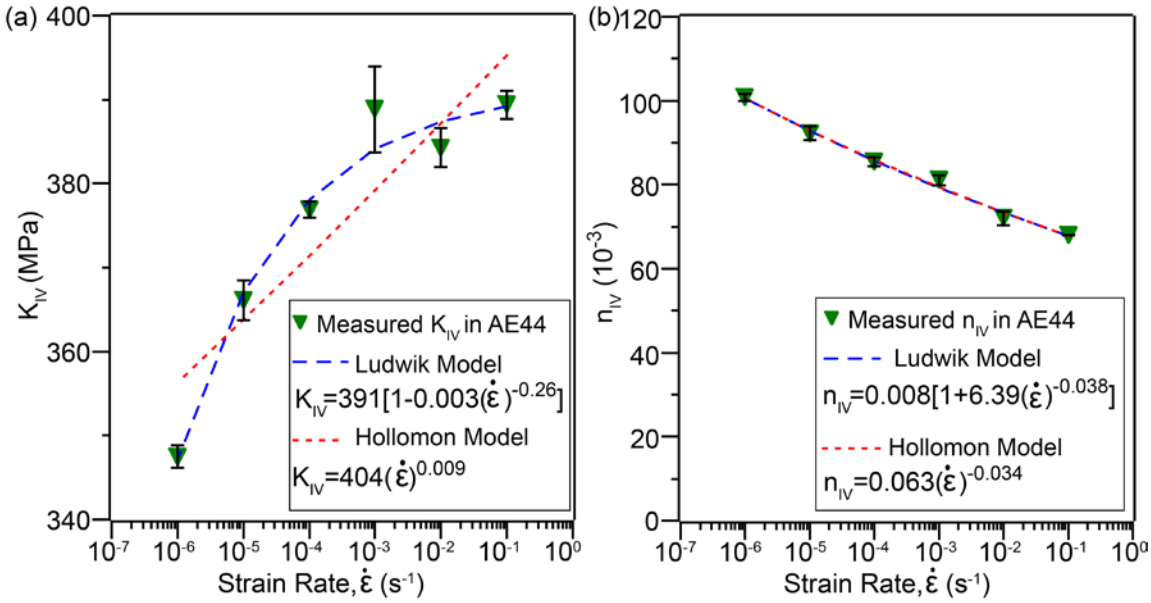

Fig. 10. Comparison of Ludwik's and Hollomon's models with K_{IV} and n_{IV} of best fit of Eq. (13).

Ludwik's model provides a slightly better fit with higher correlation to the measured K_{IV} compared to Hollomon's model. For determining n_{IV}, however, both Ludwik's and Hollomon's model are acceptable, therefore, Hollomon's model is selected to determined n_{IV}

in this study due to its simplicity as compared to Ludwik's. Using Ludwik's model for K_{IV} and Hollomon's model for n_{IV}, the values of constants are summarised in Table 4 for present die-cast alloys. Overall, Ludwik's model provides a good fit for K_{IV} while Hollomon's models the n_{IV} well for the present die-cast alloys.

Table 4. The values of constants a, b, c, d and f from Eqs. (14) and (15).

Alloy	$K_{IV}=a\,[1-b\,\dot{\varepsilon}^{c}]$			$n_{IV} = d\,\dot{\varepsilon}^{f}$	
	a	**b**	**c**	**d**	**f**
AM40	385	0.011	-0.069	0.088	-0.0128
AM60	400	0.095	0.212	0.070	-0.0230
AZ91	110	-2.926	0.014	0.099	0.0163
AE44	391	0.003	-0.261	0.063	-0.0343
AE44-T5	408	0.007	-0.232	0.047	-0.0316

3.5 Complete Stress-Strain Curve

To verify the validity of the modelling equations suggested for each stage, Eqs. (1), (3), (4) and (13) are combined and total strain, ε_t can be defined as Eq. (16) to model the complete stress-strain curve as shown in Fig. 11. It is clear that there is a good agreement between experimental (coloured) and modelled stress-strain curves (black) for all the alloys.

$$\varepsilon_t = \frac{\sigma}{E} + \frac{\sigma}{K_{II}}^{\frac{1}{n_{II}}} + \frac{\sigma-\sigma_y}{\Theta} + \frac{\sigma}{K_{IV}}^{\frac{1}{n_{IV}}} \qquad (16)$$

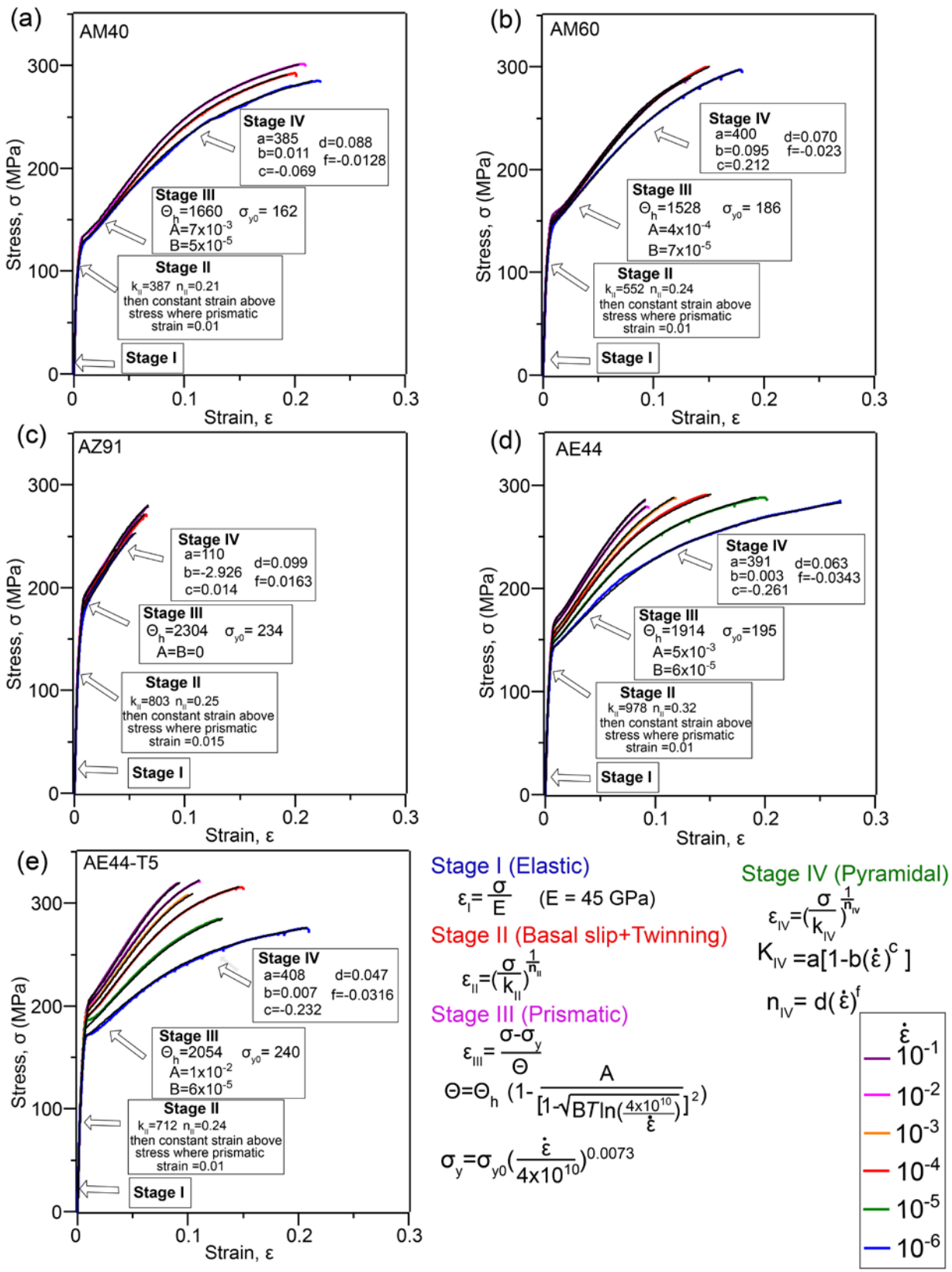

Fig. 11. Comparison of experimental (coloured) and modelled (black) stress-strain curves of (a) AM40, (b) AM60, (c) AZ91, (d) AE44, and (e) AE44-T5 at wide strain-rate range 10^{-6}-10^{-1} s^{-1}.

4. Discussion

4.1 Strain-rate Sensitivity at Different Stages

The results show that some stages of the stress-strain curve, such as Stages III and IV are more strain-rate sensitive. The change in strain-rate sensitivity is also greater in alloys with lower Al contents in solid solution, for example AE44. The discussion will now consider how the underlying deformation mechanisms affect the deformation behaviour in these stages.

Both Stages I and II are strain-rate insensitive. In Stage II, this is supported by the large statistical deviation of K_{II} in Table 1, probably resulting from experimental variation for a given strain rate. In this study, the dominant deformation mechanisms in Stage II are attributed to <a> basal slip and twinning. One piece of evidence to support this is that the critical resolved shear stress (CRSS) of <a> basal slip and twinning are known to be strain-rate independent (Barnett, 2003; Bettles and Barnett, 2012; Ma et al., 2013; Meyers et al., 2001; Ulacia et al., 2010), and this leads to the strain-rate insensitivity in this stage. While K_{II} is strain-rate independent, it is alloy dependent. K_{II} is connected to the interaction of dislocations with obstacles and is expected to increase with increasing solute content (Máthis et al., 2004). In Table 1, it is clear that among the Mg-Al based alloys AM40, AM60 and AZ91 without RE addition, AZ91 consistently shows the highest K_{II} due to its high Al solute concentrations. For alloys with RE addition, the K_{II} values of as-cast AE44 are higher than AE44-T5 for a given strain rate. AE44-T5 has lower Al solute in solution but it also contains nanoscale Al-Mn particles as a result of precipitation (Zhu et al., 2016). It is not known why AE44-T5 with precipitates has lower value of K_{II} compared to AE44. Further investigation is required. The n_{II} values which measure the ability of a metal to strain harden are also quite consistent between strain rates and alloys, and can range from 0.19-0.37.

Both Stages III and IV are more strain-rate sensitive in AE44 and AE44-T5 as compared to AM40, AM60 and AZ91 (Fig. 11). The dominant deformation mechanism in Stages III and IV are ascribed to <a> prismatic slip and <c+a> pyramidal slip, respectively. The CRSS of <a> prismatic and <c+a> pyramidal slip are known to be strain-rate sensitive (Ma et al., 2013; Ulacia et al., 2010), and this further supports the notion that it is the presence of these deformation mechanisms that leads to the strain-rate sensitivity in AE44 and AE44-T5. In contrast, the AM and AZ alloys have higher Al solute concentration and Al solute has been reported to impede slip, lowering the strain-rate sensitivity in Stages III and IV due to the dynamic strain ageing effect (Ang et al., 2017b).

Note that the notion of different deformation mechanisms dominating in the four deformation stages was mainly generated from the results reported in literature which show that the deformation first occurred by <a> basal slip and twinning followed by <a> prismatic and <c+a> pyramidal slip in Mg and alloys (Agnew et al., 2003; Yang et al., 2012a; Yang et al., 2012b). Microscopy analysis is not included in the present study due to the challenges in obtaining a single type of dislocation system under TEM.

4.2 The Delayed Saturation of Anelasticity in AZ91

Both AE44-T5 and AZ91 are high-strength alloys, but anelasticity in Stage II in AZ91 saturates at a higher ε_{III} (0.0015) as shown in Fig. 4. As previously reported (Ang et al.,

2017a), an effect of Al at high concentrations such as 9 wt.% in AZ91 is to delay the onset of <a> prismatic slip (Stage III). A delay in the onset of Stage III will extend Stage II and more twinning is necessary to accommodate the deformation, so the anelasticity saturates at higher ε_{III}.

The intergranular percolating network of eutectic $Mg_{17}Al_{12}$ may also have a measurable effect on the alloy's Stage II deformation. In a highly concentrated alloy such as AZ91, the percolating intermetallic is not only abundant, but also fully interconnected, and this further increases the strain hardening effect, but reduces the ductility due to the increased tendency of crack propagation through the interconnected micro-trusses in AZ91 (Zhang et al., 2013; Zhang et al., 2014). It is likely that the micro-trusses in AZ91 fail at ε_{III} of approximately 0.01 as suggested by (Zhang et al., 2013), which contributes an additional strain of 0.005, making up the strain of 0.015 when anelasticity saturates. In contrast, dilute alloys such as AM40 and AM60 are less likely to be affected by the micro-truss failure in Stage II due to a reduced interconnection of the percolating network. Ternary Mg-Al-RE alloy AE44 consists of a different type of Al-RE intermetallics and further investigation is required to understand the micro-trusses' strain to failure in this alloy.

4.3 Athermal and Thermal Components in Stage III

The strain hardening rate, Θ in Stage III is made up of two components: athermal component Θ_h and thermal component Θ_r. In the event at the limit of the highest strain rate or lowest temperature, when Θ_r (softening effect) becomes negligible, $\Theta=\Theta_h$. It has previously been assumed that Θ_r is negligible in Stage III (Cáceres and Blake, 2007; Yang et al., 2012a; Yang et al., 2012b) and it becomes significant only in Stage IV when dynamic recovery occurs. However, it is clear now from Fig. 7 which shows some Θ_r effect, especially for AM40, AM60, AE44 and AE44-T5. The Θ_r effect is less in AZ91 in Stage III, presumably due to its high Al solute concentration and fully interconnected percolating intermetallic network which make dislocation annihilation difficult. This also explains the high Θ_h in AZ91.

4.4 Model Limitations

While the proposed Eq. (16) provides a good fit to the experimental stress-strain data as shown in Fig. 11, there is a slight discrepancy from the experimental data for AZ91 in the Stage II-III transition region (around the "knee" of the stress-strain curve) as shown in Fig. 12.

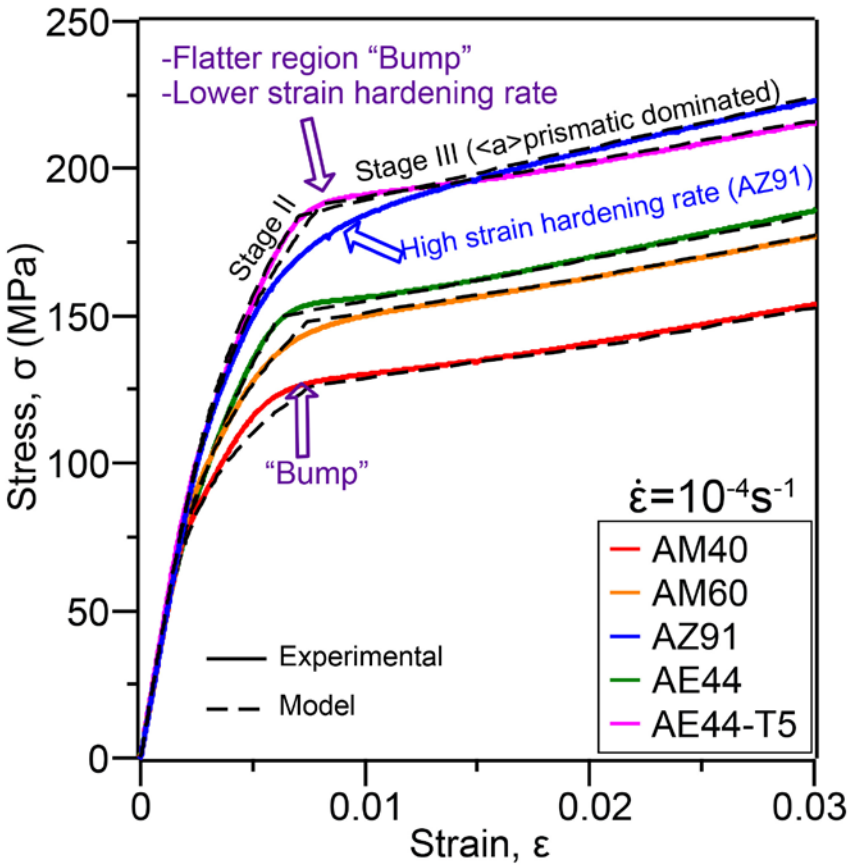

Fig. 12. Enlarged stress-strain curve in the Stage II-III transition region for the present die-cast alloys.

For the as-cast AM40, AE44 and T5-aged AE44, there appears a protuberance (bump) in the Stage II-III transition region, which has a lower strain hardening rate. In comparison, a higher strain hardening rate is noted in the Stage II-III transition for AM60, even higher for AZ91. AM40 and AE44 have low Al contents in solid solution and they are considered to be dilute alloys while AM60 and especially AZ91 are more concentrated alloys.

The observed discrepancy between the experimental and the proposed model in AZ91 could be due to two factors: a high Al solute concentration and a fully interconnected percolating intermetallic network. Firstly, a high Al concentration of 9 wt.% in AZ91 has been shown to result in solid solution hardening of <a> prismatic slip planes (Ang et al., 2017a; Nagarajan et al., 2017), delaying the activation of <a> prismatic slip. The delayed onset of <a> prismatic slip increases the tendency for twinning to occur, which is supported by the fact that there is a higher twinned area fraction (Ang et al., 2017b) and a larger maximum anelasticity (Fig. 2) in AZ91. Secondly, the fully interconnected percolating network (Zhang et al., 2013; Zhang et al., 2014) may also impede <a> prismatic slip, resulting in a higher strain hardening rate in the Stage II-III transition region. As the intermetallic network impedes slip, it becomes more highly stressed, leading to earlier fracture. Both of these phenomena could result in a more gradual Stage II-III transition. Since the proposed model (Eq. 16) assumes an abrupt saturation of Stage II at a pre-determined ε_{III}, the gradual Stage II-III transition in AZ91 due to the high Al content and intermetallic

network would affect the applicability of Eq. (16). Overall, Eq. (16) can well predict the deformation behaviour of high-pressure die-cast magnesium alloys, but care should be taken when modelling more concentrated alloys.

5. Conclusions

The tensile deformation behaviour of commercial high-pressure die-cast magnesium-aluminium based alloys has been studied and modelled. The following conclusions are drawn from this study:

1) The stress-strain curve can be separated into four stages. Stage I is the elastic region. Stage II is <a> basal slip and twinning dominated, while Stages III and IV are <a> prismatic slip and <c+a> pyramidal slip dominated, respectively.
2) The four deformation stages of stress-strain curve are modelled by semi-empirical constitutive equations. Stages I and III exhibit a linear strain hardening region and can be described by a simple linear equation while Stages II and IV exhibit a power relationship of stress and strain and are described by Hollomon's equation. These equations are combined to model the entire stress-strain curve.
3) Stages I and II are observed to be strain-rate insensitive while Stages III and IV exhibit high strain-rate sensitivity in alloys with lower aluminium contents in solid solution. This is attributed to the strain-rate sensitivity of the different deformation mechanisms. The reduced strain-rate sensitivity in Stages III and IV in alloys with higher aluminium contents in solid solution is attributed to the dynamic strain ageing effect.
4) Overall, the proposed model provides a good fit to the experimental stress-strain curve for most of the alloys, but there were some difficulties in exactly fitting the Stage II-III transition region in AZ91 alloy. This is because AZ91 has a higher strain hardening rate in the Stage II-III transition as compared to AM40 and AE44. The high strain hardening rate in AZ91 is likely due to the gradual onset of stage III, an effect of high aluminium concentration and the fully interconnected percolating network in AZ91.

Acknowledgements

This work was supported by the Australian Research Council [Grant number LP130100828]. The authors would like to thank Dr. Carlos Cáceres from the University of Queensland and Professor Matthew Barnett from Deakin University for their very helpful comments on the manuscript.

References

Agnew, S.R., Tomé, C.N., Brown, D.W., Holden, T.M., Vogel, S.C., 2003. Study of slip mechanisms in a magnesium alloy by neutron diffraction and modeling. Scr. Mater. 48, 1003-1008.

Agnew, S.R., Yoo, M.H., Tomé, C.N., 2001. Application of texture simulation to understanding mechanical behavior of Mg and solid solution alloys containing Li or Y. Acta Mater. 49, 4277-4289.

Agnew, S.R., Duygulu, Ö., 2005. Plastic anisotropy and the role of non-basal slip in magnesium alloy AZ31B. Int. J. Plast. 21, 1161-1193.

Akhtar, A., Teghtsoonian, E., 1968. Solid-solution hardening in magnesium alloys. Mater. Trans. 9, 692-697.

Ang, H.Q., Abbott, T.B., Zhu, S.M., Gu, C.F., Easton, M.A., 2017a. Anelasticity of die-cast magnesium-aluminium based alloys under different strain rates. Mater. Sci. Eng. A. 707, 101-109.

Ang, H.Q., Abbott, T.B., Zhu, S.M., Gu, C.F., Easton, M.A., 2016. Proof stress measurement of die-cast magnesium alloys. Mater. Des. 112, 402-409.

Ang, H.Q., Zhu, S.M., Abbott, T.B., Qiu, D., Easton, M.A., 2017b. Strain-rate sensitivity of die-cast magnesium-aluminium based alloys. Mater. Sci. Eng. A. 699, 239-246.

Avedesian, M., Baker, H., 1999. Magnesium and magnesium Alloys—ASM Specialty Handbook, Vol. 52. Ohio, ASM International.

Bakke, P., Pettersen, K., Westengen, H., 2003. Improving the strength and ductility of magnesium die-casting alloys via rare-earth addition. J. Miner. Metals Mater. Soc. 55, 46-51.

Barnett, M.R., 2003. A Taylor model based description of the proof stress of magnesium AZ31 during hot working. Metall. Mater. Trans. A. 34, 1799-1806.

Barnett, M.R., Bouaziz, O., Toth, L.S., 2015. A microstructure based analytical model for tensile twinning in a rod textured Mg alloy. Int. J. Plast. 72, 151-167.

Bettles, C., Barnett, M.R., (Eds.), Advances in wrought magnesium alloys: Fundamentals of processing, properties and applications. Woodhead Publishing, Cambridge, 2012.

Cáceres, C.H., Blake, A.H., 2007. On the strain hardening behaviour of magnesium at room temperature. Mater. Sci. Eng. A. 462, 193-196.

Cáceres, C.H., Lukáč, P., 2008. Strain hardening behaviour and the Taylor factor of pure magnesium. Philos. Mag. 88, 977-989.

Cáceres, C.H., Lukáč, P., Blake, A.H., 2008. Strain hardening due to $\{10\ \bar{1}\ 2\}$ twinning in pure magnesium. Philos. Mag. 88, 991-1003.

Cáceres, C.H., Sumitomo, T., Veidt, M., 2003. Pseudoelastic behaviour of cast magnesium AZ91 alloy under cyclic loading–unloading. Acta Mater. 51, 6211-6218.

Callister, W.D., Rethwisch, D.G., 2007. Materials Science and Engineering: An Introduction, eighth ed. Wiley, New York.

Christian, J.W., Mahajan, S., 1995. Deformation twinning. Prog. Mater. Sci. 39, 1-157.

Cui, Y.J., Li, Y.P., Wang, Z.C., Ding, X., Koizumi, Y., Bian, H.K., Lin, L.Y., Chiba, A., 2017. Impact of solute elements on detwinning in magnesium and its alloys. Int. J. Plast. 91, 134-159.

Dieter, G.E., 1998. Mechanical Metallurgy, SI Metric ed. McGraw-Hill Book Company, London.

Duerig, T.W., Zadno, R., 1990. An engineer's perspective of pseudoelasticity, in: Duerig, T.W., Melton, K.N., Stöckel, D., Wayman, C.M. (Eds.), Engineering Aspects of Shape Memory Alloys. Butterworth-Heinemann Publisher, Oxford, pp. 369-393.

Hirsch, P.B., Mitchell, T.E., 1967. Stage II work hardening in crystals. Canadian J. Phys. 45, 663-706.

Hollomon, J.H., 1945. Tensile deformation. Aime Trans. 12, 1-22.

Kleemola, H., Nieminen, M., 1974. On the strain-hardening parameters of metals. Metall. Trans. 5, 1863-1866.

Kocks, U.F., 1966. A statistical theory of flow stress and work-hardening. Philos. Mag. 13, 541-566.

Kocks, U.F., 1970. The relation between polycrystal deformation and single-crystal deformation. Metall. Mater. Trans. 1, 1121-1143.

Kocks, U.F., Mecking, H., 2003. Physics and phenomenology of strain hardening: the FCC case. Prog. Mater. Sci. 48, 171-273.

Lu, Z.J., Blackmore, P., 2014. Cyclic stress-Strain behaviour of AM60B and AE44 cast magnesium alloys and its impact on LCF characterisation and fatigue analysis. SAE Int. J. Mater. Manuf. 7, 446-453.

Ludwik, P., 1909. Elemente des technologischen Mechanik. Verlag von Julius Springer, Berlin.

Ma, Q., Li, B., Oppedal, A.L., Whittington, W.R., Horstemeyer, S.J., Marin, E.B., Wang, P.T., Horstemeyer, M.F., 2013. Strain rate dependence of twinning at 450° C and its effect on microstructure of an extruded magnesium alloy. Mater. Sci. Eng. A. 559, 314-318.

Mann, G.E., Sumitomo, T., Cáceres, C.H., Griffiths, J.R., 2007. Reversible plastic strain during cyclic loading–unloading of Mg and Mg–Zn alloys. Mater. Sci. Eng. A. 456, 138-146.

Máthis, K., Trojanova, Z., Lukáč, P., Cáceres, C.H., Lendvai, J., 2004. Modeling of hardening and softening processes in Mg alloys. J. Alloy. Comp. 378, 176-179.

Mecking, H., Kocks, U.F., 1981. Kinetics of flow and strain-hardening. Acta Metall. 29, 1865-1875.

Meyers, M.A., Vöhringer, O., Lubarda, V.A., 2001. The onset of twinning in metals: a constitutive description. Acta Mater. 49, 4025-4039.

Meyers, M.A., 1994. Dynamic Behaviour of Materials. John Wiley & Sons, New York.

Mises, R.V., 1928. Mechanik der plastischen Formänderung von Kristallen. J. Appl. Math. Mech. 8, 161-185.

Mordike, B.L., Ebert, T., 2001. Magnesium: Properties—applications—potential. Mater. Sci. Eng. A. 302, 37-45.

Muránsky, O., Carr, D.G., Šittner, P., Oliver, E.C., 2009. In situ neutron diffraction investigation of deformation twinning and pseudoelastic-like behaviour of extruded AZ31 magnesium alloy. Int. J. Plast. 25, 1107-1127.

Nagarajan, D., 2017. Anelasticity in cast Mg-Gd alloys. Mater. Sci. Eng. A. 695, 14-19.

Nagarajan, D., Cáceres, C.H., Griffiths, J.R., 2012. Anelastic phenomena in Mg Al alloys, in: Chmelík, F., Král, R., Martin, J.L. (Eds.), Proceedings of the 12th International Symposium on Physics of Materials. Acta Phys. Polonica A. 122, No. 3.

Nagarajan, D., Ren, X., Cáceres, C.H., 2017. Anelastic behavior of Mg-Al and Mg-Zn solid solutions. Mater. Sci. Eng. A. 696, 387-392.

Partridge, P.G., 1967. The crystallography and deformation modes of hexagonal close-packed metals. Metall. Rev. 12, 169-194.

Pekguleryuz, M., Kainer, K., Kaya, A., 2013. Fundamentals of magnesium alloy metallurgy, first ed. Woodhead Publishing, Cambridge.

Qiao, H., Agnew, S.R., Wu, P.D., 2015. Modeling twinning and detwinning behavior of Mg alloy ZK60A during monotonic and cyclic loading. Int. J. Plast. 65, 61-84.

Reed-Hill, R.E., Dahlberg, E.P., Slippy Jr, W.A., 1965. Some anelastic effects in Zirconium at room temperature resulting from prestrain at 77 deg K. Trans. Met. Soc. AIME. 233, 1766-1770.

Stanford, N., Barnett, M.R., 2013. Solute strengthening of prismatic slip, basal slip and twinning in Mg and Mg–Zn binary alloys. Int. J. Plast. 47, 165-181.

Sumitomo, T., Cáceres, C.H., Veidt, M., 2002. The elastic modulus of cast Mg–Al–Zn alloys. J. Light Metals. 2, 49-56.

Takuda, H., Morishita, T., Kinoshita, T., Shirakawa, S., 2005. Modelling of formula for flow stress of a magnesium alloy AZ31 sheet at elevated temperatures. J. Mater. Process. Technol. 164, 1258-1262.

Taylor, G.I., 1938. Plastic strain in metals. Inst. Metal. 62, 307-324.

Ulacia, I., Dudamell, N.V., Gálvez, F., Yi, S., Pérez-Prado, M.T., Hurtado, I., 2010. Mechanical behavior and microstructural evolution of a Mg AZ31 sheet at dynamic strain rates. Acta Mater. 58, 2988-2998.

Wang, H., Wu, P.D, Wang, J., 2013. Modeling inelastic behavior of magnesium alloys during cyclic loading–unloading. Int. J. Plast. 47, 49-64.

Wonsiewicz, B.C., 1966. Plasticity of magnesium crystals [dissertation], Massachusetts Institute of Technology, Cambridge.

Yang, K.V., Cáceres, C.H., Nagasekhar, A.V., Easton, M.A., 2012a. Low-strain plasticity in a high pressure die cast Mg–Al alloy. Model. Simul. Mater. Sci. Eng. 20, 024010.

Yang, K.V., Cáceres, C.H., Tomé, C.N., 2012b. The elasto-plastic transition in magnesium alloys, in: Mathaudhu, S.N., Sillekens, W.H., Neelameggham, N.R., Hort, N. (Eds.), Magnesium Technology 2012: Proceedings of the TMS (The Minerals, Metals & Materials Society). John Wiley and Sons, New York, 2012, pp. 127-131.

Yoo, M.H., 1981. Slip, twinning, and fracture in hexagonal close-packed metals, Metall. Trans. A. 12, 409-418.

Zhang, B., Nagasekhar, A.V., Sivarupan, T., Cáceres, C.H., 2013. Deformation behavior of the percolating intermetallic microstructure of high pressure die cast AZ91 alloy. Adv. Eng. Mater. 15, 1059-1067.

Zhang, B., Yang, K.V., Nagasekhar, A.V., Cáceres, C.H., Easton, M.A., 2014. Deformation behavior of the percolating eutectic intermetallic in HPDC and squeeze-cast Mg alloys. J. Miner. Metals Mater. Soc. 66, 2086-2094.

Zhu, S.M., Abbott, T.B., Gibson, M.A., Nie, J.F., Easton, M.A., 2016. Age hardening in die-cast Mg–Al–RE alloys due to minor Mn additions. Mater. Sci. Eng. A. 656, 34-38.

Chapter 8
Conclusions & Recommendations

8.1 Conclusions

This research was originated from the increasing interest in the use of high-pressure die-cast magnesium alloys in structural applications. Structural alloys must have good combinations of high room-temperature strength and high ductility. Improved mechanical properties are necessary for energy absorption in vehicle crash situations and for manufacturing processes, such as self-piercing riveting. Understanding the deformation behaviour of existing commercial die-cast magnesium alloys AM40 (Mg-4Al-0.3Mn), AM60 (Mg-6Al-0.3Mn), AZ91 (Mg-9Al-1Zn) and AE44 (Mg-4Al-4RE) is important in the future development of improved structural alloys.

The hexagonal closed-packed crystal structure of magnesium alloys further leads to a complex progression of deformation mechanisms at room temperature. The <a> basal slip system activates at low stresses and strains, and it does not provide sufficient independent slip systems to satisfy the von Mises-Taylor criterion. To further complicate the deformation behaviour, the non-basal slip (<a> prismatic and <c+a> pyramidal) systems only activate at higher stresses at room temperature. This results in profuse twinning to accommodate plastic deformation and satisfy the von Mises-Taylor criterion. However, the twins formed in magnesium alloys are unstable under loading, and they can partially revert during unloading, consequently a large part of the non-linear deformation is reversible at low stresses and strains, resulting in three deformation regions: elastic, anelastic and plastic.

This research has presented a comprehensive study on the complexity of the deformation behaviour of commercial die-cast magnesium-aluminium based alloys, specifically on the influences of strain rate (important for structural applications) and aluminium content (main alloying element in these commercial alloys) by answering the four research questions, as illustrated in Figure 8.1. The key findings of the four studies are summarised in Sections 8.1.1-8.1.4.

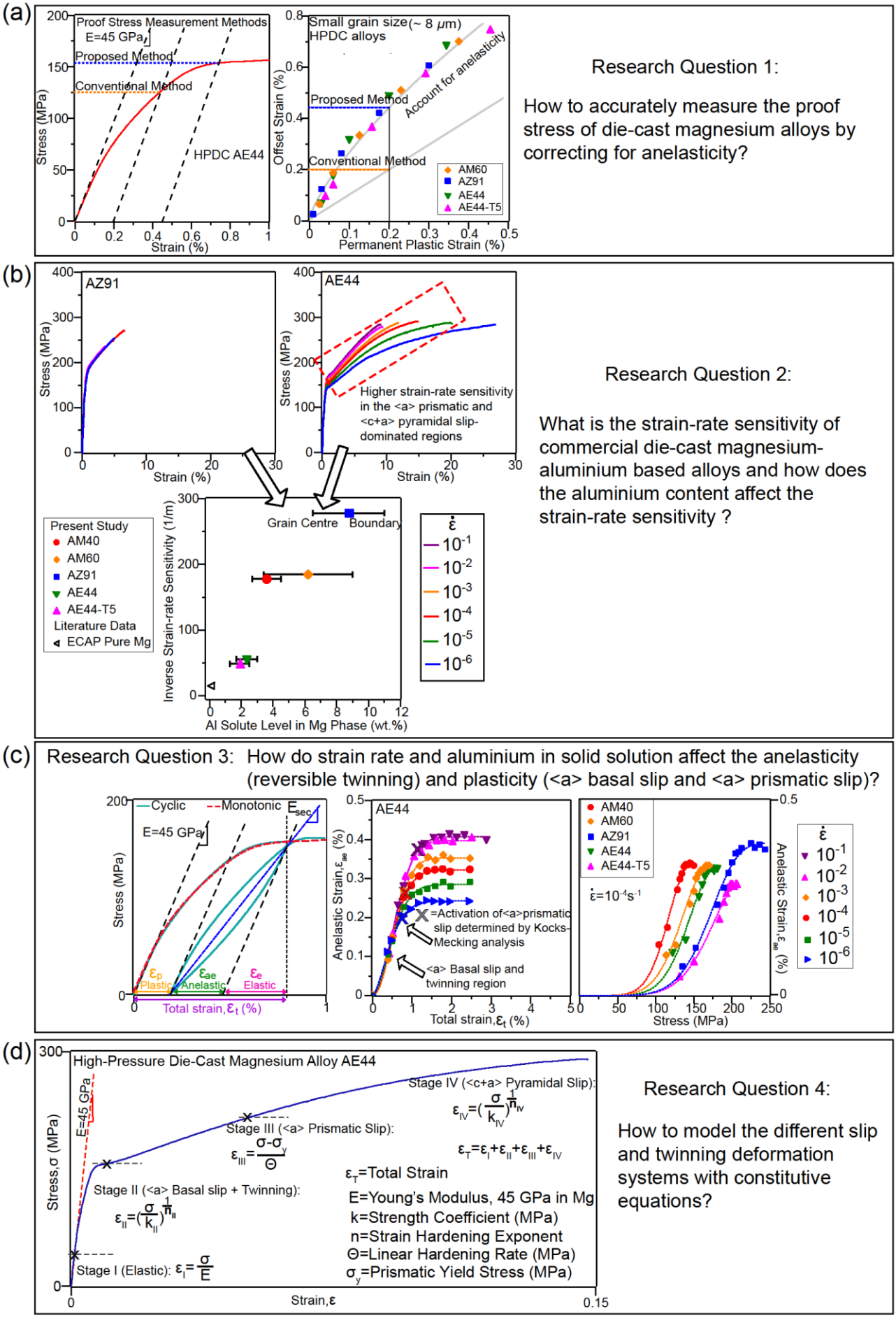

Figure 8.1: Research questions of the four studies in this thesis.

8.1.1 Study 1: Proof Stress Measurement

Studies of magnesium alloys showed a wide range of measured proof stress values even for the same alloy. This creates difficulty in comparing alloy's properties for engineering applications. In this study, the proof stress determination methods specified in ISO and ASTM standards were reviewed. Early activation of <a> basal slip and twinning complicated the conventional proof stress measurement method and a higher offset strain of 0.45% was required to achieve 0.2% permanent plastic strain in proof stress measurement of fine-grained (< 10 μm) high-pressure die-cast magnesium alloys (Figure 8.1 (a)). The proposed proof stress measurement method also provided a smaller range of proof stress values for the same alloy compared to the conventional 0.2% offset strain method, and hence, a more consistent measurement. This new approach further led to the construction of a conversion chart which can now be used to determine an appropriate offset strain for proof stress measurement for a range of magnesium alloys. This study provided insights into the effects of <a> basal slip and twinning on the proof stress of magnesium and alloys.

8.1.2 Study 2: Strain-rate Sensitivity

This study investigated the deformation behaviour of commercial die-cast magnesium alloys AM40, AM60, AZ91 and AE44 with various aluminium contents at strain rates 10^{-6}-10^{-1} s^{-1}. Understanding the strain-rate sensitivity is important towards improving the alloy's properties for structural applications. In this study, alloys with lower aluminium contents exhibited higher strain-rate sensitivity, and strain-rate sensitivity decreased with increasing aluminium solute level in the α-magnesium matrix (Figure 8.1 (b)) rather than the overall aluminium content in the alloy. The decreased strain-rate sensitivity with increasing aluminium contents in solid solution was reported to be related to dynamic strain ageing from the interactions between the aluminium solute and dislocations and this has not been previously identified. The high strain-rate sensitivity observed in alloys with lower aluminium contents in solid solution (AE44) was manifest in the <a> prismatic and <c+a> pyramidal slip-dominated regions, and there was an increase in work hardening and tensile/yield ratio. This suggested that the performance of magnesium alloy AE44 in terms of energy absorption can improve at higher strain rates, and this is beneficial for structural applications.

8.1.3 Study 3: Elastic, Anelastic and Plastic Deformations

The main objectives of this study were to determine the contributions of elasticity, anelasticity (reversible twinning) and plasticity (<a> basal slip and <a> prismatic slip) and to study their dependences on strain rate and aluminium solute level. The key findings of this study are:

(a) Anelasticity was observed to be strain-rate insensitive in the <a> basal slip and twinning-dominated region and strain-rate sensitive in the <a> prismatic slip-dominated region (Figure 8.1 (c)), especially for alloys with lower aluminium in solid solution. This was attributed to the strain-rate insensitivity of <a> basal slip and twinning and high strain-rate sensitivity of <a> prismatic slip. This suggested that anelasticity, which is attributed to reversible twinning, can also be influenced by slip. Overall, it was the strain-rate sensitivity of plasticity by <a> prismatic slip that led to a variation in maximum anelasticity with strain rate, whilst anelasticity itself was strain-rate insensitive.

(b) AZ91, which has the most aluminium in solution, exhibited the largest maximum anelasticity (Figure 8.1 (c)). Increasing the aluminium concentrations resulted in solid solution hardening in all slip systems (but not twinning), consequently plastic deformation by <a> basal slip and <a> prismatic slip became more difficult, leading to an increased amount of twinning and anelasticity.

(c) Presence of precipitates in aged AE44-T5 was reported to harden not only <a> basal and <a> prismatic slip, but also suppress twinning, lowering the anelasticity in comparison with as-cast AE44.

8.1.4 Study 4: Constitutive Modelling

Applying the knowledge from previous chapters, this study further divided the elastic, anelastic and plastic deformations into four stages of deformation: elastic (stage I); <a> basal slip and twinning (stage II); <a> prismatic slip (stage III); and <c+a> pyramidal slip (stage IV) as shown in Figure 8.1 (d). These stages of deformation were modelled with constitutive equations. Overall, the proposed consitutive model provided a good fit to the experimental stress-strain curve for most of the alloys, but it slightly overestimated the stress in the stage II-III transition region in the AZ91 alloy. This slight discrepancy was attributed to the delayed onset of <a> prismatic slip in stage III, an effect of the high aluminium concentration

and fully interconnected percolating network, leading to a higher strain hardening rate during the stage II-III transition in AZ91.

Overall, this research demonstrates that magnesium and alloys have a complex progression of deformation mechanisms due to the hexagonal closed-packed crystal structure. Within the elastic, anelastic and plastic deformations, deformation mode begins from elastic (stage I) to <a> basal slip and twinning (stage II) to <a> prismatic slip (stage III) and finally to <c+a> pyramidal slip (stage IV). Decomposition of stress-strain curve into these different stages has provided insights into:

1) the improved measurement of proof stress;
2) the role of aluminium solute in moderating strain-rate sensitivity;
3) the interactions of slip and twinning deformation systems to understand maximum anelasticity;
4) the contributions of different slip and twinning deformation mechanisms to the overall deformation behaviour of die-cast magnesium alloys.

The outcomes of this research have provided significant contributions to the fundamental understanding of the deformation mechanisms in die-cast magnesium alloys and will provide the foundation for future development of improved structural alloys.

8.2 Research Implications

Mechanical properties are important factors to consider during the process of materials selection for a particular design. To date, aluminium castings are favoured over magnesium castings, especially for applications in automotive and aerospace industries, mainly due to their availability and recyclability. In this research, presence of non-linear reversible (anelastic) deformation in magnesium alloys shows that a higher stress level is required to achieve the 0.2% permanent plastic strain. The improved understanding of magnesium yielding behaviour from this research may give magnesium castings an advantage over aluminium castings for engineering applications. Therefore, the tensile properties of some of the most frequently used magnesium and aluminium casting alloys are compared in Figure 8.2.

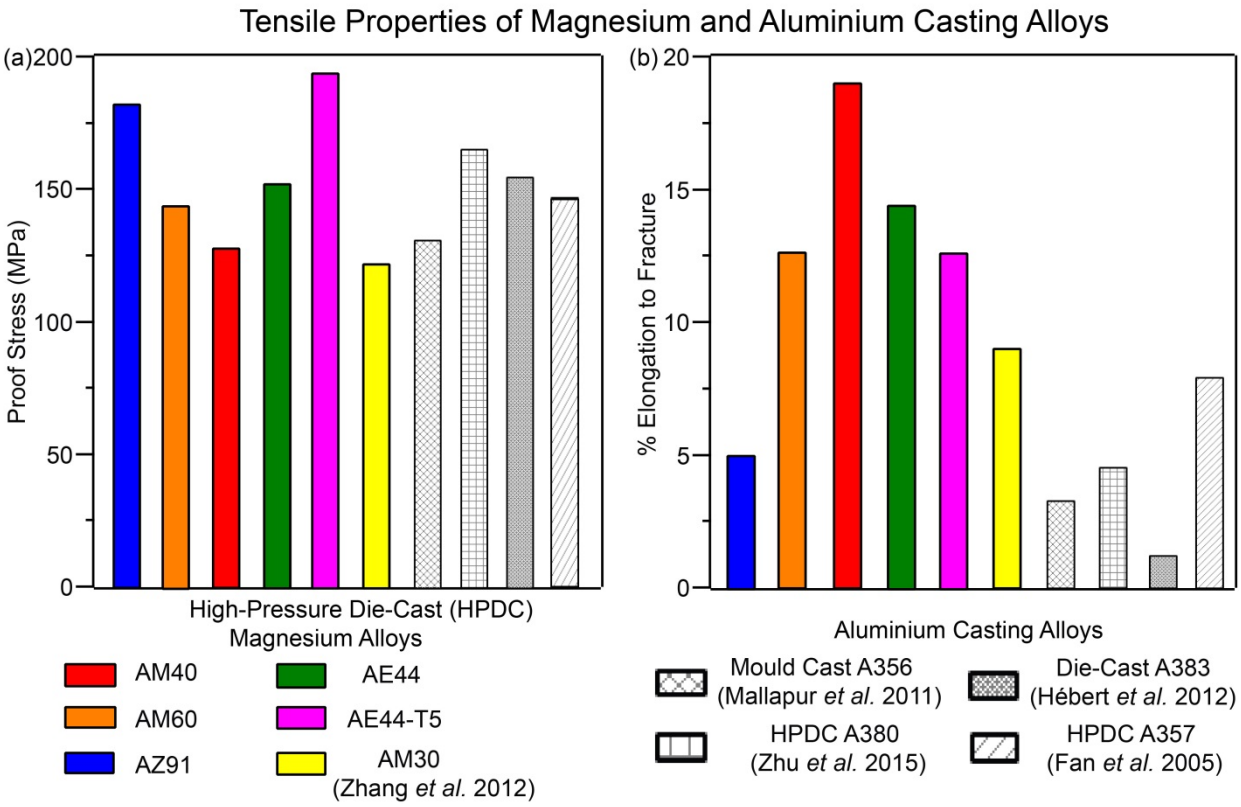

Figure 8.2: Comparison of (a) proof stress and (b) % elongation to fracture of magnesium and aluminium casting alloys. The proof stress of magnesium alloys is measured by the 0.45% offset method while the proof stress of aluminium alloys is measured by the conventional 0.2% offset method. Data of magnesium alloy AM30 [1] and aluminium alloys [2-5] are taken from the literature.

The proof stress of magnesium alloys AE44 and AM60 are now comparable with that of aluminium alloys A356, A357 and A383 with the T5-aged AE44 performing best, exceeding the proof stress of A380. The ductility (% elongation to fracture) of magnesium alloys (except AZ91) is also far superior to that of aluminium alloys. The improved proof stress measurement may have an impact on future materials selection as it shows that magnesium casting alloys on a strength-ductility basis are superior to aluminium casting alloys.

Among the commercially available magnesium alloys AM40, AM60, AZ91 and AE44, AE44 also has a better combination of strength and ductility. Interestingly, an additional T5 heat treatment (200 °C for 32 h) on AE44 results in a significant improvement in strength without a loss in ductility. Both AE44 and AE44-T5 have very low aluminium solute in the α-magnesium matrix and they exhibit higher strain-rate sensitivity compared to other alloys.

Their high strain-rate sensitivity is manifest in the <a> prismatic and <c+a> pyramidal slip-dominated regions, resulting in an increase in work hardening and tensile-yield ratio.

Whilst steels (i.e. low carbon steels) are also sensitive to strain rate, their form of strain-rate sensitivity is different from that of magnesium alloys [6]. They exhibit a distinct yield point during deformation, usually followed by a drop in load then work hardening. As the strain rate increases, the yield point increases such that it exceeds the post yielding tensile strength. Therefore, the high strain rates in low carbon steels reduce the tensile-yield ratio. This lack of effective work hardening in steels can result in strain localisation and poor energy absorption at strain rates typical of vehicle impact.

The absence of a distinct yield point and the increase in work hardening and tensile-yield ratio in magnesium alloys with lower aluminium contents in solid solution suggest that energy absorption can be improved and significant benefit can be obtained by applying magnesium alloys, such as AE44 and AE44-T5 to structural applications.

In addition, AE44-T5 may also have good fatigue properties. Based on the constitutive model proposed in this research, the stress-strain curve is decomposed into elastic and non-elastic fractions as shown in Figure 8.3. It is observed that AE44-T5 has a higher elastic fraction at low strains.

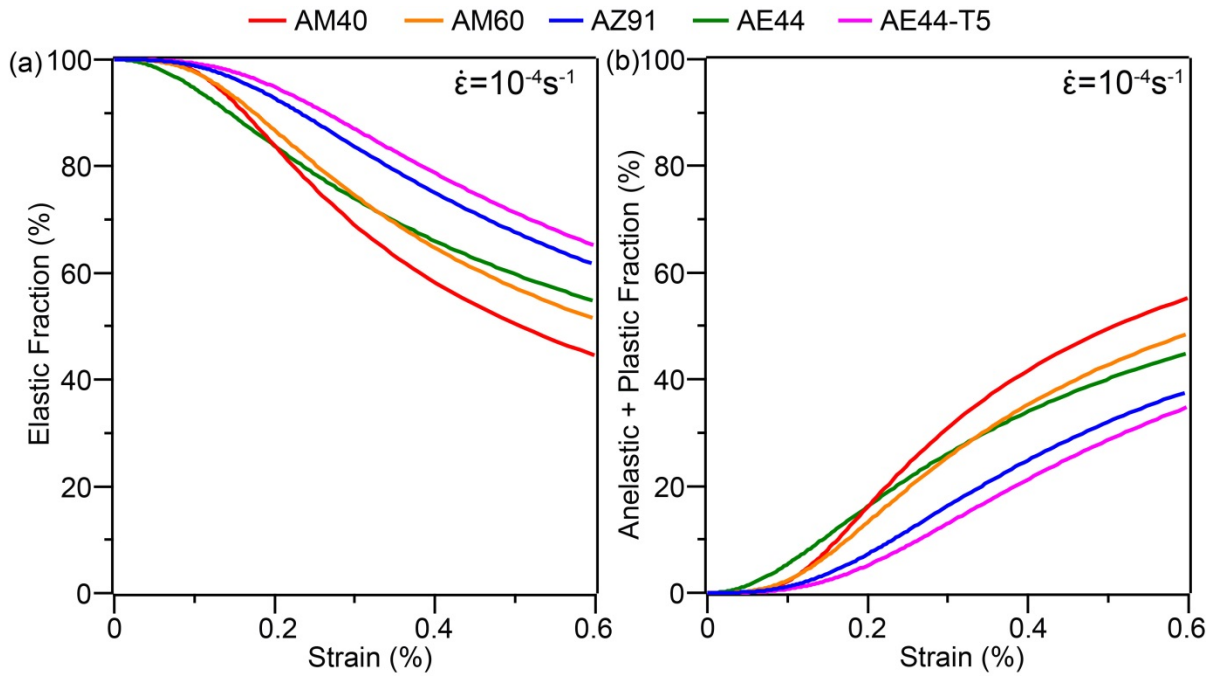

Figure 8.3: Fractions of (a) elastic and (b) anelastic + plastic for present die-cast magnesium alloys.

Although the conditions in fatigue are different in which cyclic stresses and strains are involved, a large fraction of non-elastic strain (anelastic and plastic) is likely to be detrimental to fatigue life. To sum up, the findings of this research have advanced the understanding of the mechanical properties and deformation behaviour of die-cast magnesium alloys.

8.3 Recommendations for Future Research

Whilst this research offers some new perceptions on the complex progression of deformation mechanisms of die-cast magnesium alloys, it has also identified a number of further questions. Based on the findings of the four studies, the following recommendations are made for future investigations.

Future work based on study 1: A common theme throughout this thesis is that magnesium alloys undergo a series of deformation stages, going from elastic (stage I) to <a> basal slip and twinning (stage II), to <a> prismatic slip (stage III) and finally <c+a> pyramidal slip (stage IV). The traditional meaning of yield strength has been a measure of the transition from elastic to plastic deformation but in the case of magnesium alloys presence of stage II deformation makes this ambiguous. This is because stage II consists of large fraction of non-linear reversible deformation with little permanent plastic deformation. Current standardised methods of using a 0.2% offset strain gives a stress value in stage II which is not meaningful before extensive plasticity occurs. A higher offset strain such as 0.45% (proposed in study 1 of this thesis) gives a better measure of the activation of <a> prismatic slip. Further work is needed to revise the ISO [7] and ASTM [8] standards in order to establish a more meaningful measure of yield stress for magnesium and its alloys.

Future work based on study 2: Magnesium is intrinsically strain-rate sensitive [9] due to the limited number of easily activated slip systems (only two independent basal slip directions), and the need to engage other slip systems (i.e. <a> prismatic and <c+a> pyramidal) with significant activation barriers for extensive deformation. At the strain rates studied in the present work (10^{-6}-10^{-1} s^{-1}), strain-rate sensitivity is apparent in magnesium alloys with lower aluminium contents in solid solution. In alloys with increased aluminium in solid solution, the intrinsic strain-rate sensitivity is masked by the effect of dynamic strain

ageing. Important research questions remain about the deformation behaviour outside the studied strain rates, in particular at high strain rates. The strain-rate sensitivity of alloys with low aluminium contents in solid solution seems to diminish at higher strain rates. Future work is required to determine if the strain-rate sensitivity drops to zero in the transition region towards dynamic strain rates. In the case of alloys with high aluminium contents in solid solution, it is also unclear whether the strain-rate sensitivity remains low at higher strain rates. These questions are particularly relevant to practical requirements such as crash behaviour and joining processes.

Future work based on study 3: For the first time, the anelasticity of a range of commercial high-pressure die-cast magnesium alloys has been studied. An interesting observation from this study comes from the comparison of a T5-aged AE44 with as-cast AE44. The effect of heat treatment on the anelasticity has not been studied until now, and there are more questions to be answered. In T5-aged AE44, the activation of anelasticity is shifted to higher stress levels. This is possibly due to the presence of nanoscale aluminum-manganese precipitates [10] suppresing the <a> basal slip. Further work is required to understand the mechanisms involved. More concrete evidence by transmission electron microscopy (TEM) to show the interactions of precipitates with slip and twinning would be useful. The anelasticity is also sensitive to the grain size [11-13] and alloy composition [11, 14, 15], but these studies on the effects of grain size and solute concentrations [11, 12, 14] mostly covered sand-cast and mold-cast alloys. The wide range of grain sizes in these alloys made the investigation on the solute dependence of anelasticity difficult. A more systematic study on the effect solute concentrations is required. Anelastic behaviour is important to properties such as sound dampening, yield strength and potentially fatigue strength; therefore, it is important to further study the effect of these microstructural parameters.

Future work based on study 4: The proposed constitutive model can well predict the deformation behaviour of the more dilute die-cast magnesium alloys, but it has a slightly poorer fit for the more concentrated AZ91 alloy. This is attributed to the higher strain hardening rate in AZ91, likely due to the high aluminium concentration and fully interconnected percolating network in AZ91. Yang et al.[16] has developed a theoretical model to calculate the overall strength of similar die-cast magnesium-aluminium based alloys by accounting for the contributions of Hall-Petch, solid solution and dispersion-strengthening mechanisms. Therefore, future work could incorporate their model and the effects of

microstructural features, such as grain size, eutectic morphology and intermetallic volume fraction into the modelling.

Chapter 8 References

[1] Zhang JH, Liu SJ, Leng Z, Liu XH, Niu ZY, Zhang ML et al. Structure stability and mechanical properties of high-pressure die-cast Mg-Al-La-Y-based alloy. Materials Science and Engineering A 2012; 531: p. 70-5.

[2] Mallapur DG, Kori SA, Rajendra Udupa K. Influence of Ti, B and Sr on the microstructure and mechanical properties of A356 alloy. Journal of Materials Science 2011; 46(6): p. 1622-7.

[3] Hébert G, Dubé D, Tremblay R. Tensile and fatigue behaviour of thin-walled cast A383. 0 components. Materials Science and Engineering A 2012; 552: p. 89-96.

[4] Zhu SM, Easton MA, Abbott TB, Nie JF, Dargusch MS, Hort N et al. Evaluation of magnesium die-casting alloys for elevated temperature applications: microstructure, tensile properties, and creep resistance. Metallurgical and Materials Transactions A 2015; 46(8): p. 3543-54.

[5] Fan Z, Fang X, Ji S. Microstructure and mechanical properties of rheo-diecast (RDC) aluminium alloys. Materials Science and Engineering A 2005; 412(1): p. 298-306.

[6] Abbott TB, Easton MA, Schmidt R. Magnesium for crashworthy components. In: Kaplan HI, editor. Magnesium Technology. Proceedings of the TMS Annual Meeting; 2003 March 2-6; San Diego, California; p. 463-6.

[7] ISO 6892-1 metallic materials tensile testing-part 1: method of test at room temperature. International Standards Organisation; 2009.

[8] ASTM Standard E8M-09 standard test methods for tension testing of metallic materials in annual book of ASTM standards, ASTM. West Conshohocken PA: American Society for Testing and Materials; 2009.

[9] Meyers MA. Dynamic behavior of materials. New Jersey: John wiley & sons; 1994.

[10] Zhu SM, Abbott TB, Gibson MA, Nie JF, Easton MA. Age hardening in die-cast Mg–Al–RE alloys due to minor Mn additions. Materials Science and Engineering A 2016; 656: p. 34-8.

[11] Mann GE, Sumitomo T, Cáceres CH, Griffiths JR. Reversible plastic strain during cyclic loading–unloading of Mg and Mg–Zn alloys. Materials Science and Engineering A 2007; 456(1): p. 138-46.

[12] Nagarajan D. Anelasticity in cast Mg-Gd alloys. Materials Science and Engineering A 2017; 695: p. 14-9.

[13] Cáceres CH, Mann GE, Griffiths JR. Grain size hardening in Mg and Mg-Zn solid solutions. Metallurgical and Materials Transactions A 2011; 42(7): p. 1950-9.

[14] Nagarajan D, Cáceres CH, Griffiths JR. Anelastic phenomena in Mg-Al alloys. Proceedings of the 12th International Symposium on Physics of Materials; 2011 Sep 4-8; Prague. Czech Republic: Polish Academy of Sciences Institute of Physics; 2012. p. 501-4.

[15] Nagarajan D, Ren X, Cáceres CH. Anelastic behavior of Mg-Al and Mg-Zn solid solutions. Materials Science and Engineering A 2017; 696: p. 387-92.

[16] Yang KV, Cáceres CH, Easton MA. Strengthening micromechanisms in cold-chamber high-pressure die-cast Mg-Al alloys. Metallurgical and Materials Transactions A 2014; 45(9): p. 4117-28.

Appendices

Appendix A. Conference Papers

The following pages contain the published conference papers based on the results of this research.

Flaws in Standardised Proof Stress Determination Methods for Magnesium Alloys

HuaQian Ang*, Trevor Abbott, Suming Zhu, Chengfan Gu, Mark Easton
*School of Aerospace, Mechanical and Manufacturing Engineering
Royal Melbourne Institute of Technology (RMIT) University, Victoria 3083, Australia
Email: huaqian.ang@rmit.edu.au

***Abstract* — The proof stress determination methods specified in ISO 6892-1 [1] are reviewed and discussed. Method 1 underestimates the 0.2% proof stress of magnesium alloys without considering the pseudo-elastic effect. Method 2 can accurately determine the 0.2% proof stress of magnesium alloys, but this method involves complex loading-unloading tests. Method 3 provides inconsistent proof stress values depending on the unloading stress. Inconsistencies in measured proof stress were found between and within these methods. Thus, the 0.2% proof stress measurement methods specified in ISO standard [1] analysis procedure needs to be re-evaluated.**

***Keywords*: Magnesium, Measurement, Proof Stress.**

I. INTRODUCTION

Tensile testing is one of the most commonly used methods to assess material properties. The key tensile properties include: elastic modulus, yield or 0.2% proof stress, tensile strength and elongation to failure. The tensile strength and elongation to failure are unambiguous and can be readily determined. Yield strength is used for materials with clear yielding phenomena such as plain carbon steel, for other materials the stress level required to impart 0.2% permanent strain is used to obtain proof strength where the yield strength is difficult to define definitely.

The determination of an elastic modulus value rests on the assumption that elastic behaviour is linear. Magnesium and its alloys violate this assumption and exhibit pseudo-elastic or non-linear reversible strain which has been identified in AE44 and AM60B [2], AZ91 [3] and Mg and Mg-Zn alloys [4]. Consequently, there is no single value for the elastic modulus of magnesium. The values often quoted for magnesium alloys represent the limit of elastic modulus as the stress and strain increments approach zero. The variable elastic modulus leads immediately to ambiguities in proof stress determination. The permanent plastic strain can only be determined from a monotonic stress-strain curve if the elastic strain can be determined and subtracted. With linear elastic strain this is straightforward but with non-linear elastic strain it is only possible if the elastic behaviour is fully characterised.

Scientific exchange rests on agreed standards for the measurement of properties. In the case of tensile testing standards (for example ISO 6892-1 [1]) at least three methods are presented for proof strength determination applicable to magnesium. The three methods are summarised as follows:

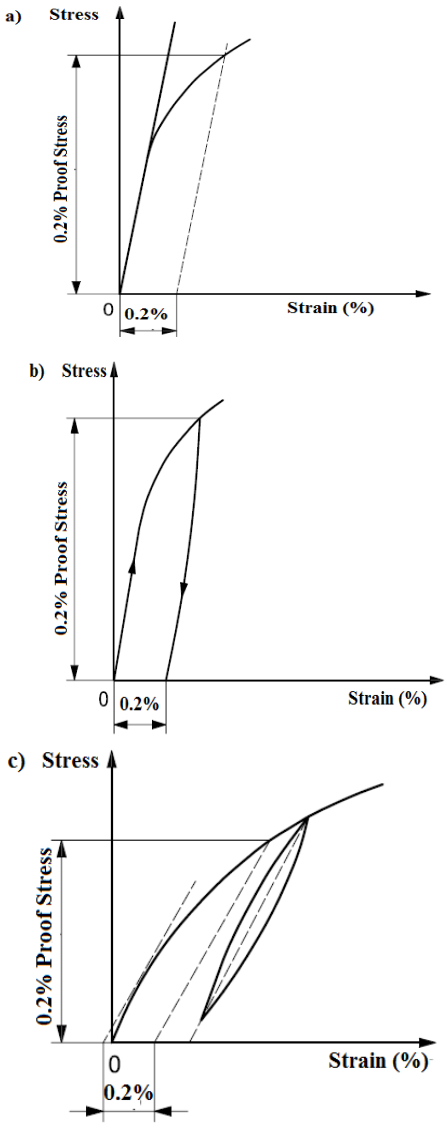

Fig. 1. Proof stress measurement (a) method 1, (b) method 2 and (c) method 3 specified in ISO 6892-1 standard [1].

1. Assumption of linear elastic behaviour with the elastic modulus estimated from the low strain and stress regions of a monotonic stress-strain curve as shown in Fig. 1(a).
2. Repeated loading and unloading to directly determine the load required to impart 0.2% permanent plastic deformation (shown in Fig. 1(b)).
3. Partial unloading once an arbitrary stress level is reached to obtain an alternative elastic modulus value to that obtained in method 1 (illustrated in Fig. 1(c)).

Inconsistencies between and within these methods frustrate attempts to investigate alloy properties. In this paper, three Mg die cast alloys, AM60, AZ91 and AE44 are tested according to the methods of ISO 6892-1 [1] and the magnitudes of inconsistencies determined.

II. Materials and Experimental Details

A. Materials

Commercial alloys, AE44, AM60 and AZ91 were high pressure die cast in a 250 ton cold chamber machine. More details about the casting parameters can be found in [5, 6]. The chemical compositions in wt.% of these three alloys are listed in Table I. The study was carried out using cast-to-shape cylindrical cross section, dog-bone shaped tensile specimens of gauge diameter 5.6 mm and gauge length 35 mm.

TABLE I
CHEMICAL COMPOSITIONS OF THE STUDIED ALLOYS (WT.%).

Alloys	Al	RE	Zn	Mn	Mg
AE44	3.97	3.76	<0.01	0.18	Bal.
AM60	6.26	/	0.1	0.29	Bal.
AZ91	8.88	/	0.74	0.19	Bal.

B. Mechanical Testing

Both monotonic (method 1) and cyclic tension loading-unloading tests (methods 2 and 3) were performed on an Instron 5569 Universal Testing Machine (UTS) with a 50 kN load cell at room temperature using a crosshead speed of 5 mm/min. Four repeats were performed per alloy composition. For method 2, the loading-unloading tests were strain-controlled, unloading at predetermined strains to 0.25 MPa. For method 3, the loading-unloading tests were stress-controlled, unloading at predetermined stress to 10% of the stress obtained. A 25 mm gauge length extensometer was attached to the specimen's gauge length and digital output files of the flow curves were converted to stress-strain.

III. Results

A. Proof Stress Measurement based on Method 1

The engineering stress-strain curves of AE44, AM60 and AZ91 are shown in Fig. 2. It is clear that the linear elastic behavior applies only up to about 20 MPa for all three alloys, where the elastic modulus of Mg alloys, E=45 GPa [7] is measured.

The relatively small elastic region makes elastic modulus determination difficult; elastic modulus decreases with increasing stress level used for modulus determination. As shown in Fig. 3, the elastic modulus is 45 GPa when it is estimated from low stress region at 20 MPa; the elastic modulus decreases to 38 GPa when it is estimated from higher stress region at 60 MPa for AE44. The inconsistency in elastic modulus used has led to a wide range of proof stress values reported in literature. For instance, offsetting a lower elastic modulus to 0.2% strain would tilt the offset line forward, leading to higher proof stress value and vice versa (as illustrated in Fig. 3).

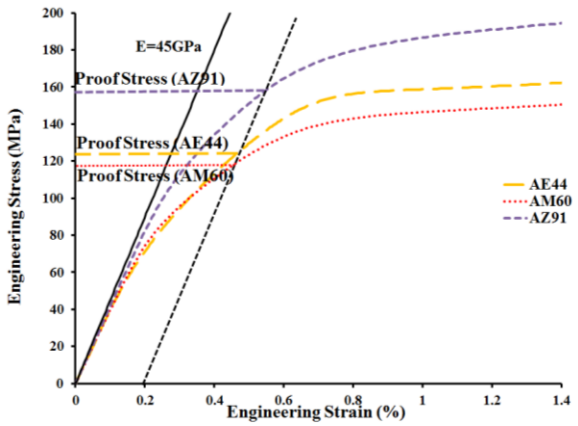

Fig. 2. Tensile curves of cast AE44, AM60 and AZ91 showing respectively proof stress values measured by method 1[1].

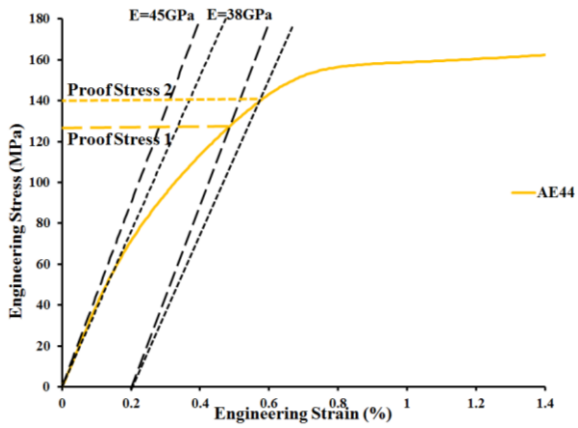

Fig. 3. Variations in elastic moduli used leading to different proof stress values obtained for cast AE44.

Here, the proof stress values measured by method 1 through offsetting a constant elastic modulus of 45 GPa [8] to 0.2% strain are summarized in Table II for cast AE44, AM60 and AZ91.

TABLE II
0.2% PROOF STRESS VALUES, σ_y (MPA) MEASURED BY METHOD 1.

Mg Alloys	σ_y (MPa) based on Method 1 (shown in Fig. 2)
AE44	124
AM60	118
AZ91	154

B. Proof Stress Measurement based on Method 2

Based on method 2, a line should be drawn across hysteresis loop unloaded to 0.2% plastic strain. The point at which this line intersects the curve gives the 0.2% proof stress. However, it is often difficult to pre-determine the applied strain and stress which would unload to 0.2% plastic strain due to the uneven hysteresis loops. Hence, each test was unloaded and reloaded a couple of times, as indicated by the hysteresis loops formed as shown in Fig. 4 for cast AE44. Similar hysteresis loops were observed for cast AM60 and AZ91. A series of secant elastic moduli are also defined in Fig. 4.

Here, the hysteresis loops still did not unload to 0.2% strain after several loading-unloading cycles. Hence, 0.2% proof stress is measured by a secant elastic modulus (as indicated by dotted line in Fig. 4), interpolated from elastic moduli drawn across hysteresis loops unloading to strains before and after 0.2%. The 0.2% proof stress values and the interpolated secant elastic moduli at 0.2% strain in method 2 for the three alloys are summarised in Table III.

TABLE III
0.2% PROOF STRESS VALUES, σ_y (MPA) AND INTERPOLATED SECANT ELASTIC MODULI USED IN METHOD 2.

Mg Alloys	σ_y (MPa)	Interpolated Secant Elastic Modulus at 0.2% Strain (GPa)
AE44	157	23.5
AM60	142	23.9
AZ91	182	26.4

Generally, secant elastic modulus decreases with increasing residual plastic strain and is similar for all alloys tested. The relationship of secant elastic modulus and residual plastic strain is shown in Fig. 5 for cast AE44, AM60, and AZ91.

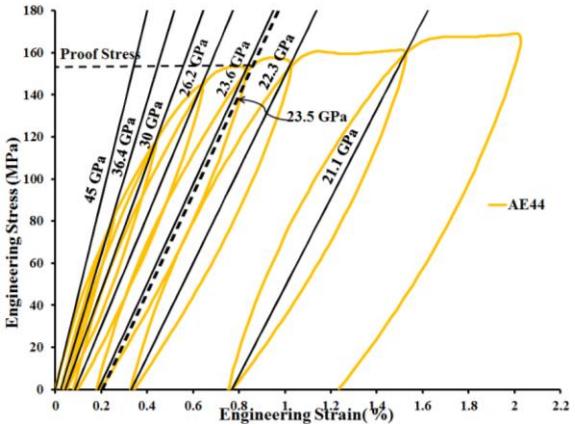

Fig. 4. Cyclic stress-strain curve of cast AE44 showing proof stress measured by method 2 [1].

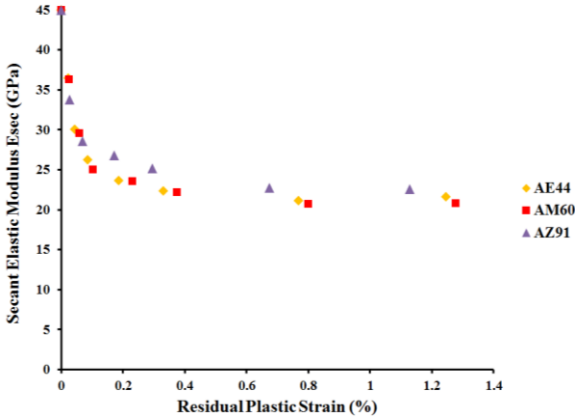

Fig. 5. Secant elastic modulus (defined in Fig. 4) as a function of residual plastic strain.

C. Proof Stress Measurement based on Method 3

Based on method 3, the stress is reduced to about 10% of the unloading stress when the presumed proof stress is reached to obtain an alternative elastic modulus for proof stress determination. But, it is impossible to pre-identify when the proof strength is exceeded unless loading-unloading tests are conducted in advance. Here, based on previously conducted monotonic tests (tensile curves shown in Fig. 2), AE44, AM60 and AZ91 were unloaded at 124 MPa, 118 MPa and 154 MPa respectively (0.2% proof stress values obtained from method 1). The cyclic stress-strain curve for AE44 and the alternative elastic modulus (shown as dotted line) following method 3 are shown in Fig. 6. According to method 3 [1], the alternative elastic modulus must be tangential to the stress-strain curve and the point where this line crosses the abscissa is taken as the corrected origin. Hence, in this case, the alternative elastic modulus is offset from negative strain rather than at the origin as shown in Fig. 6. The 0.2% proof stress values and alternative elastic moduli used in method 3 for cast AE44, AM60 and AZ91 are summarized in Table IV.

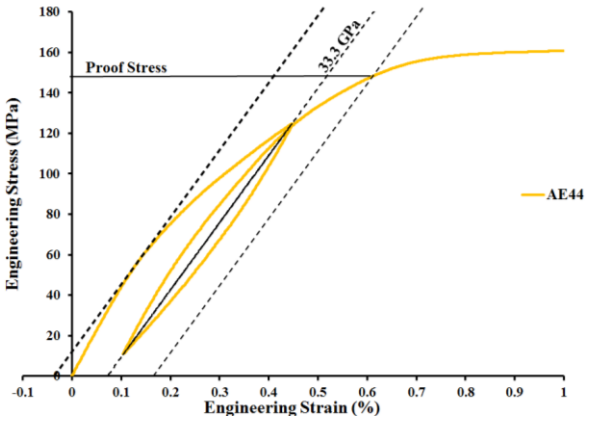

Fig. 6. 0.2% proof stress measured by method 3 [1] for cast AE44.

TABLE IV
0.2% PROOF STRESS VALUES, σ_y (MPA) AND ALTERNATIVE ELASTIC MODULUS OBTAINED FROM METHOD 3.

Mg Alloys	σ_y (MPa) based on Method 3	Alternative Elastic Modulus (GPa)
AE44	147	33.3
AM60	136	31.1
AZ91	172	32.4

IV. DISCUSSION

The 0.2% proof stress of Mg alloys reported in literature [9-15] is often defined by method 1 due to its simplicity as compared to methods 2 and 3, but several features of phenomenon suggest that method 1 does not take the anelastic effect, ε_{ae} into consideration. This is clearly seen when Fig. 2 (monotonic stress-strain curves) is overlaid onto Figs. 4 and 6 (cyclic stress-strain curves for methods 2 and 3 respectively) as shown in Fig. 7 for AE44, AM60 and AZ91. The flaws in these standardized methods are summarized as follows:

1. The 0.2% proof stress measured by method 1 unloads to a significantly lower residual plastic strain, instead of 0.2% residual plastic strain upon the disappearance of anelastic deformation. Hence, method 1 significantly underestimates the proof stress of Mg alloys.
2. Method 2 more accurately measures the 0.2% proof stress of Mg alloys, but it is almost impossible to pre-determine the stress or strain amplitudes which impart 0.2% permanent plastic deformation upon unloading. Hence, repeated loading-unloading tests have to be conducted, and this becomes time consuming and impractical.
3. Method 3 provides inconsistent 0.2% proof stress value, depending on the unloading stress level. As mentioned earlier, secant elastic modulus decreases with increasing residual plastic strain. Hence, if AE44, AM60 and AZ91 had been unloaded at higher stresses, the resulted lower alternative elastic modulus would have tilted the offset line forward, leading to higher proof stress values. In contrast, unloading at lower stress level would result in higher alternative elastic modulus, leading to a lower proof stress. value.
4. The three methods provided different proof stress values for the same alloy tested.

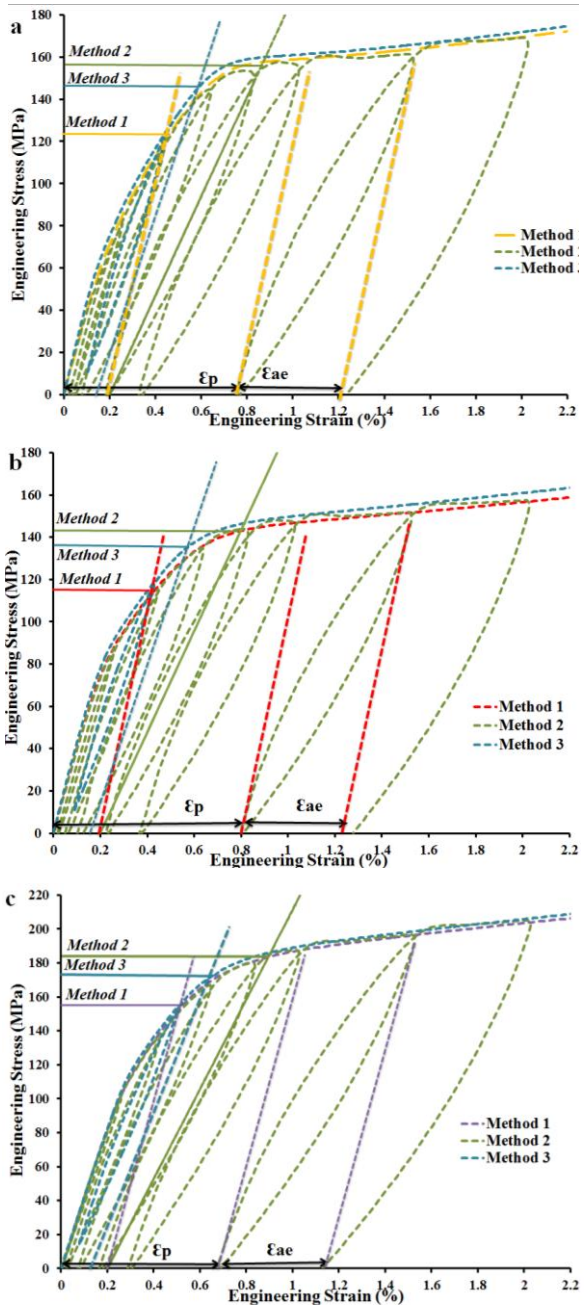

Fig. 7. 0.2% proof stress values measured by different ISO 6892-1 methods for (a) AE44, (b) AM60 and (c) AZ91.

Clearly, 0.2% proof stress measurement methods specified in ISO standard [1] analysis procedure needs to be re-

evaluated due to the existence of anelastic strain and for simplicity purposes.

Out of the three methods, method 2 is a more consistent and accurate method to follow, apart from its complexity. In contrast, methods 1 and 3 significantly underestimate the 0.2% proof stress values.

IV. CONCLUSION

The standardized ISO methods and their effects on 0.2% proof stress measurement of cast Mg alloys have been investigated. The following conclusions are drawn from this study:

1. Method 1 does not account for the anelastic effect and significantly underestimates the 0.2% proof stress of Mg alloys.

2. Method 2 is a more appropriate method, but it is often difficult to pre-determine the strain and stress which unloads to 0.2% plastic strain, unless all strains or stresses of interest are considered. Hence, repeated loading-unloading tests have to be conducted, and this becomes time consuming and impractical.

3. Method 3 is not recommended as it provides inconsistent proof stress values depending on the unloading stresses.

4. Inconsistencies in measured proof stress are found between and within these methods. Thus, the 0.2% proof stress measurement methods specified in ISO standard [1] analysis procedure needs to be re-evaluated.

REFERENCES

1. *ISO: 6892-1*, in *Metallic materials-Tensile testing* 2009, ISO Australian Standard.
2. Lu, Z. and P. Blackmore, *Cyclic Stress-Strain Behaviour of AM60B and AE44 Cast Magnesium Alloys and Its Impact on LCF Characterisation and Fatigue Analysis*. 2014, SAE Technical Paper.
3. Caceres, C., T. Sumitomo, and M. Veidt, *Pseudoelastic behaviour of cast magnesium AZ91 alloy under cyclic loading–unloading.* Acta Materialia, 2003. **51**(20): p. 6211-6218.
4. Mann, G., et al., *Reversible plastic strain during cyclic loading–unloading of Mg and Mg–Zn alloys.* Materials Science and Engineering: A, 2007. **456**(1): p. 138-146.
5. Nagasekhar, A.V., M.A. Easton, and C.H. Caceres, *Solute content and the grain microstructure of high pressure diecast magnesium–aluminium alloys.* Advanced Engineering Materials, 2009. **11**(11): p. 912-919.
6. Yang, K.V., M. Easton, and C. Caceres, *The development of the skin in HPDC Mg–Al alloys.* Materials Science and Engineering: A, 2013. **580**: p. 191-195.
7. Sumitomo, T., C. Caceres, and M. Veidt, *The elastic modulus of cast Mg–Al–Zn alloys.* Journal of Light Metals, 2002. **2**(1): p. 49-56.
8. Sumitomo, T., *Elastic and pseudoelastic behaviour of Mg-Al-Zn alloys.* 2003.
9. Zhang, J., et al., *Microstructures and mechanical properties of heat-resistant high-pressure die-cast Mg–4Al–xLa–0.3 Mn (x= 1, 2, 4, 6) alloys.* Materials Science and Engineering: A, 2010. **527**(10): p. 2527-2537.
10. Zhang, J., et al., *Effect of substituting cerium-rich mischmetal with lanthanum on microstructure and mechanical properties of die-cast Mg–Al–RE alloys.* Materials & Design, 2009. **30**(7): p. 2372-2378.
11. Zhang, J., et al., *Microstructures, tensile properties and corrosion behavior of die-cast Mg–4Al-based alloys containing La and/or Ce.* Materials Science and Engineering: A, 2008. **489**(1): p. 113-119.
12. Zhang, J., et al., *Structure stability and mechanical properties of high-pressure die-cast Mg–Al–La–Y-based alloy.* Materials Science and Engineering: A, 2012. **531**: p. 70-75.
13. Zhang, J., et al., *Effect of Ce on microstructure, mechanical properties and corrosion behavior of high-pressure die-cast Mg–4Al-based alloy.* Journal of Alloys and Compounds, 2011. **509**(3): p. 1069-1078.
14. Chia, T.L., et al., *The effect of alloy composition on the microstructure and tensile properties of binary Mg-rare earth alloys.* Intermetallics, 2009. **17**(7): p. 481-490.
15. Forsmark, J.H., et al., *An Investigation of the Effects of Cast Skin on the Mechanical Properties of an AM60 Die-Cast Magnesium Alloy.* SAE International Journal of Materials and Manufacturing, 2015. **8**(2015-01-0510).

Performance Evaluation of High-Pressure Die-Cast Magnesium Alloys

Mark Easton, Suming Zhu, Mark Gibson, Trevor Abbott, Hua Qian Ang, Xiaobo Chen, Nick Birbilis, and Gary Savage

Abstract

Over 90% of the magnesium (Mg) alloys in commercial applications are produced by high-pressure die-casting. This paper presents our efforts in evaluating castability and properties of commercial and near-commercial magnesium alloys to demonstrate how the currently available alloys can be applied to different situations across a range of property space. For high temperature applications, i.e. 175 °C and above, Mg–RE and Mg–Al–Ca based alloys have creep properties at least comparable to aluminium (Al) alloy A380 although these alloys have some challenges with casting or cost. For moderate temperatures, Mg–Al–RE based alloys, especially AE44, are most attractive due to an excellent combination of creep resistance, strength and castability. For automotive structural applications where a good combination of strength and ductility is required, Mg–Al alloys provide the baseline, but Mg–Al–RE based alloys can provide outstanding performance, especially with recent discoveries about its response to age hardening treatments. Therefore, high-pressure die-cast Mg alloys hold great promise for continued growth in automotive applications.

Keywords

Magnesium alloys • Castability • Creep • Property evaluation

Introduction

The great majority of the magnesium (Mg) alloys in commercial applications are produced by high-pressure die-casting [1]. There are a number of alloys that have been designed for high-pressure die-casting, with the great promise of better castability and improved properties particularly at higher temperatures. The main groups of alloys relate to the addition of Ca [2], Sr [3], Si [4] and/or rare earths (REs) [5, 6] to Mg–Al alloys and Mg–RE alloys [7–9]. When the properties of alloys have been compared previously it has involved in trying to collate information from different sources with alloys produced in different ways [10]. Hence it is difficult to compare the alloys directly.

Recently the current authors have assessed the castability [11, 12] and the mechanical properties of [13] of a wide range of commercial and near commercial Mg high-pressure die-cast alloys manufactured under the same conditions. This paper brings together this work in an attempt to evaluate whether there are any stand-out alloys, particularly for higher temperature applications.

M. Easton (✉) · S. Zhu · M. Gibson · T. Abbott · H.Q. Ang
School of Engineering, RMIT University, Carlton, VIC 3053, Australia
e-mail: mark.easton@rmit.edu.au

T. Abbott
CSIRO Manufacturing, Clayton, VIC 3168, Australia

X. Chen · N. Birbilis
Department of Materials Science and Engineering, Monash University, Clayton, VIC 3168, Australia

G. Savage
Magontec Ltd., Sydney, NSW 2000, Australia

K.N. Solanki et al. (eds.), *Magnesium Technology 2017*,
The Minerals, Metals & Materials Series, DOI 10.1007/978-3-319-52392-7_20

Alloys

This paper focuses on the most common commercial alloys, AZ91 and AM60 and compares the properties and castability with the range of commercial and near-commercial Mg-based alloys. AS31 and MRI alloys have been used in various powertrain applications, AJ62 was the Mg alloy used in the BMW engine block, whilst AXJ530 was developed by General Motors for similar applications. AE42/AE44 were developed by Norsk Hydro Magnesium with AE44 finding some commercial success. AE44-4 is the original version of the alloy using misch-metal additions that contain four elements (La, Ce, Pr, Nd). However, due to the demand of Nd in particular in magnets, two-element (La/Ce) misch metal is substantially cheaper and is now used as a low cost AE44 variant. AM-HP2+ is an alloy developed by the CAST Co-operative Research Centre as a premium high-temperature high-pressure die-cast alloy [14]. The compositions of the alloys are provided in Table 1.

Castability

A novel die was developed to assess the castability [12, 14]. The die was designed to create as many casting defects as possible including flow defects from diverging and converging flows, constrained difficult to feed sections that hot tear, and thin perpendicular sections to test the fluidity.

Each alloy was cast under four conditions: high and low die temperature and high and low second stage velocity. An example is shown in Fig. 1. Ten castings from each condition were rated for each of the alloys. Ratings on a 5-point scale (0 worst, 5 best) for fluidity, cracking and surface quality (spangling) were made by visual assessment of the castings and the different alloys compared. The castability rating results for the selected alloys are shown in Fig. 2.

As well as the visual assessment of the castings selected castings were sectioned to investigate the defect distribution within the casting. It was found that there was in general a reasonable correlation between the visual observations and qualitative assessment of porosity and crack distributions.

It should be pointed out that the visual assessments of the castability did not take into account how the castability was affected in two particular cases. One was that the alloys containing Ca had melt handling issues. Primarily this was evidenced by excessive blocking of the transfer tubes during casting, which appeared to be strongly correlated with the amount of Ca in the alloy. So the overall castability score should be lower for MRI153A, MRI153M, MRI230D and AXJ530 alloys compared to that based only on the visual inspection of the casting. The second was that HP2+ showed a tendency to hot tear in dog bone tensile samples, which is related to the use of REs such as Nd [15] and Y [16] which are hot tearing susceptible elements. However, through careful element selection this tendency was minimised but the overall castability score should be lower than from visual inspection only.

Mechanical Properties

Round tensile bars 5.6 mm in diameter were cast (see [13] for details) and underwent tensile testing at room temperature, 150 and 175 °C, and creep testing at 150 and 175 °C across a range of stresses so that the creep strength could be obtained. Figure 3 shows the room temperature 0.2% yield

Table 1 Chemical compositions (wt%) of the alloys in this study determined by Inductively Coupled Plasma—Optical Emission Spectroscopy

Alloy	Al	Si	Ca	Sr	Sn	Mn	Zn	Ce	La	Nd	Pr	Y
AZ91	8.88	–	–	–	–	0.19	0.74	–	–	–	–	–
AM60	6.26	–	–	–	–	0.29	0.1	–	–	–	–	–
AS31	3.52	0.56	–	–	–	0.27	–	–	–	–	–	–
AJ52[a]	5.2	–	0.07	1.86	–	0.25[a]	–	–	–	–	–	–
MRI153A	8.32	–	1.01	0.09	–	0.22	0.75	–	–	–	–	–
MRI153M	7.73	–	1.06	0.30	–	0.25	–	–	–	–	–	–
MRI230D	6.49	–	2.00	0.43	0.95	0.28	–	–	–	–	–	–
AXJ530	4.49	–	3.44	0.17	–	0.25[a]	–	–	–	–	–	–
AE42	3.45	–	–	–	–	0.31	–	1.45	0.60	0.41	0.1	–
AE44-4	3.73	–	–	–	–	0.30	–	2.47	1.21	0.51	0.1[a]	–
AE44-2	3.95					0.15		2.82	1.32			
AM-HP2+	0.05	–	–	–	–	–	0.42	0.99	1.65	0.96	–	0.08

Where the amount is not listed the composition is below the detectable range usually 0.01 wt%

[a]Note that it was planned to make AJ62, but the Al content was measured to be 5.2%, in other words AJ52

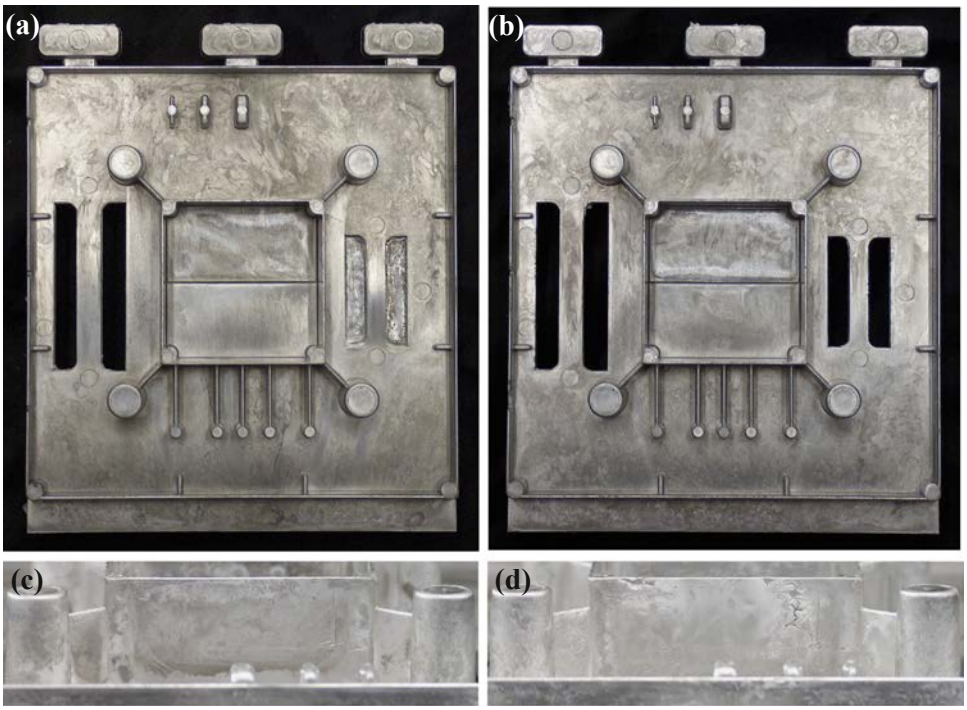

Fig. 1 Pictures of one of the better castings **a** and **c** die temperature 250 °C and injection velocity 2.0 m/s, and worst castings **b** and **d** die temperature 180 °C and injection velocity 1.3 m/s for AS31

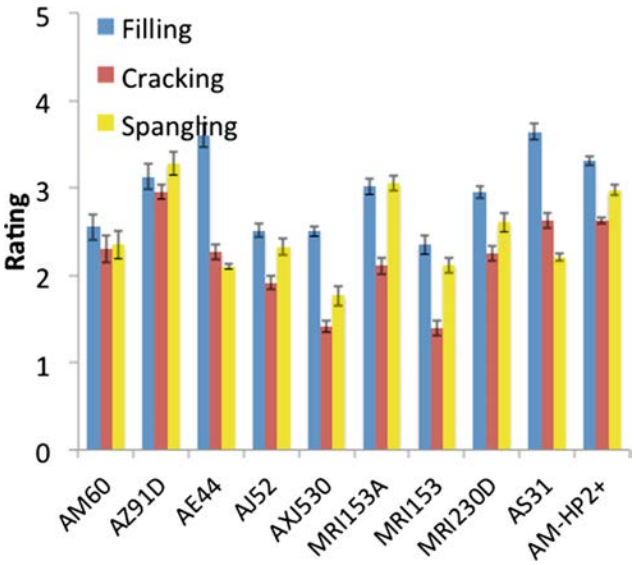

Fig. 2 Average ratings for cracking, filling and spangling for the selected Mg die casting alloys using the specially designed castability die

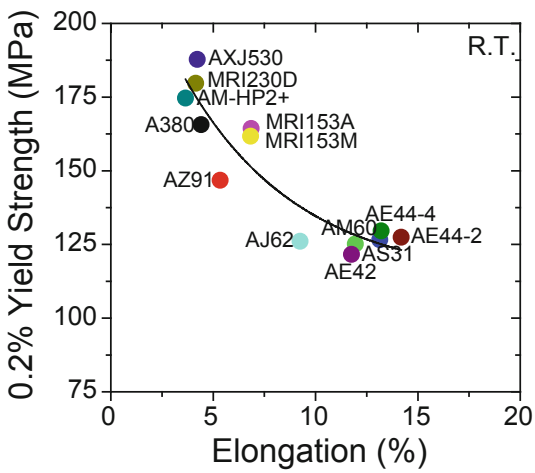

Fig. 3 The 0.2% yield strength plotted against elongation for the selected Mg alloys. Al die-casting alloy A380 is included for comparison

strength plotted against ductility (elongation) whilst the creep strength values (stress to produce 0.1% strain at 100 h) at 150 and 175 °C are presented in Fig. 4 for the selected Mg alloys. It is apparent that the HPDC Mg alloys lie on a banana curve where the alloys with the higher yield strength have a lower elongation and vice versa. At the high strength end of the spectrum AXJ530 and MRI230D possess high strength (~180 MPa) whilst maintaining elongations to fracture of approximately 5%. MRI153A/M have lower strength and better ductility, whilst AE44 appears to have a better strength-elongation combination than AM60. In general the higher strength alloys had the highest creep strength (Fig. 4) with AM-HP2+ having the highest creep strength at 175 °C, with 5 alloys surpassing Al alloy A380. AE44 had very high creep strength compared to its yield strength.

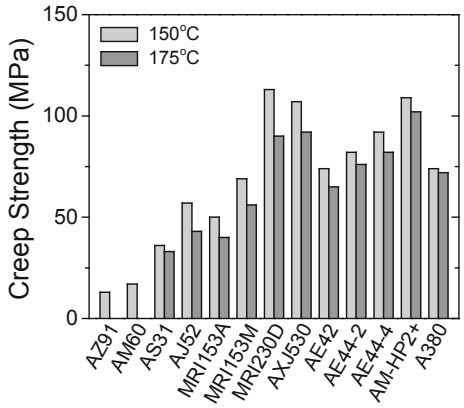

Fig. 4 Creep strength (stress to produce 0.1% strain at 100 h) at 150 and 175 °C for the selected Mg alloys. Al die-casting alloy A380 is included for comparison

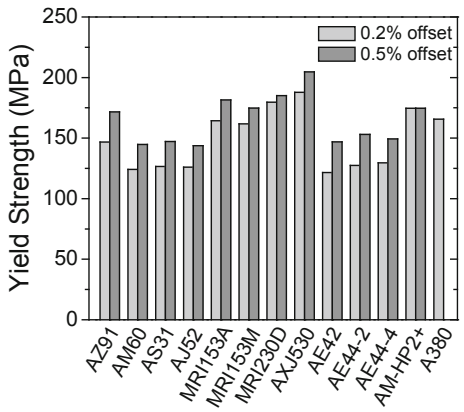

Fig. 5 Room temperature yield strength determined by 0.2% offset and 0.5% offset for the selected Mg die-casting alloys. Al die-casting alloy A380 is included for comparison

Since this work was originally published there have been a few other important developments. The first is that the approach to the measurement of yield strength has been re-evaluated based on a consideration of the anelastic behaviour of Mg alloys, where the permanent plastic strain is much lower than based on a conventional 0.2% offset as typically used. Based on loading-unloading tests of high-pressure die-cast AZ91, AM60 and AE44 alloys it was found that a 0.5% offset gives a much closer estimate of 0.2% permanent plastic deformation [17] (although it should also be noted that this seems to vary with processing conditions with decreasing grain size appearing to increase the amount of anelasticity). Revised values of yield strength of the selected Mg alloys are shown in Fig. 5.

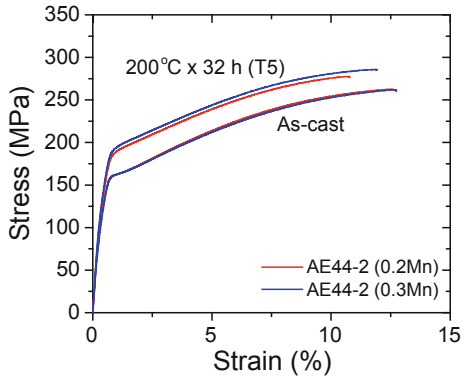

Fig. 6 Room temperature tensile curves showing the effect of ageing in AE44-2 with 0.2 and 0.3% Mn additions

The other surprising finding has been the role of Mn in promoting age-hardening behaviour in AE alloys. Figure 6 shows the room temperature tensile curves of AE44-2 with 0.2 and 0.3% Mn additions before and after ageing at 200 °C for 32 h. In AE44 yield strength increases of greater than 30 MPa for a T5 heat treatment have been observed with a 0.3%Mn addition whilst no age hardening response is observed without the Mn addition [18]. Previously it has been thought that it is the difference in creep properties in particular have varied with different rare earths [19–22]. However, it is now evident that Mn plays a major effect on the properties of these alloys and consequently all previously observed differences need to be re-evaluated. In fact, examples like the previously reported differences between AE44-2 (containing only La and Ce) and AE44-4 (containing La, Ce, Pr and Nd) [13] and the alloys containing only one of each of the rare earths, at least qualitatively relate to differences in Mn levels [22].

Corrosion

Corrosion properties on these alloys have not previously been reported by the current authors. Corrosion plates (30 × 50 × 2 mm) were cast. Polarisation tests to determine i_{corr} and immersion tests to determine the weight loss were performed (Fig. 7). See previous publications for details [23]. The main reason for this is that the corrosion response of the alloys was found to be relatively similar, with most of the alloys showing a moderate increase in corrosion rate over AZ91. AJ52 had a much higher corrosion rate because Mn was not added to the alloy. Hence it is an outlier and does not represent the actual corrosion rate of AJ52/62, which is probably similar to the other alloys.

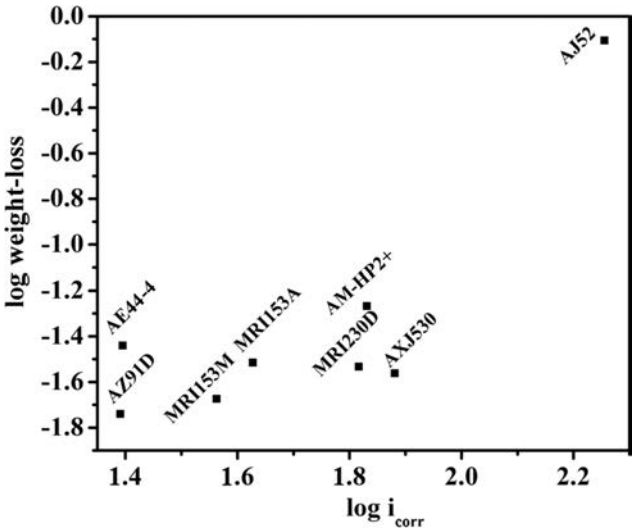

Fig. 7 Plot of two commonly used corrosion parameters, the weight loss during immersion testing and the i_{corr} from polarisation tests

Overall Evaluation

The ability to withstand high temperatures is only one factor, albeit critical, for Mg alloys to be used in powertrain components in automobiles. Two other key factors are castability and cost. An alloy that is difficult to cast into the required components, due to cracking or filling problems, will not be accepted by the automotive component industry. The cost will become an issue if the price of creep resistance enhancing elements is excessive or a non-standard procedure is required for production. To aid the selection of Mg die-casting alloys, an overall evaluation of the Mg die-casting alloys investigated is made in the present work by taking the combined influence of creep resistance, castability and cost into account.

To correlate with the creep resistance, an overall castability rating for the selected Mg die-casting alloys is used, which is an average of the quality ratings of filling, cracking and spangling. It should be pointed out that the Ca-containing alloys tend to encounter melt handling difficulties due to excessive oxidation, which can result in clogging of the transfer tube in cold chamber die casting machines. So the actual castability ratings of the Ca-containing alloys are reduced to take into account melt handing difficulties. It should also be noted that some alloys, e.g. AM-HP2+, MRI230D and MRI153M showed some propensity to hot tearing in the tensile samples, which will downgrade the castability rating. Correlations between 0.1% creep strengths at 150 and 175 °C with castability are shown in Fig. 8 with the arrows showing how the alloy ratings could be adjusted for these other factors. It is apparent that, among the selected alloys, AE44, AE44 and AM-HP2+ are the most promising, since they have a good combination of creep resistance and castability.

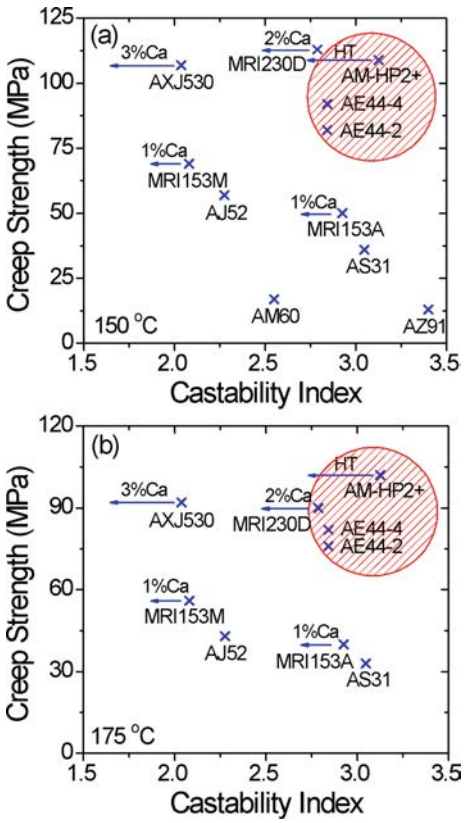

Fig. 8 0.1% creep strength at **a** 150 °C and **b** 175 °C plotted against castability index (average index of filling and cracking) for the selected Mg diecasting alloys. The *arrows* show decreases in the castability related to melt handling (MRI153M, MRI230D and AXJ530) and hot tearing resistance (AM-HP2+)

An approximate indication of the material cost of the selected Mg die-casting alloys is shown in Fig. 9, which is presented as the material cost relative to that of AZ91. The cost is calculated based on recent commodity prices (September 6, 2016) of the constituent elements in the alloys, which does not include production cost or yield loss during melting. It should be pointed out that the commodity prices vary from time to time and the materials cost data presented here are just for comparison purposes. The material cost is low for AS31, AJ52, MRI153A, MRI153M and AXJ530 while AE44-4 and AM-HP2+ are considerably more expensive than AZ91. It is noted that AE44-2 is much cheaper than AE44-4, as a result of the exclusion of the extremely expensive elements Nd and Pr. The 0.1% creep strength at 150 and 175 °C plotted against material cost is shown in Fig. 10. It can be seen that the highly creep-resistant AE44-4 and AM-HP2+ suffer from high material cost while low cost AS31, AJ52, MRI153A and MRI153M have limited creep resistance. AXJ530, AE44-2 and MRI230D represent alloys with good creep resistance yet relatively low cost.

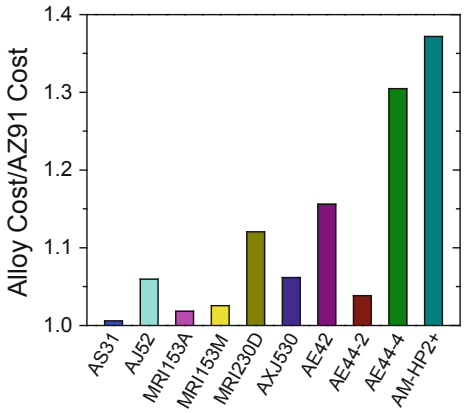

Fig. 9 The relative material cost of the selected Mg diecasting alloys as compared to AZ91. The cost is calculated based on the latest commodity prices (September 6, 2016) of the constituent elements in the alloys. It should be pointed out that the processing cost will outweigh material cost for alloys with relative material cost below about 1.1. For example, the Ca-containing alloys need special flux or flux-less production that will increase cost; the actual cost of AM-HP2+ will be considerably higher because the RE and Al contents need to be fine-tuned

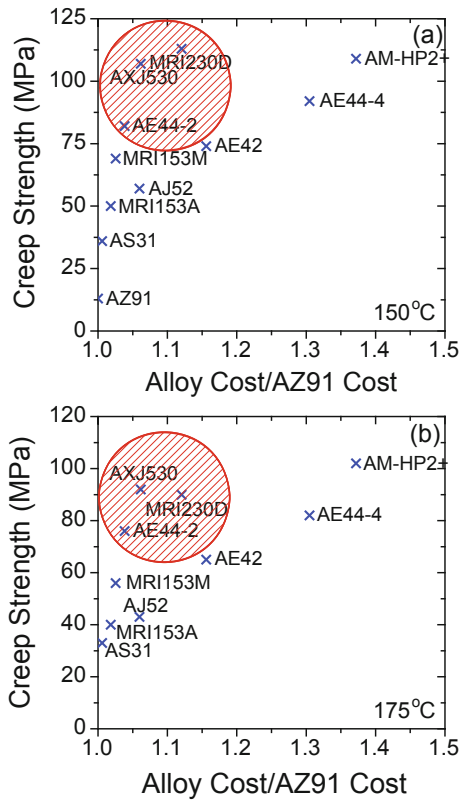

Fig. 10 0.1% creep strength at **a** 150 °C and **b** 175 °C plotted against material cost relative to that of AZ91 for the selected Mg diecasting alloys. The *circled areas* indicate alloys with high creep resistance yet low cost

Overall it is clear that high-pressure die-cast Mg alloys have a very good suite of properties, which are even better than the commonly used aluminium alloy, A380. At the high performance end of the spectrum, AM-HP2+ has an excellent set of properties and good castability but is expensive. AXJ530 and MRI230D have excellent properties and relatively low cost but there are issues with castability. For moderate improvements in creep strength over AZ91, AS31 and MRI153A seem to be good choices being low cost with relatively good castability. Overall, AE44 seems to be a stand out alloy. The creep resistance is not as good as the best alloys but still very good. It also has a very good strength-ductility combination, particularly after T5 heat treatment, and better than AM60 which is the incumbent alloy for many structural applications. Also its castability is very good. It appears that the use of low-cost RE elements, Ce and La, and the elimination of higher cost REs, such as Nd and Pr has little effect on the properties and consequently the cost increase is not great.

Conclusions

An extensive evaluation of high-pressure die-cast Mg alloys has been undertaken to evaluate the castability and properties of a range of commercial and commercial-ready alloys. It is clear that Mg alloys have properties superior to the incumbent Al alloy with relatively small cost increments over AZ91. There are alloys with excellent high-temperature properties that do have some challenges with castability (MRI230D and AXJ530) or cost (AM-HP2+). There are other alloys that provide moderate improvements in creep performance over AZ91 with little cost increase (AS31 and MRI153A). AE44 has an excellent combination of properties with good creep properties, castability and low cost with the use of the more common REs.

Acknowledgements The authors (ME, SZ, TA, XBC and MG) acknowledge the support of the Australian Research Council through linkage grant LP130100828. The authors also thank the many others who have been a part of this work including Dr. Morris Murray, who designed the castability die, Dr. Norbert Hort from HZG for the supply of the MRI alloys and the useful conversations and Prof. Jian-Feng Nie at Monash University. We also thank Mr. Andrew Yob and Ms. Maya Gershenzon of CSIRO for their highly competent production of the high-pressure die-cast samples.

References

1. T.B. Abbott, Magnesium: industrial and research developments over the last 15 years. Corrosion **71**, 120 (2015)

2. A. Luo, M.P. Balogh, B.R. Powell, Creep and microstructure of magnesium-aluminum-calcium based alloys. Metall. Mater. Trans. A **33A**, 567 (2002)
3. E. Baril, P. Labelle, M.Ö. Pekgüleryüz, Elevated temperature Mg-Al-Sr: creep resistance, mechanical properties, and microstructure. JOM **55**, 34 (2003)
4. T.K. Aune, T. Ruden, *High Temperature Properties of Magnesium Die Casting Alloys*. (SAE Technical Paper Series: SAE, Warrendale, PA, 1992), p. 920070
5. B.R. Powell, V. Rezhets, M.P. Balogh, R.A. Waldo, Microstructure and creep behaviour in AE42 magnesium die casting alloy. JOM **54**, 34 (2002)
6. P. Bakke, H. Westengen, Die casting for high performance—focus on alloy development. Adv. Eng. Mater. **5**, 879 (2003)
7. I.P. Moreno, T.K. Nandy, D.S. Jones, J.E. Allison, T.M. Pollock, Microstructural stability and creep of rare-earth containing magnesium alloys. Scripta Mater. **48**, 1029 (2003)
8. T.L. Chia, M.A. Easton, S.M. Zhu, M.A. Gibson, N. Birbilis, J.F. Nie, The effect of alloy composition on the microstructure and tensile properties of binary Mg-rare earth alloys. Intermetallics **17**, 481 (2009)
9. S.M. Zhu, M.A. Gibson, M.A. Easton, J.F. Nie, The relationship between microstructure and creep resistance in die-cast magnesium-rare earth alloys. Scripta Mater. **63**, 698 (2010)
10. A. Luo, Recent Mg alloy development for elevated temperature applications. Int. Mater. Rev. **49**, 13 (2004)
11. M.A. Easton, S.M. Zhu, T.B. Abbott, M. Dargusch, M.T. Murray, G. Savage, N. Hort, M.A. Gibson, Evaluation of magnesium die-casting alloys for elevated temperature applications: castability. Adv. Eng. Mater. **18**, 953 (2016)
12. K. Strobel, M.A. Easton, V. Tyagi, M.T. Murray, M.A. Gibson, G. Savage, T. Abbott, Evaluation of the castability of high pressure die cast magnesium based alloys. Int. J. Cast Met. Res. **23**, 81 (2010)
13. S.M. Zhu, M.A. Easton, T.B. Abbott, J.F. Nie, M. Dargusch, N. Hort, M.A. Gibson, Evaluation of magnesium die-casting alloys for elevated temperature applications: microstructure, tensile properties and creep resistance. Metall. Mater. Trans. A **46**, 3543 (2015)
14. M.A. Gibson, M.A. Easton, V. Tyagi, M.T. Murray, G.L. Dunlop, Further improvements in HPDC Mg alloys for powertrain applications, in *Magnesium Technology*, ed. by M.O. Pekguleryuz, N.R. Neelameggham, R. Beals, E.A. Nyberg (The Metals, Minerals and Materials Society, New Orleans, LA, 2008), p. 227
15. M.A. Easton, M.A. Gibson, S. Zhu, T. Abbott, An a priori hot tearing indicator applied to die-cast magnesium-rare earth alloys. Metall. Mater. Trans. A **45A**, 3586 (2014)
16. S. Gavras, M.A. Easton, M.A. Gibson, S. Zhu, J.F. Nie, Microstructure and property evaluation of high-pressure die-cast Mg–La–rare earth (Nd, Y or Gd) alloys. J. Alloy. Compd. **597**, 21 (2014)
17. H.Q. Ang, T.B. Abbott, S.M. Zhu, C. Gu, M.A. Easton, Proof stress measurement of die-cast magnesium alloys. Mater. Design **112**, 402 (2016)
18. S. Zhu, T. Abbott, M.A. Gibson, J.F. Nie, M.A. Easton, Age hardening in die-cast Mg-Al-RE alloys due to minor Mn additions. Mater. Sci. Eng. A **656**, 34 (2016)
19. J. Zhang, K. Liu, D. Fang, X. Qiu, D. Tang, J. Meng, Microstructure, tensile properties, and creep behavior of high-pressure die-cast Mg–4Al–4RE–0.4Mn (RE=La, Ce) alloys. J. Mater. Sci. **44**, 2046 (2009)
20. J. Zhang, P. Yu, K. Liu, D. Fang, D. Tang, J. Meng, Effect of substituting cerium-rich mischmetal with lanthanum on microstructure and mechanical properties of die-cast Mg–Al–RE alloys. Mater. Des. **30**, 2372 (2009)
21. J. Zhang, Z. Leng, M. Zhang, J. Meng, R. Wu, Effect of Ce on microstructure, mechanical properties and corrosion behavior of high-pressure die-cast Mg–4Al-based alloy. J. Alloy. Compd. **509**, 1069 (2011)
22. S. Zhu, M.A. Easton, T. Abbott, M.A. Gibson, J.F. Nie, The influence of individual rare earth elements(La, Ce, or Nd) on creep resistance of die-cast magnesium alloy AE44. Adv. Eng. Mater. **18**, 932 (2016)
23. N. Birbilis, M.A. Easton, A.D. Sudholz, S.M. Zhu, M.A. Gibson, On the corrosion of binary magnesium-rare earth alloys. Corr. Sci. **51**, 683 (2009)

Contributed Papers from Materials Science and Technology 2017 (MS&T17)
October 8 – 12, 2017, David L. Lawrence Convention Center, Pittsburgh, Pennsylvania USA

DOI 10.7449/2017/MST_2017_164_170

EFFECT OF STRAIN RATE ON MECHANICAL BEHAVIOUR OF COMMERCIAL DIE-CAST MAGNESIUM ALLOYS

Hua Qian Ang[1], Trevor B. Abbott[1,2], Suming Zhu[1], Mark A. Easton[1]

[1]School of Engineering, RMIT University, Bundoora, Victoria 3083, Australia
[2]Magontec Limited, Sydney, New South Wales 2000, Australia

Keywords: Magnesium alloys; High-pressure die-casting; Strain-rate sensitivity; Dynamic strain aging

Abstract

The tensile properties of high-pressure die-cast Mg-6Al-0.3Mn (AM60), Mg-9Al-1Zn (AZ91), and Mg-4Al-4RE (AE44), under strain rates ranging from 10^{-6} to 10^{-1} s^{-1} have been investigated. It was found that AE44 is highly strain rate sensitive, followed by AM60, whilst AZ91 has little strain-rate sensitivity, fitting with previous observations about a correlation between strain-rate sensitivity and the aluminium content. Ductility is improved at lower strain rates in AE44 and AM60, but it appears to be independent of strain rate in AZ91. The difference in strain-rate sensitivity among these alloys is considered to be related to dynamic strain aging (DSA) from interactions between the aluminium solute and dislocations.

Introduction

Strain-rate sensitivity (SRS) is an important parameter, especially in crash analysis. Magnesium (Mg) tends to show pronounced SRS due to the hexagonal close packed (HCP) crystal structure [1] and the SRS in Mg is manifest as an increase in work hardening and tensile/yield ratio [2]. This suggests that the performance of Mg alloys in terms of energy absorption can improve at higher strain rates, and this can benefit crashworthiness.

Several researchers have investigated the effects of Al content on the SRS of Mg and alloys [2-4]. Overall, these researchers reported a decrease in SRS with increasing Al content. However, Aune et al. [5] studied the behaviour of die-cast AM50, AM60 and AZ91 alloys at 15-130 s^{-1}, but did not observe a significant change in SRS between alloys despite a difference in Al content. Similarly, Weiler and Wood [6] investigated sand-cast AE44 in similar strain rate range (100-300 s^{-1}) and did not observe any strain rate effect in AE44 despite its low Al content. It should be noted that the investigated strain rates in Aune et al. [5] and Weiler and Wood [6] fall in between quasi-static (typically $< 10^{0}$ s^{-1}) and dynamic ($\geq 10^{3}$ s^{-1}) domains while the investigated strain rates in these work [2-4] covered only the quasi-static strain rate range 10^{-6}-10^{-1} s^{-1}. Hence, it appears that SRS may vary with the applied strain rates.

To further understand the effects of Al content and strain rate on the SRS of various commercial available die-cast Mg alloys AM60, AZ91 and AE44, uniaxial tensile tesing are performed to achieve strain rates ranging from 10^{-6}-10^{-1} s^{-1}. AM60 are most commonly used in applications where energy absorption is required while AZ91 is widely used for some structural components of automobiles, aircraft, and computers, because of its good combination of mechanical

properties and die-castability. AE44 was originally developed as a creep resistant alloy, but it has good combination of strength and ductility, especially after aging [8], this makes it attractive for structural applications [9].

Experimental Procedures

Commercial high-pressure die-cast (HPDC) AM60, AZ91 and AE44 alloys cast into round tensile bars (100 mm long with a 36 mm parallel section in the gauge length and a diameter of 5.6 mm) [7]. The chemical compositions in wt.% of these alloys analysed using inductively coupled plasma atomic emission spectroscopy (ICP-AES) are listed in Table I. Tensile tests were performed using a constant rate of crosshead displacement with nominal strain rates in the range from 10^{-6}-10^{-1} s^{-1}. A more comprehensive data has been submitted for review [8].

Table I. Chemical Compositions (wt.%) Determined by ICP-AES for the Alloys used in This Study.

Alloy	Al	Mn	RE (Ce+La)	Zn	Mg
AM60	6.26	0.29	<0.01	0.1	Bal.
AZ91	8.88	0.19	<0.01	0.74	Bal.
AE44	3.67	0.31	3.83	<0.01	Bal.

Results

The tensile flow curves of AM60, AZ91, and AE44 Mg alloys tested at various strain rates, $\dot{\varepsilon}$ are shown in Figure 1. The flow curves of AE44 consistently shift higher with increasing $\dot{\varepsilon}$, increasing proof strength. The shift in flow curves of AM60 is a lot less visible, and even less so in AZ91.

The effects of strain rate on strength and fracture strain (ductility) are shown in Figures 2 (a) and (b), respectively. In Figure 2 (a), 0.5% proof strength is used because die-cast Mg alloys tend to show pronounced anelasticity and the 0.5% offset is a closer approximation to the 0.2% permanent plastic strain [9]. The 0.5% proof strength shows a more visible increase with strain rate for AE44 while the increase is moderate for AM60 and AZ91. It is noted that tensile strength appears to be less sensitive to strain rate and remains almost constant across strain rates for all alloys. This could be due to the fact that the present alloys do not reach necking and the tensile strength is the stress at fracture. Ductility appears to increase with decreasing strain rate in AE44 and AM60 while it appears to be independent of strain rate in AZ91 (Figure 2 (b)).

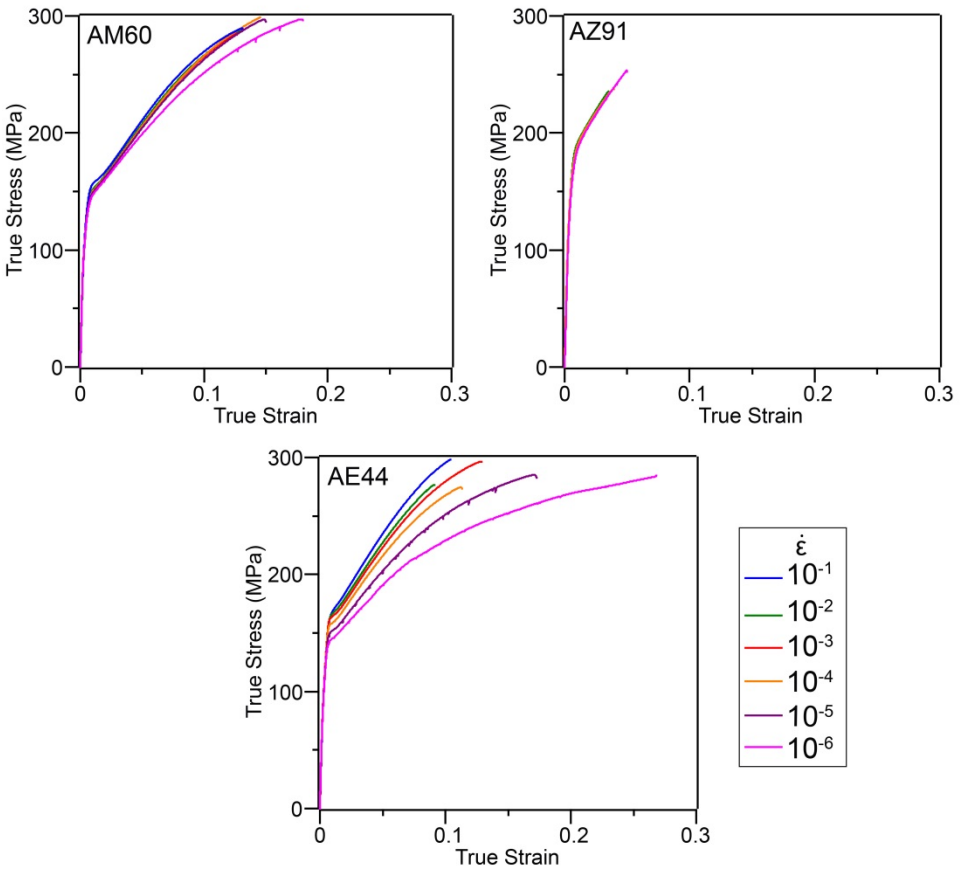

Figure 1. True stress-strain curves of (a) AM60, (b) AZ91 and (c) AE44 at different nominal strain rates, $\dot{\varepsilon}$.

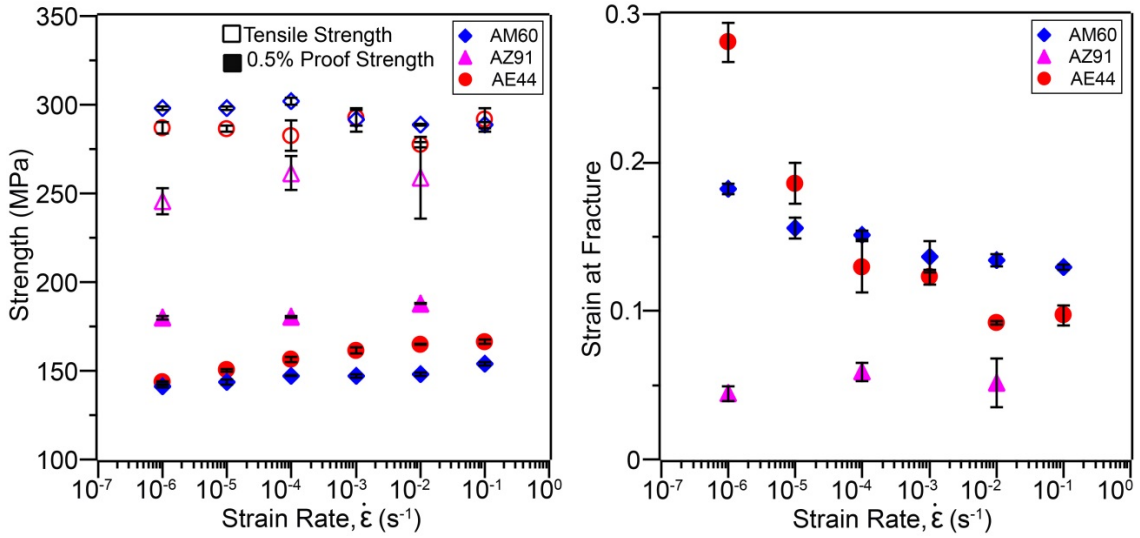

Figure 2. Effects of strain rate on (a) strength (MPa) and (b) strain at fracture of AM60, AZ91, and AE44. The solid and empty filled symbols in (a) indicate the 0.5% proof strength and tensile strength, respectively. Data reproduced from [8].

The differences in the levels of flow stress for different strain rates are indicative of SRS, represented by $m = \frac{\delta \ln(\sigma)}{\delta \ln(\dot{\varepsilon})}$ [1, 10, 11]. Figure 3 shows the variations of SRS with strain rate. It is clear that SRS appears to increase with decreasing strain rate in AE44, which is consistent with the observations from studies of pure Mg and other alloys [12-14]. There is, however, no consistent trend with AM60, where the SRS exhibits a slight decrease, followed by a slight increase with decreasing strain rate, but the difference in SRS is still small. Meanwhile, there is no visible change in SRS observed in AZ91. Overall, AE44 has the highest SRS, followed by AM60 and AZ91.

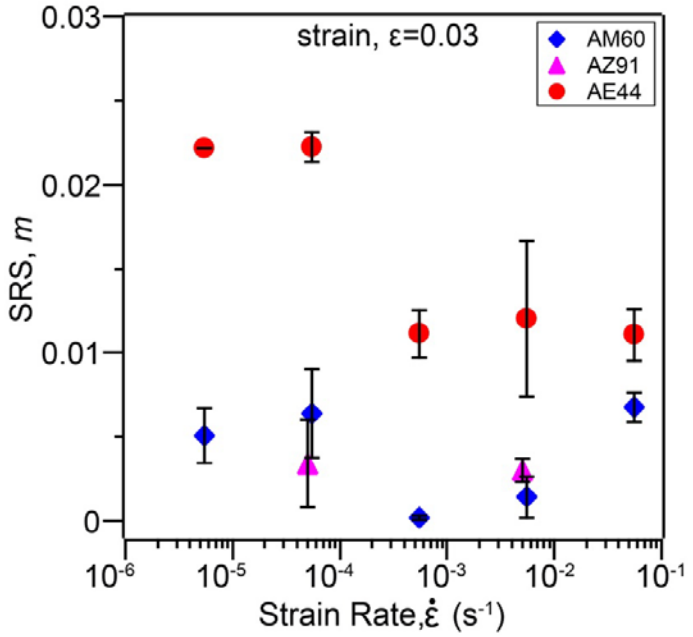

Figure 3. The variations of SRS with strain rate at strain=0.03 for different alloys. The strain rate corresponds to the average of the upper and lower values. Reproduced from [8].

Discussion

Present results show that strain rate can greatly influence the strength and ductility of AE44, while the effect of strain rate is moderate in AM60, and small in AZ91. The main difference between these alloys is the Al content. The reduced SRS with increasing Al content is considered to be related to dynamic strain aging (DSA) due to the interaction of Al solute and dislocations. DSA effect does not always manifest itself as serrations on stress-strain curves as reported earlier [15, 16]. DSA in solid solutions involves diffusion of solute atoms to mobile dislocations while dislocations are temporarily arrested by other forest dislocations piercing through their slip planes [15, 17, 18]. As a consequence of DSA, the stress to keep the dislocations moving will increase at constant strain rates. As the time taken for dislocations to cut through the forest obstacles is inversely proportional to strain rate, the strengthening effect is lower at higher strain rates, bringing the flow curves closer and reducing the SRS.

For AM and AZ Mg alloys, increasing Al content also increases the Al solute in α-Mg matrix, which further enhances the DSA effect and reduces the SRS. In the case of AE44, although Al is

still the dominant alloying element (4 wt.%), AE44 has significantly lower Al solute level in the α-Mg matrix as most of Al is in the form of Al-RE intermetallics [19-21]. Therefore, it is less likely to be affected by DSA. The net result is that the intrinsic SRS in Mg which is often attributed to the HCP crystal structure [1] is observed. AE44 also shows a higher SRS at lower strain rates (Figure 3) which is consistent with the SRS behaviour of pure Mg [13]. The diminished influence of DSA in AE44 causes the SRS behaviour to approach that of pure Mg.

Conclusions

In summary, this study has investigated the effect of strain rate on the commercial die-cast Mg alloys AM60, AZ91 and AE44 over a wide strain rate range 10^{-6}-10^{-1} s^{-1}. It is shown that the Al content can affect the SRS. The decrease in SRS with increasing Al content is likely related to DSA from the interaction of Al solute with dislocations.

Acknowledgements

This work was supported by the Australian Research Council [Grant number LP130100828]. The samples were produced by the CSIRO Manufacturing Flagship with acknowledgement of Mr. Gary Savage and Mr. Andrew Yob.

References

[1] M.A. Meyers, Dynamic Behaviour of Materials, John Wiley & Sons, New York, 1994.

[2] T.B. Abbott, M.A. Easton, R. Schmidt, Magnesium for crashworthy components, in: M. Byko (Ed.), Journal of The Minerals, Metals, and Materials Society, TMS Annual Meeting, California, 2003, pp. 227-230.

[2] C.A. Newland, M.T. Murray, Strain rate dependent behaviour of magnesium-based alloys, in: Proceedings of the First Australasian Congress on Applied Mechanics, Institution of Engineers, Australia, 1996, pp. 73-76.

[4] N. Stanford, M.R. Barnett, Effect of Al and Gd solutes on the strain rate sensitivity of magnesium alloys, Metall. Mater. Trans. A 41 (2010) 734-743.

[5] T.K. Aune, D. Albright, H. Westengen, T.E. Johnsen, B. Anderson, Behavior of die cast magnesium alloys subject to rapid deformation, SAE Technical Paper, 2000 pp. 2000-01-1116.

[6] J.P. Weiler, J.T. Wood, Strain-rate effects of sand-cast and die-cast magnesium alloys under compressive loading, in: S.N. Mathaudhu, W.H. Sillekens, N.R. Neelameggham, N. Hort (Eds.), Magnesium Technology 2012, John Wiley & Sons, Florida, 2012, pp. 365-370.

[7] A.V. Nagasekhar, M.A. Easton, C.H. Cáceres, Solute content and the grain microstructure of high pressure die cast magnesium–aluminium alloys, Adv. Eng. Mater. 11 (2009). 912-919.

[8] H.Q.Ang, S.M.Zhu, T.B.Abbott, Q.Dong, M.A.Easton, Strain-rate sensitivity of die-cast magnesium-aluminium based alloys [Accepted]. http://dx.doi.org/10.1016/j.msea.2017.05.093

[9] H.Q. Ang, T.B. Abbott, S.M. Zhu, C.F. Gu, M.A. Easton, Proof stress measurement of die-cast magnesium alloys, Mater. Des. 112 (2016) 402-409.

[10] E. Karimi, A. Zarei-Hanzaki, M.H. Pishbin, H.R. Abedi, P. Changizian, Instantaneous strain rate sensitivity of wrought AZ31 magnesium alloy, Mater. Des. 49 (2013) 173-180.

[11] W.S. Lee, T.H. Chen, Rate-dependent deformation and dislocation substructure of Al–Sc alloy, Scr. Mater. 54 (2006) 1463-1468.

[12] T. Matsunaga, H. Somekawa, H. Hongo, M. Tabuchi, Deformation mechanism transition with strain rate in Mg–3Al–1Zn alloy at room temperature, Mater. Sci. Eng. A 647 (2015) 212-215.

[13] R.B. Figueiredo, F. Poggiali, C. Silva, P.R. Cetlin, T.G. Langdon, The influence of grain size and strain rate on the mechanical behavior of pure magnesium, J. Mater. Sci. 51 (2016). 3012-3024.

[14] X.Z. Lin, D.L. Chen, Strain hardening and strain-rate sensitivity of an extruded magnesium alloy, J. Mater. Eng. Perform. 17 (2008). 894-901.

[15] L.P. Kubin, Y. Estrin, Dynamic strain ageing and the mechanical response of alloys, J. Phys. III 1 (1991) 929-943.

[16] L. Jiang, J.J. Jonas, R. Mishra, Effect of dynamic strain aging on the appearance of the rare earth texture component in magnesium alloys, Mater. Sci. Eng. A 528 (2011) 6596-6605.

[17] A. Van den Beukel, Theory of the effect of dynamic strain aging on mechanical properties, Phys. Stat. Sol. (a) 30 (1975) 197-206.

[18] Z. Trojanová, P. Lukác, K.U. Kainer, V. Gärtnerová, Dynamic strain ageing during stress relaxation in selected magnesium alloys containing rare earth elements, Adv. Eng. Mater. 7 (2005) 1027-1032.

[19] S.M. Zhu, J.F. Nie, M.A. Gibson, M.A. Easton, P. Bakke, Microstructure and creep behavior of high-pressure die-cast magnesium alloy AE44, Metall. Mater. Trans. A 43 (2012) 4137-4144.

[20] S.M. Zhu, M.A. Easton, T.B. Abbott, M.A. Gibson, J.F. Nie, The influence of individual rare earth elements (La, Ce, or Nd) on creep resistance of die-cast magnesium alloy AE44, Adv. Eng. Mater. 18 (2016) 932-937.

[21] M.I. Khan, A.O. Mostafa, M. Aljarrah, E. Essadiqi, M. Medraj, Influence of cooling rate on microsegregation behavior of magnesium alloys, J. Mater. (2014) 1-18.

Appendix B. Copyrights Permissions

Permissions have been granted by Elsevier to reproduce the published articles in full in this thesis.

ELSEVIER LICENSE
TERMS AND CONDITIONS

Sep 13, 2017

This Agreement between Hua Qian Ang ("You") and Elsevier ("Elsevier") consists of your license details and the terms and conditions provided by Elsevier and Copyright Clearance Center.

License Number	4187070644572
License date	Sep 13, 2017
Licensed Content Publisher	Elsevier
Licensed Content Publication	Materials & Design
Licensed Content Title	Proof stress measurement of die-cast magnesium alloys
Licensed Content Author	Hua Qian Ang,Trevor B. Abbott,Suming Zhu,Chengfan Gu,Mark A. Easton
Licensed Content Date	Dec 15, 2016
Licensed Content Volume	112
Licensed Content Issue	n/a
Licensed Content Pages	8
Start Page	402
End Page	409
Type of Use	reuse in a thesis/dissertation
Intended publisher of new work	other
Portion	full article
Format	both print and electronic
Are you the author of this Elsevier article?	Yes
Will you be translating?	No
Title of your thesis/dissertation	Mechanical Properties and Deformation Behaviour of High-Pressure Die-Cast Magnesium-Aluminium Based Alloys
Expected completion date	Oct 2017
Estimated size (number of pages)	128
Requestor Location	Hua Qian Ang
	Attn:
Total	0.00 AUD

ELSEVIER LICENSE
TERMS AND CONDITIONS

Sep 13, 2017

This Agreement between Hua Qian Ang ("You") and Elsevier ("Elsevier") consists of your license details and the terms and conditions provided by Elsevier and Copyright Clearance Center.

License Number	4187070288437
License date	Sep 13, 2017
Licensed Content Publisher	Elsevier
Licensed Content Publication	Materials Science and Engineering: A
Licensed Content Title	Strain-rate sensitivity of die-cast magnesium-aluminium based alloys
Licensed Content Author	Hua Qian Ang,Suming Zhu,Trevor B. Abbott,Dong Qiu,Mark A. Easton
Licensed Content Date	Jun 24, 2017
Licensed Content Volume	699
Licensed Content Issue	n/a
Licensed Content Pages	8
Start Page	239
End Page	246
Type of Use	reuse in a thesis/dissertation
Intended publisher of new work	other
Portion	full article
Format	both print and electronic
Are you the author of this Elsevier article?	Yes
Will you be translating?	No
Title of your thesis/dissertation	Mechanical Properties and Deformation Behaviour of High-Pressure Die-Cast Magnesium-Aluminium Based Alloys
Expected completion date	Oct 2017
Estimated size (number of pages)	128
Requestor Location	Hua Qian Ang
	Attn:
Total	0.00 AUD

ELSEVIER LICENSE
TERMS AND CONDITIONS

Sep 15, 2017

This Agreement between Hua Qian Ang ("You") and Elsevier ("Elsevier") consists of your license details and the terms and conditions provided by Elsevier and Copyright Clearance Center.

License Number	4190520838587
License date	Sep 15, 2017
Licensed Content Publisher	Elsevier
Licensed Content Publication	Materials Science and Engineering: A
Licensed Content Title	Anelasticity of die-cast magnesium-aluminium based alloys under different strain rates
Licensed Content Author	Hua Qian Ang,Trevor B. Abbott,Suming Zhu,Mark A. Easton
Licensed Content Date	Nov 7, 2017
Licensed Content Volume	707
Licensed Content Issue	n/a
Licensed Content Pages	9
Start Page	101
End Page	109
Type of Use	reuse in a thesis/dissertation
Intended publisher of new work	other
Portion	full article
Format	both print and electronic
Are you the author of this Elsevier article?	Yes
Will you be translating?	No
Title of your thesis/dissertation	Mechanical Properties and Deformation Behaviour of High-Pressure Die-Cast Magnesium-Aluminium Based Alloys
Expected completion date	Oct 2017
Estimated size (number of pages)	128
Requestor Location	Hua Qian Ang
	Attn:
Total	0.00 USD